Imperial College London

Department of Bioengineering

Evolutionary Biomechanics Group

Biomechanics of the insect bite apparatus

Frederik Püffel, BSc

Submitted for the degree of Doctor of Philosophy

December 2022

Main supervisor:
Dr. David Labonte

Co-supervisor:
Dr. Spyridon Masouros

Examiners:
Dr. Angela Kedgley
Prof. Jérôme Casas

Statement of Originality

I, Frederik Püffel, declare that this thesis is an original report of my research, has been written by me and has not been submitted for any previous degree. The experimental work is almost entirely my own work; the collaborative contributions have been indicated clearly and acknowledged. Due references have been provided on all supporting literature and resources.

Copyright Declaration

The copyright of this thesis rests with the author. Unless otherwise indicated, its contents are licensed under a Creative Commons Attribution-Non Commercial 4.0 International Licence (CC BY-NC). Under this licence, you may copy and redistribute the material in any medium or format. You may also create and distribute modified versions of the work. This is on the condition that: you credit the author and do not use it, or any derivative works, for a commercial purpose. When reusing or sharing this work, ensure you make the licence terms clear to others by naming the licence and linking to the licence text. Where a work has been adapted, you should indicate that the work has been changed and describe those changes. Please seek permission from the copyright holder for uses of this work that are not included in this licence or permitted under UK Copyright Law.

Publications

Some ideas and figures have appeared previously in the following preprints/publications:

F. Püffel et al. (2021). "Morphological determinants of bite force capacity in insects: a biomechanical analysis of polymorphic leaf-cutter ants". In: *Journal of the Royal Society Interface* 18.182, p. 20210424

F. Püffel et al. (2022). "Strong positive allometry of bite force in leaf-cutter ants increases the range of cuttable plant tissues". In: *bioRxiv*

F. Püffel et al. (2023a). "A biomechanical model for the relation between bite force and mandibular opening angle in arthropods". In: *Royal Society Open Science* 10.2, p. 221066

F. Püffel et al. (2023b). "Developmental biomechanics and age polyethism in leaf-cutter ants". In: *bioRxiv*

See Appendix F for list of permissions to republish data, text and images.

Acknowledgements

I am deeply grateful to my supervisor, David Labonte. Ever since we met, David did everything to support me, my social environment and my scientific endeavours. Your high academic and ethical standards have made a deep impression on me, shaped my scientific mind, and helped me to progress within and outside my PhD. I learned a ton, and I hope our journey will continue for a long while.

I thank the Evolutionary Biomechanics Group, and all its members throughout the years, for the friendly and supportive environment, for all the memorable nights in the Union bar, the Pasta Fridays, and the delicious cakes — I have eaten more than I could ever bake. I give special thanks to Maria, for your never-ceasing positive energy; to Andrea, my 'Schicksalgenosse', for your great heart; to Aurélie, for bringing éclairs into my life; to Victor, for all your support and cheekiness; to Liv, my 'lab buddy', for your inspiring efforts; to Henny, for the countless 'middle-of-the-night-cycling-home' conversations; to Haaris, for your considerate nature; to Tanel, for reminding me to be brave; to Fabi, for bringing me to climbing; to Nat, for your spontaneity; to Dilanka, for your readiness to help; to Ginny, for your self-deprecating humor; and lastly, to the coffee machine, the secret motor of the group, for obvious reasons.

I thank the Department of Bioengineering and its technical staff; the students that contributed to my thesis, Anaya Pouget and Xinyue Liu; my mentor, Reiko Tanaka; and my external collaborators, Rich Johnston, Thomas van de Kamp and Flavio Roces. I am indebted to Flavio for your support, hospitality, and abundance of knowledge and resources. I thank Jörg Müssig for the inspiring lectures that prompted my curiosity for science. I thank the Cusanuswerk for funding my PhD.

I thank Estelle for all the squash and beers, and my family, Mama, Papa, Mari, Lisa, Andi and Thea, for who you are and your support. I am deeply thankful to Myriam, my life partner and best friend. Myriam is my refuge and mirror, I could not have done this without you. Lastly, I thank Matti, my child and greatest gift, who gave me a new world.

"If a congress of naturalists were to gather to choose the seven wonders of the animal world, they would be compelled to include the bizarre and mighty civilizations of the attine leafcutters."

from *The Leaf-cutter Ants: Civilization by Instinct* by Bert Hölldobler and Edward O. Wilson

Abstract

Frederik Püffel

Biomechanics of the insect bite apparatus

In this thesis, I investigate the morphology and biomechanics of the insect bite apparatus using polymorphous leaf-cutter ants as study organism. I first quantify the key morphological determinants of bite force and discuss the spatial constraints of muscle geometry imposed by the insect exoskeleton. Across the substantial size-range of leaf-cutter ant workers, the bite force capacity increases with a strong positive allometry, driven by a disproportional increase in the volume of the mandible closer muscle combined with a muscle fibre arrangement that enables high volume-specific muscle forces. Second, I derive and validate a biomechanical model that links the geometry of the musculoskeletal bite apparatus to changes of the mandibular opening angle. I then deploy this model to extract the force-length properties of the mandible closer muscle via *in-vivo* bite force measurements. Third, based on these results and the previously extracted morphological parameters, I predict the scaling relationship between maximum bite force and body mass, and compare this prediction to direct force measurements. Leaf-cutter ants generate among the highest weight-specific bite forces ever reported for any animal, displaying an exceptional level of morphological and physiological adaptation to the high mechanical demands of herbivory. Fourth, I turn my attention to ontogenetic changes of the bite apparatus, from freshly-eclosed adults to fully-matured foragers. In the week following eclosion, the bite apparatus undergoes a considerable biomechanical development, driven by substantial muscle growth and increasing head capsule rigidity. As a result, young leaf-cutter ants are likely incapable of engaging in any colony tasks involving leaf-cutting. Fifth, although fully-matured foragers can generate much larger bite forces than callows, their mandibles require significantly higher forces to cut the same material. These mandibular cutting forces are largely size-independent, and for callows, they approach a theoretical minimum for the tested material, suggesting geometric adaptations for high mandible 'sharpness'. The results of this work add important aspects to the discussion on age- and size-related foraging behaviour in social insects, and more generally, underline the importance of biomechanics in insect herbivory.

Contents

Acknowledgements **ix**

Abstract **xiii**

1 Introduction **1**
1.1 Insect herbivory . . . 1
1.1.1 Plant-insect interactions . . . 2
1.1.2 Pest management . . . 3
1.1.3 Plant-mechanical properties . . . 4
1.2 The insect bite apparatus . . . 5
1.3 Leaf-cutter ants . . . 6
1.3.1 Natural history . . . 7
1.3.2 Division of labour . . . 9
1.3.3 Effects of size and shape . . . 9

2 Morphological determinants of bite force capacity **13**
2.1 Introduction . . . 13
2.2 Materials & methods . . . 16
2.2.1 Study animals . . . 16
2.2.2 Micro computed-tomography and tissue segmentation . . . 16
2.2.3 Morphometric analysis . . . 18
2.2.4 Error analysis . . . 20
2.2.5 Data analysis . . . 21
2.3 Results and discussion . . . 21
2.3.1 Functional constraints on mechanical advantage and pennation angle favour positive allometry of A_{phys} . . . 22
2.3.2 Positive allometry of bite force capacity requires substantial changes to external and internal head anatomy . . . 25
2.3.3 Why vary shape to boost bite performance? . . . 30

3 Relationship between bite force and mandibular opening angle **33**
3.1 Introduction . . . 33
3.2 A biomechanical analysis of biting in arthropods . . . 35
3.3 Materials & methods . . . 42

3.3.1 Study animals . . . 42
3.3.2 Tomography and morphometric analysis for model validation . . . 43
Sample preparation and scanning . . . 43
Morphometry . . . 43
3.3.3 Bite force measurements . . . 45
Experimental protocol . . . 46
Video analysis . . . 47
Electrical stimulation . . . 48
Data analysis . . . 50
3.4 Results and discussion . . . 50
3.4.1 Variation of morphological bite force determinants is in excellent agreement with model predictions . . . 51
3.4.2 Leaf-cutter ants are extremely specialised for large bite forces, and bite strongest at opening angles relevant for cutting . . . 54
3.4.3 Minimal models for the magnitude of bite force and its variation with gape . 57
3.5 Conclusion and outlook . . . 61

4 Scaling of maximum bite forces 63
4.1 Introduction . . . 63
4.2 Materials & methods . . . 65
4.2.1 Study animals . . . 65
4.2.2 Experimental set-up . . . 65
4.2.3 Sensor calibration, accuracy and precision . . . 66
4.2.4 Experimental protocol . . . 68
4.2.5 Extraction of landmarks . . . 69
4.2.6 Confounding effects due to size-differences . . . 69
4.2.7 Data curation and statistical analysis . . . 72
4.3 Results . . . 73
4.3.1 Leaf-cutter ant bite forces increase with strong positive allometry . . . 73
4.4 Discussion . . . 75
4.4.1 Bite force allometry can be accurately predicted from muscle architecture and head morphology . . . 75
4.4.2 Positive allometry of bite force has substantial benefits at colony level . . . 76
4.4.3 Positive allometry of bite force is common within, but rare across species . . 79
4.5 Conclusion and outlook . . . 83

5 Biomechanical development of the bite apparatus 85
5.1 Introduction . . . 85
5.2 Materials & methods . . . 87
5.2.1 Study animals . . . 87

5.2.2 Bite force measurements . . . 88
5.2.3 Cuticle brightness . . . 89
5.2.4 Nanoindentation . . . 90
5.2.5 Tomography and morphometric analysis . . . 92
5.2.6 Statistical analysis . . . 93
5.3 Results and discussion . . . 93
5.3.1 Co-development of bite force and muscle post eclosion . . . 93
5.3.2 Flexural rigidity and the mechanical demands of the head capsule during biting 97
5.3.3 Biomechanical limitations of foraging ability in leaf-cutter ants . . . 100
5.4 Conclusion and outlook . . . 101

6 Scaling of mandibular cutting forces 103
6.1 Introduction . . . 103
6.2 Materials & methods . . . 105
6.2.1 Study animals . . . 105
6.2.2 Mandible preparation and wear determination . . . 106
6.2.3 Polymer synthesis and mechanical testing . . . 107
6.2.4 Cutting force setup . . . 109
6.2.5 Experimental protocol . . . 110
6.2.6 Data curation and statistical analysis . . . 112
6.3 Results . . . 112
6.3.1 Effects of cutting speed . . . 112
6.3.2 Cutting forces are independent of mandible size . . . 112
6.3.3 Cutting forces increase significantly with mandibular wear . . . 115
6.4 Discussion . . . 116
6.4.1 Cutting mechanics and mandible 'sharpness' . . . 116
6.4.2 Mandibular wear and size-related cutting ability . . . 118
6.5 Conclusions and outlook . . . 120

7 Concluding remarks 121

A Morphological determinants of bite force capacity 127
A.1 Tomography . . . 127
A.2 Fibre-tracking algorithm . . . 127
A.3 Cuticle saving via filament-attachment . . . 129
A.4 Area coverage of apodeme . . . 129
A.5 Estimation of A_{apo} and σ_{apo} . . . 130
A.6 A simple geometric model of the ant head capsule . . . 130

B Relationship between bite force and mandibular opening angle 135
B.1 Model derivations . . . 135

B.2 Filament strain, head deformation and ligament rotation . . . 137
B.3 Bite force extraction for 2D sensors . . . 138
B.4 Ant preparation for tomography . . . 138
B.5 Sensor calibration and bite force measurement . . . 140
B.6 Passive joint forces enabled by the opener muscle . . . 140

C Scaling of maximum bite forces **143**
C.1 Effects of bite plate deflection during biting . . . 143
C.2 Force sensor circuit and user interface . . . 143
C.3 Projection of the mandibular joint rotational axis . . . 143
C.4 Filament length . . . 144

D Biomechanical development of the bite apparatus **147**
D.1 Further notable differences between callows and foragers . . . 147
D.2 Plate model . . . 147

E Scaling of mandibular cutting forces **151**
E.1 Tooth length measurements and wear determination . . . 151

F Permissions for republication **155**

Bibliography **157**

List of Figures

1.1 Evolutionary arms race between plants and insect herbivores . . . 2
1.2 Basic anatomy of the insect bite apparatus . . . 5
1.3 Leaf-cutter ant foraging . . . 7
1.4 Ecology of leaf-cutter ant colonies . . . 8
1.5 Worker-size distribution of a mature *Atta cephalotes* colony . . . 10
1.6 Isometric and allometric growth of head size . . . 11

2.1 Leaf-cutter ant herbivory and size-polymorphism . . . 14
2.2 Internal head anatomy of a medium-sized worker . . . 17
2.3 Scaling of bite force capacity and its musculoskeletal determinants . . . 24
2.4 Geometrical model of the head capsule . . . 26
2.5 Head geometry and theoretical optima . . . 28
2.6 Scaling of internal and external head anatomy . . . 30

3.1 Biomechanical model on the variation of bite force with mandibular opening angle . 37
3.2 Bite force measurements at varying opening angles . . . 46
3.3 Electrical muscle stimulation . . . 48
3.4 Voluntary vs stimulated bite forces . . . 49
3.5 Morphological changes with opening angle . . . 52
3.6 Bite force variation with opening angle and the effects of model components . . . 57
3.7 Error propagation from rotational axis . . . 61

4.1 Bite force setup and video analysis . . . 66
4.2 Sensor calibration and error estimation . . . 68
4.3 Impact of bite force corrections on scaling analysis . . . 70
4.4 Scaling of maximum bite forces – prediction and measurement . . . 74
4.5 Ecological significance of bite force allometry and interspecific comparison . . . 78

5.1 Callows inside the nest and leaf-cutting foragers . . . 87
5.2 Cuticle brightness and bite force measurement . . . 89
5.3 Nanoindentation experiments and morphometric analysis . . . 91
5.4 Biomechanical development of workers with varying cuticle brightness . . . 94
5.5 Bite force variation with muscle volume . . . 95
5.6 Flexural rigidity and bite force-induced head deformation . . . 99

6.1 Ant head preparation for callows and foragers . . . 106
6.2 Polymer characterisation and cutting force measurements . . . 108
6.3 Effects of cutting speed and sample mounting . . . 113
6.4 Scaling of mandibular cutting forces . . . 114
6.5 Mandibular wear and cutting forces . . . 116

A.1 Method to extract fibre length and orientation . . . 133

B.1 Muscle fibre analysis . . . 139
B.2 Bite force sensor calibration . . . 140

C.1 Bite force sensor circuit and user interface . . . 144

D.1 Muscle detachment in callows . . . 148
D.2 Plate model of head capsule . . . 149

E.1 Mandible tooth length measurement . . . 152
E.2 Fibre optic sensor calibration . . . 153

List of Tables

2.1 OLS regression results of bite force determinants with body mass 22

4.1 Intraspecific and intrageneric bite force scaling studies across various taxa 80

5.1 Correlation tests between biomechanical parameters and cuticle brightness 96

6.1 OLS regression results of cutting force and mandibular wear with body mass 113

A.1 SMA regression results of bite force determinants with body mass 132

C.1 RMA regression results of bite force with body mass and head volume 145

C.2 RMA regression results of critical opening angle with body mass 145

E.1 OLS regression results of various mandible dimensions with body mass 151

List of Symbols

$\hat{\mathbf{A}}$	Closer apodeme main axis
A_{apo}	Cross-sectional area of the closer apodeme
A_{eff}	Effective cross-sectional area of the closer muscle
A_{int}	Internal muscle attachment area
A_{phys}	Physiological cross-sectional area of the closer muscle
α	Misalignment angle between $\mathbf{F}_{b,m}$ and $\mathbf{F}_b$
β	Muscle force-length shape parameter
b_{RGB}	Cuticle brightness
D	Flexural rigidity of the head capsule
Δ	Closer apodeme displacement
E	Young's modulus
E_I	Indentation modulus of the head cuticle
$\mathbf{E}_l$	Vector connecting joint centre with left eye centre
$\mathbf{E}_r$	Vector connecting joint centre with right head eye centre
$\mathbf{e}_1$, $\mathbf{e}_2$, $\mathbf{e}_3$	Local head coordinate system
η	Fraction of the available head volume occupied by the closer muscle
$\mathbf{F}_b$	Applied bite force
$\mathbf{F}_{b,m}$	Measured bite force
$\mathbf{F}_{b,\theta}$	Maximum bite force at opening angle θ
$\mathbf{F}_{b,max}$	Maximum bite force at an equivalent mandibular opening angle, θ_{max}
$\hat{\mathbf{F}}$	Bite force-opening angle relationship, normalised with its maximum
$\hat{\mathbf{F}}_\theta$	Relative bite force at opening angle θ
F_c	Cutting force
$F_{c,min}$	Minimum cutting force
F_f	Friction force
F_{nc}	Net cutting force
f_h	Ratio between head cylinder length and external muscle attachment radius
f_r	Ratio between internal and external muscle attachment radii
γ	Closer apodeme angle
Γ	Correction term for differences in lever arm around the beam pivot
G_c	Fracture toughness
h	Head cylinder length
H_h	Head height

κ	Approximated cuticle deformation resulting from biting
$\hat{\kappa}$	Approximated cuticle strain resulting from biting
L_d	Average length of directly-attached muscle fibres
L_f	Average length of filament-attached muscle fibres
L_{fil}	Filament length
L_h	Head length
L_{mb}	Mandible blade length
$\mathbf{L}_{i,eff}$	Effective mandible inlever
$\mathbf{L}_{o,c}$	Mandible outlever at bite contact point
$\mathbf{L}_{o,eff,c}$	Effective mandible outlever at bite contact point
$\mathbf{L}_{o,d}$	Most distal (largest) mandible outlever
$\mathbf{L}_{o,eff,d}$	Most distal (largest) effective mandible outlever
L_{opt}	Optimal muscle fibre length at which muscle stress is maximal
$\mathbf{L}_p$	Lever arm around the beam pivot during biting experiment
$\mathbf{L}_{p,cal}$	Lever arm around the beam pivot during sensor calibration
L_t	Average total length of muscle fibres
MA	Mechanical advantage of the force transmission system
ϕ	Average fibre pennation angle
r	Internal muscle attachment radius
R	External muscle attachment radius
$\hat{\mathbf{R}}$	Rotational axis of the mandible joint
$\mathbf{S}_l$	Vector connecting joint centre with left head spike
$\mathbf{S}_r$	Vector connecting joint centre with right head spike
σ_{apo}	Yield strength of the closer apodeme
σ_m	Muscle stress
σ_{max}	Maximum muscle stress
T_1	Most distal tooth length
T_2	Second most distal tooth length
ΔT_1	Length difference between most distal tooth and its expected pristine length
ΔT_2	Length difference between second most distal tooth and its expected pristine length
θ	Mandibular opening angle
θ_{max}	Mandibular opening angle at which bite force is maximal
θ_{opt}	Mandibular opening angle at which muscle stress is maximal
T_{hc}	Head capsule thickness
t	Sheet thickness
V_{hc}	Head cuticle volume
V_m	Muscle volume
V_{func}	Functional volume of the closer muscle
V_{ext}	Head volume available for the closer muscle

V_h	Head volume
W_h	Head width
W	Mandibular wear index
χ	Muscle volume occupancy

1 Introduction

There are more than one million described insect species, constituting around two-thirds of all described species in the animal kingdom (Z.-Q. Zhang, 2013a,b). This unmatched diversity is reflected by an abundance of shape adaptations and mechanisms that enable insects to cope with the multitudinous environmental demands imposed on them. To give but a small glimpse: Aquatic beetles bind an air bubble around their body allowing them to respirate underwater (Stride, 1953). Water striders posses long and thin legs enabling them to support their entire body weight based on surface tension alone (Hu et al., 2003). Where there is little water, desert beetles keep hydrated by extracting water from air via alternating 'waxy' and 'non-waxy' regions on their elytra (Parker and Lawrence, 2001). To cover large distances in little time, some insects such as fleas, froghoppers and planthoppers use their skeleton as springs to store muscle work as elastic energy; when released, this energy drives powerful jumps within a single millisecond (Burrows, 2006; G. P. Sutton and Burrows, 2011; Burrows and G. Sutton, 2013; G. Sutton and Burrows, 2018). Speed and dexterity are often key to success in predator-prey encounters (Gronenberg, 1996): snap-jaw and trap-jaw ants use their mandibles to launch powerful strikes on prey, reaching peak velocities in as little as tens of microseconds (Gronenberg, 1995; Patek et al., 2006; Larabee and Suarez, 2015; Larabee et al., 2018; Hao et al., 2018); larvae of some mosquito species use hemostatic pressure to rapidly extend their necks and capture prey in just a few milliseconds (Hancock et al., 2022); dragonflies deploy an intricate visual guidance system in combination with precise flight control to capture airborne prey with relative ease (Combes et al., 2013; Bomphrey et al., 2016; Fabian et al., 2019). In order to defend themselves, some carabid beetles utilise an explosive chemical reaction in their abdomen to discharge harmful organic compounds against aggressors (Moore and Wallbank, 1968; Di Giulio et al., 2015). Clearly, predator-prey interactions have driven the evolution of fascinating phenotypes, but not all insects live on a carnivorous diet. At least several hundred thousand insect species are herbivorous (Futuyma and Agrawal, 2009; Wiens et al., 2015; Douglas, 2018), and plant-herbivore interactions are believed to have substantially driven the unparalleled diversification of both insects and plants (Ehrlich and Raven, 1964; Futuyma and Agrawal, 2009; Wiens et al., 2015).

1.1 Insect herbivory

Insect herbivores play a vital role in most terrestrial ecosystems: By transforming living plant biomass into frass, they accelerate the cycling of carbon, nitrogen and phosphor (H. G. Fowler et al., 1989; Weisser and Siemann, 2004; Yang and Gratton, 2014). Insect herbivory is so ubiquitous that virtually all plant species are utilised by at least one insect species (Fürstenberg-Hägg et al., 2013; Douglas,

2018), but plant-herbivore interactions are not a 'one-way street': The evolutionary arms race between plants and insects began several hundred million years ago and is characterised by ingenious chemical and physical plant-defence mechanisms and sophisticated 'strategies' to overcome them (Fürstenberg-Hägg et al., 2013; Wiens et al., 2015, see Fig.1.1). In the following paragraphs, I will describe some of the involved mechanisms and eventually converge on a particular set of insect traits critical to overcome the physical barrier of plant tissues: the insect bite apparatus, which is the main subject of this thesis.

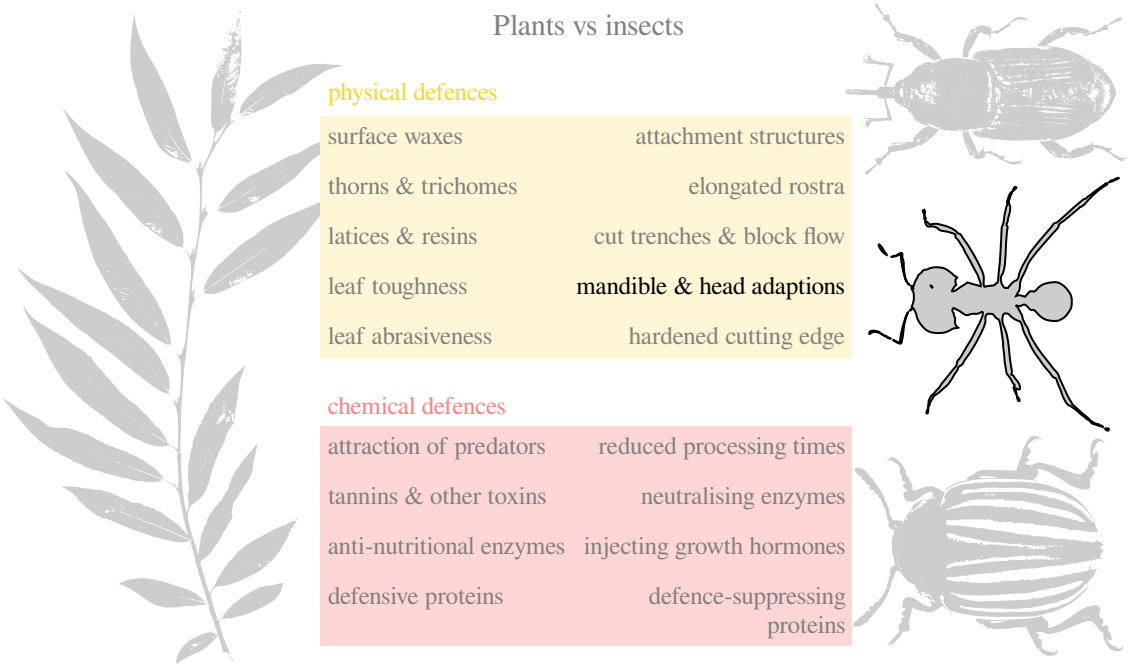


FIGURE 1.1: The evolutionary arms race between plants and insect herbivores has led to the emergence of intricate physical and chemical plant-defence mechanisms, and insect-feeding adaptations to overcome them (collated from E. Bernays, 1986; E. A. Bernays, 1991; Howe and Schaller, 2008; Reynolds et al., 2009; War et al., 2012; Fürstenberg-Hägg et al., 2013; Giron et al., 2018; Beran and Petschenka, 2022). Plant-insect interactions are fascinatingly complex (and not always antagonistic, see e. g. Hung et al., 2018; Magalhães et al., 2018), and I acknowledge that this simple schematic cannot do this complexity justice: e. g. microbial factors are entirely neglected here (but see Giron et al., 2018). In my thesis, I investigate insect traits that are particularly important to overcome leaf toughness: the morphology and biomechanics of the bite apparatus (black font). To this end, I use one of the most effective herbivores as study organism: leaf-cutter ants (middle). Other hazardous insect pests include the red palm weevil (top) and the Colorado potato beetle (bottom) (Abraham et al., 1998; Oerke, 2006); insects are not shown to scale.

1.1.1 Plant-insect interactions

In order to plant-feed, insects first need to gain access to the sought-after plant tissues. Tissue access can be rendered difficult via the application of epicuticular wax layers, which increase the slipperiness of the plant surface (Federle et al., 1997; Howe and Schaller, 2008; Scholz et al., 2010), and thus require insect-tarsal structures with strong attachment abilities (E. A. Bernays, 1991; Federle et al., 2000). Another physical barrier are trichomes, small hair-like structures of varying shapes which extend from the plant epidermis; trichromes negatively affect insect mobility, oviposition success and

feeding rates of insects (E. A. Bernays, 1991; Howe and Schaller, 2008; War et al., 2012; Fürstenberg-Hägg et al., 2013). To bypass this barrier, some piercing-sucking froghopper and aphid species develop elongated rostra, allowing them to access their preferred feeding sites (E. A. Bernays, 1991).

Some plants use latices and resins to fight off insect herbivores; when the lactifiers or resin ducts get severed, they exude latex and resin, respectively, and so push out, entrap, or even poison the attacking insect (Howe and Schaller, 2008; Agrawal and Konno, 2009; Fürstenberg-Hägg et al., 2013). Some herbivores, in turn, block and redirect the flow of latices and resins before feeding (Carroll and Hoffman, 1980; Fürstenberg-Hägg et al., 2013): For example, *Epilachna tredecimnotata* lady beetles cut trenches in the leaf to prevent the exudation of latex onto the feeding site (Carroll and Hoffman, 1980).

The arms race between plants and insects is not only characterised by physical interactions; plant-chemical defence mechanisms and corresponding insect adaptations also play a role (e. g. Howe and Schaller, 2008; War et al., 2012; Fürstenberg-Hägg et al., 2013; Simon et al., 2015; Giron et al., 2018; Douglas, 2018; I. K. Singh and A. Singh, 2021; A. C. Jones et al., 2022; Beran and Petschenka, 2022, see Fig. 1.1). In fact, the chemical interactions are so complex, describing them in detail is a book-filling exercise (literally, e. g. I. K. Singh and A. Singh, 2021), and far exceeds the scope of this introduction. I will hence constrain myself to a few examples: Plants use secondary metabolites such as tannins and proteins to deter and intoxicate insects, and so reducing herbivory and insect survival rates (War et al., 2012; Douglas, 2018). Insects counter this by injecting their own set of chemicals into the plant which can suppress plant-defences or even create new resource sinks via hormone-induced tissue growth (Giron et al., 2018). Some insects can neutralise or excrete ingested plant toxins (Giron et al., 2018; Beran and Petschenka, 2022), or store them to later defend themselves against parasitoids and predators (Simon et al., 2015); predators, in turn, can be recruited via damage-induced plant volatiles and extrafloral nectar (Fürstenberg-Hägg et al., 2013).

1.1.2 Pest management

Evidently, insect herbivory is multifaceted and of great ecological and evolutionary importance. But, it has also substantial effects on our agriculture: Global crop losses due to insect pests and other arthropods may be around 20 % (Sharma et al., 2017), excluding the indirect losses to insect-transmitted pathogens (see Oerke, 2006; Giron et al., 2018); as a result, insect pests cause hundreds of billions of US dollars in economic damage, every year (Dhaliwal et al., 2010; Oliveira et al., 2014; Sharma et al., 2017). The combined losses of wheat, rice and maize mount up to over 150 Mt per year (Deutsch et al., 2018), and these figures are likely to increase in the future: Due to climate change, insect pest populations are projected to grow substantially, migrate to previously inaccessible regions, and operate at increased metabolic rates (Deutsch et al., 2018; Giron et al., 2018). In combination with an increasing human population (Tilmen et al., 2011), insect pests may seriously threaten global food security in the upcoming decades (Battisti and Naylor, 2009; Rosenzweig et al., 2014; Deutsch et al., 2018). To make matters even worse, insecticides used for crop protection become increasingly

ineffective due to the emergence of resistances (Oerke, 2006; Sparks, 2013; Borel, 2017), and the development of new insecticides gets increasingly difficult and expensive (Sparks, 2013; Borel, 2017). For these reasons, alternative strategies for pest management are urgently needed (see e. g. Borel, 2017; Douglas, 2018; Kamatham et al., 2021).

A desirable starting point for such strategies may be to increase the resistance of the host plant itself (Sandhu and Kang, 2017; Douglas, 2018), so restrengthening the natural physical and chemical defences against pests, which were partially lost during crop domestication (Olsen and Wendel, 2013; Douglas, 2018). Increasing crop resistance by altering the plant-chemical profile may be a promising avenue, but it comes with challenges: The richness and diversity of plant secondary metabolites (> 200,000 different molecules), in combination with the multitude of insect-specific adaptations to them, renders general approaches difficult and limits the predictability of outcomes from such manipulations (Douglas, 2018). An alternative approach may thus be to enhance the physical resistance of plants. From a mechanical perspective, the ability to feed on plants appears remarkably predictable: if the insect cannot pierce, drill or bite into the plant tissue, it cannot feed on it. And indeed, plant-mechanical properties can be a good predictor for herbivory success: 'Tough' plant tissues deter insect herbivores (J. M. Cherrett, 1972; Barrer and J. M. Cherrett, 1972; Waller, 1982; P. D. Coley, 1983; Nichols-Orians and Schultz, 1989; Nichols-Orians and Schultz, 1990; P. Coley and Barone, 1996; P. J. Peeters et al., 2007, but see Howard, 1988; Folgarait et al., 1996), reduce feeding and growth rates (Raupp, 1985; F. J. Clissold et al., 2009; R. M. Schofield et al., 2011), and induce mandibular wear (Raupp, 1985; Roitberg et al., 2005; Depieri et al., 2010; R. M. Schofield et al., 2011).

1.1.3 Plant-mechanical properties

The key determinants of plant toughness and hardness are the composition, density and thickness of cell walls (Choong, 1996; P. W. Lucas et al., 2000; War et al., 2012), and the local inclusion of amorphous silica (P. W. Lucas et al., 2000; Reynolds et al., 2009). Silicon-augmented plants are more abrasive and less digestible for insects (and for mammals, see Baker et al., 1959), and may even induce the production of defensive plant-enzymes (Reynolds et al., 2009). Insect adaptations include behavioural, morphological, and biomechanical aspects: Some caterpillar species mainly feed on the leaf lamina, avoiding tougher regions such as midribs and veins (Choong, 1996); leaf-cutter ants incorporate heavy metals in their mandibular cutting edge, which may increase wear resistance (R. M. Schofield et al., 2002; R. Schofield et al., 2021); the mandible and gut morphology of grasshoppers may have adapted to fit dietary needs (E. A. Bernays, 1991), and grass-feeding caterpillars developed larger mandible muscles compared those reared on softer tissues (E. Bernays, 1986). The underlying biomechanical principles of insect herbivory have received some attention (e. g. Chapman, 1995; Tautz et al., 1995; Wright and Vincent, 1996; P. W. Lucas et al., 2000; Read and A. Stokes, 2006; Sanson, 2006; F. Clissold, 2007; R. M. Schofield et al., 2011), but we still lack fundamental knowledge about the musculoskeletal system that determines the ability of plant-chewing insects to process food: the bite apparatus.

1.2 The insect bite apparatus

In essence, the insect bite apparatus is composed of a pair of mandibles, controlled via antagonistic opener and closer muscles (Chapman, 1995, see Fig. 1.2). In most insects, these mandibles rotate about a single axis of rotation, defined by two mandibular condyles (Blanke et al., 2015; Blanke, 2019); dicondylic joints may provide more stable mandible movements compared to monocondylic articulations, and perhaps increase the capacity for bite force (Staniczek, 2001; Blanke et al., 2012, 2015).

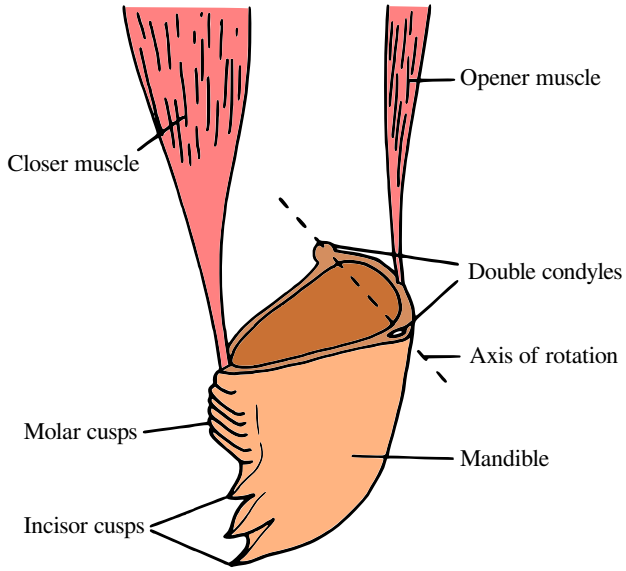


FIGURE 1.2: Basic anatomy of the insect bite apparatus, consisting of a pair of mandibles controlled via antagonistic opener and closer muscles (only the left head hemisphere is shown here; adapted from Chapman, 1995, see Appendix F for permission to republish). Each mandible rotates about a single axis of rotation defined by two condyles. In some insects, the mandible blade is divided into a molar region for mastication, and a more distally located incisor region for cutting. In Chapter 3 of this thesis, investigate the relationship between bite force and mandibular opening angle, based on changes to the morphology and physiology of the bite apparatus.

Bite forces are of critical importance to insect herbivores as they determine whether or not a plant tissue can be cut (e. g. Wright and Vincent, 1996; F. Clissold, 2007). In addition to herbivory, bite forces determine various other aspects of insect ecology such as access to feeding sites and mating partners (Hall et al., 2010; Goyens et al., 2014b) and the escape chances from predation (Hao et al., 2018). Despite this significance, studies on insect bite forces are extremely scarce: When I started my PhD in 2018, there existed only nine studies reporting *in-vivo* bite forces of insects, covering a total of 25 species (Wheater and Evans, 1989; Paul and Gronenberg, 2002; Hall et al., 2010; M. H. Huang, 2012; Goyens et al., 2014b; Weihmann et al., 2015a; David et al., 2016b,a; Hao et al., 2018). In 2022, a more comprehensive study with bite force measurements of 654 insect species was published (Rühr et al., 2022), which I will discuss in more detail in Chapter 4. Still, only two of these ten studies considered the effect of mandibular opening angle on bite forces (Goyens et al., 2014b; Weihmann et al., 2015a); the opening angle is relevant because it determines the functional range of the mandibles and may relate to dietary needs; as I will mention later, this aspect of bite performance has received a

lot more attention in vertebrates (e. g. Dumont and Herrel, 2003; S. H. Williams et al., 2009; Gidmark et al., 2013; Santana, 2016; Kaczmarek and Gidmark, 2020).

In this thesis, I explore biomechanical aspects of the insect bite apparatus in five experimental chapters: In Chapter 2, I quantify the morphological determinants of bite force with a focus on the constraints of muscle size and geometry imposed by the insect head capsule. Space-constraints are particularly relevant for insects and other arthropods, because unlike vertebrates they cannot put on muscle tissue outside their skeleton. Instead, they are confined by an exoskeleton, which leads to an optimisation problem how to best use the limited available head volume. In Chapter 3, I extract the morphological changes of the bite apparatus across a large range of mandibular opening angles. Combined with a biomechanical model to predict these chances, I then extract the force-length properties of the mandible closer muscle from *in-vivo* bite force measurements, and provide a detailed discussion on the various predictors of bite force. In Chapter 4, I use the results from the previous two chapters to predict the variation of bite force from morphological data alone, which I then compare against *in-vivo* force measurements. I discuss the difficulties of measuring bite forces of small animals, and place my results in a comparative and ecological context with a focus on the ability to plant-feed. In Chapter 5, I study ontogenetic changes of the musculoskeletal bite apparatus in conjunction with associated changes in bite performance. The ability to generate bite forces depends on both muscle-developmental and skeletal aspects, which I quantify and discuss in a biomechanical framework. At last, I turn my attention to another critical force that determines a herbivore's ability to feed: the mandibular cutting force. In contrast to bite forces, cutting forces depend not only on the biting animal, but also on the geometry and mechanical properties of the cutting substrate, which makes a clear definition of mandible 'sharpness' difficult. I quantify mandibular cutting forces using homogenous polymer sheets as 'synthetic leaves' in order to reduce mandible-independent variation, and I contextualise the results in an ecological framework. I end my thesis with a brief general discussion to synthesise the key findings of my experimental chapters. For each of the experimental chapters, I added an introduction with details on the relevant literature pertaining to the respective topics. To not repeat myself, I will thus keep this section short and instead move on to a subject I have not yet touched upon: my study organism.

1.3 Leaf-cutter ants

Any suitable study organism should be an ecologically and economically relevant insect herbivore with a bite apparatus, from which general conclusions on other insects can be drawn. Leaf-cutter ants fulfil these criteria because (i) they are the principal herbivore in the Neotropics, cutting up to 15 % of the foliar biomass (see Fig. 1.3, Herz et al., 2007; Costa et al., 2008), which makes them key players in their native ecosystems (H. G. Fowler et al., 1989); (ii), they are considered an important pest, frequently attacking crops such as coffee, cocoa, citrus, cassava, maize, cotton, sugar cane and oil palm (H. G. Fowler et al., 1989; Montoya-Lerma et al., 2012), which causes billions of US$ in annual economic damages (Montoya-Lerma et al., 2012); and (iii), the internal head anatomy consists of the

same basic elements typical for most insect species (see Fig. 1.2, Chapman, 1995; Gronenberg et al., 1997; F. Clissold, 2007; Blanke, 2019), which enables a broader interpretation of the results. In the next paragraphs, I will give a broader introduction to the biology of leaf-cutter ants, in an attempt to convey my fascination for an organism that captivated me for the last few years.

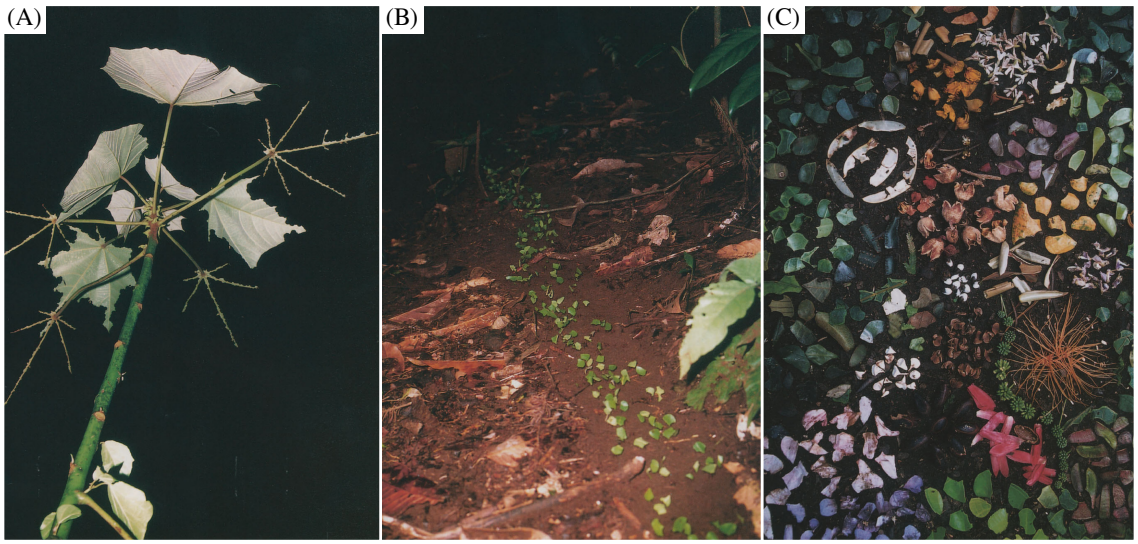


FIGURE 1.3: **(a)** Leaf-cutter ants are a notorious pest species in the Neotropics, frequently attacking economically important crops such as oil palm, coffee, cocoa, maize and cotton (Montoya-Lerma et al., 2012). They also cause substantial damage to trees; an individual tree may loose almost half its leaves to leaf-cutter ant foragers (Wirth et al., 2003; Montoya-Lerma et al., 2012), where young (tender) leaves are often preferred to old (tough) leaves (e. g. Nichols-Orians and Schultz, 1990). **(b)** The characteristic foraging trails of leaf-cutter ants may be as long as 80 m (Rockwood, 1976; Wirth et al., 2003), densely populated by leaf-carrying workers. **(c)** A single colony may forage on leaves, petals and fruit from more than 100 different plant species (Shepherd, 1985), here displayed in an artistic arrangement for a *Atta columbica* colony, collected during a one-year period; all three photos were taken from Wirth et al. (2003), see Appendix F for permission to republish.

1.3.1 Natural history

Leaf-cutter ants are eusocial insects of the fungus-growing myrmicine tribe Attine; mature colonies consist of up to several million workers with only one reproductive individual: the queen (Wirth et al., 2003; Hölldobler and E. O. Wilson, 2010). The numerous tasks arising in the colony include brood and fungus care, grooming, excavation, waste disposal, nest defence and the cutting and carrying of fresh vegetation to the nest (E. O. Wilson, 1980a, see Fig. 1.4). The harvested vegetation may consist of leaves, petals and fruits from up to 130 plant species in the colony surroundings (J. M. Cherrett, 1968; Shepherd, 1985); this dietary breadth makes leaf-cutter ants 'generalised' herbivores as opposed to much more common 'specialists' who feed on a small set of plant species (E. A. Bernays, 1998; Futuyma and Agrawal, 2009; Forister et al., 2015). 'Generalists' can typically tolerate a wide range of plant defences (Fürstenberg-Hägg et al., 2013). In leaf-cutter ants, however, some of these defences may be 'sidestepped' via a symbiotic fungus that pre-processes less palatable plant components (Littledyke and J. M. Cherrett, 1976). The symbiosis between ants and fungus is mutualistic:

The ants protect the fungus from microbial pathogens and parasites (Rodrigues et al., 2008; Hölldobler and E. O. Wilson, 2010, but see Currie et al., 1999; Currie, 2001), actively foster growth by incorporating leaf fragments into the fungal comb (E. O. Wilson, 1980a; Garrett et al., 2016), and help dispersing fungal spores (Mueller et al., 2001; Hölldobler and E. O. Wilson, 2010). The fungus, in turn, provides a rich and easily digestible diet (Martin et al., 1969; Martin and Weber, 1969), which feeds the ants during larval growth; adult workers may often supplement their diet with sugary plant sap (Littledyke and J. M. Cherrett, 1976; Quinlan and J. Cherrett, 1979).



FIGURE 1.4: **(a)** Leaf-cutter ant colonies consist of up to several million workers with only one reproductive individual: the queen. From the outside, only piles of excavated soil are visible; the majority of the nest lies below the ground, and may consist of hundreds and thousands of fungus and waste chambers (Wirth et al., 2003, photo credit: Flavio Roces). **(b)** To maintain the subterranean fungus as crop, polymorphic foragers cut semi-circular fragments from fresh vegetation in the colony surroundings (Hölldobler and E. O. Wilson, 2010). These fragments are carried back to the nest, 'shredded' to smaller pieces, and incorporated in the fungal gardens (Garrett et al., 2016). **(c)** The symbiosis between ants and fungus is mutualistic: the fungus breaks down nutrients otherwise inaccessible to the ants (Martin et al., 1969; Martin and Weber, 1969; Littledyke and J. M. Cherrett, 1976), while the ants protect the fungus from parasites and harmful bacteria (Hölldobler and E. O. Wilson, 2010). **(d)** In addition to food, the fungus also provides accommodation for the colony's brood: eggs, larvae and pupae are housed in the close-knit structure of the fungal garden. Photo credit (b-d): Samuel T. Fabian.

1.3.2 Division of labour

The ecology of leaf-cutter ants is characterised by an extensive division of labour based on both size and age polyethism; e. g. smaller and freshly-eclosed workers are more likely to perform nursing tasks inside the nest, whereas only workers exceeding a certain age and size engage in outside foraging tasks (E. O. Wilson, 1980a; Camargo et al., 2007). The size-differences between workers of the same colony can be substantial: Between smallest minims and largest majors, the body mass may vary by a factor of almost 300 (0.4-110 mg in *Atta cephalotes*, see Wetterer, 1994a); notably, majors only exist in colonies exceeding a certain size and age, and even then, they are comparatively rare (E. O. Wilson, 1983b, see Fig. 1.5). Size polymorphism and the associated behavioural differences are hypothesised to increase colony fitness via ergonomic task allocation (E. O. Wilson, 1980a,b, 1983a,b; Wetterer, 1999; Wirth et al., 2003; Clark, 2006; Hölldobler and E. O. Wilson, 2010; R. M. Schofield et al., 2011). However, such hypotheses are difficult to test as they require the functional analysis of size-related ability and efficiency to perform certain tasks. In order to assess the effects of worker size and age on the ability to partake in leaf-cutting tasks, I conducted most of my experiments with individuals of different sizes and/or age post eclosion: In Chapter 5 and 6, I investigate the biomechanical development and effects of mandibular wear, respectively, of differently-aged workers following eclosion. In Chapter 2, 4 and 6, I study the morphology, bite forces and cutting forces, respectively, across almost the entire size-range of workers in *A. vollenweideri* ($\approx 1 - 50$ mg). The results of these chapters provide a biomechanical basis for the ability to leaf-cut, and so add quantitatively to our understanding of the intricate foraging behaviour of leaf-cutter ants – a biological phenomenon which has captivated researchers across more than a century and has accumulated a large body of literature (e. g. W. M. Wheeler, 1907; Walter et al., 1938; J. M. Cherrett, 1968; Barrer and J. M. Cherrett, 1972; Jaffe and Howse, 1979; E. O. Wilson, 1980a,b, 1983a; Shepherd, 1985; Rudolph and Loudon, 1986; Howard, 1988; Waller, 1989; Nichols-Orians and Schultz, 1989; Nichols-Orians and Schultz, 1990; Roces, 1990; Wetterer, 1990; Wetterer, 1991a,b; Shutler and Mullie, 1991; Roces and Núñez, 1993; Wetterer, 1994a,b; Roces and Hölldobler, 1994; Wetterer, 1995a,b; Burd, 1995, 1996; Roces and Hölldobler, 1996; Burd, 2000a,b, 2001; Hart et al., 2002; Röschard and Roces, 2003b,a; Burd and Howard, 2005; Clark, 2006; Evison and Ratnieks, 2007; Lewis et al., 2008; Dussutour et al., 2008; Helanterä and Ratnieks, 2008; Moll et al., 2010; Röschard and Roces, 2011; Moll et al., 2013; Garrett et al., 2016; Arenas and Roces, 2018).

1.3.3 Effects of size and shape

The ability to leaf-cut across workers of vastly different sizes may be expected to vary based on differences in size alone. In order to assess to what extent different polymorphs are 'specialised' to leaf-cutting, I need to consider shape differences as well. To differentiate between effects based on size or shape, I will make use of an important concept in biological sciences termed 'relative growth' or 'allometry' (see Gayon, 2000, for historical review). Allometry describes "changes in relative dimensions of parts of an organism that are correlated with changes in overall size" (Gayon, 2000). Three different types of allometry are typically distinguished: ontogenetic, static and evolutionary

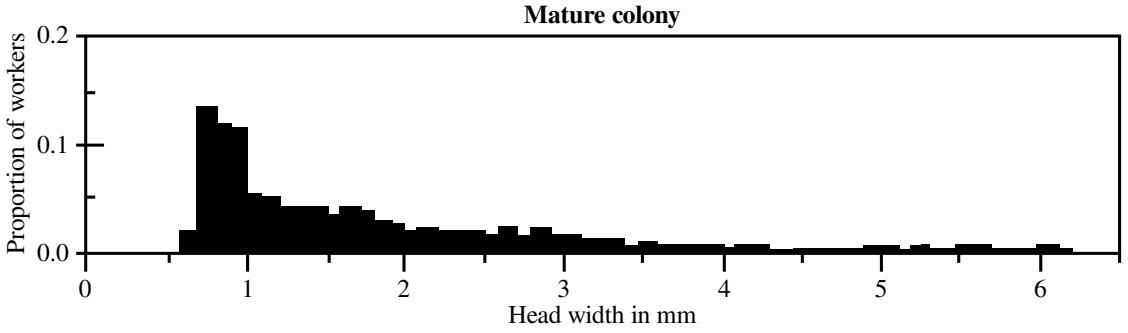


FIGURE 1.5: Worker-size distribution of a mature *Atta cephalotes* colony (adapted from Wetterer, 1999, see Appendix F for permission to republish; original data from Stradling, 1978), spanning an order of magnitude in head width, which corresponds to an approximately 250-fold difference in body mass (Wetterer, 1994a). The size distribution of younger colonies with fewer workers have a shorter right tail, i. e. the largest workers are only 'produced' in colonies that exceed a certain minimum size (E. O. Wilson, 1983b). Size-polymorphism in leaf-cutter ants is associated with an extensive division of labour: The smallest workers attend to the queen, brood and fungus; a range of medium-sized workers harvests fresh plant matter; and the largest workers, so-called 'soldiers', defend the colony against intruders (E. O. Wilson, 1980a).

allometry (Gould, 1966; Gayon, 2000; Pélabon et al., 2013). Ontogenetic allometry describes relative changes during an individual's development, static allometry is defined across individuals from the same population and equal developmental stage, and evolutionary allometry is measured across species (Gould, 1966; Pélabon et al., 2013). Leaf-cutter ants do not grow externally after eclosion, so that the observed size-range covers workers of the same developmental stage. The scaling relationships across fully-matured workers in Chapter 2, 4 and 6 are hence 'static'. In contrast, most available intraspecific studies on bite forces describe 'ontogenetic' allometries (see Chapter 4), which may underlie different constraints (Pélabon et al., 2013); the various developmental and evolutionary constraints on allometry are highly complex and beyond the scope of this introduction (for the interested reader, I recommend Gould, 1966; Egset et al., 2012; Pélabon et al., 2013; Voje et al., 2014; Bolstad et al., 2015).

In contrast to this complexity, allometric relationships are typically described by a simple equation: $y = ax^b$, where trait y scales proportionally to trait x to the power of scaling coefficient b (Huxley, 1924). After logarithmic transformation, this power equation takes a linear form: $\log y = b \log x + \log a$ (Huxley, 1924; Gould, 1966), which I use as the basis to characterise most scaling relationships in this thesis. If traits x and y have the same dimension, b should equal one if geometric similarity (isometry) is maintained; if x is a volumetric quantity (such as mass) and y is a length, $b = 1/3$ for isometric growth (Gould, 1966). Allometry occurs when b deviates from its isometric prediction; 'positive allometry' is indicated for larger values of b and 'negative allometry' for smaller values. To illustrate the effects of allometry, imagine a small leaf-cutter ant with body mass, m, and head width, H_w (see Fig. 1.6). For isometric scaling, $H_w \propto m^{0.33}$, a large leaf-cutter ant with a body mass of 100 times m would have a head 4.6 times wider, $100^{0.33} \approx 4.6$. For positive allometry, $H_w \propto m^{0.40}$, the head width would be 6.3 times larger. The increase in head width due to shape differences alone is thus about 40 %, $100^{0.40-0.33} \approx 1.4$. Naturally, a strong allometry across many

orders of magnitude in body size can be biologically implausible, if not physically impossible (Gould, 1966). A hypothetical allometric worker of 10 g, far exceeding the maximum body mass measured for leaf-cutter ants (≈110 mg for *A. cephalotes*, Wetterer, 1994a, and about 50 mg for *A. vollenweideri*), would have a head width similar to its body length (excluding the head, see Fig. 1.6).

In the following chapter, I will show how different parameters of the musculoskeletal bite apparatus vary across more than two orders of magnitude in body mass, and discuss the relative contributions of size and shape adaptations to the variation of bite force capacity in polymorphous leaf-cutter ants.

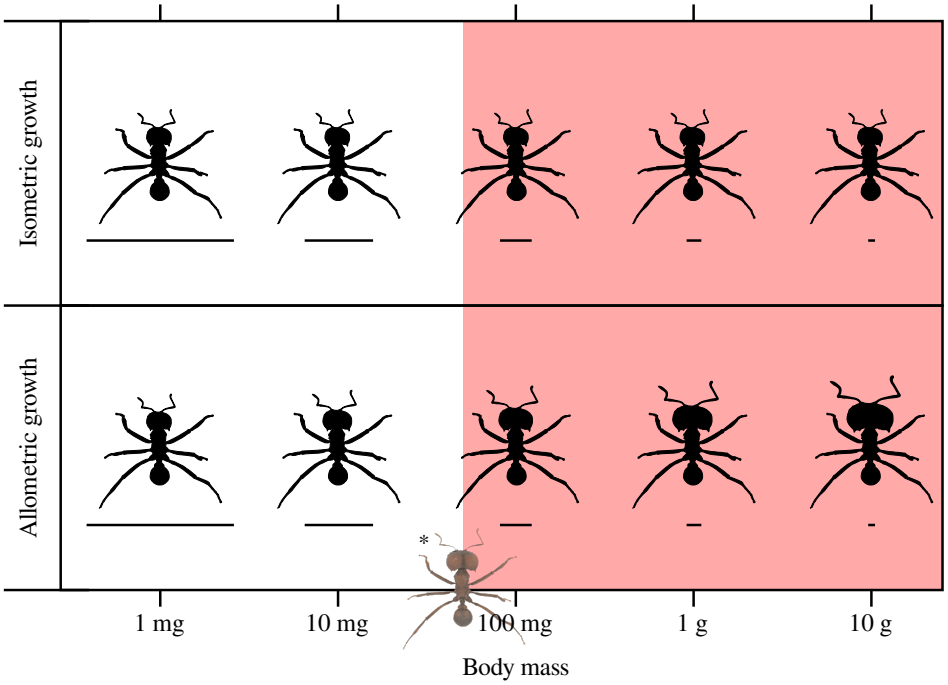


FIGURE 1.6: The difference between isometric and allometric growth of head size in *Atta vollenweideri* leaf-cutter ants (see Chapter 2). The original ant was a 50.1 mg worker with a body length of 9.58 mm, digitised by Fabian Plum (labelled with *, see Plum and Labonte, 2021). To illustrate isometric growth, the relative head dimensions were scaled to a 1 mg worker using the allometric scaling coefficients from Chapter 2, and kept constant across sizes. For allometric growth, relative head width and height were adjusted in accordance to the observed allometry. Workers on the right side (red area) exceed the naturally occurring size-range, illustrating the effects and limitations of allometric scaling across large scales. With increasing body mass, the head proportions of allometric workers seem increasingly 'absurd'; at its most extreme, the head width of a hypothetical allometric worker of 10 g is similar to the length of its thorax and abdomen combined. All scale bars represent 5 mm and are based on the assumption that body length scales isometrically with body mass; for simplicity, any body length changes due to head size allometry were neglected.

2 Morphological determinants of bite force capacity

I acknowledge the contributions of Thomas van de Kamp and Marcus Zuber, who conducted the μCT scans, Xinyue Liu, who segmented a subset of the resulting scans, Anaya Pouget, who manually traced muscle fibres for method validation, and Flavio Roces, who kindly provided the ant colony.

Summary

The extraordinary success of social insects is partially based on 'division of labour', i. e. individuals exclusively or preferentially perform specific tasks. Task-preference may correlate with morphological adaptations so implying task-specialisation, but the extent of such specialisation can be difficult to determine. Here, I demonstrate how the physical foundation of some tasks can be leveraged to quantitatively link morphology and performance. I study the allometry of bite force capacity in *Atta vollenweideri* leaf-cutter ants, polymorphic insects in which the mechanical processing of plant material is a key aspect of the behavioural portfolio. Through a morphometric analysis of tomographic scans, I show that the bite force capacity of the heaviest colony workers is twice as large as predicted by isometry. This disproportionate 'boost' is predominantly achieved through increased investment in muscle volume; geometrical parameters such as mechanical advantage, fibre length or pennation angle are likely constrained by the need to maintain a constant mandibular opening range. I analyse this preference for an increase in size-specific muscle volume and the adaptations in internal and external head anatomy required to accommodate it with simple geometric and physical models, so providing a quantitative understanding of the functional anatomy of the musculoskeletal bite apparatus in insects.

2.1 Introduction

Colonies of social insects are stereotypically characterised by a 'division of labour', i. e. individuals favour some tasks over others (Oster and E. O. Wilson, 1978; Beshers and Fewell, 2001). Such task-preferences may be the 'plastic' result of complex interactions between genetic predisposition, neural and hormonal factors, and varying levels of experience (Beshers and Fewell, 2001; D. M. Gordon, 2016), but they may also correlate with more 'rigid' morphological differences in the colony workforce (Hölldobler and E. O. Wilson, 1990; Schmid-Hempel, 1992). A natural aim, then, is to connect morphological variation with the task-specialisation it enables.

A textbook example of polymorphic social insects are leaf-cutter ants, in which workers fall on a more or less continuos size-spectrum covering more than two orders of magnitude in body mass (see Fig. 2.1). Workers may not only differ in size, but also in shape, i. e. specific body parts may not scale according to geometric similarity hypotheses (E. O. Wilson, 1953, 1980a; Feener et al., 1988; Wetterer, 1991a; Wetterer, 1999; Helanterä and Ratnieks, 2008; Groh et al., 2014; Arganda et al., 2020). Both size- and shape-variation may indicate task-specialisation and so help to increase colony fitness through ergonomic task allocation (Weber, 1972; E. O. Wilson, 1980a,b, 1983a,b; Wetterer, 1999; Wirth et al., 2003; R. M. Schofield et al., 2011; Hölldobler and E. O. Wilson, 2010), but this link is speculative where it is not rationalised through a quantitative functional analysis. For some tasks, e. g. brood care or gardening, such an analysis may be difficult to conduct, but there exists a subset of tasks where it can be made both explicit and quantitative: Where tasks have a physical foundation, it is possible to derive exact relationships between morphology and performance from first principles.

A key mechanical task arising in leaf-cutter ants is to cut leaf- or fruit-fragments to supply and maintain a fungus used as crop (see Fig. 2.1; Evison and Ratnieks, 2007; Hölldobler and E. O. Wilson, 2010; Garrett et al., 2016). Leaf-cutting occurs on an almost industrial scale, and at significant metabolic cost: Leaf-cutter ants are responsible for up to 15 % of the defoliation in the Neotropics (Wirth et al., 2003; Herz et al., 2007; Costa et al., 2008), and the aerobic scope of leaf-cutting is comparable to that of insect flight (Roces and Lighton, 1995). It thus appears both plausible and necessary that leaf-cutter ants show morphological adaptations which render them particularly apt at cutting plants.

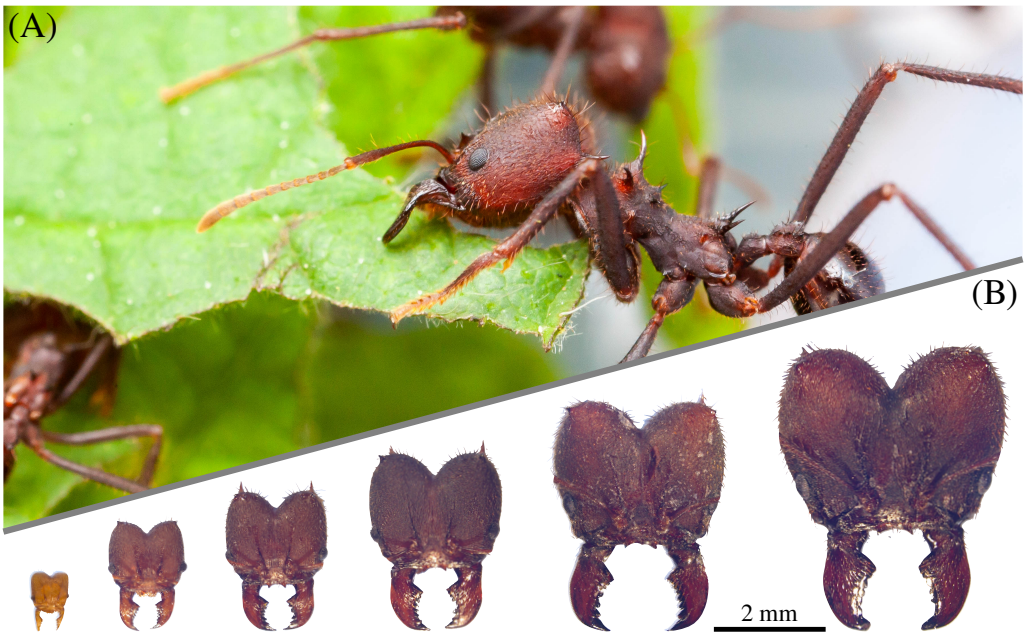


Figure 2.1: (**A**) *Atta vollenweideri* leaf-cutter ants cut and carry fresh plant fragments using their mandibular bite apparatus to supply a fungus used as crop (photo: Samuel T. Fabian). (**B**) This task is performed by workers which may vary by approximately two orders of magnitude in body mass, as illustrated here with photographs of head capsules representing this size-spectrum (dorsal view).

In all insects with chewing mouthparts, bite forces are generated by large muscles located in the head

capsule, and transmitted to the cutting edge of the mandible via an apodeme and a mandibular joint (Chapman, 1995; E. A. Bernays, 1998; F. Clissold, 2007). Because this musculoskeletal bite system is both of behavioural, ecological and evolutionary relevance *and* can be analysed with first principles, it has received increasing attention from biomechanists (Goyens et al., 2014b,a; Weihmann et al., 2015a,b; Kundanati et al., 2020), evolutionary biologists (Spagna et al., 2008; D. Li et al., 2011; David et al., 2016b,a; Blanke et al., 2017; Booher et al., 2021), functional morphologists (Heethoff and Norton, 2009; Schmitt et al., 2014; Weihmann et al., 2015b; Wipfler et al., 2016; Khalife et al., 2018; Larabee et al., 2018; Lillico-Ouachour et al., 2018; A. Richter et al., 2019, 2020, 2021) and (behavioural) ecologists alike (Wheater and Evans, 1989; Gronenberg et al., 1997; Paul and Gronenberg, 1999; Paul, 2001; F. Clissold, 2007; Hall et al., 2010; Muscedere et al., 2011; Paul and Roces, 2019; Klunk et al., 2020). Concretely, for an isometric contraction at zero fibre stretch, the force exerted at any point of the mandible, F_b, may be written as the product between the ratio of muscle volume V_m and the average fibre length L_f (the physiological cross-sectional area of the muscle, $A_{phys} = V_m/L_f$), the muscle stress σ_m, the cosine of the pennation angle ϕ, and the mechanical advantage MA (Wheater and Evans, 1989; Paul and Gronenberg, 1999; F. Clissold, 2007; Heethoff and Norton, 2009):

$$F_b = \underbrace{\sigma_m}_{\text{Physiology}} \cdot \overbrace{\underbrace{V_m}_{\text{Investment}} \cdot \underbrace{L_f^{-1} \cdot \cos\phi \cdot MA}_{\text{Geometry}}}^{A_{eff}} \tag{2.1}$$

Parametrising the bite force in this way has two distinct advantages. First, it illustrates that F_b may be modulated by changing one of three distinct determinants: muscle *physiology* (represented by muscle stress), total muscle *investment* (represented by muscle volume), and the *geometry* of the musculoskeletal apparatus, defined by the arrangement of muscle fibres and the lever system. The product between the latter two terms may be interpreted as the effective cross-sectional area A_{eff} of a muscle which acts directly at the point of force application; A_{eff} is thus a suitable proxy for bite force capacity.

Second, because A_{eff} is defined entirely by morphological quantities, it is possible to quantitatively link both size- and shape-variation across workers to a specialisation in terms of bite force capacity. Concretely, the parsimonious assumption of geometric similarity implies $V_m \propto m$, $L_f \propto m^{1/3}$ and $\cos\phi \propto MA \propto m^0$, so that $A_{eff} \propto m^{2/3}$ (where m is body mass). Any deviation from this prediction indicates shape-variation that correlates with a modulation of bite force capacity. Here, I use this predictive model as a quantitative guideline for a morphometric analysis of the bite force apparatus of *Atta vollenweideri* leaf-cutter ants across the entire size range. I (i) investigate if bite force capacity is modulated solely by size or also by shape differences; (ii) analyse if and why such specialisation may occur predominantly via changes in muscle investment vs geometry; and (iii) discuss how any specialisation requires a variation of the external and internal head morphology, due to geometric and mechanical constraints.

2.2 Materials & methods

2.2.1 Study animals

Individual ants were sampled from a colony of *Atta vollenweideri*, founded and collected in Uruguay in 2014. The colony was kept in a climate chamber at 25 $^{\circ}C$, 60 % relative humidity, in a 12/12 h light and dark cycle (FitoClima 12.000 PH, Aralab, Rio de Mouro, Portugal), and was fed with bramble and honey water *ad libitum*. About 30 ants, across the size spectrum, were collected from the foraging area and weighed (Explorer Analytical EX124, max. 120 g x 0.1 mg, OHAUS Corp., Parsippany, NJ, USA). From these 30 ants, I then selected 16 individuals including the heaviest (43.3 mg) and lightest (0.3 mg) specimen to achieve an approximately even spacing between log-transformed masses. The sample size was limited by the time-intense segmentation process. However, the consistently high R^2 values of my scaling regressions, and the narrow confidence intervals of the associated slopes suggest that my conclusions are robust (see section 2.3).

Ants were sacrificed by freezing and decapitated using a razor blade. In order to facilitate fixative penetration, the antennae and labrum were removed with fine forceps (Dumont #5, Montignez, Switzerland), and about five holes were pierced into the head capsule using '00' insect pins for specimens $>$1 mg. All heads were fixed in a paraformaldehyde solution (4 % in PBS, Thermo Fisher Scientific, Waltham, MA, US) for 18 h and subsequently stored in 100 % ethanol.

2.2.2 Micro computed-tomography and tissue segmentation

Computed-tomography (CT) scans were performed at the Imaging Cluster at the KIT light source (see Appendix A for details). Prior to segmentation, the tomographic image stacks were preprocessed using 'Fiji' (Schindelin et al., 2012). Each stack was aligned such that the lateral, dorso-ventral and antero-posterior axes coincided with the principal axes of Fiji's coordinate system (see Fig. 2.2). The lateral and dorso-ventral axes were defined based on the bilateral symmetry of the heads. The antero-posterior axis was defined as the line connecting the distal end of the dorsal mandible with the centre of the posterior head opening in lateral view. The oriented image stacks were imported in 'ITK-SNAP' (v 3.6, Yushkevich et al., 2006) for threshold-based segmentation. Head capsule, mandibles, as well as mandible opener and closer apodemes and muscles were separated with the semi-automatic 'active contour' mode; directly- and filament-attached muscles were segmented as individual tissues. The grayscale thresholds, set individually for each tissue, were kept constant within a sample, but were manually adjusted between samples to account for variation in contrast and brightness. For each individual, a second segmentation was performed to quantify characteristic linear dimensions of the head capsule and its volume. Artificial segmentation boundaries were added where the head capsule was open: At the anterior side, the segmentation was 'cut-off' at the mandible joints; the posterior head opening was closed at the lateral edge of the postocciput (see A. Richter et al., 2020).

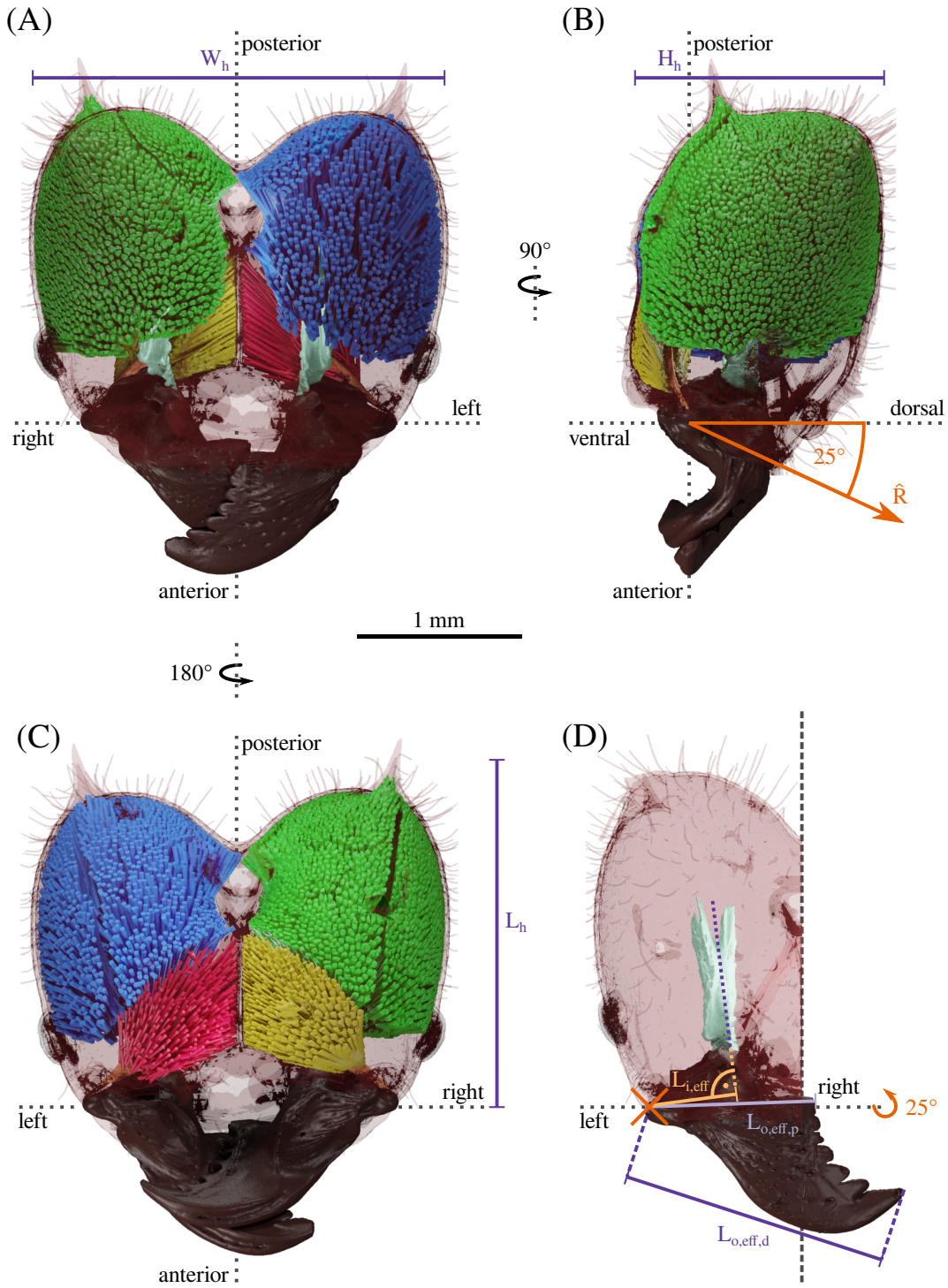


FIGURE 2.2: (**A**) Dorsal, (**B**) lateral and (**C**) ventral view of the internal head anatomy of a medium-sized *Atta vollenweideri* worker (10.9 mg). Tissues as segmented from micro-computed tomography scans are shown in green (closer muscle), yellow (opener muscle), turquoise (closer apodeme) and light brown (opener apodeme). Muscle fibres as reconstructed with a custom fibre-tracking algorithm are coloured in blue (closer muscle) and red (opener muscle); dashed lines indicate the lateral (left-right), antero-posterior and dorso-ventral axes. Head width W_h, height H_h, and length L_h are indicated. (**D**) The effective inlever $|\mathbf{L}_{i,eff}|$, proximal and distal outlevers, $|\mathbf{L}_{o,eff,p}|$ and $|\mathbf{L}_{o,eff,d}|$, respectively, are defined as the perpendicular distances to the rotational axis of the mandible joint $\hat{\mathbf{R}}$.

2.2.3 Morphometric analysis

I extracted a series of parameters from the CT scans in order to characterise changes in the key morphological determinants of bite force, and associated changes in head and apodeme morphology.

Head dimensions: Head width and height were extracted from the 'head volume' segmentation, using Fiji's native 2D particle analysis on all slices perpendicular to the antero-posterior axis. Based on the bilateral symmetry of the heads, head width and height were defined as the width or height of the bounding box with maximum lateral or dorso-ventral expansion, respectively. Head length, in turn, was defined as the antero-posterior distance between the first and last image slice containing segmented head volume.

Volume occupancy: Segmentation volumes were directly exported from 'ITK-SNAP'. I measured the 'functional volume' occupied by muscle as the volume of a convex hull surrounding the segmented muscle tissue, extracted with the '3D convex hull' plugin in Fiji (Sheets et al., 2011). The functional volume encapsulates all muscle fibres and the space between them including filaments and apodeme. Volume occupancy was defined as the ratio between functional volume and head volume.

Apodeme dimensions and orientation: In order to functionally analyse the apodeme, I first needed to identify its main axis. This task may seem trivial because apodemes in leaf-cutter ants are approximately linear structures (see Fig. 2.2). However, to enable an unbiased and quantitative analysis across all scans, I standardised the procedure as follows: First, I extracted the centres-of-area of the apodeme cross-sections perpendicular to the antero-posterior axis. Second, I performed a principal component analysis on the xyz coordinates of these centres-of-area, akin to a three-dimensional regression analysis. The first principal component then represents the axis around which the apodeme is most 'centred' — the apodeme main axis. Next, the apodeme image stack was rotated such that it was perpendicular to the main axis using 'TransformJ' (Meijering et al., 2001). Apodeme length was defined as the distance between first and last image slice containing segmented apodeme; cross-sectional areas and perimeters were extracted via 2D particle analysis for each slice. Apodeme centre-of-mass and surface area were extracted with Fiji's native 3D particle analysis routines.

Muscle fibre dimensions and orientation: Length and orientation of segmented muscle fibres were extracted with a custom tracking algorithm written in Python 3.7.6 (Van Rossum and Drake, 2009). A detailed description of the algorithm is provided in Appendix A. In short, the origins of individual muscle fibres were identified by dilating the head capsule, and extracting the intersections with the muscle tissue. These intersections were used as 'seed points' to grow fibres in an iterative process, designed to maximise fibre length and homogeneity. I extracted muscle fibre length and pennation angle for a total of 62,380 fibres across all samples.

Fibre pennation angle was defined as the angle between the fibre and the main axis of the apodeme (Paul and Gronenberg, 1999). Implicit in this definition is the assumption that muscle contraction moves the apodeme along its main axis. This assumption is supported by the fact that the main axis approximately coincides with the resulting net muscle force vector, which has been used as an

alternative reference axis for the calculation of pennation angles in previous studies (Goyens et al., 2014b; Weihmann et al., 2015b). Pennation angles, averaged for each muscle tissue, were about two degrees smaller using this definition, but this difference was independent of worker size [Analysis of covariance (ANCOVA): $F_{1,56}$ = 0.10, p = 0.75], within the accuracy of the angle estimation (see section 2.2.4), and thus does not affect conclusions on the scaling of the average pennation angle.

The muscle physiological cross-sectional area A_{phys} was defined as the ratio between segmentation volume and average muscle fibre length. Note that all morphological muscle parameters are from scans with closed mandibles and maximum muscle contraction. Thus, closer muscle fibre are shorter, have higher pennation angles, and larger physiological cross-sectional areas than in the uncontracted state (see Paul and Gronenberg, 1999).

Mandible dimensions: Mandible inlever was defined as the distance between (i) the insertion of the apodeme ligament to the mandible and (ii) the mandible joint (see Fig. 2.2D). The apodeme ligament is the segment between the anterior cranio-mandibular muscle apodeme (henceforth referred to as closer apodeme) and the mandible base (see Gronenberg et al., 1998b; T. S. Silva and Feitosa, 2019); the location of the mandible joint was defined as the centre of the ridge between the ventral mandibular articulation and the atalar acetabulum (see A. Richter et al., 2020). In contrast to the inlever, the outlever is not solely defined by anatomy, but can be adjusted to serve behavioural needs. For example, leaf-cutter ants may use only the distal end of their mandibles to anchor or cut through the leaf lamina, or engage the entire blade when cutting thicker veins (Tautz et al., 1995; R. M. Schofield et al., 2011). The minimum and maximum functional outlevers were defined as the distance between point (ii) and the tip of the most proximal or distal mandibular tooth, respectively.

I then estimated the effective in- and outlevers, $|\mathbf{L}_{i,eff}|$, and $|\mathbf{L}_{o,eff}|$, respectively, defined as the moment arms perpendicular to the axis of rotation (and the apodeme main axis for the inlever, see Fig. 2.2D). This calculation required three assumptions on the kinematics of the mandibles: (i) the mandible joint is a revolute joint (Gronenberg et al., 1998a; Paul, 2001; Paul and Gronenberg, 2002; Patek et al., 2006; Larabee et al., 2018; A. Richter et al., 2019, 2020), (ii), the joint rotational axis has a constant relative orientation with respect to a head-fixed coordinate system (see W. Zhang et al., 2020a), and (iii), the apodeme force vector lies in the plane of rotation (I account for this misalignment in Chapter 3 and 4, but the resulting difference is minimal). The second assumption was supported by preliminary kinematics analysis suggesting that the rotational axis is approximately parallel to the sagittal plane, and forms an angle of about 25° to the dorso-ventral axis (see Fig. 2.2 and Chapter 3 and 4). In comparable studies on cockroaches, dragonflies and stag beetles, the axis of rotation was deduced from morphology alone (Goyens et al., 2014b; Weihmann et al., 2015a,b; David et al., 2016b,a). Ants, however, posses more complex joints, rendering morphological inference difficult (but see A. Richter et al., 2019, 2020, 2021). I observed no obvious changes in joint morphology across sizes, so that any errors introduced by this estimation are unlikely to result in a systematic effect on my scaling analysis. The mechanical advantage MA was defined as the ratio between effective in- and outlevers.

2.2.4 Error analysis

The accuracy of the fibre identification and tracking procedure is defined by four distinct sources of error: (i) identification error, (ii) intrinsic error, (iii) segmentation error, and (iv) tracking error. I assessed these errors by comparing the result of the tracking algorithm with manual measurements of length and orientation of a subset of 278 fibres across the ant size-range (see Appendix A for details).

Identification error: In order to track fibres, they first need to be correctly identified. My approach based on head capsule dilation may identify too many fibres – by considering 'noise' as a seed point – or too few, by assigning the origin of multiple fibres to one single seed point. As it was unfeasible to manually count fibres, I quantified this error indirectly, by comparing the average physiological cross-sectional areas per fibre, A_f, calculated in two different ways. First, I rotated the image stacks of manually tracked fibres to be perpendicular to the fibre's long axis (see section 2.2.3 and Appendix A); the cross-sectional area of these fibres was then measured by placing an ellipse around the fibre at three locations along its length. Second, I estimated A_f as the ratio between the total physiological cross-sectional area and the estimated numbers of fibres (this definition conflates identification and length estimation errors). An ANCOVA on $\log_{10}$-transformed data showed neither a significant difference between the two methods, nor an effect of size [method: $F_{1,38}$ = 1.11, p = 0.30, interaction: $F_{1,38}$ = 3.82, p = 0.06]. Thus, identification error is negligible.

Intrinsic error: Even a perfectly tracked fibre is limited in accuracy by an error intrinsic to the tracking method: the fibre with the highest quality connects the *centre* of the fibre origin at the head capsule with the *edge* of the fibre end - the longest line that contains only segmented tissue. As a result, both the fibre orientation and the fibre length have an accuracy which depends on the aspect ratio, ρ, of the fibres, defined as the fibre radius divided by fibre length. The fibre orientation will deviate from its main axis by $E_\alpha = \arctan(\rho)$, whereas the fibre length will be overestimated by a factor $E_{length} = \sqrt{\rho^2 + 1}$. For typical muscle fibres, $\rho \approx 0.04$, so that the angles have an accuracy of approximately 2°, and the length is overestimated by less than one per mille.

Segmentation error: Because both angle and length are estimated from the segmented tissue, the accuracy is defined with respect to it. In order to quantify segmentation error, fibre orientation and length were measured manually from both segmented and unsegmented image stacks. On average, segmented fibres were 4 ± 6 % shorter than those measured directly from the CT-scans (One-sample t-test: $p < 0.05$). This error decreased significantly with size, approached zero for the largest workers [ANCOVA: $F_{1,10}$ = 10.72, $p < 0.01$; Ordinary Least Squares (OLS) slope on semi-log data: -0.04, 95 % CI:(-0.10 | 0.01)], and is small compared to the overall variation in fibre length (about sixfold). Pennation angles did not differ significantly between unsegmented and segmented fibres (One-sample t-test: p = 0.33).

Tracking error: I quantified tracking error by direct comparison of manual and automated measurements. Fibres were matched between manual and automatic measurements by minimising the distance between respective fibre origins. My custom-written algorithm overestimated the fibre

length by 12 ± 21 % independent of size [ANCOVA: $F_{1,10} = 1.23$, $p = 0.29$]. Average pennation angles were overestimated by $5 \pm 3^{\circ}$ independent of size [ANCOVA: $F_{1,10} = 0.46$, $p = 0.51$]. These results compare favourably to the performance of commercial alternatives (Sullivan et al., 2019; Katzke et al., 2022).

2.2.5 Data analysis

All data analysis was performed in jupyter lab v 2.1.2 (Kluyver et al., 2016), using R v 3.6.1 (R Core Team, 2020) and Python v 3.7.6 (Van Rossum and Drake, 2009). Unless stated otherwise, all values are given as mean $\pm$ standard deviation. There was no significant difference between tissues in the left and right head hemispheres [ANCOVA: $p > 0.05$], so I used the average. Analyses involving morphological traits, their derived quantities and body mass were performed on $\log_{10}$-transformed data. I used OLS and Standardised Major Axis (SMA) regressions models implemented in the R package 'SMATR' to describe scaling relationships (Warton et al., 2012). The suitability of these models is subject to debate, as they involve assumptions on 'observational' and 'biological' errors (Warton et al., 2006; R. J. Smith, 2009; Egset et al., 2012). Fortunately, the main conclusions of this paper are supported by either model. The text reports the results for OLS regressions for simplicity; SMA regression results are provided in Appendix A.

Allometric scaling in polymorphic ants has sometimes been described with bi- or curvilinear models, i. e. a single log-log slope may not allow an adequate description of the observed allometry (E. O. Wilson, 1953; Feener et al., 1988; Wetterer, 1991a; D. E. Wheeler, 1991; Seid et al., 2011; Wills et al., 2018; Arganda et al., 2020). Visual inspection of key morphological traits in my data suggested an approximately linear relationship on a log-log-scale, i. e. a constant differential growth factor (Huxley, 1924). However, the smallest workers (head width < 1 mm), appeared to depart from this linear relationship: 'Minims' systematically 'underperformed', i. e. they had significant negative residuals (see e. g. Fig. 2.3D). Indeed, the assumptions of a linear model were only met when minims were excluded (assessed via a global procedure following Peña and Slate, 2006), which also increased the coefficient of determination R^2 considerably for all regressions on opener and closer muscle volumes, inlever and outlevers. On the basis of this statistical observation, as well as the biological argument that minims preferentially engage in brood care and gardening, and only rarely partake in foraging activities which involve cutting (E. O. Wilson, 1980a), I excluded them from all subsequent analyses.

2.3 Results and discussion

Cutting plant fragments is a central part of the behavioural repertoire of leaf-cutter ants. Bite force capacity is thus a biologically relevant performance metric for the suitability of an individual worker to partake in foraging. All morphological determinants of bite force capacity apart from fibre length differ significantly from isometry (see Table 2.1 for detailed statistics). As a cumulative result of these changes, the effective cross-sectional area, A_{eff} scales as $A_{eff} \propto m^{0.88}$ [95 % CI: (0.81 | 0.95)], in significant excess of the isometric prediction, $A_{eff} \propto m^{0.67}$. This difference in scaling coefficients

may appear small, but it results in a substantial enhancement of the absolute bite force capacity: the largest workers have an effective cross-sectional area twice as large as predicted from changes in body mass, $(45/1)^{0.88-0.67} \approx 2$; achieving this increase in bite force capacity through changes in size alone would require workers of a maximum size approximately $2^{3/2} \approx 3$ times larger than the largest workers in the colony. Two key questions emerge from this result. First, which of the 'morphological dials' are turned to achieve the departure from isometry? Second, what additional adaptations of internal and external head morphology are required to implement those changes?

TABLE 2.1: Results of Ordinary Least Squares regressions describing the relationship of $\log_{10}$-transformed determinants of bite force capacity, A_{eff}, internal and external head dimensions with $\log_{10}$(body mass in mg). 95 % confidence intervals are provided in parentheses.

Quantity	Unit	Elevation	Slope	R^2
A_{eff}	mm^2	-1.49 (-1.56, -1.42)	0.88 (0.81, 0.95)	0.99
V_m	mm^3	-1.43 (-1.52, -1.33)	1.15 (1.06, 1.25)	0.98
L_f	μm	2.4 (2.36, 2.44)	0.3 (0.26, 0.34)	0.96
A_{phys}	mm^2	-0.83 (-0.9, -0.76)	0.86 (0.79, 0.92)	0.99
cosϕ	(-)	-0.1 (-0.11, -0.08)	-0.02 (-0.04, -0.01)	0.49
MA	(-)	-0.57 (-0.6, -0.54)	0.05 (0.02, 0.08)	0.54
$\lvert\mathbf{L}_{i,eff}\rvert$	mm	-0.75 (-0.79, -0.72)	0.38 (0.35, 0.42)	0.98
$\lvert\mathbf{L}_{o,eff,p}\rvert$	mm	-0.43 (-0.46, -0.4)	0.35 (0.32, 0.38)	0.99
$\lvert\mathbf{L}_{o,eff,d}\rvert$	mm	-0.19 (-0.21, -0.16)	0.34 (0.31, 0.36)	0.99
V_h	mm^3	-0.56 (-0.63, -0.49)	1.15 (1.08, 1.21)	0.99
W_h	mm	-0.02 (-0.04, 0)	0.4 (0.38, 0.42)	0.99
H_h	mm	-0.23 (-0.25, -0.21)	0.38 (0.36, 0.4)	0.99
L_h	mm	-0.08 (-0.11, -0.04)	0.36 (0.33, 0.39)	0.98
A_{apo}	mm^2	-2.71 (-2.77, -2.65)	0.89 (0.83, 0.95)	0.99

2.3.1 Functional constraints on mechanical advantage and pennation angle favour positive allometry of A_{phys}

The maximum bite force capacity is determined by the investment in muscle volume V_m, and by the average fibre length L_f, pennation angle ϕ and the mechanical advantage MA of the force transmission system (see Eq. 2.1). About 70 % of the observed disproportionate increase in A_{eff} is achieved by a disproportionate increase in muscle volume V_m. MA and L_f, in turn, make a contribution of about 40 %; the systematic decrease of ϕ seemingly reduces size-specific bite force capacity by about 10 % (see Table 2.1 and Fig. 2.3A). Thus, bite force capacity is substantially enhanced through an increased investment in muscle volume as opposed to adjustments in the geometry of the musculoskeletal apparatus. What are the advantages and disadvantages of altering the relative force capacity through a

systematic increase in volume investment over changes in geometry, and what constraints may limit one strategy or favour another?

Mechanical advantage: Across worker sizes, MA shows limited but significant positive allometry; MA increases by about 20%, irrespective of whether it is defined with respect to the distal or proximal sections of the gnathal edge (*sensu* (S. Richter et al., 2002); see Table 2.1 and Fig. 2.3B). A systematic change in MA may be achieved by an increase of the effective inlever ($|\mathbf{L}_{i,eff}|$), a decrease in the effective outlever ($|\mathbf{L}_{o,eff}|$), or a combination of both. In *A. vollenweideri*, the positive allometry in MA is solely driven by the first option (see Fig. 2.3C). Although halving $|\mathbf{L}_{o,eff}|$ would result in the same numerical change of MA as doubling $|\mathbf{L}_{i,eff}|$, these two changes are not functionally equivalent: An increase in $|\mathbf{L}_{i,eff}|$ increases the force available at *any* point along the mandibular cutting edge. In contrast, a shortening of $|\mathbf{L}_{o,eff}|$ merely reduces the functional length of the mandible without providing a clear functional advantage – smaller outlevers can also be achieved by simply biting with a more proximal part of the mandible. Because this behavioural flexibility is not afforded to $|\mathbf{L}_{i,eff}|$ – which is anatomically fixed – it is functionally sensible to drive systematic changes in MA through changes in inlever length.

Notably, both the absolute value of the MA and its variation, $0.27 < MA < 0.32$ for the distal outlever, are at the lower end of values reported across numerous insect taxa (typically $0.3 < MA < 0.8$, see Blanke, 2019). Thus, the ants appear to utilise only a small fraction of the theoretically available scaling capacity – a change from 0.3 to 0.8 across worker sizes would result in $MA \propto m^{0.26}$, a factor of five in excess of the observed scaling. I argue that the scaling capacity of MA is constrained for at least two reasons. First, systematic increases in $|\mathbf{L}_{i,eff}|$ are difficult to implement, because inlevers are internal to the head-capsule. Second, the magnitude of the bite force is not the sole functional determinant of bite performance. Instead, ant workers may have to maintain an approximately similar opening range across sizes, which results in a functional coupling of in- and outlever. To retain an equivalent mandibular opening range, a strong positive allometry of MA would require relatively longer muscle fibres, or an increase in characteristic muscle strain. Implementing either option likely requires substantial changes to head anatomy or muscle physiology, and may therefore only be possible across more distantly related species, where developmental and phylogenetic constraints are relaxed. Indeed, the MA of the mandibular system contains significant phylogenetic signal (Blanke, 2019), and extreme variations in outlever such as between male and female stag beetles are matched by corresponding changes in inlever (Goyens et al., 2014b), both consistent with this interpretation.

Pennation angle: Across worker sizes, the cosine of the average pennation angle ϕ decreases significantly by about 8%, i. e. ϕ increases from about 37° to 43° (see Table 2.1 and Fig. 2.3B). Thus, the systematic change in ϕ seemingly *decreases* the bite force capacity of larger workers. However, this conclusion is premature. Pennate muscle fibres require an attachment area which exceeds their cross-sectional area by a factor $csc(\phi)$ (Pfuhl, 1937; Benninghoff and Rollhäuser, 1952; Alexander, 1969; Wheater and Evans, 1989; Paul and Gronenberg, 1999; Paul, 2001). This dependency of the

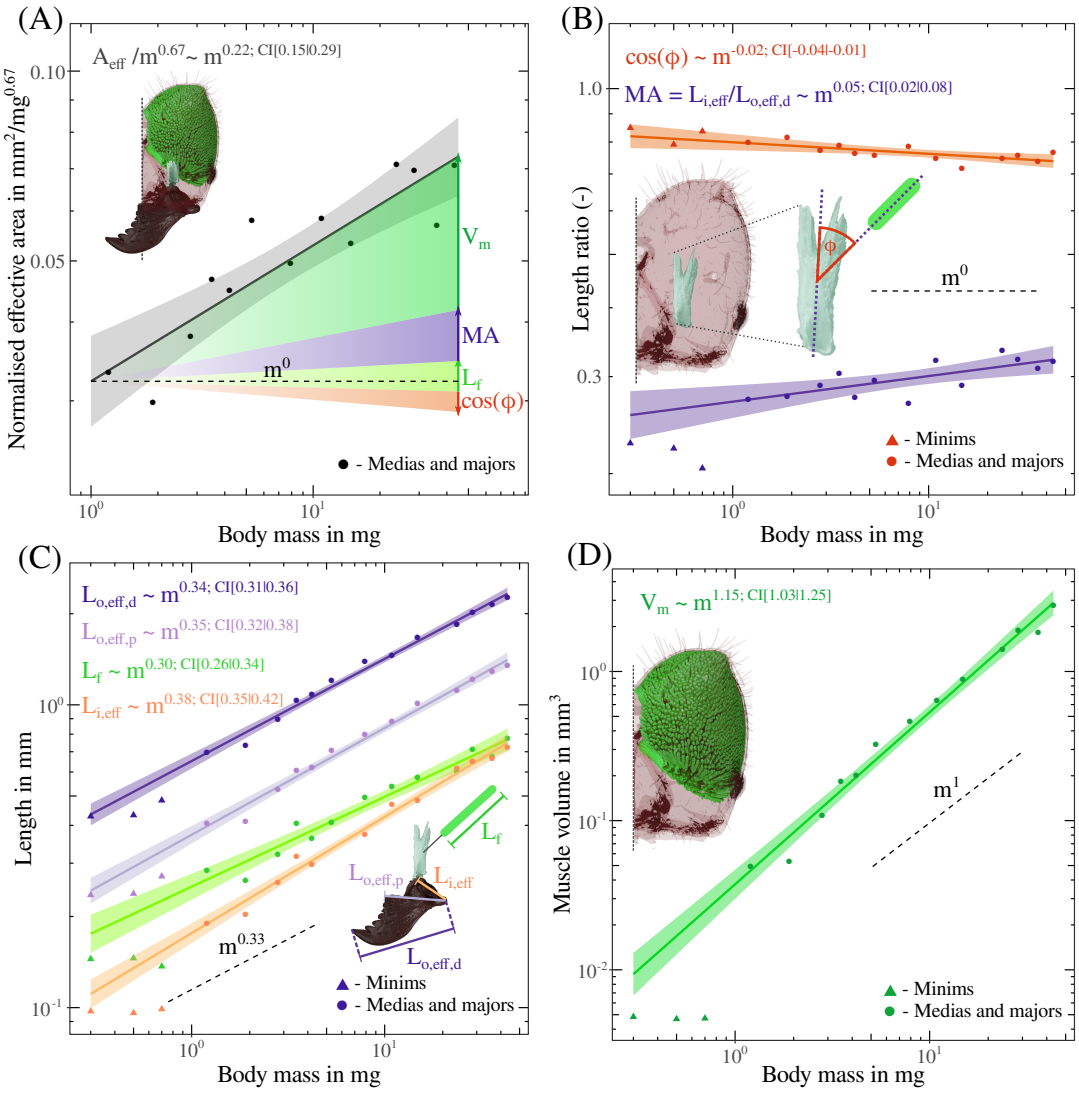


FIGURE 2.3: Scaling of bite force capacity and its morphological determinants in *A. vollenweideri* leaf-cutter ants. Solid lines show the results of Ordinary Least Squares regressions on $\log_{10}$-transformed data excluding the minims (triangles), shadings show the 95% confidence intervals, and dashed lines show predictions from isometry. (**A**) Bite force capacity is determined by investment in muscle volume V_m and the geometry of the musculoskeletal apparatus, and shows strong positive allometry. The shaded areas indicate the extent to which the size-specific increase in bite force capacity is determined by the different morphological determinants. (**B**) The mechanical advantage, MA and cosine of the average pennation angle, cosϕ, both change systematically but moderately with size. (**C**) The change in mechanical advantage is solely achieved by a positive allometry of the inlever $|\mathbf{L}_{i,eff}|$; both the distal and proximal effective outlevers, $|\mathbf{L}_{o,eff,p}|$ and $|\mathbf{L}_{o,eff,d}|$, respectively, are isometric. Fibre length, L_f, shows a weak but non-significant trend to negative allometry. (**D**) Muscle volume grows with strong positive allometry, and because fibre length is isometric, this increase largely reflects an increase in the physiological cross-sectional area of the muscle.

physiological cross-sectional area on ϕ introduces a sin-term into Eq. 2.1, so that the maximum bite force capacity occurs not for $\phi = 0°$, as may be concluded from Eq. 2.1. Instead, the maximum occurs for $\frac{d}{d\phi}[\sin\phi\cos\phi] = 0$, i. e. for $\phi = 45°$, remarkably close to the values measured for the largest workers (also see Paul and Gronenberg, 1999). Concretely, although the fraction of the force acting along the apodeme decreases as $m^{-0.02}$, the potential for an increase in A_{phys} scales as $m^{0.03}$ so that the net result of the increase in ϕ may well be an increase in bite force capacity; I discuss how the disproportionate increase in A_{phys} is implemented below. Because small workers already have average pennation angles close to the theoretical optimum for force capacity, the net change in bite force capacity arising from changes in ϕ is negligible. Indeed, the similarity of ϕ across sizes likely reflects a functional limitation in analogy to the constraint imposed on $|\mathbf{L}_{i,eff}|$: changes in ϕ at constant size-specific muscle length would either alter the functional opening range of the mandible, or require a systematic variation in characteristic muscle strain (see Benninghoff and Rollhäuser, 1952; Brainerd and Azizi, 2005).

Muscle length and volume: The segmented volume of the closer muscles fibres scales with positive allometry, $V_m \propto m^{1.15}$. In contrast, the length of the muscle fibres scales close to isometry, $L_f \propto m^{0.30}$ (see Table 2.1 for detailed statistics). Thus, the positive allometry of V_m exclusively reflects a strong positive allometry of $A_{phys} \propto m^{0.86}$, and hence bite force capacity. Leaf-cutter ants thus deploy a 'hybrid strategy' of combining positive allometry of muscle volume with isometry of fibre length, simultaneously satisfying two biological demands: the differential growth of L_f and $\sqrt{A_{phys}}$ systematically increases bite force capacity, and the isometric growth of L_f ensures that mandibular opening range remains approximately size-invariant.

2.3.2 Positive allometry of bite force capacity requires substantial changes to external and internal head anatomy

I have demonstrated that larger *A. vollenweideri* leaf-cutter ants boost their bite force capacity via an increase investment in muscle volume, while the geometric arrangement defined by muscle length, pennation angle and the mechanical advantage only shows minor size-specific changes. This positive allometric growth results in a substantial increase of bite force capacity (see Fig. 2.3A), but poses a significant challenge for external and internal head anatomy: Internal adaptations are required to provide the attachment area for a relatively larger A_{phys}; external adaptations are necessary to combine the positive allometry of A_{phys} with isometry of L_f, and to provide sufficient space for other functional tissues.

Internal anatomy: The disproportionate increase in A_{phys} needs to be matched by an equivalent increase of the internal attachment area. In order to model this increase, I approximate the shape of each half of the head capsule as a cylinder with radius R and height $h = f_h R$ (with $f_h \geq 0$). This cylinder is terminated with a spherical cap, also with radius R, at its posterior end. The internal attachment area, in turn, is defined by a cylindrical part with equal height h, but radius $r = f_r R$ for the cylindrical section and the spherical cap (with $0 \leq f_r \leq 1$. The internal area is not equal to

the apodeme surface area, because most muscle fibres attach via filaments, see Fig. 2.4). I estimate h as the apodeme length, R as a quarter of the head width, and $r = R - L_f \sin\phi$. This simple model predicts the functional volume occupied by muscle to 3 % accuracy ($V_{func} \approx V_{ext}$), and A_{phys} to 19 % accuracy ($A_{phys} \approx \sin\phi A_{int}$). Having demonstrated that my geometric approximation captures the salient features of the internal and external head geometry pertaining to the arrangement of the closer muscle, I turn my attention to two functional predictions it enables.

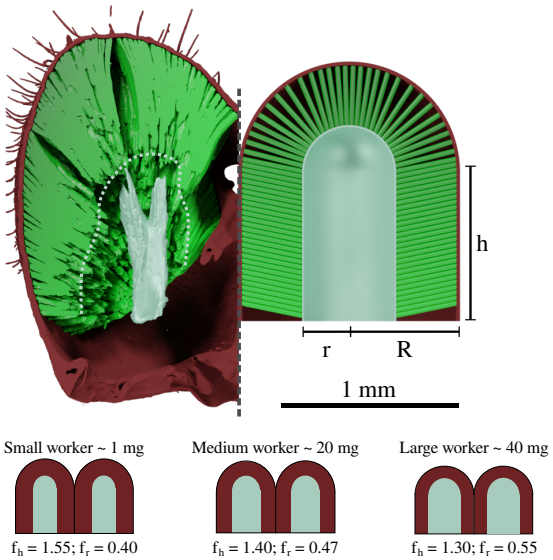


FIGURE 2.4: The volume of half a head capsule may be modelled as a cylinder of length h and radius R, terminated by a spherical cap. The internal fibre attachment area surrounds an internal volume of identical geometry, but with radius $r \leq R$; this volume contains both the apodeme, and muscle-filaments (see main text).

First, I note that, although A_{phys} can be increased by increasing either h or r, deviating from the isometric prediction of $A_{phys} \propto V_m^{0.67}$ requires a systematic variation in $r/R = f_r$, which controls the surface to volume ratio of the muscle (see Appendix A):

$$\frac{A_{phys}}{V_m} = \frac{\sin\phi}{R\,(1 - f_r)} \tag{2.2}$$

Indeed, in *A. vollenweideri*, r grows more quickly than R, so that f_r increases systematically with size [$r \propto m^{0.49}$. 95 % CI: (0.45 | 0.52); $f_r \propto m^{0.09}$. 95 % CI: (0.05 | 0.12), see Fig. 2.5A]. As a consequence of this shift in internal anatomy, the positive allometry of muscle volume is disproportionally invested into A_{phys} instead of L_f. Additional support for the hypothesis that a disproportionate increase in A_{phys} is the dominant objective is provided by the observation that h grows more slowly with mass than r [$h \propto m^{0.37}$. 95 % CI: (0.34 | 0.39)].

Second, I seek to demonstrate that heads of *A. vollenweideri* workers occupy a morphological space where a shift of volume from fibre length to area can be achieved without a significant variation of the total muscle volume. The origin of the complex relationship between length, area and volume is rooted in the space-constraint imposed by an exoskeleton: The area occupied by a cross-section

through a muscle fibre is independent of its length, but the internal area available to attach it decreases as the fibre gets longer (Paul and Gronenberg, 1999; Paul, 2001). For a given head volume, there thus exists a trade-off between maximising fibre length or fibre cross-sectional area: At one extreme are fibres of maximum length which have no internal area to attach to; at the other extreme are fibres with a maximum A_{phys} equal to the internal surface area of the head capsule, but of miniscule length. The *volume* of the muscle, then, is maximised at some compromise between investment in fibre length vs area. In order to calculate the geometric arrangement which optimises muscle volume, I consider the fraction of the available head volume occupied by the closer muscle, η, which is a function of f_r and f_h (see Appendix A):

$$\frac{V_m}{V_{ext}} = \eta = \frac{f_r^2\,(1-f_r) + f_h f_r\,(1-f_r)}{1/3 + f_h/2} \tag{2.3}$$

The maximum for η falls between two extremes set by a high-aspect ratio cylinder ($f_h >> f_r$, $\eta_{max} = 0.5$, $f_r(\eta_{max}) = 0.5$) and a hemisphere ($f_h = 0$, $\eta_{max} = 0.44$, $f_r(\eta_{max}) = 0.67$; see Appendix A). Thus, the maximum volume that can be utilised is roughly half of the head capsule, which requires $f_r \approx 0.5$. For *Atta*-workers, my data suggest $0.36 < f_r < 0.55$ and $1.30 < f_h < 1.53$, covering a functionally meaningful range (see Fig. 2.5): For $f_r << 0.5$, muscle length is favoured over area at the steep expense of muscle volume. For $f_r >> 0.5$, in turn, volume is sacrificed to maximise area. For $f_r \approx 0.5$ as observed in *A. vollenweideri*, the partitioning of volume into fibre length and cross-sectional area can be altered without a large variation in total muscle volume (see Fig. 2.5B): The geometric changes in internal head morphology increase the size-specific A_{phys} by more than 50 %, but only alter η by about 12 %.

The internal attachment area surrounds an internal volume. In principle, this internal volume could be filled entirely with apodeme, but in insects, individual muscle fibres may alternatively attach via a single, thin, filament-like process of the apodeme (Gronenberg et al., 1997). The fraction of filament- vs directly attached muscle fibres differs across species, and likely reflects functional specialisation (Gronenberg et al., 1997; Paul and Gronenberg, 1999; Paul, 2001). In *A. vollenweideri*, 98 ± 2 % of muscle fibres are filament-attached, independent of worker size [ANOVA: $F_{1,11}$ = 1.98, p = 0.18]. What is the advantage of such a strong bias towards filament-attached fibres?

Hypotheses on the functional significance of filament-attached muscle fibres are scarce, but previous work has suggested that using filaments optimises area utilisation (Paul and Gronenberg, 1999; Paul, 2001). Although filaments indeed result in an increase of the available attachment area, this is only a sufficient, but not a necessary condition: the same increase could be achieved by increasing the volume occupied by the apodeme instead. Indeed, filament-attached fibres appear to be an alternative to secondary and tertiary branching of the apodeme (Paul and Gronenberg, 1999; Paul, 2001), suggesting that the optimisation of volume utilisation may not be the dominant driving factor for filament-attachment. I demonstrate in Appendix A that the use of filaments in *A. vollenweideri* substantially reduces the required cuticle volume by an amount approximately equal to the cuticle

volume of the entire head capsule. Thus, filament-attachment has the advantage of significantly reducing material investment; such 'light-weight' construction may be particularly important in insects which operate close to maximum volume occupancy.

Filament-attachment may also alter how muscle shortening translates to apodeme motion. For example, filament-attached fibres are shorter, and thus slower (Paul and Gronenberg, 1999; Paul, 2001). In addition, the relationship between apodeme displacement and pennation angle change differs between filament- and directly-attached muscle fibres of equal resting length. The resulting complex interaction between filament length, apodeme displacement, pennation angle, muscle contraction and average force is beyond the scope of this chapter, but will be addressed in Chapter 3.

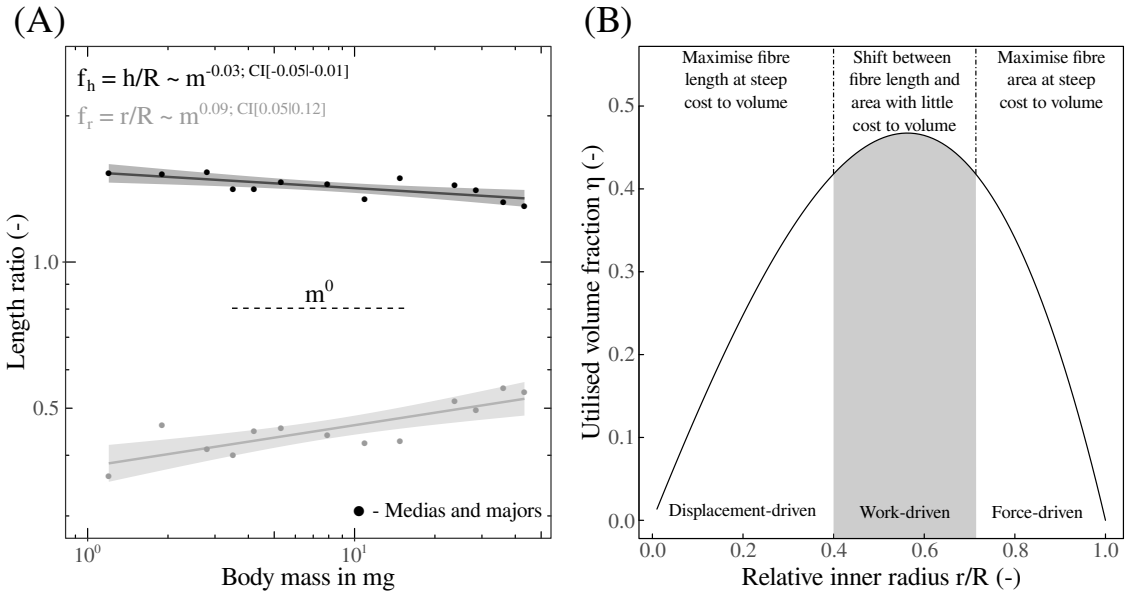


FIGURE 2.5: (**A**) The ratio between cylinder length and external radius, h/R, is negatively allometric so that heads of larger ants appear more 'heart-shaped'. The ratio between internal and external radius, r/R, in turn, is positively allometric, indicating a change in the surface to volume ratio of the attaching muscle (see main text). (**B**) The internal head morphology of *A. vollenweideri* leaf-cutter ants achieves approximately optimal volume utilisation (here shown for a mean value of $h/R = 1.4$), and lies in a morphological region where fibre length and area can be 'exchanged' without a significant variation in utilised volume.

Filament-attachment of muscle fibres constitutes a powerful strategy to reduce material investment, but the apodeme itself cannot be arbitrarily small. Instead, apodeme size is bound by two constraints. First, the apodeme needs to have a surface area large enough to attach all muscle fibres. Only about 6 ± 4 % of the apodeme surface area is covered with either filaments or directly-attached muscle fibres (see Appendix A). Consequently, the surface area is unlikely to be a limiting constraint for apodeme size. Second, the apodeme needs to have a cross-sectional area sufficiently large to withstand the muscle force without risking failure. This demand may be formally described as the condition that the ratio between two characteristic forces is to remain constant:

$$\text{Apodeme safety factor} = \frac{\sigma_{apo} A_{apo}}{\sigma_m A_{phys} \cos\phi} \propto m^0 \tag{2.4}$$

Here, A_{apo} is the cross-sectional area of the apodeme at the location of maximum stress, and σ_{apo} is the yield strength of the apodeme. If both characteristic stresses are size-invariant, the above condition is satisfied if the scaling of A_{apo} is close to the scaling of $A_{phys}\cos\phi \propto m^{0.84}$. Consistent with this condition, I find that $A_{apo} \propto m^{0.89}$ [95 % CI: (0.83 | 0.95), Fig. 2.6A; see Appendix A for how I determined A_{apo}]. Hence, ants possess apodemes with cross-sectional areas just large enough to keep the stress approximately constant, $\sigma_{apo} \propto m^{-0.06}$ [95 % CI: (-0.10 | -0.02)]. The simple expression for the safety factor highlights a second important functional demand: the extent to which volume can be saved through the use of filament-attached fibres is modulated by the ratio σ_{apo}/σ_m. For representative values of $\sigma_m \approx 0.30\,MPa$, similar to values for striated muscles in vertebrates (Alexander, 1985), and well within the range reported for arthropods (G. M. Taylor, 2000; Guschlbauer et al., 2007; Siebert et al., 2010; Meijden et al., 2012; Goyens et al., 2014b; Weihmann et al., 2015a, but see Chapter 3), and $\sigma_{apo} \approx 100 - 600$ MPa (Jensen and Weis-Fogh, 1962; Bennet-Clark, 1975; Labonte et al., 2017, see Appendix A), this ratio is typically $\sigma_{apo}/\sigma_m \approx 300 - 1800$. The implemented area ratio, in turn, is $\cos\phi A_{phys}/A_{apo} = 55 \pm 5$, suggesting that the apodeme operates at a safety factor of $\approx 5 - 30$.

External anatomy: The positive allometry of muscle volume poses a challenge, as larger ants need to accommodate disproportionally larger closer muscles. This challenge can be addressed by (i) increasing volume occupancy, and/or (ii), increasing the relative head volume. Volume occupancy χ indeed increases from 70 to over 80 % (in accordance with previous studies on ant mandible muscles, e. g. Gronenberg et al., 1997; Paul, 2001), $\chi \propto m^{0.05}$ [95 % CI: (0.03 | 0.06)]. This increase accounts for about 20 % of the increase in the functional volume in excess of isometry $V_{func} \propto m^{1.19}$, as $(45/1)^{1.19-1.00} \approx 2$. The remaining 80 % are enabled by disproportionally larger head capsules, $V_h \propto m^{1.15}$ [95 % CI: (1.08 | 1.21)]. Larger ants tend to have proportionally smaller brains (Gronenberg, 2008; Seid et al., 2011; Groh et al., 2014; Lillico-Ouachour et al., 2018; Arganda et al., 2020), which may provide some flexibility for muscle occupancy. However, smaller ants already have the majority of their heads filled by muscle, and larger ants likely need to provide space for other tissues inside the head capsule, so that the strong allometry of V_{func} must be predominantly achieved by a positive allometry of overall head volume.

The positive allometry of head volume can be modulated by scaling head length, width and height. I find that head width displays the strongest positive allometry, $W_h \propto m^{0.40}$ (as previously reported for *Atta*, see E. O. Wilson, 1980a; Wetterer, 1999; Helanterä and Ratnieks, 2008), followed by head height, $H_h \propto m^{0.38}$. Head length, in turn, only shows a weak tendency for positive allometry $L_h \propto m^{0.36}$ [95 % CI: (0.33 | 0.39)] (see Fig. 2.6B). What explains this seeming preference for increasing some head dimensions more strongly than others?

One possible explanation might lie in the expansion of the internal attachment area: changing the surface-to-volume ratio requires a strong positive allometry of the internal radius $r \propto m^{0.49}$. Coupled with the isometric growth of fibre length, this allometric expansion affects the relative spatial demand in width and height more strongly than it does in length, as a larger fraction of head width

and height is occupied by r. In other words, the effect of the strong positive allometry of r on head length is likely attenuated by the apodeme length, and the space occupied by the opener muscle (see Fig. 2.2). Head width allometry, in comparison to head height, might be further driven by the need to accommodate longer mandible inlevers, which are approximately aligned with the lateral axis.

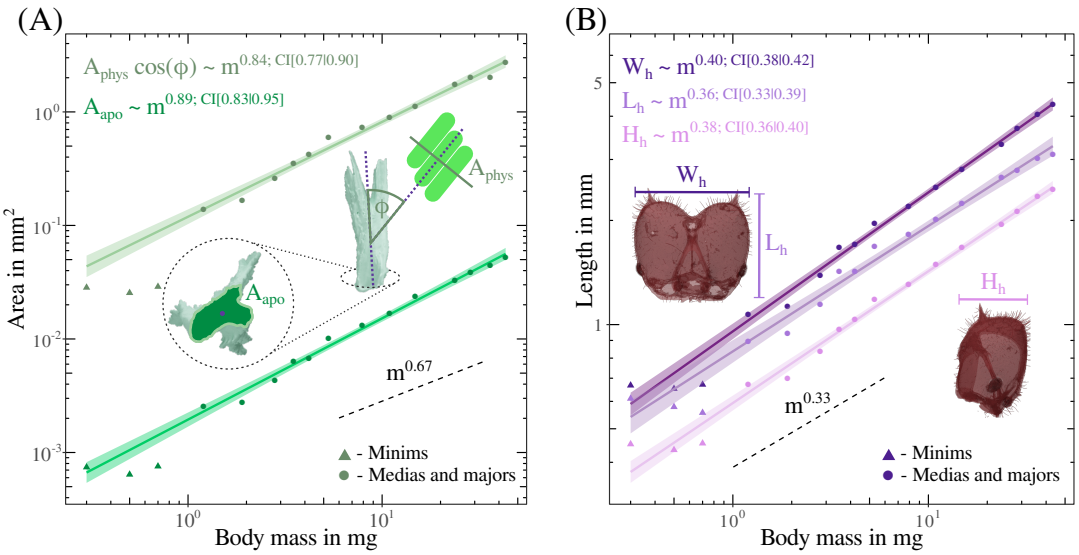


FIGURE 2.6: Scaling of allometric changes in internal and external head anatomy in *A. vollenweideri* leaf-cutter ants. (**A**) The size-specific increase in bite force associated with the positive allometry of A_{phys} is countered by disproportionally larger apodemes; the apodeme cross-sectional area A_{apo} also scales with a strong positive allometry, so maintaining an approximately equal apodeme stress. (**B**) The increase in size-specific muscle volume is accommodated mainly by a positive allometry of head width W_h and height H_h; head length L_h is isometric.

2.3.3 Why vary shape to boost bite performance?

The bite force capacity in *A. vollenweideri* leaf-cutter ants shows strong positive allometry, mainly achieved by a disproportionate increase in muscle investment. Bite force capacity is of particular relevance for leaf-cutter ants, as it influences the diversity of plant materials that can be processed by colony workers (J. M. Cherrett, 1972; E. O. Wilson, 1980a,b; Wetterer, 1994b). Hence, my results add further support to the hypothesis that size-polymorphism in leaf-cutter ants, and the associated adaptations in shape, may enable them to forage on a broader spectrum of food sources (E. O. Wilson, 1980a; Waller, 1989; Wetterer, 1999; Clark, 2006; Hölldobler and E. O. Wilson, 2010). Why alter force capacity not only via size- but also via shape-differences?

I propose three potential reasons. First, achieving the same bite force with isometry would require a worker three times heavier than the largest worker in an allometric colony workforce. The positive allometry thus increases the effective size range of the colony workforce by a factor of three, but at reduced 'production cost' (which is proportional to mass). It is well established that larger workers cut tougher leaves (J. M. Cherrett, 1972; E. O. Wilson, 1980a,b; Nichols-Orians and Schultz, 1989; Wetterer, 1994a,b), and my results suggest that they may even cut *relatively* tougher leaves. Second, a disproportionate increase in bite force may be required to compensate an increase in mandibular

cutting force – the force required to cut a material with mandibles – which may scale in proportion to a characteristic mandible length (J. G. Williams, 2015b; R. M. Schofield et al., 2016, but see Chapter 6). Third, disproportionally large heads may enable an increase in size-specific bite force capacity, but they may limit or reduce the ability of workers to perform other tasks, i. e. they render them less generalist. For example, the increased head size may reduce mobility at the nest entrance and within the nest where small heads may be beneficial to successfully manoeuvre through the close-knit structure of the fungal garden (see Fig. 2.6B; Rodríguez-Planes and Farji-Brener, 2019). Indeed, significant numbers of larger workers typically only exist in colonies which exceed a minimum size (E. O. Wilson, 1983b), consistent with the hypothesis of specialised large workers but generalist small workers.

Leaf-cutter ant workers show substantial, size-specific modifications to internal and external anatomy which increase their bite force capacity. The extent to which this specialisation improves colony performance requires to integrate the morphological findings of this study with quantitative measurements of cutting performance to assess 'efficiency', and with behavioural assays to assess how differences in efficiency are reflected in task allocation. I hope that such work will provide a comprehensive and integrative picture of the interaction between worker polymorphism, task specialisation, and foraging efficiency.

3 Relationship between bite force and mandibular opening angle

I acknowledge the contributions of Richard Johnston, who conducted the μCT scans.

Summary

Bite forces play a key role in animal ecology: they affect mating behaviour, fighting success, and the ability to mechanically process food. Although feeding habits of arthropods have an enormous ecological and economical impact, we lack fundamental knowledge on how the morphology and physiology of their bite apparatus controls bite performance and its variation with mandible gape. To address this gap, I derived a comprehensive biomechanical model that characterises the relationship between bite force and mandibular opening angle from first principles. I validate the model by comparing its geometric predictions with direct morphological measurements on CT-scans of *Atta cephalotes* leaf-cutter ant majors. I then demonstrate its deductive and inductive power with four exemplary use cases: First, I extract the physiological properties of the leaf-cutter ant mandible closer muscle from *in-vivo* bite force measurements, and so add to the few studies on force-length properties of arthropod muscle. Second, I show that leaf-cutter ants are extremely specialised for biting: they generate maximum bite forces equivalent to about 2600 times their average body weight – at least a factor of five in excess of the largest weight-specific forces reported in the literature for any animal. Third, I discuss the relative importance of morphology and physiology in determining the magnitude and variation of bite force, so providing guidance for comparative work. And last, through rational analysis of the model, I suggest a hierarchy of model simplifications and assess the performance of 'minimum' models which predict bite force from a reduced set of easily accessible parameters. I hope that my work will facilitate future comparative studies on the insect bite apparatus, and advance our knowledge of the behaviour, ecology and evolution of arthropods.

3.1 Introduction

Bite forces are a performance metric paramount to animal behaviour, ecology and evolution (R. A. Anderson et al., 2008). They determine access to food sources (Verwaijen et al., 2002; Meij and Bout, 2004; Gidmark et al., 2013; Lappin et al., 2017; Herrel et al., 2018; Kaczmarek and Gidmark, 2020), fighting ability and reproductive success (Husak et al., 2009; Hall et al., 2010; Goyens et al., 2014b; McLain et al., 2015), and the ability to escape predators (Hao et al., 2018). Strikingly, the vast majority

of bite force studies has been conducted on vertebrates and crustaceans (e. g. Pruim et al., 1980; Elner and Campbell, 1981; Govind and Blundon, 1985; Blundon, 1988; Dessem and Druzinsky, 1992; Levinton and Judge, 1993; L. D. Smith and Palmer, 1994; Block and Rebach, 1998; Yamada and Boulding, 1998; Herrel et al., 1999; G. M. Taylor, 2000; Aguirre et al., 2002; Meyers et al., 2002; Verwaijen et al., 2002; Dumont and Herrel, 2003; G. M. Erickson et al., 2003; Meij and Bout, 2004; Herrel et al., 2005; Huber et al., 2005; Herrel and O'Reilly, 2006; Huber et al., 2006; R. S. Wilson et al., 2007; Bywater et al., 2008; Claussen et al., 2008; Freeman and Lemen, 2008; Husak et al., 2009; M. E. Jones and Lappin, 2009; Lailvaux et al., 2009; S. H. Williams et al., 2009; Pfaller et al., 2010; Becerra et al., 2011; Grubich et al., 2012; Marshall et al., 2012; Becerra et al., 2013; Gidmark et al., 2013; Yap et al., 2013; G. Erickson et al., 2014; McLain et al., 2015; Senawi et al., 2015; Oka et al., 2016; Santana, 2016; Lappin et al., 2017; Penning, 2017; Herrel et al., 2018; Malavé et al., 2018; M. E. Jones et al., 2020; Kaczmarek and Gidmark, 2020; South et al., 2020). In sharp contrast, comparatively few studies exist for the hyperdiverse non-crustacean arthropods (but see Wheater and Evans, 1989; Paul and Gronenberg, 2002; Spagna et al., 2008; Heethoff and Norton, 2009; Hall et al., 2010; Meijden et al., 2010; M. H. Huang, 2012; Meijden et al., 2012; Goyens et al., 2014b; Weihmann et al., 2015a; David et al., 2016b,a; Hao et al., 2018; Rühr et al., 2022).

This disparity is as striking as it is surprising; arthropods rely on bite forces just as much as vertebrates: to fight over access to food and mating partners (Hall et al., 2010; Goyens et al., 2014b), and in other key behaviours such as nest building (Pielström and Roces, 2014). The arguably most important role of bite forces in arthropods, however, is that they determine the ability to mechanically process food (E. Bernays, 1986; Chapman, 1995; F. Clissold, 2007). Indeed, plant-eating insect have an enormous impact on our lives – they destroy around 11-20 % of our crops, causing billions of US dollars in economic damage, and may thus jeopardise global food security in a warming climate (Battisti and Naylor, 2009; Dhaliwal et al., 2010; Oliveira et al., 2014; Rosenzweig et al., 2014; Sharma et al., 2017; Deutsch et al., 2018) – and affect entire ecosystems (Crespo-Pérez et al., 2020). To provide but two illustrative examples, leaf-cutter ants accelerate the cycling of nutrients in the Neotropics through massive defoliation and decomposition of plant material (H. G. Fowler et al., 1989), and seed-harvesting ants increase the dispersion rate and regeneration of myrmecochorous plants (Magalhães et al., 2018). The need to mechanically process plant-material to feed is likely one of the driving factors in the evolutionary arms race between plants and insects, and thus constitutes a significant aspect of insect diversity (E. A. Bernays, 1991; E. A. Bernays, 1998; Krenn, 2019).

Despite this broad significance, fundamental knowledge about the bite performance across the arthropod tree of life is scarce. A reasonable and indeed common starting point to characterise bite performance within and between species may be the magnitude of the peak bite force (Alexander, 1985). This peak force, however, can be difficult to measure, because arthropods are often small, and tricky to predict, as it depends on the geometry of the bite apparatus and the physiology of muscle; both vary substantially across arthropods (G. M. Taylor, 2000; Krenn, 2019). To make matters worse, bite force typically varies with the mandibular opening angle or gape, adding further complexity (S. W. Herring and S. E. Herring, 1974; Dumont and Herrel, 2003; Heethoff and Norton, 2009; S. H.

Williams et al., 2009; Gidmark et al., 2013; Yap et al., 2013; Goyens et al., 2014b; Weihmann et al., 2015a; Santana, 2016; Kaczmarek and Gidmark, 2020). This variation is not merely a complication, but is functionally relevant and may reflect species-specific demands. For example, masticating bats produce largest bite forces at small opening angles (Dumont and Herrel, 2003; Santana, 2016), whereas snail-eating carps produce maximum forces at comparatively larger angles (Gidmark et al., 2013); predatory king salmons produce maximum bite force at a relatively larger mandible gape than filter-feeding pink salmons (Kaczmarek and Gidmark, 2020); and stag beetles generate largest bite forces at opening angles that are typical during combat (Goyens et al., 2014b). The ecological and behavioural needs of each species hence likely drive the morphological and physiological properties of the musculoskeletal bite apparatus which determine the variation of bite force with mandibular opening angle.

Notwithstanding this considerable complexity and richness of factors which contribute to and influence bite forces, bite forces have a mechanical origin, which makes them amenable to exact analysis from first principles. A quantitative model which predicts the magnitude and variation of bite force with opening angle from morphology and physiology of the bite apparatus would provide a powerful tool to study comparative bite performance and head anatomy, and may thus increase our understanding of arthropod behaviour, ecology and evolution. In the following paragraphs, I derive such a model and then validate it using *Atta cephalotes* leaf-cutter ants as model organism. I demonstrate the utility of the model by extracting the force-length properties of the mandible closer muscle from *in-vivo* bite force measurements, discuss the morphology and exceptional performance of the leaf-cutter ant bite apparatus in an ecological and comparative context, and discuss the possibility and accuracy of 'minimum' bite force models which allow colleagues to predict the magnitude of the bite force and its variation with opening angle from a reduced set of accessible parameters.

3.2 A biomechanical analysis of biting in arthropods

The magnitude of the bite force, $|\mathbf{F}_b|$, is determined by the morphological architecture and the physiological properties of the musculoskeletal bite apparatus. These two components are fully captured by two simple terms: the net muscle force which pulls on the apodeme (later referred to as apodeme force); and the mechanical advantage of the force-transmission system, MA, i. e. the ratio of two characteristic moment arms (Wheater and Evans, 1989; Heethoff and Norton, 2009, and Chapter 2). The net muscle force is the vector sum of the forces generated by individual fibres. Combined, all fibres produce a force with a magnitude equal to the product between a characteristic muscle stress, σ, and a characteristic cross-sectional area, A_{phys}. However, unless the fibres are perfectly aligned, only some fraction of the fibre force magnitude contributes to the magnitude of the net force. This fraction is typically characterised by an average angle of pennation, ϕ (throughout this thesis, all vectors are bold, and all unit vectors are indicated by a hat). We may thus write:

$$|\mathbf{F}_b|(\theta) = \sigma(\theta) A_{phys} \cos[\phi(\theta)] MA(\theta) \tag{3.1}$$

I note that only one of the four key parameters in this equation, A_{phys}, is independent of the mandibular opening angle θ, defined here as the angle between the lateral head axis and the projection of the outlever on the plane of rotation (see Fig. 3.1A-C and Weihmann et al., 2015b). In the following paragraphs, I derive the critical functions $\sigma(\theta)$, $\cos[\phi(\theta)]$ and $MA(\theta)$ from first principles. Understanding how the morphology and physiology of the bite force apparatus control the variation of bite force with opening angle is not just an enjoyable exercise in mechanics, but has substantial biological implications, for it determines the accessibility of food items of different size (e. g. Gidmark et al., 2013), and potentially prey handling times (Yap et al., 2013). However, this problem has received relatively little quantitative attention (e. g. S. W. Herring and S. E. Herring, 1974; Gidmark et al., 2013; Yap et al., 2013; Goyens et al., 2014b; Weihmann et al., 2015b).

I derive bite force as a function of the opening angle because this relationship is biologically meaningful and directly relates to the typical experimental procedure to measure bite forces (e.g. Herrel et al., 1999; Dumont and Herrel, 2003; Weihmann et al., 2015a). Physically, however, the bite force is not a function of the opening angle, but of the muscle activation and the muscle fibre stretch ratio λ. The causal relationship $|\mathbf{F}_b| = f(\lambda)$ is provided in Appendix B. Throughout the derivation, I use the following assumptions: mandible kinematics are fully characterised by a single axis of rotation; the tendon-like apodeme connects to the mandible base via a single attachment point and displaces along its main morphological axis which coincides with the net muscle force vector; and the head capsule, apodeme and mandible are rigid. Due to the abundance of dicondylic mandible joints across the insecta, which are putative hinge joints (Blanke et al., 2015; Blanke, 2019), and the comparatively high elastic modulus of sclerotised cuticle (Young's modulus $\geq$ 1 GPa, Vincent and Wegst, 2004; Labonte et al., 2017), these assumptions likely hold for the vast majority of all insect species with chewing-biting mouthparts, as well as many other arthropods. The model thus has considerable generality, but I stress that it may not be readily applicable to vertebrate biting, which may involve multiple muscle insertion points, non-rigid tissue deformation, jaw articulations with multiple degrees of freedom, and more complex muscle deformations (e. g. Azizi et al., 2017).

Mechanical advantage: Musculoskeletal lever systems are often characterised in terms of their mechanical advantage; the ratio between two characteristic moment arms (e.g. see Wheater and Evans, 1989; F. Clissold, 2007; Goyens et al., 2014b). These moment arms are determined by the location of two force transmission points, the joint centre, and the orientation of the relevant force vectors and the joint rotational axis (see Fig. 3.1).

The points of force transmission are readily identified: *internally*, it is the attachment point of the apodeme to the mandible base (in most insects, muscle force is transmitted to the mandible via a single closer apodeme, see Blanke, 2019); *externally*, it is the bite contact point on the mandibular blade. The rotational axis, $\hat{\mathbf{R}}$, is determined by joint morphology, and may often be inferred from the axis connecting the two joint condyles (Blanke et al., 2012; Goyens et al., 2014b; Weihmann et al., 2015b; David et al., 2016b,a). I use the apodeme main axis $\hat{\mathbf{A}}$ as proxy for the orientation of the *internal* apodeme force vector, because it is easier to measure and closely aligned with the net muscle

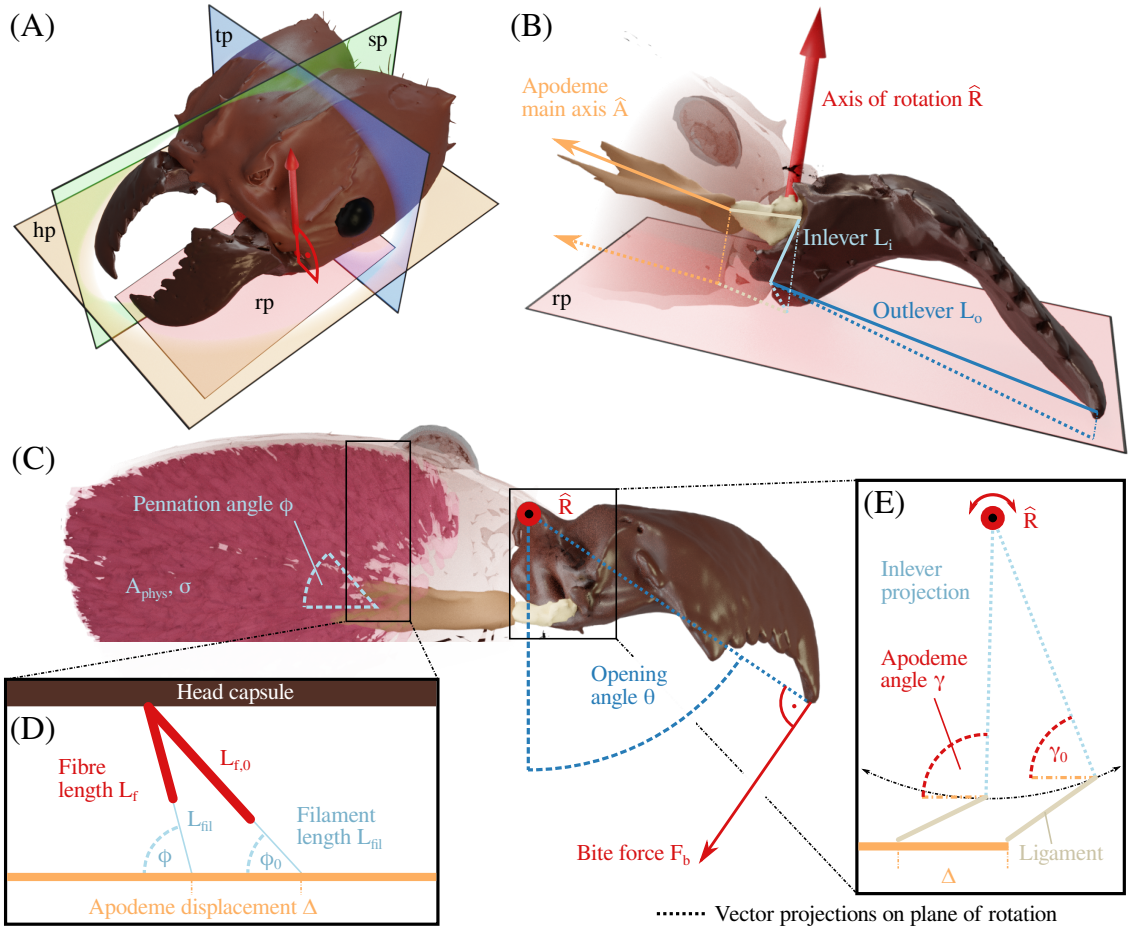


FIGURE 3.1: (**A-C**) The bite force $\mathbf{F}_b$ is a function of muscle stress σ, physiological cross-sectional area A_{phys}, pennation angle ϕ, apodeme angle γ, and the mechanical advantage determined by inlever $\mathbf{L}_i$ and outlever $\mathbf{L}_o$, the axis of rotation $\hat{\mathbf{R}}$, and the apodeme main axis $\hat{\mathbf{A}}$. The mechanical advantage and muscle stress, as well as the apodeme and pennation angle, vary with the mandibular opening angle θ, so affecting the magnitude of the maximum bite force that can be generated at different opening angles. γ and θ are defined with respect to the vector projections of $\hat{\mathbf{A}}$, $\mathbf{L}_i$ and $\mathbf{L}_o$ onto the rotational plane (rp). The position of this plane with respect to the head coordinate system, defined by the horizontal (hp), transversal (tp) and sagittal (sp) plane, can often be inferred from joint morphology (see Chapter 2). (**D**) Muscle fibres attach either directly or via thin filaments to the apodeme. When muscle fibres shorten ($L_{f,0}$ to L_f), the pennation angles increase (ϕ_0 to ϕ), and the apodeme is displaced (Δ); the filament length remains approximately constant (see main text). (**E**) As a result of the apodeme displacement, the inlever rotates about $\hat{\mathbf{R}}$ and γ changes. Notably, the apodeme appears to move in pure translation, i. e. its main axis has a constant orientation. The lateral displacement of the attachment point which must accompany mandible rotation is likely accommodated by rotation of the putatively soft apodeme ligament, which connects the apodeme to the mandible base.

force vector (see Chapter 2). The *external* bite force vector $\mathbf{F}_b$, in turn, is perpendicular to both the rotational axis and the mandible outlever by definition (see Fig. 3.1C).

To calculate the mechanical advantage, I extract the shortest distance between $\hat{\mathbf{R}}$ and the points of force transmission. To this end, I first define a specific plane of rotation by choosing a point on the rotational axis as the joint centre, in order to then find the planar (2D) components of the relevant 3D position vectors (see Fig. 3.1A). In theory, the choice of this point is arbitrary as it does not affect the moment arm calculation. In practice, however, it can be informed by joint morphology and may, in fact, be used to define the physical location of $\hat{\mathbf{R}}$, e. g. by using the centre of a joint condyle. Second, I define the in- and outlever, $\mathbf{L}_i$ and $\mathbf{L}_o$, respectively, as the vectors connecting the joint centre with the internal and external points of force transmission. I project these vectors onto the plane of rotation and calculate the length of the projections, $|\hat{\mathbf{R}} \times \mathbf{L}_i|$ and $|\hat{\mathbf{R}} \times \mathbf{L}_o|$, respectively (see Fig. 3.1B); these lengths are equal to the shortest distance between the axis of rotation and the two points of force transmission.

The length of the projected in- and outlever represents the maximum possible moment arm. The effective lever length, however, may be shorter, depending on its orientation relative to the relevant force vector. Because the bite force is perpendicular to the outlever by definition, $\mathbf{F}_b$ rotates with $\mathbf{L}_o$ as the mandible opens and closes; it follows that $|\mathbf{L}_{o,eff}| = |\hat{\mathbf{R}} \times \mathbf{L}_o|$ for all opening angles.

For the inlever, in contrast, the geometric dependency is considerable more complex. The orientation of the apodeme force remains approximately constant across mandibular opening angles, because the apodeme does not rotate. However, because the joint converts apodeme translation into mandible rotation, the angle between inlever and $\hat{\mathbf{A}}$ changes with opening angle (see Fig. 3.1C & E). Calculating the magnitude of the effective inlever $|\mathbf{L}_{i,eff}|$ at different opening angles thus requires to define the angle γ between the vector projections of inlever and apodeme main axis onto the plane of rotation. γ can be written as a direct function of opening angle, $\gamma(\theta) = \theta_0 - \theta + \gamma_0$, where γ_0 is measured at an arbitrary reference opening angle θ_0 (for a similar calculation, see S. W. Herring and S. E. Herring, 1974; Goyens et al., 2014b; Weihmann et al., 2015b). For $\gamma \approx 90°$, the effective inlever takes a maximum value of approximately $|\hat{\mathbf{R}} \times \mathbf{L}_i|$, and a small change in opening angle will be associated with a small change in effective inlever. If γ is acute or obtuse, however, the effective inlever is small, and rapidly varies with opening angle. These results may be understood in analogy to the effect of pennation angle on apodeme displacement: both angles control the amount of rotation associated with a unit of translational displacement. The two characteristic angles ϕ and γ thus crucially determine the gearing of the muscle force across opening angles. However, the importance of γ in this context has received comparatively little attention (but see Weihmann et al., 2015a).

As a last step in the calculation of the mechanical advantage, I account for the fact that the apodeme force vector may not lie in the plane of rotation. The orientation of $\hat{\mathbf{A}}$ relative to $\hat{\mathbf{R}}$ matters because only the force components in the plane of rotation can be transmitted through the mandible joint; all other components result in joint reaction forces instead. I calculate the fraction of the force acting

in the plane of rotation as the cross-product between the two relevant unit vectors, $|\hat{\mathbf{R}} \times \hat{\mathbf{A}}|$. The magnitude of the effective inlever as a function of the opening angle then follows as:

$$|\mathbf{L}_{i,eff}(\theta)| = \sin(\theta_0 - \theta + \gamma_0)|\hat{\mathbf{R}} \times \mathbf{L}_i||\hat{\mathbf{R}} \times \hat{\mathbf{A}}| \tag{3.2}$$

Note that this definition of $|\mathbf{L}_{i,eff}|$ differs from the one in Chapter 2 in two ways: First, I acknowledge that $|\mathbf{L}_{i,eff}|$ is a function of the opening angle. Second, I remove the assumption that the apodeme force vector lies in the plane of rotation. I define the mechanical advantage as the ratio between effective in- and outlever, $MA = |\mathbf{L}_{i,eff}|/|\mathbf{L}_{o,eff}|$.

Apodeme displacement: Any rotation of the mandible is associated with a displacement of the apodeme attachment point. This displacement has two components in the plane of rotation: one longitudinal component along the projection of the apodeme main axis, and one lateral component perpendicular to it. Previous work has noted that the lateral component is small for small changes in opening angle, and can thus be neglected (Weihmann et al., 2015b). This simplifying assumption, based on the small angle approximation, holds if the length of the inlever projection onto the plane of rotation is small, and the apodeme angle remains close to 90° throughout the opening range. However, for large variations in opening angle, it is inaccurate. As an illustrative example, if θ changes by 40°, the lateral displacement is about one-third of the longitudinal displacement, $1/3 \approx (1 - \sin 50°)/\cos 50°$ (see Fig 3.1E). The longitudinal displacement is likely associated with an equivalent displacement of the apodeme along its main axis; the lateral displacement, however, is likely not: If the apodeme was to translate laterally or rotate significantly, a fraction of the closer muscle would lengthen considerably while another fraction may be slack. Indeed, the apodeme would eventually hit the head capsule. Lateral translation or rotation of the apodeme is thus biologically implausible, and to the best of my knowledge, has never been reported. However, lateral displacements of the attachment point must occur, because it moves along a circular path (see Fig. 3.1 E).

I hypothesise that these lateral displacements are enabled by the rotation of the apodeme ligament, a putatively flexible connective tissue which bridges the sclerotised apodeme and the mandible (Gronenberg et al., 1998b,a; T. S. Silva and Feitosa, 2019, see Fig. 3.1E). It remains unclear how exactly the apodeme, ligament, and mandible are mechanically linked. I conjecture that both longitudinal *and* transversal forces can be transmitted from the apodeme through the ligament, so effectively shifting the apodeme force vector to the point where the ligament attaches to the mandible. At this attachment point, I assume a hinge-like connection, which enables variation in γ.

Based on the above hypothesis, the displacement of the apodeme along its main axis, Δ, is equal to the longitudinal displacement of the apodeme attachment point corrected by the misalignment between $\hat{\mathbf{A}}$ and the plane of rotation; in analogy to the effective inlever, only apodeme displacement components in the plane of rotation contribute to mandible rotation. The associated out-of-plane displacements are likely also enabled by the ligament (and may typically be very small, see Appendix B). As a consequence and in analogy to Eq. 3.2, the apodeme displacement follows as:

$$\Delta(\theta) = [\cos(\gamma_0) - \cos(\theta_0 - \theta + \gamma_0)] \frac{|\hat{\mathbf{R}} \times \mathbf{L}_i|}{|\hat{\mathbf{R}} \times \hat{\mathbf{A}}|} \tag{3.3}$$

I define Δ such that it increases as the mandible closes; it can however be defined with respect to any reference opening angle θ_0, for $\Delta(\theta_0) = 0$. Similar to the effective inlever, the change of Δ with θ depends on the apodeme angle γ. If $\gamma \approx 90°$, a small change in opening angle will be associated with a large apodeme displacement; if γ is acute or obtuse, the opposite holds.

Pennation angle: All muscle fibres attach to the rigid head capsule on one side, and insert onto the surface of the apodeme on the other. Consequently, muscle fibres that attach at a reference angle $\phi_0 > 0°$ with respect to the apodeme main axis change their relative orientation when they shorten to move the apodeme – they rotate. The associated change in pennation angle ϕ, first derived by (Pfuhl, 1937), depends on ϕ_0 and the average distance between muscle fibre origins and insertion points, $L_{t,0}$ (see Fig. 3.1D and Appendix B for derivation):

$$\phi(\theta) = \arctan\left(\frac{\sin\phi_0}{\cos\phi_0 - \Delta(\theta)/L_{t,0}}\right) \tag{3.4}$$

Muscle stress: Muscle stress is a function of fibre length, as the relative overlap and lattice spacing between thick and thin myofilaments varies when fibres are stretched or contract (A. Gordon et al., 1966; Josephson, 1975; C. D. Williams et al., 2013). I am not aware of a first-principle form of this force-length relationship (but see Rockenfeller et al., 2022), and it has been modelled with a variety of empirical functions. One simple choice is a Gaussian probability density function (e. g. Otten, 1987a; Wakeling et al., 2021):

$$\sigma(\theta) = \sigma_{max} e^{-\beta(1-L_f(\theta)/L_{opt})^2} \tag{3.5}$$

This function has a maximum σ_{max} at an optimal fibre length $L_f = L_{opt}$; β is a shape parameter which determines how quickly the stress decays as the fibre is stretched or contracts. In contrast to all previous parameters, σ_{max}, L_{opt} and β cannot be easily measured from Computed-tomography (CT) scans; they are physiological parameters which vary with the microanatomy of the muscle, such as the relative length of the myofilaments (Josephson, 1975; Otten, 1987b). Note that σ_{max}, L_{opt} and β may vary within the muscle between directly- and filament-attached fibres (Gronenberg et al., 1997), but the form of Eq. 3.5 holds for both.

Fibre length: To predict muscle stress, the relationship between muscle fibre length and opening angle needs to be known. In insects, this relationship has previously been modelled with a simple linear function (Goyens et al., 2014b), which may be sufficiently accurate provided that the range of opening angles is small. For a large range of opening angles, however, the small angle approximation is inaccurate, and the functional relation is more complex. Consider a muscle fibre of total length

L_t which attaches directly to the apodeme. The variation of fibre length L_d with apodeme displacement is determined by the reference fibre length $L_{d,0}$, the fibre pennation angle ϕ_0, and $\Delta(\theta)$ (see Benninghoff and Rollhäuser, 1952, and Appendix B for derivation):

$$L_d(\theta) = \sqrt{[\cos\phi_0 L_{d,0} - \Delta(\theta)]^2 + [\sin\phi_0 L_{d,0}]^2} \tag{3.6}$$

However, in some insects, fibres may attach via thin cuticular filaments instead (Paul and Gronenberg, 1999, and Chapter 2). Filament-attachment increases volume occupancy and cross-sectional area of the muscle while keeping the apodeme compact; it is a light-weight solution to strongly increase bite force capacity in the limited space provided by the rigid head capsule (Paul, 2001, and Chapter 2). In addition to these *static* effects, filament-attachment also has *dynamic* effects: Consider two muscle fibres of equal length; one is directly- and one filament-attached. The same fibre shortening will lead to a different apodeme displacement, because filaments reduce the amount of rotation per unit fibre strain (see Fig. 3.1D). As a consequence, the change in pennation angle associated with fibre-shortening is smaller in the filament-attached fibre.

In analogy to Eq. 3.6, the relation between the length of filament-attached fibres and apodeme displacement depends on the initial fibre length $L_{f,0}$, pennation angle ϕ_0, $\Delta(\theta)$ and filament length L_{fil} as (see Appendix B for derivation):

$$L_f(\theta) = \sqrt{\begin{matrix}[\cos\phi_0(L_{f,0} + L_{fil}) - \Delta(\theta)]^2 \\ + [\sin\phi_0(L_{f,0} + L_{fil})]^2\end{matrix}} - L_{fil} \tag{3.7}$$

where I assumed that filament length is independent of pennation angle (the strain in the filaments across the opening range is less than 2%, see Appendix B).

The last parameter in Eq. 3.1 is the physiological cross-sectional area of the muscle, A_{phys}. The physical cross-sectional area of the muscle changes as fibres change length, because muscle is approximately incompressible. A_{phys}, however, is a characteristic cross-sectional area, and thus invariant to strain. In vertebrates, A_{phys} is often measured for a relaxed muscle (e. g. Sullivan et al., 2019), but this definition is problematic in comparative work, because the relaxed fibre length may be a different fraction of L_{opt} in different muscle. In order to avoid a systematic under- or overestimation of σ_{max}, I thus define A_{phys} as the physiological cross-sectional area at an equivalent point of the force-length curve, and the natural choice for this point is the cross-sectional area for fibres of length L_{opt} at which stress is maximal.

Based on the derived geometric relations, I substitute the place-holding functions of θ in Eq. 3.1, $MA(\theta)$, $\phi(\theta)$, and $\sigma(\theta)$, with Eq. 3.2 (divided by $|\mathbf{L}_{o,eff}|$), Eq. 3.4, and Eq. 3.5, respectively. Muscle stress is expressed as a function of fibre length, so that Eq. 3.6 (for directly-attached fibres) and Eq. 3.7 (for filament-attached fibres) need to be inserted into Eq. 3.5. Total muscle stress is equal to the sum of the fractional contributions of directly- and filament-attached fibres. Last, fibre length and pennation

angle are expressed as functions of the apodeme displacement, so that Eq. 3.3 needs to be inserted into Eq. 3.4, Eq. 3.6 and Eq. 3.7. The resulting equation contains a total of 20 parameters, including θ.

The above model fully captures the determinants of bite force in arthropods and its variation with opening angle. Practically, the bite force is rarely measured directly. Instead, its magnitude, $|\mathbf{F}_b|$, is inferred from measurements with 1D or 2D force sensors (e. g. see Wheater and Evans, 1989; Herrel et al., 1999; Weihmann et al., 2015a; Rühr and Blanke, 2022). As a consequence, at least one of the vector components has to be inferred from geometry. For 1D sensors, the key geometric variable is the angle α between the force sensitive axis, and the bite force, $\mathbf{F}_b$; the measured force, $\mathbf{F}_m$, is equal to the projection of $\mathbf{F}_b$ onto the sensitive axis:

$$|\mathbf{F}_b| = \frac{|\mathbf{F}_m|}{\cos\alpha} = \frac{|\mathbf{L}_o \times \hat{\mathbf{R}}||\mathbf{F}_m|^2}{(\mathbf{L}_o \times \hat{\mathbf{R}}) \cdot \mathbf{F}_m} \tag{3.8}$$

where the term $\mathbf{L}_o \times \hat{\mathbf{R}}$ represents the orientation of $\mathbf{F}_b$ (see Fig. 3.2)B). The inner product between $\mathbf{L}_o \times \hat{\mathbf{R}}$ and $\mathbf{F}_m$, divided by their respective magnitudes, is equal to $\cos\alpha$. The sensitive axis is determined by the sensor design; the orientation of $\mathbf{F}_b$, however, is subject to experimental variation, for it depends on the orientation of the mandible outlever relative to the axis of rotation. The corresponding relationship between $|\mathbf{F}_b|$ and $|\mathbf{F}_m|$ for 2D sensors is provided in Appendix B.

3.3 Materials & methods

3.3.1 Study animals

In order to validate the derived geometric relations (Eqs. 3.2-3.7), I extracted the morphological determinants of bite force from insect heads of similar size, but with a wide variation in mandibular opening angles. I then used the validated model to extract the force-length properties of mandible closer muscles by conducting *in-vivo* bite force measurements. For both sets of experiments, I use leaf-cutter ants (genus *Atta*). Leaf-cutter ants constitute an excellent model organism for at least three reasons. First, biting is key to their ecology; they cut food sources of varying thickness and toughness to feed a fungus grown as crop (J. M. Cherrett, 1972; Nichols-Orians and Schultz, 1989). Second, the mandible closer muscle consists of both directly- and filament-attached muscle fibres (Paul and Gronenberg, 1999), which enables me to verify the two separate geometric relations between fibre length and apodeme displacement (Eqs 3.6 and 3.7). Third, mandibular opening angles observed during natural behaviour span a large range of around 70°, allowing me to validate the model across a maximum range.

Ants were collected from an *Atta cephalotes* colony, kept in a climate chamber (FitoClima 12.000 PH, Aralab, Rio de Mouro, Portugal) at 25 $^\circ C$ and 60 % relative humidity, with a 12/12 h light-dark cycle. The colony was fed with bramble, laurel, cornflakes and honey water *ad libitum*. I selected

only majors with a body mass between 50 and 60 mg in order to minimise variation due to size, reduce the complexity of handling small individuals during the experiments, and to enable bite force measurements across a maximal opening range. All individuals were weighed to the nearest 0.1 mg after collection (Explorer Analytical EX124, max. 120 g x 0.1 mg, OHAUS Corp., Parsippany, NJ, USA).

3.3.2 Tomography and morphometric analysis for model validation

Sample preparation and scanning

To obtain information on the morphological determinants of bite force, I conducted tomographic scans of five ant heads (body mass 55.0 ± 3.8 mg), prepared such that the mandibular opening angles approximately spanned the naturally observed range. In order to experimentally control the opening angle, live ants were clamped using a 3D printed device, and offered PLA rods of varying thickness to bite onto. The rods were positioned asymmetrically between the mandibles, so that the opening angles between left and right mandible differed (see Appendix B for details). This procedure was followed for four of the five ants; one ant was prepared without PLA rod, which resulted in mandibles that were maximally closed. I thus collected data for ten opening angles across the entire opening range. Ants were then sacrificed by freezing, decapitated using micro scissors, and fixed in paraformaldehyde solution (4% in PBS, Thermo Fisher Scientific, Waltham, MA, USA). After 90 - 95 h, the samples were transferred to 100 % ethanol via a series of dehydration steps in 70, 80 and 90 % ethanol solutions for an hour each. To prepare the heads for CT scanning, they were stained with 1 % iodine in ethanol for at least 4.5 days (see Metscher, 2009). The samples were analysed via X-ray microscopy using a Zeiss Xradia Versa 520 X-ray microscope (Carl Zeiss XRM, Pleasanton, CA, USA; for more details, see Appendix B).

The tomographic image stacks were reoriented such that the lateral, dorso-ventral and anterior-posterior head axes aligned with the coordinate system internal to Fiji (Schindelin et al., 2012, for more details, see Chapter 2). Tissue segmentation of head capsule, mandible closer muscle and closer apodemes were performed in ITK-SNAP (v 3.6, Yushkevich et al., 2006).

Morphometry

From the segmented tomographic scans, a series of morphological parameters relevant to the generation of bite forces were extracted: mechanical advantage, mandibular opening angle and the corresponding mandibular gape, the rotational axis of the mandible joint, apodeme orientation and displacement, volume of the mandible closer muscle, as well as average muscle fibre length and average pennation angle.

Mechanical advantage: The mechanical advantage was calculated as defined by Eq. 3.2. The relevant lengths, $\mathbf{L}_i$ and $\mathbf{L}_o$, and angles, γ_0 and θ_0, were extracted separately for each head hemisphere. The joint centre was placed at the ventral articulation of the joint (for an exact definition, see Chapter 2). The outlever may be defined with respect to any point on the mandibular cutting edge; I used

the most distal tooth tip to provide an upper bound, $\mathbf{L}_o = \mathbf{L}_{o,d}$. I calculated the mandible gape as twice the shortest distance between the distal tooth tip and the sagittal plane. The gape is thus negative when mandibles overlap.

Axis of rotation: In order to obtain the orientation of the rotational joint axis, $\hat{\mathbf{R}}$, I invoke a simple result from rigid body kinematics: If the mandible rotates about a single axis, then the angle between any vector which connects two points on the mandible and $\hat{\mathbf{R}}$ remains constant throughout mandible motion. $\hat{\mathbf{R}}$ was thus determined by minimising the squared angular residuals between $\hat{\mathbf{R}}$ and three such vectors, $\mathbf{L}_i$, $\mathbf{L}_{o,d}$, and the outlever to the most proximal tooth tip, $\mathbf{L}_{o,p}$, using a numerical solver in Python (v 3.9, Van Rossum and Drake, 2009, V Kang, F Püffel and D Labonte, in preparation). In order to integrate vector coordinates from different scans into the same coordinate system, the image origins were first transposed to the respective joint centres. Second, the coordinates were normalised with head length, defined as anterior-posterior distance between mandible joint and the rear of the head capsule. Last, to combine data from the left and right head hemisphere, the coordinates of the latter were mirrored across the sagittal plane.

Apodeme displacement: In order to obtain the apodeme displacement, I first extracted the apodeme centres-of-masses via 3D particle analysis in Fiji (for more details, see Chapter 2). The centre-of-mass coordinates were transposed and normalised as described for the rotational axis to integrate results from different individuals into the same coordinate system. Next, I performed a principal component analysis on the normalised coordinates; the first component explained the dominant part of the variation of coordinates, $R^2 = 0.931$, and was thus selected as the axis of displacement. I defined the apodeme displacement as the distance between the normalised coordinates along this axis, multiplied with the average head length. In support of the model assumption, the axis of displacement is close to the apodeme main axis $\hat{\mathbf{A}}$, defined as in Chapter 2; it differs only by $8 \pm 2^\circ$ (mean $\pm$ standard deviation). In the following, both axes are hence treated as equivalent.

Muscle architecture: The muscle volume was directly measured via ITK-SNAP. I have previously described an automated algorithm to extract fibre length and pennation angles from segmented tomography scans (Chapter 2). However, this tracing algorithm was developed for scans with a resolution and contrast only achievable with synchrotron scanning, to which I did not have access for this work. In addition, preliminary inspection of the scans revealed little 'free volume' between fibres, on which the automated tracing algorithm relies. I thus developed an alternative method, based on a simple sorting algorithm. This algorithm leverages the observation that all muscle fibres originate from the internal surface of the head capsule, and connect as approximately straight lines to a central apodeme either directly, or via thin sclerotised filaments (Paul and Gronenberg, 1999, and Chapter 2). Obtaining pennation angle and fibre length with this algorithm involves three simple steps (see Fig. B.1 in Appendix B).

First, the 3D location of the fibre attachment points (seeds) on the head capsule are identified using Fiji as described previously (see Chapter 2 for details). Second, each fibre seed is connected to its insertion point on the apodeme surface. To identify the insertion point, I assume that the density of

fibre attachments on the apodeme is approximately constant along its length, and that muscle fibres rarely cross. On the basis of these assumptions, the fibre insertion point can be found by sorting fibre seeds and apodeme surface points by their anterior-posterior positions, to then match fibre seeds and apodeme surface points with the same relative rank. As a result, fibre seeds originating at the rear of the head are connected to posterior points on the apodeme, and seeds located closer to the mandible are connected to anterior points (see Fig. B.1C in Appendix B). To prevent fibres from crossing the apodeme, the apodeme surface point closest to the fibre seed was selected from all points with the same anterior-posterior rank. The orientation of the lines connecting fibre seeds to apodeme surface was then used to calculate fibre pennation angles with respect to the apodeme main axis. The length of the connection lines, L_t, was used to extract muscle fibre length. For directly-attached fibres, $L_d = L_t$. For filament-attached fibres, the fibre length was calculated as $L_f = L_t - L_{fil}$, where L_{fil} is the filament length, obtained in a last step.

Third, I extract filament length, L_{fil}, for each fibre. To this end, filaments are grown from their insertion points on the apodeme along the orientation of the respective fibre. After crossing at least 5 pixels of muscle tissue, approximately equal to the fibre diameter, the growth was terminated, and the filament length extracted. Muscle fibres for which $L_{fil} < 5$ pixels were classified as directly-attached; fibres shorter than twice the fibre diameter were excluded from further analysis.

In order to quantify the quality of this ranking method, I manually extracted length and pennation angle of 200 fibres. The results of these direct manual measurements were compared with the results of the ranking method by matching the corresponding fibre seeds. On average, fibres from the ranking method were $1 \pm 18\,\%$ shorter than those measured manually, independent of opening angle [Linear Mixed Model (LMM) with random intercepts and opening angle as fixed effect: $\chi^2_1 = 0.51$, p = 0.48]; the error of the pennation angle was small, $0 \pm 1°$. Although this error changed significantly with opening angle – pennation angles were increasingly underestimated at larger opening angles [LMM: $\chi^2_1 = 8.53$, p < 0.01] – it remained small even for large opening angles, $< 3°$. The quality of my simple sorting algorithm thus compares favourably to that of state-of-the-art commercial tracing software (Sullivan et al., 2019; Katzke et al., 2022).

3.3.3 Bite force measurements

In order to extract the force-length properties of the mandible closer muscle, I measured bite forces of *A. cephalotes* majors using a custom-built setup, described in detail in Chapter 4. In brief, a capacitive force sensor (maximum load: 1 N, resolution: 0.002 N) is compressed when a force is applied to a bite plate connected to a pivoting lever (see Fig. 3.2A). The position of a second slidable lever can be controlled by a stepper motor, so adjusting the distance between two bite plates. To extract mandible and head position during biting, a camera recorded the experiment simultaneously from top-down at 30 fps. A 45 °-angled mirror provides a side view for a 3D reconstruction of landmarks (see section 3.3.3). Force sensor, motor and camera were controlled by a Raspberry Pi (v 3B+, Raspberry Pi Foundation, Cambridge, UK), and operated via a graphical user interface. Details on the

sensor calibration are provided in Appendix B.

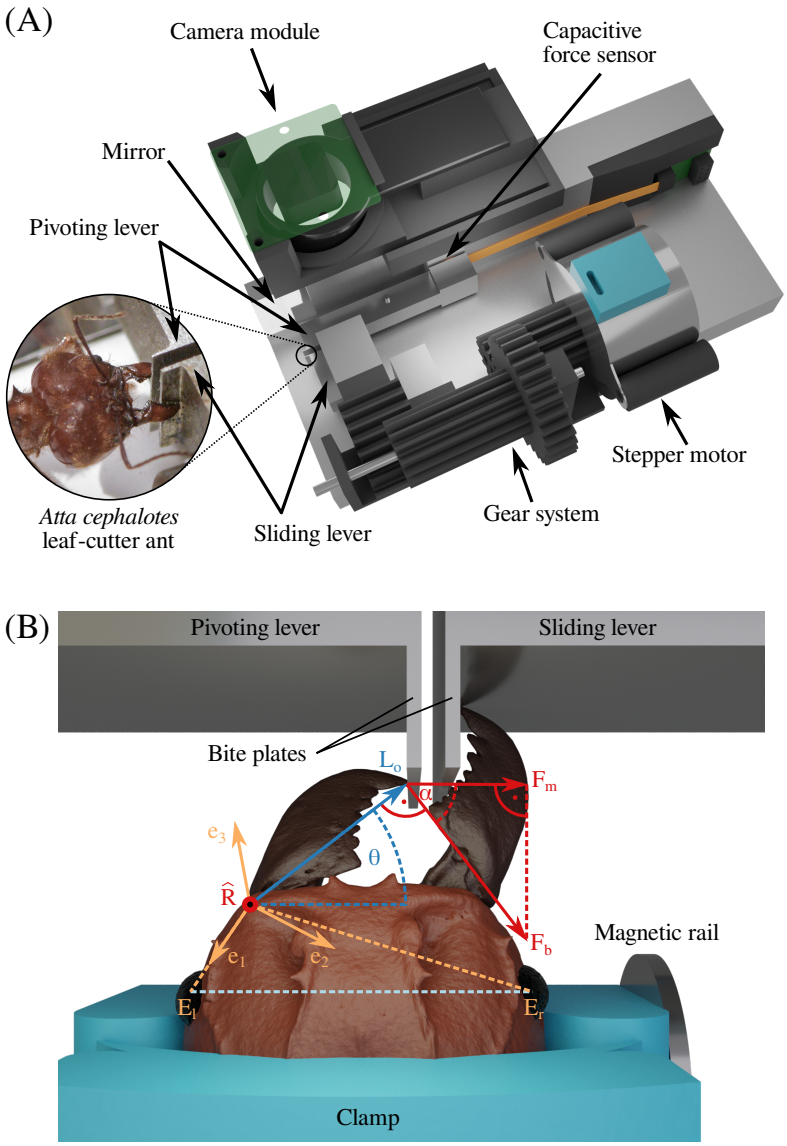


FIGURE 3.2: (**A**) A custom-built force rig was used to measure bite forces of *Atta cephalotes* majors (photo by Victor Kang). In short, a force-sensitive capacitor was attached to a rigid metal frame. A pivoting lever presses onto it as a force is applied at the opposite end of the lever. A second sliding lever, controlled by a stepper motor, provides control over the distance between the bite plates. (**B**) To measure bite forces at small opening angles θ, ants were positioned off-centre using a 3D printed clamp attached to a magnetic rail. Bite force $|\mathbf{F}_b|$ was extracted from the measured force $|\mathbf{F}_m|$ using the angle α, the outlever $\mathbf{L}_o$ and the joint axis of rotation $\hat{\mathbf{R}}$, as defined in Eq. 3.8. $\hat{\mathbf{R}}$ was projected onto a head-fixed coordinate system ($\mathbf{e}_1$, $\mathbf{e}_2$, $\mathbf{e}_3$), defined by the vectors connecting the mandible joint with left ($\mathbf{E}_l$) and right eye centres ($\mathbf{E}_r$).

Experimental protocol

Ant majors were collected from the foraging area or the fungus garden as available, and held in front of the bite plates of the force sensor using insect tweezers. Force recordings were terminated as soon as at least five distinct bites occurred. Subsequently, the ant was marked (Edding 4000 paint

marker, Edding AG, Ahrensburg, Germany), and placed into a separate container with fresh bramble leaves and around 20 minors and medias to provide a resting period. After around two minutes, the same ant was measured again, but with a different plate distance. This process was repeated once more, so that bite forces of a single individual were measured three times in total at three different plate distances. Plate distances were chosen at random from three equally-sized bins between 0.7 and 3.6 mm, approaching the maximum mandible gape range of the ants. In order to test if muscle fatigue may confound the results (Larabee et al., 2022), an additional five ants were measured using the same protocol, but at a constant plate distance of 1 mm. A LMM with random intercepts revealed no significant effect of trial number on bite forces ($\chi^2_1 = 3.75$, p = 0.053; I note that this result is almost significant, but in the opposite direction than expected: bite forces were around 15 % larger at the last trial compared to the initial measurement).

To comprehensively characterise the relationship between bite force and mandibular opening angle, it is necessary to measure bite forces across the largest possible range of opening angles. The upper end of this range can be approached by simply increasing the distance between the bite plates; the smallest angle, however, is structurally limited by bite plate thickness (approximately 150 μm each for my set-up). To overcome this limit, I fixed the ant heads with a custom 3D printed clamp, magnetically connected to a metal frame. The clamp allowed me to position the ant heads off-centre relative to the bite plates, so enabling bites at lower opening angles (see Fig. 3.2B). Clamped ants did bite much less frequently, and sometimes only after stimulation with polite air blows (also see Weihmann et al., 2015a). To test if clamping affected bite forces, five ants were clamped and positioned centrally in front of the sensor. The plate distance was selected at random to fall between 1.7 and 2.5 mm, and bite forces were measured. There was no significant difference in force between unclamped and clamped bites of the same gap class (Two Sample t-test: t_{28} = 1.19, p = 0.24).

Video analysis

I extracted the maximum force from each bite force trace (see Appendix B for raw data examples). To avoid confounding effects due to variation in mandible outlever, only bites transmitted with the most distal tooth were considered. The following 3D coordinates were extracted from the video frame corresponding to the peak bite force: the bite contact point (most distal tooth tip), joint centre, and the geometric centres of both eyes. The depth component of the 3D coordinates was measured from the mirrored side view (see Chapter 4). The vectors connecting mandible joint with both eyes $\mathbf{E}_l$ and $\mathbf{E}_r$ were used to define a local head-fixed coordinate system: $\mathbf{e}_1 = \mathbf{E}_l/|\mathbf{E}_l|$, $\mathbf{e}_3 = (\mathbf{E}_l \times \mathbf{E}_r)/|\mathbf{E}_l \times \mathbf{E}_r|$ and $\mathbf{e}_2 = \mathbf{e}_3 \times \mathbf{e}_1$. The rotational axis, $\hat{\mathbf{R}}$, extracted from the tomographic scans, was projected onto this coordinate system using the same relative orientation to $\mathbf{e}_1$, $\mathbf{e}_2$ and $\mathbf{e}_3$ (see Fig. 3.2B). The mandibular opening angle was calculated with respect to the lateral axis, here defined by the vector connecting both eye centres.

The capacitive force sensor has only one sensitive axis, i. e. it is a 1D sensor. $|\mathbf{F}_b|$ was hence extracted as defined by Eq. 3.8. Due to the design of the setup, an additional correction factor Γ was introduced

to account for differences in moment arms due to variation in contact point on the bite plate. This correction factor reads $\Gamma = |\mathbf{L}_{p,cal}|/|\mathbf{L}_p|$; $|\mathbf{L}_{p,cal}|$ is the moment arm used for calibration, and $|\mathbf{L}_p|$ is the moment arm defined by the mandible contact point on the bite plate.

Electrical stimulation

To correctly interpret my bite force measurements, I tested (i) if voluntary bites involve maximum muscle activation, and (ii), if activation is independent of mandibular opening angle. I conducted these tests by eliciting maximum muscle activation through electrical stimulation of the mandible closer muscle.

To this end, a microcontroller (Raspberry Pi Pico, Raspberry Pi Foundation, Cambridge, UK) was programmed to output a square function of stimulation impulses at 100 Hz frequency with a duty cycle of 10 % (parameters used to elicit muscle contraction in moths (Daly et al., 2009) and beetles (Cao et al., 2014; Choo et al., 2016)). The output voltage was regulated using voltage dividers with resistors between 70 and 2230 Ω. A custom-designed device, consisting of two insect pins (size '0', power and ground) and a 3D printed pin holder, was connected to the circuit (see Fig. 3.3).

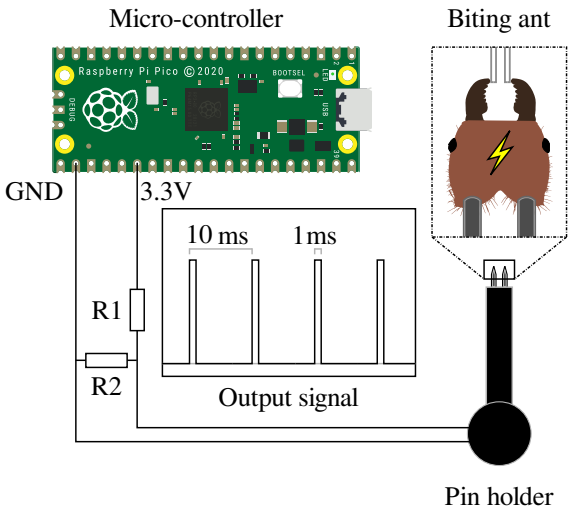


FIGURE 3.3: A custom-built device was used to stimulate the mandible closer muscle, so eliciting maximum bite forces. A Raspberry Pi Pico was used to generate a square function as output signal with 100 Hz frequency and a duty factor of 0.1. The voltage was regulated using a voltage divider with varying resistors (0.08 $\leq$ R1 $\leq$ 2.24 $k\Omega$, R2 = 1 $k\Omega$). A 3D printed device was connected to the circuit. This device holds two insect pins, 1.5 mm apart and each protruding 2 mm. The pins were inserted into the head of live ants, positioned in front of the bite plates, and the device was activated.

Unclamped bite force experiments were performed following the above protocol with a fixed bite plate distance of 1 mm. This time, however, the measurement was not stopped after a sufficient number of bites. Instead, the pins were inserted into the head capsule of the biting ant. Subsequently, the stimulation was turned on for 1 s, and the resulting bite force was recorded. Due to the approximate

positioning and size of the pins, I cannot exclude that the opener muscle was also stimulated. However, due to its small relative size in *Atta* ants (≈5 % of the closer muscle in volume, see Chapter 2), any co-contraction would only have minor effects on the net bite force.

Two maxima were extracted from the recorded force trace: the maximum force of distal bites during natural and stimulated bites. Voltages between 1 and 3 V were used to find the minimum voltage at which the muscles where stimulated maximally, similar to the range used for beetle leg muscles (Cao et al., 2014). At 1 V, bites were not always elicited; the extracted second maximum may thus often represent voluntary bites. At 1.5 V the muscle may have been sub-maximally stimulated, causing lower bite forces than from the voluntary bites (see Fig. 3.4A). A marked increase of stimulated bite force was visible at 2 - 2.5 V, and for voltages $\geq 2\,V$, the average ratio between maximum voluntary and maximum elicited bite force remained constant [ANOVA: $F_{1,9} = 1.17, p = 0.31$]. On the basis of these results, I selected 2.75 V as excitation voltage for further stimulated bite force measurements at small (1 mm) and large (2.5 - 3 mm) plate distances. Occasionally, stimulated bites did not occur at the distal end of the mandible blade. In these cases, the calculated maximum bite force was corrected as $|\mathbf{F}_{b,s}| = |\mathbf{F}_b||\mathbf{L}_{o,c,eff}|/|\mathbf{L}_{o,d,eff}|$ to account for differences in effective outlever, where $\mathbf{L}_{o,c,eff}$ and $\mathbf{L}_{o,d,eff}$ are the effective outlevers at the point of bite contact and the most distal tooth tip, respectively. I excluded stimulated measurements for which the difference in opening angle between unstimulated and stimulated bite exceeded 20 ° to reduce confounding effects, and one additional measurement that exceeded the force range of sensor calibration.

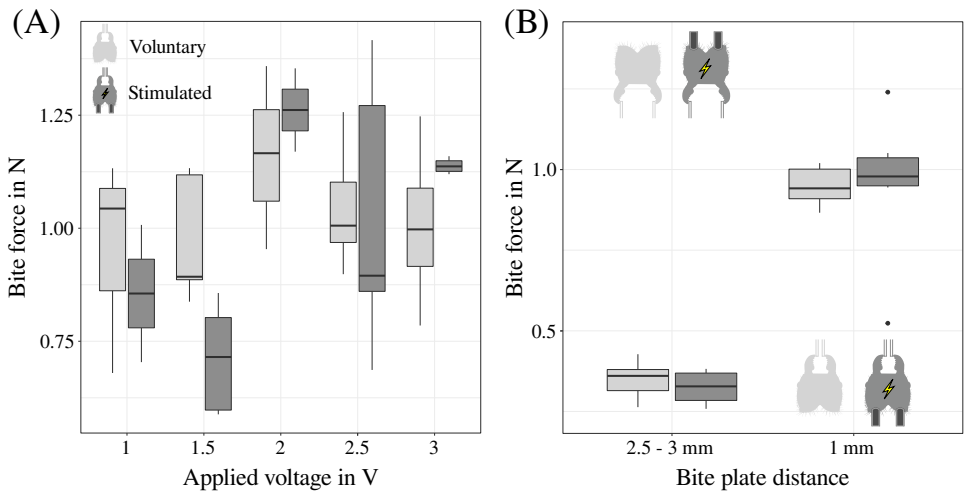


FIGURE 3.4: (**A**) Stimulated bite forces (dark grey) were compared against the maximum voluntary forces (light grey), recorded prior to stimulation for voltages between 1 and 3 V (voluntary: n_{1V} = 3, $n_{1.5V}$ = 5, n_{2V} = 3, $n_{2.5V}$ = 6, n_{3V} = 4; stimulated: n_{1V} = 2, $n_{1.5V}$ = 5, n_{2V} = 2, $n_{2.5V}$ = 5, n_{3V} = 4). For voltages $\geq$2 V, stimulated forces were approximately constant. For 1 V (shaded area), bites did not always occur after activating the device; the 'stimulated' forces hence likely include voluntary bites. (**B**) Maximum voluntary and stimulated bite forces were of similar magnitude for both small and large opening angles (measured with a stimulation voltage of 2.75 V). Hence, ants bite with close to maximum available force independent of opening angle, and undeterred by the rigid, metallic material of the levers and the clamping.

Data analysis

The variation of morphological force determinants with mandibular opening angle can be directly predicted from the derived geometric relations (see Eqs. 3.2-3.7). As reference parameters for these predictions, I selected the corresponding arithmetic average across all scans. To test for significant effects of opening angle on a variety of morphological parameters of the bite apparatus, I deployed LMMs: I tested if adding opening angle as fixed parameter improves the model significantly compared to a random intercept model (see Field et al., 2012). To extract the force-length properties of the muscle (see Eq. 3.5), maximum muscle stress, optimum fibre length and shape parameter β were estimated using a non-linear least squares fitting function in Python (SciPy, Virtanen et al., 2020), invoking Eq. 3.1. To enforce physical and biological plausibility, boundaries were set such that the maximum muscle stress and β are positive; the optimum fibre length was forced to remain within the range of measured fibre lengths. The physiological properties of directly- and filament-attached fibres likely differ (Gronenberg et al., 1997); however, due to the small fraction of directly-attached fibres, $15 \pm 8\,\%$, I lacked sensitivity to determine their physiological properties with sufficient confidence. The physiological muscle parameters of these fibres were thus assumed to be equal to those of the filament-attached fibres; L_{opt} was assumed to be at the equivalent stretch with respect to the average fibre lengths of both fibre populations. I merged data from all bite force experiments, as neither clamping, nor measurement order affected bite force. I excluded the stimulated bites to avoid pseudo-replication and four further data points: three measurements from one individual that produced outliers at low opening angles ($55° < \theta < 65°$; $|\mathbf{F}_b| < \mu - 3\sigma$), and one measurement where the second mandible interfered during the experiment. Overall, I analysed 138 force measurements from 81 individuals (54.8 ± 3.2 mg).

3.4 Results and discussion

Bite force influences animal behaviour and relates directly to muscle physiology and head morphology. It has significant consequences for animal fitness, and is thus under selection. As a consequence, bite forces may be considered a nonpareil performance metric for comparative studies at several levels of organismal biology (R. A. Anderson et al., 2008). I derived a comprehensive first principles model to describe the variation of bite force with mandibular opening angle across arthropods. In order to validate the geometric derivations of my model, I measured the relevant parameters from tomography scans of *A. cephalotes* majors across a large mandibular opening range. I then used my model to extract the physiological properties of the mandible closer muscle from *in-vivo* bite force measurements via Eq. 3.1. In the next paragraphs, I (i) demonstrate the accuracy and predictive power of the model; (ii) discuss the magnitude and variation of leaf-cutter ant bite forces with opening angle in an ecological and comparative context; and (iii) present a 'minimal' model to predict bite forces from simple morphological measurements.

3.4.1 Variation of morphological bite force determinants is in excellent agreement with model predictions

Our model derivation involved four key assumptions: First, I assumed that filament strain is negligible. This conjecture is supported by the observation that filament length is independent of opening angle (LMM: $\chi^2_1 = 0.32$, p = 0.58, see Appendix B). Second, I assumed that the head capsule is effectively rigid. This assumption is supported by the fact that head dimensions vary little with opening angle (see Appendix B). Third, I conjectured the apodeme ligament rotates, and so enables the lateral displacement imposed by mandible rotation. Indeed, I report evidence for such changes in the lateral expansion of the ligament in Appendix B. Fourth, I modelled the mandible joint as a one degree-of-freedom hinge. The mandible joint in some ants, including leaf-cutter ants, has an unusual morphology (A. Richter et al., 2021), but mandible motion nevertheless approximates planar rotation across the change in opening angle relevant to this study [V Kang, F Püffel and D Labonte, in preparation].

Having provided empirical support for the simplifying assumptions involved in the model derivation, I turn my attention to the predictions it enables. Mechanical advantage, apodeme displacement, fibre pennation angle and fibre length are important morphological determinants of bite forces, which all change with mandibular opening angle (see Eqs. 3.2-3.7). Direct morphological measurements of these parameters across a large range of opening angles are in excellent agreement with theoretical predictions based on arithmetic means, without exception (see Fig. 3.5).

I measured opening angles between 35 and 105° for fully closed and maximally opened mandibles, respectively. At the maximum opening angle, the gape is 3.6 mm, or approximately 75 % of the head width. At the minimum gape, in turn, the most distal mandible teeth overlap by about 1.3 mm. To move the mandible from maximally opened to fully closed, the apodeme displaces by around 0.7 mm corresponding to about one-fifth of the average head length (see Fig. 3.5A). This displacement may appear small, but it constitutes more than 50 % of the average fibre length, and thus requires large fibre strains. At small opening angles, the apodeme angle, γ is close to 90°, and varies approximately linearly with apodeme translation (this follows from the small angle approximation, $\cos(d\theta + 90°) = -\sin(d\theta) \approx -d\theta$, see Eq. 3.3). At large opening angles, this linearity no longer holds, and the same change in opening angle is associated with a smaller longitudinal displacement of the apodeme attachment point, and a larger lateral displacement (see Fig. 3.1E).

The mechanical advantage takes a maximum value of 0.29 at an opening angle of 51°, where $\gamma \approx 90°$. As a consequence, at most 29 % of the apodeme force is transmitted at the distal end of the mandible blade (see Fig. 3.5B). The maximum MA is at the lower end of values reported for insects across numerous taxa ($0.3 < MA < 0.8$, see Blanke, 2019). The MA decreases with increasing opening angle in direct proportion to the effective inlever, and is reduced by a factor of 1.7 at the largest opening angle, at which γ has decreased to about 40°. The increasing steepness of this decline directly reflects the change in slope of sin(γ) (see Eq. 3.2). If the variation of MA was neglected, $MA(\theta) = MA_{max}$, the capacity for bite forces at large opening angles would thus be overestimated by about

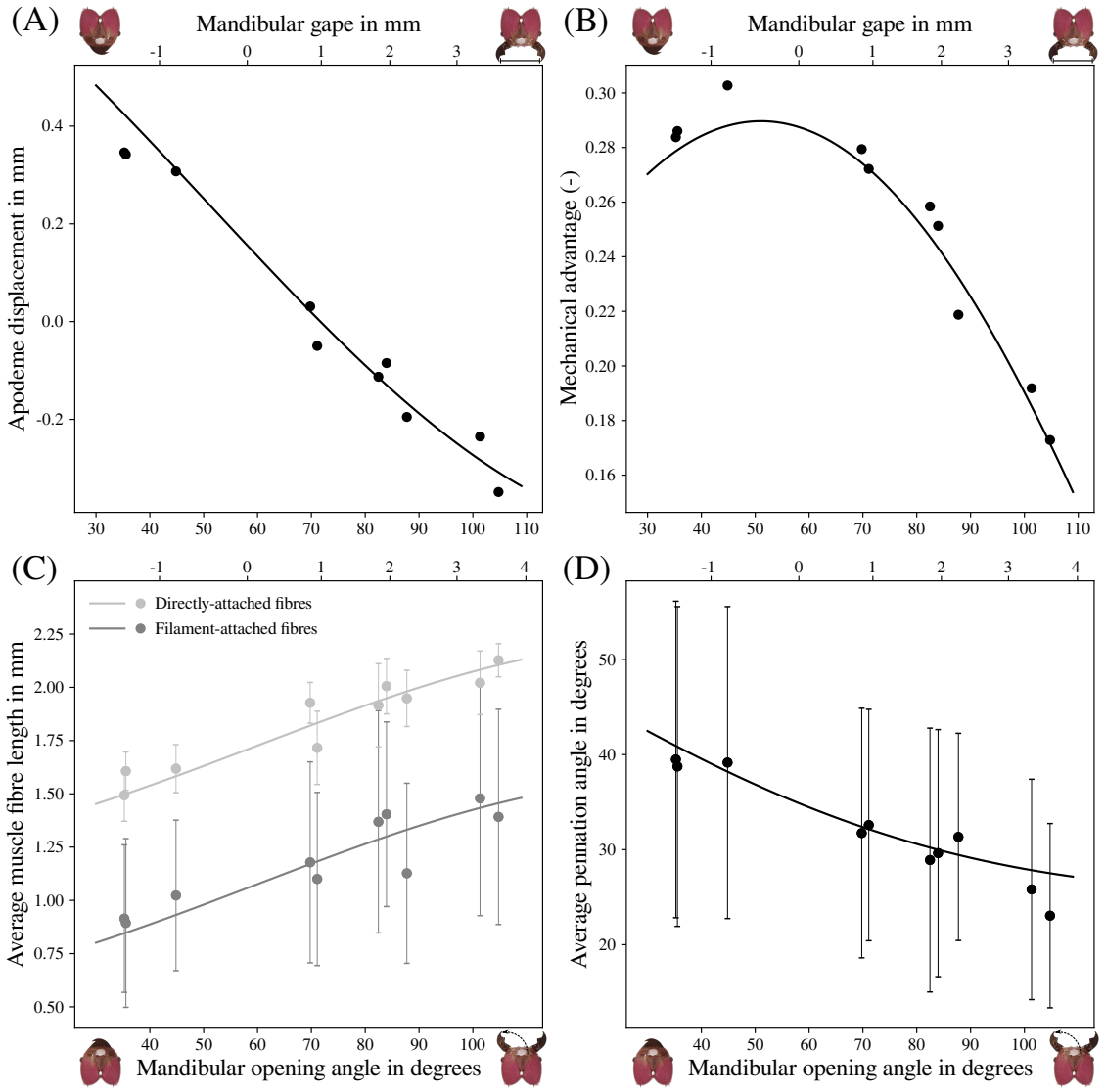


FIGURE 3.5: The variation of the relevant morphological parameters with mandibular opening angle, extracted from tomographic scans of *Atta cephalotes* majors, is in excellent agreement with the theoretical predictions. Points and error bars represent the extracted mean $\pm$ standard deviation. The solid lines show the model predictions based on the sample means (see main text); they are not fitted lines. The mandible gape is shown on the upper abscissa. (**A**) Mandible closure is associated with a displacement of the apodeme. Across the opening range, this displacement amounts to around 0.7 mm, or about one-fifth of the average head length. Positive values represent displacements away from the average apodeme position in the posterior direction, and negative values indicate anterior displacements relative to the average position. (**B**) The mechanical advantage is maximal at 51°, close to zero mandible gape, and decreases by a factor of almost two at the largest opening angle. (**C**) The displacement of the apodeme is associated with a change in fibre length, which follows different relationships for directly- and filament-attached fibres (see Eqs. 3.6 and 3.7 in the main text). The resulting *absolute* length changes are similar between both fibre populations ($\approx 0.6\,mm$). However, as directly-attached fibres are much longer on average, their *relative* length change is much smaller. (**D**) As fibres shorten, they rotate and thus change their orientation. Across the opening range, the associated decrease in average pennation angle is around 13°.

70 %. This variation is similar to the range of possible effective outlevers from the most distal to the most proximal sections of the mandibular blade for my study organism and across various insect taxa (Blanke, 2019). The fact that animals can control MA by changing the outlever has previously been discussed in an evolutionary context (Blanke, 2019); that a similar effect, which alters bite force just as much across the opening range, arises from variations in opening angle, however, has received very little attention in both the vertebrate and invertebrate literature (but see S. W. Herring and S. E. Herring, 1974; Weihmann et al., 2015b).

The displacement of the apodeme is associated with a change in fibre length. Both directly- and filament-attached fibres shorten by around 0.60 mm across the opening range, starting from a similar maximum *total* length of 2.11 and 2.07 mm, respectively (see Fig. 3.5C). The absolute changes in fibre length are similar, but with an average filament length of 0.60 mm – equivalent to around 75 % of the smallest fibre length – the relative changes in fibre length differ substantially. The ratio between largest and smallest fibre length is 1.41 for directly-attached fibres, but 1.73 for filament-attached fibres, considerably larger than ratios reported for other insects (1.35 and 1.55 for the mandible closer muscle in stag beetles and cockroaches, respectively, (Goyens et al., 2014b; Weihmann et al., 2015b), and 1.50 for the extensor tibiae muscle in stick insects (Guschlbauer et al., 2007)). Such large changes in relative muscle length are associated with a substantial decrease in muscle stress (A. Gordon et al., 1966; Josephson, 1975, and see section 3.4.3), which seemingly favours a direct muscle attachment over filament-attachment. The abundance of directly-attached fibres, however, is likely limited by space constraints in the head capsule; filament-attachment increases the effective internal muscle attachment area to the apodeme, so that its net effect may still be an increase in muscle force (Paul and Gronenberg, 1999, and Chapter 2).

In addition to changes in fibre length, the apodeme displacement is associated with changes in average pennation angle (see Fig. 3.5D). ϕ is around 41° at low opening angles and decreases to 27° at large angles. The notable standard deviation of the measured angles (and fibre lengths, see Fig. 3.5C) does not reflect measurement error (see method validation), but the multi-pennate architecture of the closer muscle in *Atta* ants (see Gronenberg et al., 1997, and Chapter 2). The decrease of ϕ is steepest at small opening angles, and flattens towards larger angles (see Fig. 3.5D). This pattern is driven by two effects: First, at large opening angles, the apodeme attachment point displaces mostly laterally, due to the small apodeme angle. As a consequence, the longitudinal displacement, which controls fibre rotation, is small. Second, the change in pennation angle per unit apodeme displacement is determined by the magnitude of the pennation angle itself, and is largest for large pennation angles.

The decrease in ϕ increases the fraction of the muscle force aligned with the apodeme by about 20 %, $\cos(27°)/\cos(41°) \approx 1.18$, more than twice as much as reported for cockroaches (Weihmann et al., 2015b). This increase is nevertheless small, and insufficient to balance the reduction in force due to the decrease in MA (Fig. 3.5B). There exists a further notable difference between the two parameters: the pennation angle will always be maximal for small opening angles and then decrease

monotonously to a minimum at large opening angles (see Fig. 3.1). In sharp contrast, the effective in-lever is largest at $\gamma = 90^{\circ}$, which could be achieved at any opening angle by relatively small changes in mandible shape, so resulting in non-monotonous variation across the opening angle range. These observations suggest two different functional roles for the pennation and apodeme angle: The variation in pennation angle is likely irrelevant for the change in force magnitude across opening angles. However, large pennation angles increase the maximum possible physiological cross-sectional area in the limited volume of the rigid head capsule, and thus control the total magnitude of the bite force (Wheater and Evans, 1989; Paul and Gronenberg, 1999, and Chapter 2). Pennation also results in 'displacement' gearing (see Brainerd and Azizi, 2005; Azizi et al., 2008), which reduces the fibre strain required to cover the same range of opening angles. This reduction is important, because muscle stress may decay steeply with fibre length; it is, however, difficult to draw direct conclusions from it, because the interactions between pennation angle, fibre strain, muscle stress, and the maximum possible muscle size in a closed volume are subtle and require a more detailed parametric analysis than is within the scope of this study. The apodeme angle, in turn, does not meaningfully alter the maximum magnitude of the bite force. However, because it can increase or decrease with opening angle, it can be used to counter or magnify any changes in bite force arising from force-length effects – it is a more flexible gearing parameter across the opening range than the pennation angle. The possible 'design space' spanned by these two parameters is thus large, and presents an interesting area for comparative work.

I have demonstrated that the variation of the key morphological design parameters of the insect bite apparatus with opening angle can be accurately predicted from first principles. Next, I show that the knowledge of these relationships can be used to extract the physiological properties of insect muscle, which remain understudied (but see Gronenberg et al., 1997; Guschlbauer et al., 2007).

3.4.2 Leaf-cutter ants are extremely specialised for large bite forces, and bite strongest at opening angles relevant for cutting

I used the deductive power of my geometrically validated biomechanical model to extract the force-length properties of the mandible closer muscle. To this end, I performed *in-vivo* bite force measurements across a large range of opening angles, 50-105°, and extracted the magnitude of the maximum bite force at each opening angle via Eq. 3.8. To test if the ants bit with maximum activation, I compared voluntary and electrically stimulated bite forces. There was no significant difference between the maximum voluntary and stimulated bite forces for neither small nor large bite plate distances [Welch Two Sample t-test, 1 mm distance: $t_{5.68}$ = -0.04, p = 0.97; 2.5 - 3 mm distance: $t_{9.69}$ = -1.76, p = 0.11, see Fig. 3.4B]. Consequently, ants appear to maximally activate their muscle during the bite force measurements, independent of the mandibular opening angle, and undeterred by the rigid material of the bite plates (but see Lappin and M. E. Jones, 2014).

In order to characterise the physiology of the mandible closer muscle, I extracted maximum muscle stress, optimum fibre length, and the force-length shape parameter β, via a non-linear least squares

fit of Eq. 3.1. The resulting fit yielded optimum fibre lengths of $L_{opt} = 1.42$ mm [95 % CI (1.17; 1.66)] for directly-attached fibres, and $L_{opt} = 0.92$ mm [95 % CI (0.79; 1.07)] for filament-attached fibres. I used L_{opt} to extract the physiological cross-sectional area of the muscle at a defined point on the force-length curve (see 3.2), $A_{phys} = V_m/L_{opt} = 4.3 \pm 0.4\,\text{mm}^2$. The maximum muscle stress was fitted as 1.16 MPa [95 % CI (1.06; 1.26)], at the upper end of values reported for arthropod muscle, which are typically below 1 MPa (Wheater and Evans, 1989; Full and A. Ahn, 1995; Guschlbauer et al., 2007; Goyens et al., 2014b; Weihmann et al., 2015a; David et al., 2016a, but see Blundon, 1988; G. M. Taylor, 2000). I caution against strong conclusions on the basis of this comparison, because most of the published muscle stress estimates do not represent the 'true' maximum muscle stress, as they do not stem from direct or indirect measurements of force-length properties. Based on the difference in average sarcomere length, it is likely that the true stress of some crab pincher muscles, for example, exceeds my estimate for leaf-cutter ant closer muscle (see Gronenberg et al., 1997; G. M. Taylor, 2000), which may suffer further from shrinkage effects arising from CT sample preparation (Barbosa et al., 2015).

The shape parameter was fitted as $\beta = 5.34$ [95 % CI (0.09; 10.59)]. Data on the force-length properties of arthropod muscle are surprisingly scarce. In order to assess the plausibility of this result, force-length data were extracted from published work, all forces were normalised with maximum force, all lengths with optimum length, and Eq. 3.5 was fitted with a non-linear least-squares algorithm. The shape parameter for *Atta* closer muscles is close to the shape parameter for fibres from the extensor carpopoditi muscle of the European crayfish ($\beta = 6.27$, 95% CI (5.72; 6.84), Zachar and Zacharová, 1966), the extensor tibiae muscle of Indian stick insects ($\beta = 3.95$, 95% CI (3.29; 4.71), Guschlbauer et al., 2007), fibres from the meropodite muscle of walking legs of Orconectes crayfish ($\beta = 6.61$, 95% CI (5.87; 7.41), April and Brandt, 1973), and the abdominal ventral superficial muscle of Hermit crabs ($\beta = 6.46$, 95% CI (5.25; 7.87), Chapple, 1983). However, it is substantially smaller than values for extensor muscles in the coxa of discoid cockroaches ($\beta = 12.18$, 95% CI (11.10; 13.30), A. N. Ahn et al., 2006), the respiratory muscle in green crabs ($\beta = 26.66$, 95% CI (13.07; 56.23), Josephson and D. R. Stokes, 1987), and the (synchronous) mesothoracic dorso-longitudinal muscle of *Manduca sexta* moths ($\beta = 58.65$, 95% CI (52.89; 64.59), Tu and Daniel, 2004). In light of the considerable variation in both sarcomere lengths and the ratio between thick and thin filaments in arthropod muscle (G. M. Taylor, 2000; Shimomura et al., 2016), this large range may not be surprising, and suggests exciting opportunities for comparative muscle physiology.

My biomechanical model captures the general shape of the variation of bite force with opening angle both quantitatively and qualitatively. The agreement between prediction and observation, however, is arguably less convincing than for the geometric relations alone in at least two aspects (see Fig. 3.6A). First, at the largest opening angles, the fit systematically underestimates the measured bite forces, which remain approximately constant for $\theta > 90^\circ$. This disagreement partially reflects passive joint forces, which may contribute about 50 mN (see Appendix B, and Weihmann et al., 2015a), as well as passive muscle forces, which can reach 20 % of the maximum isometric force at large fibre strains (Azizi, 2014). Second, close to the fitted maximum, the spread of measured bite forces is large. At

small opening angles, the misalignment angle between measurable and bite force vector is most extreme (see Eq. 3.8). The increased variation may thus represent a combination of biological variation and small errors in landmark placement, amplified by larger correction factors. For measurements at small opening angles (< 65°), the average correction was $28 \pm 25\,\%$, compared to only $5 \pm 4\,\%$ for measurements at larger angles.

I measured maximum bite forces of 1.4 N, equivalent to about 2600 times of the mean body weight of the ant workers. Maximum bite forces were measured at small opening angles ($< 65°$, see Fig. 3.6A), and bite force decreased steeply with opening angle to a minimum of 0.3 N at 100° - a total variation of a factor of five. Considering the comparatively small size of the ants (50-60 mg), these forces are rather remarkable indeed: Alexander conducted a literature review of the maximum forces exerted during various activities, including biting, by animals spanning ten orders of magnitude in mass (Alexander, 1985). He reported an upper bound for weight-specific forces of $F_{max} = 20\,\mathrm{m}^{-1/3}$, where m is the body mass in kg. The expected value for a 55 mg leaf-cutter ant is $F_{max} = 20\,(55\ 10^{-6})^{-1/3} \approx 500$. Leaf-cutter ants thus bite with a force around five times larger than expected for an animal of their size; these values even surpass those from other unusually strong animals such as crabs (G. M. Taylor, 2000). The specialisation of leaf-cutter ants to produce large bite forces is even more startling in the context of muscle force: Leaf-cutter ants exert maximum muscle forces of $\sigma_m A_{phys} \approx 5\,\mathrm{N}$ – around 9000 times their body weight. A typical upper bound for maximum weight-specific muscle force is $50\,\mathrm{m}^{-1/3}$ (Alexander, 1985), or ≈ 1300 for leaf-cutter ant majors – almost an order of magnitude smaller than the observed value. Clearly, leaf-cutter ants are extremely specialised to produce large bite forces.

Having fully characterised peak bite forces, and the key physiological and morphological parameters of the mandible closer muscle in *Atta* majors, I can asses the relative importance of physiology or morphology for the bite force-gape relationship (see Eq. 3.1). The majority of this variation is driven by changes in muscle stress, which varies by a factor of 5.7 (see Fig. 3.6B); the mechanical advantage decreases by a factor of 1.7. These effects are slightly attenuated by the decrease in pennation angle, which effectively increases the bite force for large opening angles by 18 %. Remarkably, if all parameters were optimum at the same opening angle, the maximum bite force would increase by only ≈ 15 %. Compared to the significant variation in muscle stress and mechanical advantage, this 'lost' potential appears rather small, and it is mainly driven by the pennation angle, which is anatomically constrained. The bite apparatus in leaf-cutter ants thus seems to have an architecture close to a theoretical optimum; the muscle volume density approaches its theoretical maximum (see Chapter 2), and pennation angle, apodeme angle and optimum fibre length are all 'synchronised' such that bite force peaks in a narrow range of opening angles (centred around 47°). The opening angle range where bite forces are maximal corresponds to small mandible gapes (< 0.5 mm). This range is most critical in the context of the typical behaviour displayed during leaf-cutting, because fresh cuts are often initiated with 'scissor-like' cuts through the leaf lamina, and the average lamina thickness of tropical leaves is around 0.25 mm (Onoda et al., 2011). When propagating cuts through the lamina, ants often use a large range of opening angles (Tautz et al., 1995); however when encountering thick

veins that require high bite forces, mandibles open only very little (see SI in R. M. Schofield et al., 2011). Leaf-cutter ants may thus adjust their cutting behaviour in accordance with the steep decrease of bite force for opening angles $> 75°$. These results represent a key step towards understanding the intricate relationship between cutting behaviour, maximum bite force and mandibular opening angle in *Atta* foraging (also see Chapter 4).

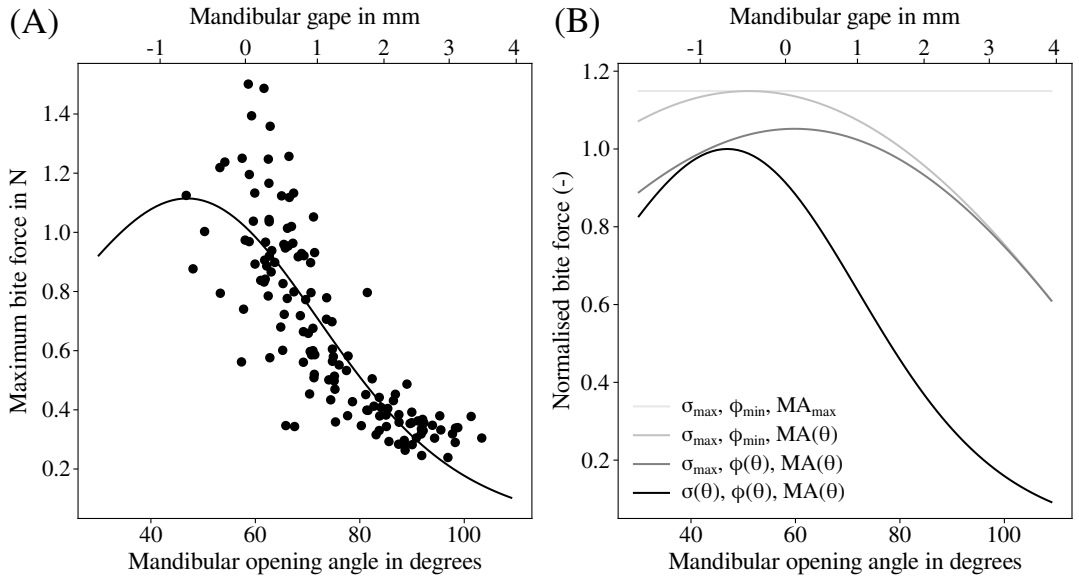


FIGURE 3.6: (**A**) Bite forces of *Atta cephalotes* majors were measured across mandibular opening angles between 50 and 105°. Bite forces peak at small opening angles, and decreased to around one-fifth of that maximum at 100°. The solid line is a least-squares fit of Eq 3.1 which accounts for the variation of both morphological and physiological determinants of bite force. For the largest opening angles, the model underestimates the measured forces, which may be partially attributed to passive joint forces (see Appendix B). The peak muscle force associated with peak bite forces is 9,000 times larger than the mean body weight of the ants – a factor of seven larger than expected for animals of this size (see main text). (**B**) The variation in bite force is driven by changes in muscle stress and mechanical advantage. The pennation angle, on the other hand, mainly modulates the maximum bite force magnitude. The black line represent the fitted relationship between bite force magnitude and opening angle, $|\mathbf{F}_b|(\theta)$, normalised with its maximum. The grey lines show the theoretical relationships between bite force and opening angle, if muscle stress, the cosine of the pennation angle, and the mechanical advantage were progressively fixed at constant values equal to their respective maxima. If these parameters were all maximal at the same opening angle, the maximum bite force would increase by a mere 15 %. Because muscle volume occupancy is also close to its maximal theoretical value (see Chapter 2), leaf-cutter ant heads are close to a morphological optimum for maximum bite forces.

3.4.3 Minimal models for the magnitude of bite force and its variation with gape

I have demonstrated that both the magnitude of bite force and its variation with gape can be accurately predicted from first principles. Many individual components of my biomechanical model have been discussed by colleagues previously (e. g. S. W. Herring and S. E. Herring, 1974; Wheater and Evans, 1989; Heethoff and Norton, 2009; Freeman and Lemen, 2010; Habegger et al., 2012; Goyens et al., 2014b; Weihmann et al., 2015a; Lowie et al., 2022, and Chapter 2). However, a comprehensive analysis which combines all elements into one single model has to my knowledge been absent from

the literature. The advantage of a complete first principle model is that it is as accurate as the estimates of the relevant parameters which define it. The problem is that many of these parameters are time-consuming and costly to measure. Accordingly, there has been considerable interest in 'minimal' bite force models, where some parameters are either replaced with first order approximations, scaling relationships, or proxies identified via statistical analysis (G. M. Erickson et al., 1996; Dumont and Herrel, 2003; Meij and Bout, 2004; Herrel et al., 2005; R. A. Anderson et al., 2008; Heethoff and Norton, 2009; Freeman and Lemen, 2010; Santana et al., 2010; Sakamoto et al., 2019; Lowie et al., 2022). As an illustrative example, head width has repeatedly been shown to correlate tightly with bite force in vertebrates, which seemingly makes bite force predictions rather straight forward (e. g. Herrel et al., 2005, 2018; Lowie et al., 2022). Due the extraordinary attractiveness of a minimal bite force model for ecologists, palaeontologists, evolutionary biologists and biomechanists alike, I next discuss the implications of my analysis for such models in insects; first with respect to the magnitude of the absolute bite force, and then for its variation with gape. In probing the accuracy with which the magnitude of the maximum bite force can be predicted without full knowledge of all parameters, I am assessing an upper bound, corresponding to the assumption that all relevant parameters take their maximum value at the same opening angle (see Fig. 3.6B). By separating the question of bite force variation with gape from its absolute value, I am then considering only *relative* changes of bite force with gape.

The maximum distal mechanical advantage of the mandible bite apparatus in insects varies between 0.3 - 0.8 across a broad range of insect orders (Blanke, 2019). Using a value in the middle range of $MA \approx 0.55$ is thus associated with an uncertainty of less than a factor of two. A more accurate proxy may be obtained by measuring the ratio between mandible width and length (see e. g. Wheater and Evans, 1989). The mandible length is likely a relatively accurate proxy for the outlever, because the uncertainty associated with the location of the joint centre will be small compared to its length. The mandible width, however, may be a poor proxy for the inlever, which is typically shorter than the outlever, but subject to the same absolute uncertainty.

Average pennation angles of mandible closer muscles in insects are smaller than 45° (data exists for ants, beetles, and cockroaches, Paul and Gronenberg, 1999; D. Li et al., 2011; Weihmann et al., 2015b, and Chapter 2). The direct influence of pennation on bite force magnitude is thus negligible, $\cos\phi \approx 1$.

An accurate measure of A_{phys} is perhaps most challenging to obtain: it requires knowledge of muscle volume, and crucially, the optimal fibre length. L_{opt} is typically unknown, and can only be estimated from transmission electron microscopy images of muscle tissue (to measure thick and thin filament length and lattice spacing), or via knowledge of all other parameters and bite force measurements (this study). Using the physical cross-sectional area of muscle at an arbitrary but naturally occurring muscle length is associated with an error directly related to the strain range of the muscle: because muscle is incompressible, any change in its length is associated with a change in its cross-sectional

area such that volume is conserved, $A = V/L$. If L_{opt} was overestimated by 70 %, corresponding to the maximum fibre length ratio extracted in this study, A_{phys} would be underestimated by $1 - 1/1.7 \approx 40$ %. However, even this proxy requires knowledge of muscle volume and fibre length, and thus CT data and advanced fibre tracing algorithms (see Chapter 2). Due to these difficulties, a large number of proxies have been used in the literature, including head size, the surface area of the apodeme (Elner and Campbell, 1981), or the muscle attachment area to the head capsule (Goyens et al., 2014b). Head size is arguably the most attractive proxy for A_{phys}, for it represent the best compromise between accuracy and ease of measure; head volume can be readily estimated from head length, width and height, $V_h \approx H_w H_h H_l$, with simple light microscopy. In insects, both mandible closer muscles typically occupy between 10 and 50 % of the total head volume V_h (D. Li et al., 2011; Weihmann et al., 2015b; Lillico-Ouachour et al., 2018 and Chapter 2, but see Paul, 2001). The volume of a single closer muscle can thus be estimated as $V_m \approx 0.3/2\, H_w H_h H_l$. L_{opt}, in turn, is some fraction of a linear head dimension. The most suitable dimension may be head height, as the region where it takes its maximum value is mainly occupied by closer muscle (see D. Li et al., 2011; Weihmann et al., 2015b; Lillico-Ouachour et al., 2018, and Chapter 2). It follows that $L_{opt} \approx 0.5 H_h$, and $A_{phys} = V_m / L_{opt} \approx 0.3 H_w H_l$. This estimate has an error similar to the suggested approximation for the mechanical advantage, and is as good as the implicit yet untested assumption of isometry across animals of wildly different sizes.

The maximum muscle stress is the parameter most prone to variation; estimates for arthropods vary by almost two orders of magnitude (0.04 - 2.2 MPa, see Blundon, 1988; Full and A. Ahn, 1995; G. M. Taylor, 2000; Guschlbauer et al., 2007; Weihmann et al., 2015a). This large range limits the accuracy of a mean stress to one order of magnitude at best (Weihmann et al., 2015a), and is likely at least partially owed to the experimental methods with which stress has been estimated. Force measurements with isolated insect muscle let alone single fibres are rare (e. g. Full and A. Ahn, 1995; A. N. Ahn et al., 2006; Guschlbauer et al., 2007). Most often, stress is estimated from more integrated bite/pinch force measurements instead (e. g. Wheater and Evans, 1989; G. M. Taylor, 2000; Weihmann et al., 2015a, and this study). Any such estimation of muscle stress, however, is subject to the uncertainties in determining MA and A_{phys} discussed above. A more accurate peak muscle stress estimate may be obtained from the average fibre sarcomere length, S_l (G. M. Taylor, 2000, but see Oka et al., 2016). To this end, all non-vertebrate data were extracted from the classic work of Taylor, and a standardised major axis regression was conducted, $\sigma \sim S_l$, in log-log space. For sacromere lengths between 3 - 17μm, this relationship reads $\sigma_{max} = 50 S_l$, where S_l is in μm and σ_{max} is in kPa, which explains about 75% of the variation in stress with sarcomere length. The remaining variation is likely attributed to variations of the relative fibre length at which forces were measured and generic measurement error. The scaling coefficient of unity is robust (and has a theoretical foundation), but the proportionality constant of 50 kPa μm^{-1} is again subject to uncertainty in A_{phys}, required to convert the measured force to a stress (for example, my measurements in *Atta* are a noteworthy outlier). Taylor estimated A_{phys} as the surface area of the apodeme multiplied with sin(ϕ) (G. M. Taylor, 2000, also see Govind and Blundon, 1985; Wheater and Evans, 1989). The error in measuring apodeme

surface area is likely small, but the error in assuming that it is equal to the muscle attachment area is $\geq$ 10% (the maximum packing density of a lattice of circles). The total uncertainty associated with this approximation for stress is thus at least 35%. Although measuring sarcomere length is technically involved, the significant reduction in uncertainty for the maximum stress associated with it may make these measurements well worthwhile.

I conclude the discussion for maximum bite force by summarising that the simplest reasonable estimate for the maximum bite force requires only knowledge of head width and length. However, this estimate may at worst only be accurate to less than an order of magnitude. The next best estimation replaces the maximum stress with a proxy based on sarcomere length, and reads:

$$F_{max} = \underbrace{MA}_{0.55} \underbrace{\cos\phi}_{1} \underbrace{A_{phys}}_{0.3H_wH_l} \underbrace{\sigma_{max}(S_l)}_{50S_l} \approx 8.25\,\mathrm{kPa}\,\mu\mathrm{m}^{-1} H_w H_l S_l \tag{3.9}$$

If we use an intermediate sarcomere length of 10 μm (G. M. Taylor, 2000), Eq. 3.9 simplifies to $F_{max} \approx 83\,\mathrm{kPa}\,H_wH_l$. The effort required to measure sarcomere length is rewarded with a reduction in the worst-case error by at least a factor of about five.

Next, I address the variation of bite force with gape, which has received even less attention than maximum bite force, but is of similar ecological significance (e. g. S. W. Herring and S. E. Herring, 1974; Dumont and Herrel, 2003). The cosine of the average pennation angle will typically vary at most between unity and 0.7 between maximally open and fully closed mandibles, respectively ($\cos 0°$ and $\cos 45°$, see section 3.4.1); this variation is small enough that it can be neglected, $\cos[\phi(\theta)] \approx$ constant. Instead, the variation of bite force with opening angle is likely dominated by changes in muscle stress due to changes in muscle length; such effects are particularly pronounced when fibre strain and shape parameter β are large, and L_{opt} occurs at fully open or closed mandibles (this study). β appears to cluster around $\approx$ 6, but may be twice as large in some muscle (see section 3.4.2). The variation of the mechanical advantage can be significant, but much of this variation is governed by the apodeme angle γ, which can be measured relatively easily. Perhaps the most important *and* most often neglected source of variation comes from the joint rotational axis. $\hat{\mathbf{R}}$ affects virtually all bite force determinants, apart from A_{phys}, and also influences the accuracy of bite force measurements themselves (see Eq. 3.8). In order to gain some intuition for both the error and the variation of force-gape curves which can be associated with variations in $\hat{\mathbf{R}}$, I calculated the relationship between $|\mathbf{F}_b|$ and opening angle using a set of 50 alternative rotational axes, located at the same joint centre, but oriented at an angle between 5 and 25° relative to the original $\hat{\mathbf{R}}$ (all other parameters were kept constant). The resulting variation, normalised with the original relationship $|\mathbf{F}_b|(\theta)$, is substantial, and includes a large range of different force-gape relationships (see Fig. 3.7). As illustrative examples, an axis deviating by only 10° alters the force prediction by up to 20% compared to the original relationship $|\mathbf{F}_b|(\theta)$; an axis deviating by 25° causes changes of up to 50%. Misidentifying the joint centre would lead to additional significant variation affecting both levers, the predicted apodeme

displacement, and all associated parameters. For species with two well-developed condyles, the location and orientation of $\hat{\mathbf{R}}$ may be identified with reasonable accuracy from joint morphology alone, as previously done for beetles (D. Li et al., 2011; Goyens et al., 2014b), cockroaches (Weihmann et al., 2015b) and dragonflies (David et al., 2016b). Other insects such as some hymenopterans, however, have more complex mandible joints (A. Richter et al., 2019, 2020), which may also have more than one degree of freedom (Gronenberg et al., 1998b; W. Zhang et al., 2020b; Kamp et al., 2022), rendering such deductions difficult (but see A. Richter et al., 2021, V Kang, F Püffel and D Labonte, in preparation). Given the sensitivity of bite forces to the joint axis, it is surprising how little attention has been paid to rigorously determine joint kinematics across the insect tree of life using the tools of rigid body mechanics (but see W. Zhang et al., 2020b, and V Kang, F Püffel and D Labonte, in preparation). Any attempt to predict or measure the bite force-gape relationship needs to take due note of the importance of $\hat{\mathbf{R}}$ in order to avoid significant errors.

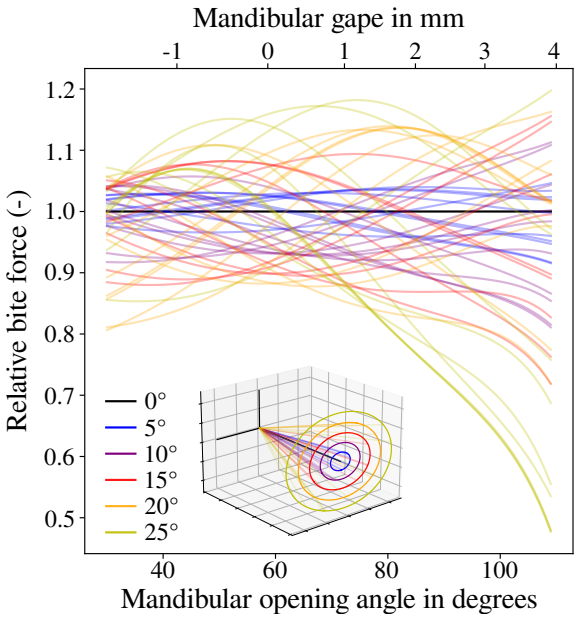


FIGURE 3.7: The variation of bite force with opening angle strongly depends on the mandible joint axis of rotation. A seemingly small variation in this axis of only 15°, changes the relative bite force prediction by up to 30 %. The coloured lines represent the theoretical relationships between bite force and opening angle for 50 randomly generated axes of varying angles to the actual axis (black), normalised with the fitted relationship, $|\mathbf{F}_b|(\theta)$. Clearly, the axis of rotation is an absolutely crucial parameter if the variation of bite force with opening angle is to be predicted accurately.

3.5 Conclusion and outlook

I presented a validated model which predicts the bite force-gape relationship in arthropods from first principles, based on a minimum set of assumptions. I hope that my work will be useful for future studies on the bite performance in arthropods in at least three aspects. First, it enables *in-vivo* extraction of force-length properties from bite force measurements, which remain scarcely reported in the literature. The significant variation of the physiological make-up of insect muscle suggests exciting

avenues for comparative muscle physiologists, and my model allows colleagues to side-step challenging measurements with tiny isolated muscle fibres. Second, my model identifies the key determinants of maximal bite forces, including a 'minimal' bite force model, and so facilitates comparative analyses of the functional morphology of the insect bite apparatus, including rare, small or extinct species, for which bite force measurements may be impossible. Third, it provides clear guidance on how muscle morphology and physiology translate into a variation of bite force with gape, which is of significant ecological and behavioural relevance, for example in the analysis of feeding guilds or niche formation. Indeed, the increasing number of high-resolution CT scans of insect heads offers tantalising opportunities to study the bite force-gape relationship across the insect tree of life without the need for direct bite force measurements. Notably, systems that operate close to the maximum possible bite force, such as in leaf-cutter ants, will suffer from a steeper decrease in bite force at opening angles departing from the optimum, suggesting that the functional morphology of the bite apparatus is subject to a trade-off. All three points will contribute to our general understanding of the performance, behaviour, ecology and evolution of arthropods.

4 Scaling of maximum bite forces

I acknowledge the contributions of Flavio Roces, who kindly provided the ant colonies.

Summary

Atta leaf-cutter ants are the prime herbivore in the Neotropics: polymorphic foragers harvest plant material from the nest surroundings to grow a fungus as crop. Efficient foraging involves complex interactions between worker-polymorphism, task-preferences and plant-fungus-suitability; it is, however, ultimately constrained by the ability of differently-sized workers to generate forces large enough to cut vegetation. In order to quantify this ability, I measured bite forces of *A. vollenweideri* leaf-cutter ants spanning more than one order of magnitude in body mass. Maximum bite force scaled almost in direct proportion to mass; the largest workers generated peak bite forces 2.5 times higher than expected from isometry. This remarkable positive allometry can be explained via a biomechanical model that links bite forces with substantial size-specific changes in the morphology of the musculoskeletal bite apparatus. In addition to these morphological changes, I show that bite forces of smaller ants peak at larger mandibular opening angles, suggesting a size-dependent physiological adaptation, likely reflecting the need to cut leaves with a thickness that corresponds to a larger fraction of the maximum possible gape. Via direct comparison of maximum bite forces with leaf-mechanical properties, I demonstrate (i) that bite forces in leaf-cutter ants need to be exceptionally large compared to body mass to enable them to cut leaves; and (ii), that the positive allometry enables colonies to forage on a wider range of plant species without the need for extreme investment into larger workers. My results thus provide strong quantitative arguments for the adaptive value of a positively allometric bite force.

4.1 Introduction

Leaf-cutter ants are remarkable in many ways: They are the world's first farmers; their colonies collect plant material to grow a fungus as crop – a mutualism that originated around 50 million years ago (Mueller et al., 2001; Hölldobler and E. O. Wilson, 2010). They are considered the principal herbivore in the Neotropics; *Atta* ants are estimated to consume about 15 % of the foliar biomass produced by Neotropical trees (H. G. Fowler et al., 1989; Costa et al., 2008). And last, they display a level of polymorphism, linked to size-dependent task-preferences and a complex ecology, exceptional even within social insects (e. g. E. O. Wilson, 1980a; Wirth et al., 2003).

Among the diverse tasks arising in a leaf-cutter ant colony are brood care, fungus gardening, worker transport, soil excavation, nest defence and foraging (E. O. Wilson, 1980a; Hölldobler and E. O. Wilson, 2010; Pielström and Roces, 2013). In particular foraging behaviour has received considerable attention, as it is central to leaf-cutter ant ecology (e. g. E. O. Wilson, 1980a,b, 1983a,b; Rudolph and Loudon, 1986; Wetterer, 1990; Roces, 1990; Roces and Núñez, 1993; Roces and Hölldobler, 1994; Wetterer, 1994a,b, 1995a,b; Burd, 1995; Roces and Hölldobler, 1996; Burd, 1996, 2000a,b, 2001; Farji-Brener, 2001; Röschard and Roces, 2002; Farji-Brener and Sasal, 2003; Röschard and Roces, 2003b; Burd and Howard, 2005; Dussutour et al., 2008; Moll et al., 2010; Röschard and Roces, 2011; Moll et al., 2013). Key to foraging success is the cutting of small fragments from vegetation – the energetically most demanding task faced by the colony (Roces and Lighton, 1995). Although many aspects of foraging involve complex biological interactions (e. g. Roces, 2002), cutting plant fragments is, to first order, a mechanical problem: The ability to cut a leaf or fruit is determined by the maximum available bite force, the morphology of the mandible, and the material and structural properties of the plant. Perhaps surprisingly, this mechanical foundation of leaf-cutting has received comparatively little quantitative attention (e. g. Tautz et al., 1995; R. M. Schofield et al., 2011, 2016). Larger workers may be reasonably expected to produce larger bite forces, and may thus be able to cut a wider range of plant materials. Indeed, they tend to be more likely to cut tougher and denser leaves (J. M. Cherrett, 1972; E. O. Wilson, 1980a,b; Nichols-Orians and Schultz, 1989; Nichols-Orians and Schultz, 1990; Wetterer, 1991a). Understanding the exact relation between bite force and worker size is crucial for the analysis of leaf-cutter ant foraging behaviour, because it holds the key to distinguish between foraging assignments based on ability (which ants can cut a given leaf) vs. suitability (which ants should cut a given leaf).

This distinction is relevant for assessing the evolution and possible adaptive advantage of worker polymorphism, and for predictions on 'optimal' foraging strategies based on ergonomic considerations (e. g. E. O. Wilson, 1980b; Wetterer, 1991a; Burd and Howard, 2005).

I previously predicted the scaling of bite force based on the morphology of the bite apparatus in *Atta vollenweideri* leaf-cutter ants (see Chapter 2). However, direct experimental confirmation of this prediction is missing and is difficult to obtain, because ants are small. To make matters worse, bite forces in insects generally depend on the mandibular opening angle (Goyens et al., 2014b; Weihmann et al., 2015a, and Chapter 3), which is challenging to control experimentally. Here, I address both difficulties with the help of a custom-built bite force set-up and first principles biomechanical analysis. I report direct bite force measurements for ant workers spanning more than one order of magnitude in body mass, relate my results to the foraging behaviour of leaf-cutter ant colonies, and discuss both the magnitude and scaling of bite forces in a comparative framework.

4.2 Materials & methods

4.2.1 Study animals

Bite force experiments were conducted with *A. vollenweideri* ants from three colonies, all founded and collected in Uruguay in 2014 (see Fig. 4.1A). The colonies were kept at 25°C and 50 % humidity in a climate chamber under a light:dark cycle of 12 h:12 h, and were fed with fresh bramble leaves, cornflakes and honey water *ad libitum*. I collected around 80 workers from the foraging areas of each colony (n = 248), covering approximately the entire size range (1 - 50 mg). I excluded minims (body mass < 1 mg), because their bite apparatus is morphologically distinct, and they do not generally partake in foraging (see Chapter 2, and N Imirzian, F Püffel and D Labonte, in preparation).

4.2.2 Experimental set-up

Bite forces were measured with a custom-built set-up based on a capacitive force sensor (SingleTact S8-1N, Pressure Profile Systems, Inc., California, USA, data acquisition frequency 33 Hz, maximum force 1 N, resolution 2 mN). In order to distribute the force equally across the sensor area, I used a lever mechanism to convert *point*-like bite forces into an *areal* compression (see Fig. 4.1B). Ants bit onto two thin bite plates (1 mm long, and $\approx$ 0.15 mm thick, see Fig. 4.1C), protruding from two mechanically uncoupled beams (6 x 6 x 40 mm and 6 x 12 x 6 mm, respectively). Both beams and the terminating bite plates were manufactured in one single piece from stainless steel to minimise compliance, using electrical discharge machining. The beam that transmits the bite force to the sensor was connected to a metal base plate, made from a single aluminium block using CNC milling, via a small hinge placed in the beam centre. As an ant bites onto the bite plates, the opposite end of this pivoting beam is pressed onto the sensor, which is glued to a vertical wall protruding from the base. At the maximum load of 1 N, the sensor only deforms approximately 10 μm [manufacturer data]. Because the gear ratio of the pivoting beam is unity, the magnitude of this deformation is equivalent to the maximum displacement of the bite plate arising from beam rotation. As bite plate bending is also negligible (see Appendix C), I measured approximately isometric bite forces. The second beam, in turn, was connected to a lubricated rail, so that its position relative to the pivoting beam can be altered via a stepper motor (28BYJ-48, 5 V), connected to a gearing system 3D printed from PLA. This design allowed me to vary the distance between the two bite plates by less than 100 μm per motor step. The minimum required gape to bite both bite plates, equivalent to the shortest distance between their outer surfaces, was 0.5 mm, and the largest gape used during experiments was 3.0 mm. This range is similar to the range of head widths of the ants used in this experiment (1.1 - 4.5 mm).

In order to extract coordinates of key landmarks (see section 4.2.5), a top-down camera was synchronised to the sensor recording, and recorded the bite experiments at 30 fps, (camera module v 2.1, 8 MP, Raspberry Pi Foundation, Cambridge, UK; with a Black Eye HD macro lens, Eye Caramba Ltd., Helsinki, Finland). A mirror, tilted 45° with respect to the camera plane, provided depth information. Force sensor, motor, camera and a touchscreen (7 inch HDMI-LCD Display, Elecrow, Shenzhen, China) were connected to a Raspberry Pi (v 3B+, Raspberry Pi Foundation, Cambridge,

UK). The system was operated via a custom software written in Python (v 3.5, see Van Rossum and Drake, 2009, and Appendix C for details on the user interface and circuit).

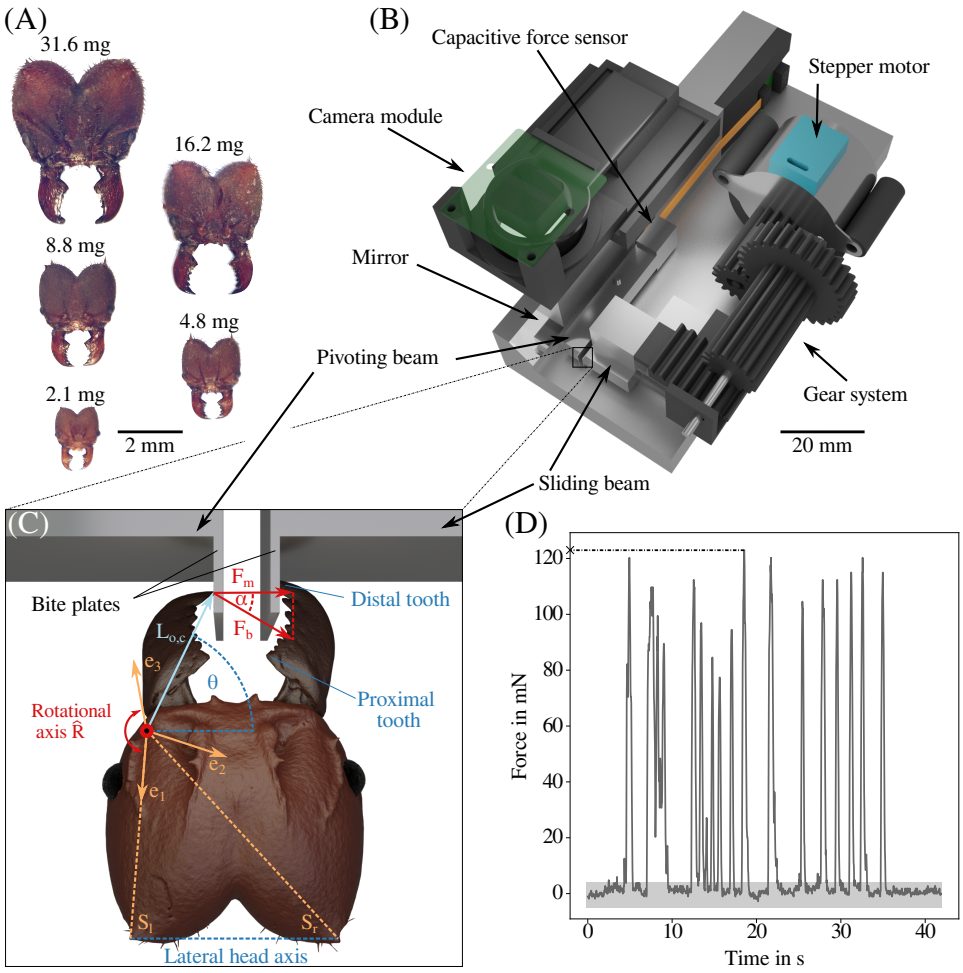


FIGURE 4.1: (**A**) I measured bite forces of polymorphic *Atta vollenweideri* leaf-cutter ants ranging between 1.5 and 46.8 mg in body mass. (**B**) To measure bite forces, I built a custom-designed force setup based on a capacitive force sensor and a lever mechanism. The ants bit onto two bite plates, one protruding from a pivoting beam connected to the force sensor, the other protruding from a sliding beam. The distance between the two bite plates can be varied by moving the sliding beam via a geared stepper motor. Bite experiments were filmed with a top-down camera, which also recorded a side view from a 45° mirror. (**C**) From the video recordings, I extracted the coordinates of the mandible joint centre, head spikes $\mathbf{S}_l$ and $\mathbf{S}_r$, outlever length $\mathbf{L}_{o,c}$, and the most distal and proximal tooth tips. The rotational axis of the mandible $\hat{R}$ was projected onto the local head coordinate system ($\mathbf{e}_1$, $\mathbf{e}_2$, $\mathbf{e}_3$). The mandibular opening angle θ was defined as the angle between the lateral head axis, span by the head spikes, and the projection of the largest outlever onto the plane of rotation. The magnitude of the bite force $|\mathbf{F}_b|$ was extracted from the measured force $|\mathbf{F}_m|$ and the misalignment angle α, measured from the video recordings, as defined by Eq. 4.1. (**D**) From each force trace, the maximum force (cross) was extracted for further analysis. Maximum measured forces exceeded the sensor noise (shaded area) by at least a factor of eight.

4.2.3 Sensor calibration, accuracy and precision

The sensor was calibrated using a series of calibration weights (Kern & Sohn GmbH, Balingen, Germany), suspended from the pivoting lever via a thin cotton thread (the weight of the cotton thread

was small, $\approx 0.015\,\mathrm{g}$, and hence neglected). The thread was placed at around one-quarter of the length of the bite plate measured from its base, resulting in a moment arm around the pivot of $|\mathbf{L}_{p,cal}| \approx 20.25\,\mathrm{mm}$. The set-up was rotated such that the measurable force vector aligned with gravity (see Fig. 4.2A). I used 20 weights between 5 and 100 g; a weight of 1.4 g was required to establish equilibrium around the pivot, and was consequently subtracted from all readings. The range of effective weight forces was hence 35 - 970 mN, approximately spanning the range of measured bite forces. Each weight was suspended five times in random order, and the steady-state sensor reading averaged across $\approx 2\,\mathrm{s}$ was used for sensor calibration. The relationship between weight and sensor output was characterised via an Ordinary Least Squares regression on $\log_{10}$-transformed data in order to prioritise minimisation of relative error over absolute error; the high R-squared of the regression line indicates robust calibration (R^2 = 0.993, see Fig. 4.2A).

To quantify calibration accuracy and precision, five additional weights (7 - 87 g) were measured three times each, and the relative error was calculated as $\epsilon = 1 - |\mathbf{F}_w|/|\mathbf{F}_x|$, where $\mathbf{F}_x$ is the predicted and $\mathbf{F}_w$ is the measured force, respectively (see Fig. 4.2B). The average measurement error, the sensor accuracy, was $2 \pm 6\,\%$ independent of weight [Linear Mixed Model (LMM) with weight as fixed and repetition as random effect: $\chi^2_1 = 0.38$, p = 0.53; the average magnitude of the measurement error was $5 \pm 4\,\%$]; the standard deviation indicates the precision of the measurements.

To quantify sensor noise, the output of the unloaded sensor was recorded for 100 s. Discrete Fourier transformation suggested a constant power spectral density, indicating white noise (Haykin, 2001, p. 61) This noise had a standard deviation of 1 mN and a range of -5 to 4 mN. The maximum positive value of this range was about eight times smaller than the smallest measured bite force (see Fig. 4.1D). Sensor drift was significant [Spearman's correlation coefficient: $r_{s,2867}$ = -0.26, p < 0.001; see manufacture data sheet], but small enough to be inconsequential across the time scale of my measurements (cf. 1 mN/min vs ≈30 - 60 s).

In a last validation step, I directly compared measurements from my set-up with those of an established set-up based on a substantially more expensive piezoelectric sensor (Herrel et al., 1999; Rühr and Blanke, 2022). To this end, maximum bite forces of three house crickets (*Acheta domesticus*) were measured with three repetitions on both set-ups, by two independent operators each. A LMM with set-up and operator as fixed and specimen as random effect showed no significant influence of neither set-up nor operator on bite forces [LMM versus random intercept model: $\chi^2_2 = 3.83$, p = 0.15; set-up: t_{31} = 1.68, p = 0.10; operator: t_{31} = 0.95, p = 0.35].

The camera was calibrated assuming an inverse size-distance relationship, $L_2S_2 = L_1S_1$, where S_1 and S_2 are the apparent sizes of an object at distances L_1 and L_2 to the camera aperture. The apparent size of a calibration target (5 units on 1 mm-grid paper), placed on the top surface of the metal base at a distance $L_1 \approx 32\,\mathrm{mm}$ to the camera, was measured from ten images, and the pixel-to-mm conversion factor C_1 was extracted. This conversion factor changes approximately in direct proportion to the camera distance as $C_2 = C_1L_2/L_1$, where L_2 is the distance between the camera

and the imaged object. In contrast to L_1, L_2 is not constant, but varies with the vertical position of the object coordinate, which was extracted using the mirrored side view.

For validation, the grid paper was photographed at 25 different positions along the bite plate, extracted from five trials, and its physical size was calculated from the calibration. The relative error was 1 ± 2 %. This error changed significantly with grid paper-lens distance – the physical dimensions were increasingly underestimated at smaller distances [LMM with lens distance as fixed effect and trial as random effect: $\chi^2_1 = 6.94$, $p < 0.01$]. This effect, however, was miniscule (1.5 % across the entire bite plate length, 6 mm), corresponding to only $\approx 60\,\mu$m, or about 10 % of the smallest measured mandible length; it is thus considered negligible.

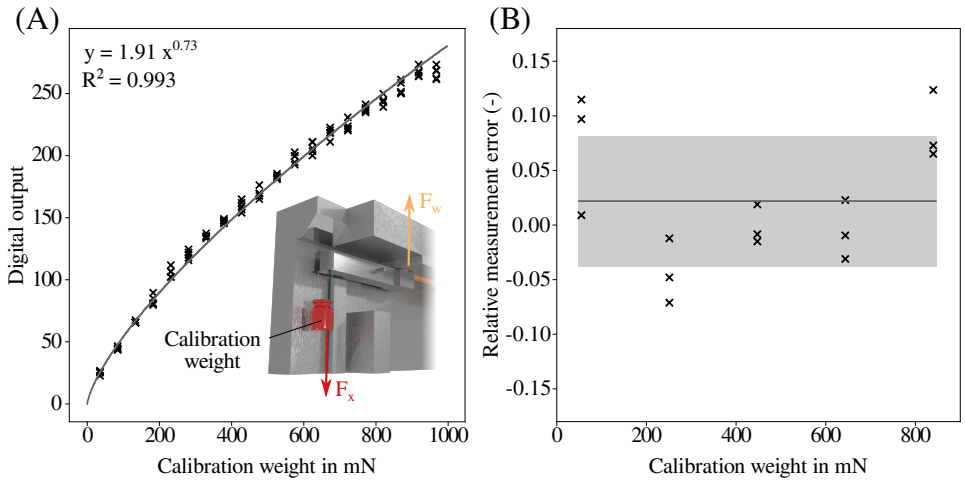


FIGURE 4.2: (**A**) For sensor calibration, I suspended weights between 5 and 100 g from the bite plate of the pivoting lever. A linear regression on $\log_{10}$-transformed data characterised the relationship between measured output and force with high accuracy ($R^2 = 0.993$). (**B**) A subsequent error analysis using intermediate weights between 7 - 87 g yielded relative errors between measured and expected forces of 2 % (accuracy, black line) with a standard deviation of 6 % (precision, shaded area), independent of weight (see main text).

4.2.4 Experimental protocol

To measure bite forces, individual ants were held in front of the bite plates using insect tweezers. Ants were pleasantly eager to bite, typically executing numerous bite cycles in quick succession (see Fig. 4.1D). After completing at least five bite cycles, or exceeding a total bite duration of 10 s, the measurement was terminated, each ant was weighed (AX304 Microbalance, 310 g x 0.1 mg, Mettler Toledo, Greifensee, Switzerland) and isolated, and the maximum force was extracted. To obtain bite forces from a maximum range of sizes and varying opening angles without pseudoreplication, I measured each ant only once at a single bite plate distance. In practice, I gradually increased the bite plate distance from 0.5 to 3.0 mm; for each distance, I used ants of all sizes capable of biting onto the plates. For small plate distances, this included almost all ants; for the largest plate distance, however, only larger specimen were able to bite. I assume that ants bit with maximum muscle activation at all opening angles, as indicated by measurements involving direct muscle stimulation in closely related *Atta cephalotes* (see Chapter 3).

4.2.5 Extraction of landmarks

In order to obtain the opening angle, the orientation of the bite force vector, and the length of the mandible outlever, I extracted the coordinates of a series of landmarks from the video frame corresponding to the time of maximum bite: (i) the contact point between mandible and bite plate; (ii) the tip of the most distal and proximal mandibular teeth; (iii) the mandible joint centre (defined as in Chapter 2); and (iv) a pair of distinct head spikes (see Fig. 4.1C). In addition, I extracted the orientation of the mandible joint axis $\hat{\mathbf{R}}$ via kinematics analysis of the mandible motion (see Chapter 3, and V Kang, F Püffel and D Labonte, in preparation). In order to position $\hat{\mathbf{R}}$ on the biting ant, I introduced a local head coordinate system ($\mathbf{e}_1$, $\mathbf{e}_2$, $\mathbf{e}_3$) based on the vectors connecting the joint centre with the tips of both head spikes, $\mathbf{S}_l$ and $\mathbf{S}_r$, respectively. The coordinate axes were defined as $\mathbf{e}_1 = \mathbf{S}_l/|\mathbf{S}_l|$, $\mathbf{e}_3 = (\mathbf{S}_l \times \mathbf{S}_r)/|\mathbf{S}_l \times \mathbf{S}_r|$, and $\mathbf{e}_2 = \mathbf{e}_3 \times \mathbf{e}_1$. The estimated rotational axis was then projected onto this local head coordinate system (for more details, see Appendix C). In line with previous work (Weihmann et al., 2015b), I define the opening angle as the angle between the lateral head axis and the largest effective outlever $\mathbf{L}_{o,eff,d}$. The lateral head axis was defined as the vector connecting both head spikes (see Fig. 4.1C).

4.2.6 Confounding effects due to size-differences

Measuring bite forces across a large size range poses at least two challenges. First, the signal-to-noise ratio typically decreases with animal size, as smaller animals generally bite with less force. I addressed this challenge by selecting a force sensor capable of measuring small and large bite forces with sufficiently high resolution (see section 4.2.2). Second, the characteristic dimensions of the set-up are relatively larger for small animals. The implications of this size-effect are perhaps less obvious and, unfortunately, more complex. To appreciate the problem, consider a small ant of 3 mg body mass biting onto bite plates that are 1 mm apart. This bite plate distance is approximately equal to the distance between both mandible joints; a bite with the distal-most teeth would thus involve a mandibular opening angle of about $90°$. For a bite with the most proximal teeth, in turn, the opening angle is larger, around $110°$ (see Fig. 4.1A), and the effective outlever is smaller. Consider next a large ant of 45 mg biting onto the same bite plates. For a distal bite, the bite plate distance corresponds to only 40 % of the joint distance, and thus a much lower opening angle of about $70°$. Notably, the ant's ability to bite proximally is limited because the length of the mandible blade exceeds the length of the bite plate by about 20 % (see Fig. 4.1C). Evidently, for a given configuration of the experimental setup, both the range of possible mandibular opening angles and bite positions along the mandible blade vary systematically with size. Because both directly affect the magnitude of bite force (see Eq. 4.2 and Chapter 3), an unbiased comparison of bite force magnitude across animal sizes, requires four corrective steps, implemented here with the ultimate aim to extract the maximum bite force an ant worker can produce when biting with an equivalent point of her mandible (see Fig. 4.3). First, I correct for the misalignment between *measurable* force vector and *applied* bite force vector. Second, I correct for differences in moment arms around the lever pivot, arising from variation of the bite contact point. Third, I account for variation in bite position along the mandible blade, which

alters the mechanical advantage of the force transmission system. Fourth, I account for differences in mandibular opening angle during exertion of the maximum bite force.

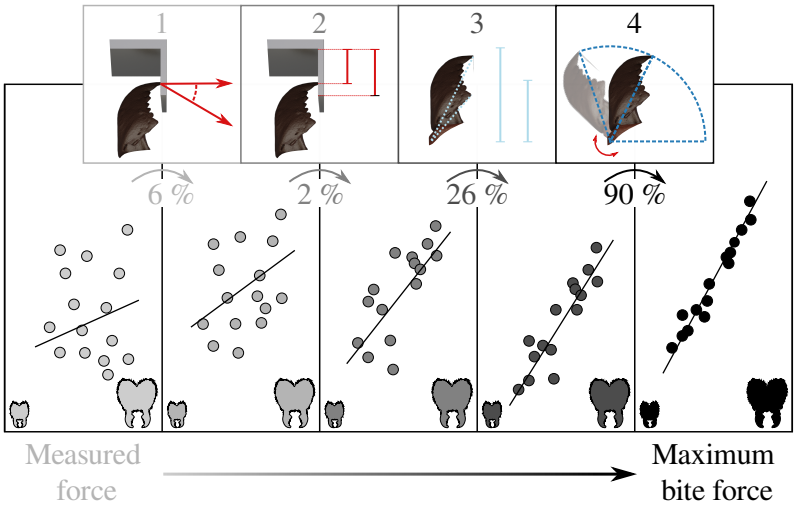


FIGURE 4.3: In order to extract the maximum bite force from the measured data, I account for four confounding effects: First, I account for the misalignment between bite force orientation and the force-sensitive axis. Second, I account for variation in bite contact point on the bite plate, which results in different moment arms. Third, I account for differences in bite position along the mandible blade, which determines the mechanical advantage of the musculoskeletal force transmission system. Fourth, I account for variation in mandibular opening angle, which is associated with variation in mechanical advantage, fibre length and pennation angle, all of which influence bite forces. Implementation of these corrections reduces the size-dependent variation introduced by the experimental design and animal behaviour, and thus enables an unbiased comparison of maximum bite force capacity across animals of different sizes. The data depicted in this schematic is not 'real' data, but merely serves for illustration. The 'actual' relative change in force caused by each correction, averaged for all ants, is shown in percent.

The first correction is necessary, because the sensor measures 1D compression, $\mathbf{F}_m$, but the applied bite force vector, $\mathbf{F}_b$, may deviate from this line of action by a misalignment angle α (see Fig. 4.1C). The orientation of $\mathbf{F}_m$ is approximately equal to the plane normal of the bite plate; the orientation of the bite force vector is defined by the cross product between mandible outlever $\mathbf{L}_{o,c}$ and the rotational axis, where $\mathbf{L}_{o,c}$ is the vector connecting joint centre and the bite contact point (for more details, see Chapter 3). This correction was typically larger for larger animals, which more frequently bit at opening angles below 90° (see section 4.3), leading to larger misalignment angles.

The second correction is necessary, because the point of force application on the bite plate itself may vary across ants – smaller ants have shorter mandibles and are thus more likely to bite at the distal part of the bite plates, so changing the lever arm around the pivot, $\mathbf{L}_p$. To account for variation in lever arm, I introduce the correction term $\Gamma = |\mathbf{L}_{p,cal}|/|\mathbf{L}_p|$. Γ was always close to 1, as the length of the bite plate is small in comparison to the total length of the lever arm ($\approx 5\,\%$); the effect of this correction was thus miniscule.

The third correction is necessary, because the bite force may be transferred onto the bite plate at an arbitrary position along the mandible; an ant biting with the distal end of its mandible may use the same muscle effort but nevertheless produce a smaller measured bite force than an ant biting with

the proximal end of its mandible, because the mechanical advantage of the force transmission system differs (see e. g. Lappin and M. E. Jones, 2014). To correct for this variation, I converted the measured bite force into an equivalent bite force at a fixed point on the mandible blade (the most distal tooth tip). To this end, two effective mandible outlevers, each defined as the projection of the outlever onto the plane of rotation, were calculated for the contact point and the most distal tooth tip, respectively, as $\mathbf{L}_{o,eff} = \mathbf{L}_o - (\hat{\mathbf{R}} \cdot \mathbf{L}_o)\hat{\mathbf{R}}$ (for more details, see Chapter 3).

After implementation of corrections (i-iii), the magnitude of the bite force $|\mathbf{F}_b|$ follows as:

$$|\mathbf{F}_b| = \Gamma \frac{|\mathbf{F}_m|}{\cos\alpha} \frac{|\mathbf{L}_{o,eff,c}|}{|\mathbf{L}_{o,eff,d}|} \tag{4.1}$$

The fourth and last correction is necessary, because changes in opening angle are associated with changes in both muscle length and mechanical advantage. The resulting variation in bite force magnitude can be substantial; in *A. cephalotes* majors, bite forces at small opening angles are around five times larger than those at large opening angles (see Chapter 3 and Fig. 4.3).

In order to implement this correction, I first recognise that bite force is a function of both morphological and physiological parameters; it is determined by muscle stress σ, the physiological cross-sectional area of the mandible closer muscle A_{phys}, the average fibre pennation angle ϕ, and the mechanical advantage of the mandible lever system, defined as the ratio between effective in- and outlever $|\mathbf{L}_{i,eff}|/|\mathbf{L}_{o,eff,d}|$ (see Chapters 2 and 3 for details):

$$|\mathbf{F}_b|(\theta) = \sigma(\theta) A_{phys} \cos[\phi(\theta)] \frac{|\mathbf{L}_{i,eff}(\theta)|}{|\mathbf{L}_{o,eff,d}|} \tag{4.2}$$

I analysed 13 tomographic scans of *A. vollenweideri* leaf-cutter ants across the size range but excluding minims in order to extract muscle volume, average muscle fibre length, pennation angle, and the effective mandible levers (for details, see Chapter 2). Fibre length, pennation angle and effective inlever are functions of the mandibular opening angle. I previously demonstrated that these functions can be accurately predicted from first principles, using a small set of assumptions, geometry and reference measurements at a single opening angle (see Chapter 3). For this study, I assume that all fibres of the closer muscle attach to the tendon-like apodeme via thin filaments (which holds for 98 % of fibres in *A. vollenweideri,*, see Chapter 2); the length of these filaments determines the change of fibre length with opening angle, and was extracted from the scans (for more details, see Appendix C). I define the physiological cross-sectional area as the muscle volume divided by the optimal fibre length at which the muscle stress is maximum, L_{opt} (see Chapter 3). Muscle fibres which are stretched or shorten deviate from this optimum length, and as a result the muscle stress decreases due to characteristic force-length effects (A. Gordon et al., 1966; Josephson, 1975; Otten, 1987b). The magnitude of the decrease may be characterised by an empirical shape parameter β via $\sigma(\theta) = \sigma_{max} e^{-\beta(1-L_f(\theta)/L_{opt})^2}$ (see Chapter 3). The maximum muscle stress $\sigma_{max} = 1.16\,\text{MPa}$ and $\beta = 5.34$ were taken from Chapter 3, where they were determined experimentally for closely related *A. cephalotes* majors. I

make the simplifying assumption that these parameters are size-independent, and this assumption is supported by the resulting agreement between theoretical prediction and measured bite force (see section 4.3).

The mandibular opening angle at which the muscle stress is maximum, $L_f(\theta_{opt}) = L_{opt}$, was then estimated via a non-linear least squares numerical fitting routine of Eq. 4.2 in Python (v 3.9, Van Rossum and Drake, 2009). Notably, θ_{opt} may be reasonably expected to vary with body size, as it is sensitive to head capsule geometry which changes with size in *A. vollenweideri* (see Chapter 2, and N Imirzian, F Püffel and D Labonte, in preparation). In order to investigate the size-dependence of θ_{opt}, I selected bite force measurements from individuals with a body mass that differed by no more than $\approx 25\,\%$ from the individuals for which I obtained morphological data from μCT scans. Each size-class bin contained at least eight bite force measurements, except for the largest and smallest ant, which contained two and three bites, respectively.

In order to implement the opening angle correction across worker sizes, I first characterised the size-dependent relationship between bite force and opening angle as outlined above. Next, I calculated a database containing the relationship between predicted bite force, normalised with its maximum, $\hat{\mathbf{F}}$, opening angle and size. I rescaled the measured forces, corrected via Eq. 4.1, to the force expected at an *equivalent* mandibular opening angle; the angle θ_{max} at which bite forces are maximal, $|\mathbf{F}_{b,max}| = |\mathbf{F}_{b,\theta}|/|\hat{\mathbf{F}}_{\theta}|$. The magnitude of this correction thus depends on both the size and the mandibular opening angle of the biting ant; the corrected value used for the final analysis is the maximum force the animal can transmit at the distal mandibular tooth (see Fig. 4.1C).

4.2.7 Data curation and statistical analysis

I pooled bite force data from all three colonies, because the relationship between bite force and body mass was independent of colony both before and after correcting for differences in opening angle [Analysis of covariance (ANCOVA) on $\log_{10}$-transformed data, before correction: $F_{2,242} = 1.26$, p = 0.28; after correction: $F_{2,242} = 0.85$, p = 0.43]. Out of 248 bite force measurements, three slightly exceeded the range of calibration forces; two were lower and one higher, but all within 15 % to the nearest calibration force. These measurements neither appeared to be outliers, nor altered the scaling relationship (see section 4.3), and were hence kept for the analysis. Scaling relationships were characterised with Ordinary Least Squares (OLS) and Reduced Major Axis (RMA) regression models on $\log_{10}$-transformed data in R (v 4.1, R Core Team, 2021). For simplicity, I only report the results of the OLS regressions in the text; the RMA regression results are provided in Appendix C. Scaling coefficients tend to be higher for RMA regressions (also see LaBarbera, 1989); however, the main conclusions of this study are supported by both.

4.3 Results

4.3.1 Leaf-cutter ant bite forces increase with strong positive allometry

I measured bite forces of *A. vollenweideri* leaf-cutter ants spanning more than one order of magnitude in body mass, m. Measured bite forces $|\mathbf{F}_m|$ ranged from a minimum of 31 mN to a maximum of 1029 mN, and were proportional to $m^{0.79}$ [OLS 95 % CI: (0.74 | 0.85), R^2 = 0.75], suggesting positive allometry (isometry predicts $m^{0.67}$). After correcting for force orientation, and bite position along the bite plate and mandible blade, respectively, bite forces, $|\mathbf{F}_{b,\theta}|$, ranged between 19 and 901 mN (see Fig. 4.3 and Eq. 4.1), and were proportional to $m^{0.85}$ [OLS 95 % CI: (0.79 | 0.92), R^2 = 0.74], in substantial excess of the scaling coefficient of $|\mathbf{F}_m|$ (see Fig. 4.4B). However, this scaling relationship is still influenced by systematic differences in mandibular opening angle, which, as expected, were systematically smaller for larger animals [Analysis of variance (ANOVA) on $\log_{10}$-transformed data: $F_{1,246}$ = 15.24, p < 0.001].

In order to correct for the systematic differences in opening angle, I first assessed the size-dependence of the opening angle, θ_{opt}, at which muscle stress is maximum (see section 4.2 and Chapter 3). Notably, θ_{opt} decreased significantly with body mass [OLS: slope = -0.09, 95 % CI: (-0.15 | -0.04), p < 0.01, R^2 = 0.56]: $\theta_{opt} \approx 70^\circ$ for a 1.5 mg ant, but $\theta_{opt} \approx 50^\circ$ for a 45 mg ant. Next, I calculated the opening angle at which the bite force is maximum, θ_{max}. θ_{max} may differ from θ_{opt}, because bites with larger or smaller opening angles may involve a higher mechanical advantage, so counteracting any loss of force associated with isometric contractions at non-optimal fibre length (see Chapter 3). θ_{max} decreased significantly with size [OLS: slope = -0.06, 95 % CI: (-0.10 | -0.03), p < 0.01, R^2 = 0.59, represented by the crosses in Fig. 4.4A]; the bite forces of a 1.5 mg and 45 mg ant are maximal at around 65° and 50°, respectively. Thus, the difference between θ_{max} and θ_{opt} is small, supporting my earlier conclusion that the musculoskeletal bite apparatus of leaf-cutter ants has a morphology which maximises the magnitude of the peak bite force (see Chapter 3).

Equivalent bite forces at θ_{max} and the most distal bite point scale with an even stronger positive allometry, $|\mathbf{F}_{b,max}| \propto m^{0.90}$ [OLS 95 % CI: (0.86 | 0.95), R^2 = 0.86]. The increase in scaling coefficient is surprising, because larger ants bit at significantly smaller opening angles; the intuitive expectation is thus that the bite forces of small ants were underestimated, and the scaling coefficient overestimated. However, this argument neglects the significant decrease of θ_{max}, which reverts the effect: because θ_{max} decreases more quickly than the opening angle increases, larger ants were measured at less favourable opening angles, and the scaling coefficient was underestimated.

Together, the four corrections result in a significant increase of the scaling coefficient by 0.11, or about 15 % [LMM with correction as fixed and sample number as random effect: $\chi^2_1 = 118$, p < 0.001], and in an increase of the R^2 from 0.75 to 0.86. The difference in scaling coefficient may appear small, but this impression is misleading: the difference in maximum bite force between ants varying in body mass by a factor of 30 is $30^{0.90} \approx 22$ compared to $30^{0.79} \approx 15$ – a drop by about

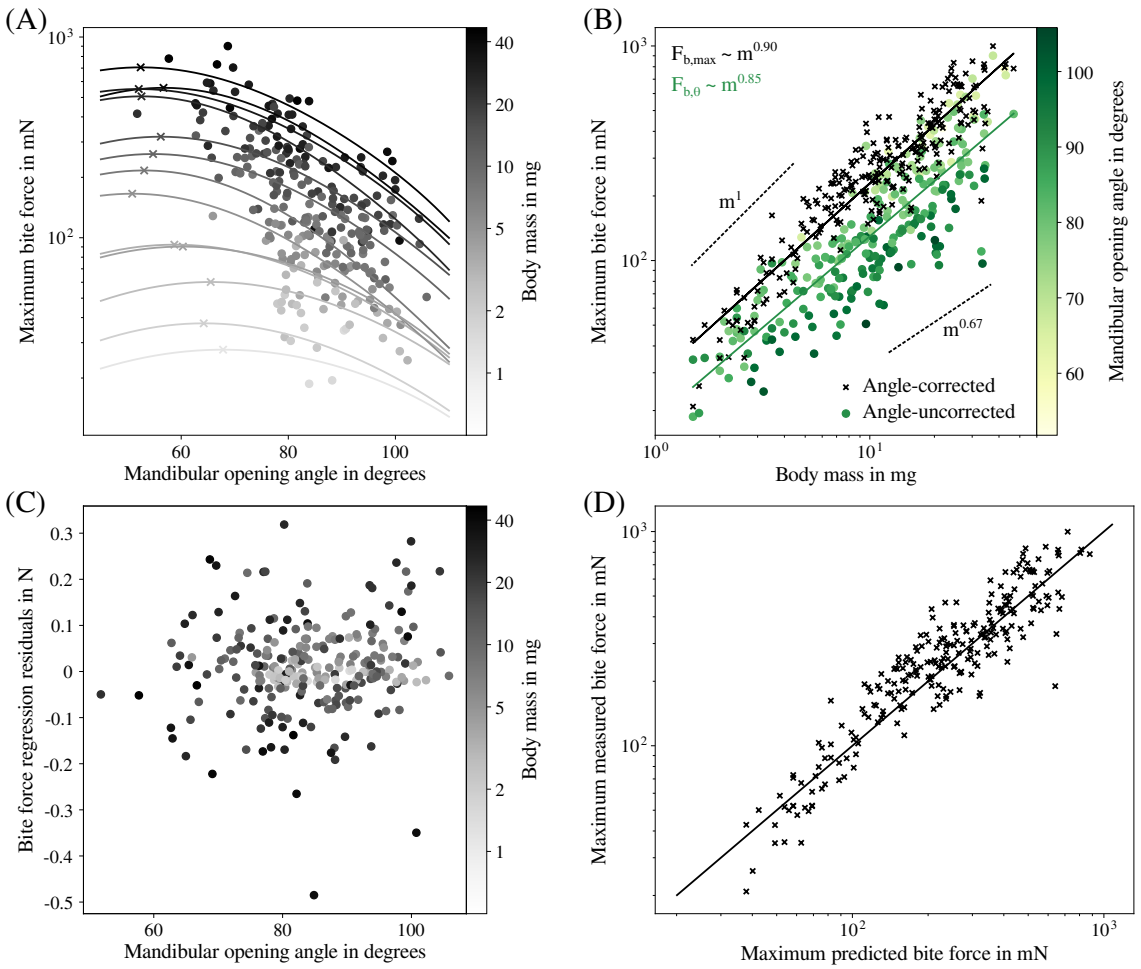


FIGURE 4.4: (**A**) Maximum bite force is determined by the morphology of the bite apparatus and the physiology of the mandible closer muscle. The morphological force determinants were extracted from 13 tomographic scans of *Atta vollenweideri* scans across all sizes excluding minims. The physiological determinants were determined experimentally for closely related *Atta cephalotes* majors (see Chapter 3), except for the mandibular opening angle at which the muscle stress is maximum. This 'optimum' angle was fitted numerically using bite forces measured for ants similar in size to those for which tomographic scans were available (circles). The solid lines represent the predicted bites forces from morphology and physiology across mandibular opening angles, calculated via a first-principle biomechanical model derived in Chapter 3. The maxima of these predictions (crosses) shift to significantly larger opening angles for smaller ants [Ordinary Least Squares (OLS) regression: slope = -0.09, $p < 0.01$]. (**B**) Bite forces, corrected to an equivalent mandibular opening angle and bite points on the mandible (crosses), scale with strong positive allometry [$mass^{0.90}$, OLS 95 % CI: (0.86 | 0.95), $R^2 = 0.86$], far surpassing the parsimonious prediction from isometry ($mass^{0.67}$); bite forces are almost directly proportional to body mass. The scaling coefficient exceeds the estimate from angle-uncorrected data [$mass^{0.85}$, OLS 95 % CI: (0.79 | 0.92), $R^2 = 0.74$], represented by the green line and circles. (**C**) The residuals of the regression on corrected maximum bite forces are independent of mandibular opening angle [ANOVA: $F_{1,246} = 2.43$, $p = 0.12$], supporting the validity of the angle-correction. (**D**) The corrected measured bite forces are in excellent agreement with a quantitative prediction from morphology and physiology, as demonstrated by the identity function (solid line). The predicted forces are the result of an OLS regression on $\log_{10}$-transformed data between force maxima (crosses in figure part A) and body mass of the scanned ants. I note that predicted and corrected forces are not strictly independent; the optimum opening angle, affecting the force prediction, was fitted using the measured bite forces, and the correction factor, applied to the measured forces, was determined via the normalised predictions.

30 %. Clearly, a careful analysis of bite force measurements is required in order to draw meaningful conclusions on scaling relationships.

4.4 Discussion

Leaf-cutter ants are an ecologically and economically important herbivore (Wirth et al., 2003; Costa et al., 2008), foraging on a wide variety of plants with different mechanical properties (J. M. Cherrett, 1972; Nichols-Orians and Schultz, 1989). Key to foraging success is the ability of workers to produce bite forces sufficiently large to cut plant tissues (F. Clissold, 2007). How does this ability vary with worker size? In order to address this question, I measured the maximum bite forces of *A. vollenweideri* leaf-cutter ants spanning more than one order of magnitude in body mass. In the following discussion, I (i) connect the bite force allometry with its morphological and physiological determinants; (ii) discuss the magnitude and scaling of maximum bite forces in the context of foraging ecology; and (iii) place my findings in an evolutionary and comparative context.

4.4.1 Bite force allometry can be accurately predicted from muscle architecture and head morphology

Maximum bite forces of *A. vollenweideri* workers show strong positive allometry, $|\mathbf{F}_{b,max}| \propto m^{0.90}$. Due to the large variation in worker size, the effect of this positive allometry is rather extreme: the largest ant workers generate maximum bite forces about 2.5 times higher than a theoretical isometric worker with the same body mass, $(45/1)^{0.90-0.67} \approx 2.5$. Can this extreme positive allometry be understood from the morphology and physiology of the *Atta* bite apparatus?

I have previously extracted the relevant morphological bite force determinants in *A. vollenweideri* workers from tomographic scans (see Chapter 2). On the basis of these data, I predicted that bite force should scale as $m^{0.88}$, a positive allometry largely driven by a disproportional increase in physiological cross-sectional area of the mandible closer muscle (see Chapter 2). This prediction is in rather close agreement with my bite force measurements. The small difference stems from the fact that I previously extracted the morphological bite force determinants from scans, where the mandibles were maximally closed, whereas θ_{max} varies across sizes (see Fig. 4.4A). In order to account for this variation in my morphological prediction, and to estimate the intercept of the scaling relationship, I use the stress and force-length shape parameter measured for closely related *A. cephalotes* (see Chapter 3), the change in θ_{opt} as observed in this work, and a biomechanical model which links morphology, opening angle and bite force to directly predict maximum bite forces (see Chapter 3, and Fig. 4.4A).

This calculation predicts a scaling of $m^{0.91}$ [OLS 95 % CI: (0.82 | 1.01), R^2 = 0.98], and an intercept of 1.42 [units: mN, mg; OLS 95 % CI: (1.32 | 1.52]. Both estimates are almost identical to the results obtained from direct measurements: $m^{0.90}$ (scaling coefficient), 1.46 (intercept) [units: mN, mg; OLS 95 % CI: (1.41 | 1.51)]. In other words, the ratio between maximum measured and predicted bite

forces is close to unity (1.11 ± 0.30), and independent of body mass [ANOVA on $\log_{10}$-transformed data: $F_{1,246} = 0.23$, $p = 0.63$, see Fig. 4.4D]. I thus conclude that the scaling of bite forces can be predicted to reasonable accuracy from morphological measurements.

Predicting bite performance from morphology is of considerable interest to evolutionary biologists, palaeontologists and biomechanists alike, as *in-vivo* force measurements are often challenging if not impossible to obtain. Consequently, theoretical models to predict maximum bite force have been developed and deployed for numerous taxa (e. g. G. M. Erickson et al., 1996; Huber et al., 2006; Heethoff and Norton, 2009; Habegger et al., 2012, and Chapter 3). In arthropods, the two key obstacles facing such theoretical efforts are the extraordinary variation in reported muscle stresses (e. g. G. M. Taylor, 2000; Guschlbauer et al., 2007), and the uncertainty in estimates of the physiological cross-sectional area, which requires knowledge of the optimal fibre length (see Chapter 3). The fact that I was able to accurately predict both the magnitude and scaling of bite forces in *A. vollenweideri* using physiological parameters measured in closely related *A. cephalotes* suggests that muscle stress and shape parameter β are conserved across sizes and within *Atta*, cautiously indicating that the intraspecific and intrageneric variation of bite forces may be predictable based on morphological data alone.

4.4.2 Positive allometry of bite force has substantial benefits at colony level

Bite forces are a non-pareil performance measure which influences access to food sources and high-quality mating partners (R. A. Anderson et al., 2008). As a result, the variation in morphology and physiology of the bite apparatus across species often reflects species-specific needs (Dumont and Herrel, 2003; Gidmark et al., 2013; Goyens et al., 2014b; Santana, 2016; Kaczmarek and Gidmark, 2020). What needs have shaped the evolution of bite performance in *Atta*?

Atta ants are known for their 'catholicity of taste' (J. M. Cherrett, 1968; Rockwood, 1976); a single colony may forage on more than 100 plant species at once, spanning a large range of chemical and mechanical properties (J. M. Cherrett, 1972; Shepherd, 1985). Foraging is not completely indiscriminate, however: for example, foragers seem to prefer young (tender) over old (tough) leaves from the same plant (J. M. Cherrett, 1972; Waller, 1982; Shepherd, 1985; Nichols-Orians and Schultz, 1990). Notably, this preference disappears when pre-cut leaf fragments are offered instead (Nichols-Orians and Schultz, 1989; Nichols-Orians and Schultz, 1990), suggesting that foraging decisions are not solely driven by plant chemistry, but also by mechanical considerations. Because larger ants typically cut tougher and denser leaves than smaller ants (J. M. Cherrett, 1972; E. O. Wilson, 1980a,b; Nichols-Orians and Schultz, 1989; Wetterer, 1994a,b), I surmise that these mechanical considerations are further confounded by size. From these simple observations emerge two key demands on bite forces in *Atta*: its magnitude must be large enough to cut a representative leaf, and its scaling determines the range of plant leaves that can be cut by workers of different size.

In order to contextualise the magnitude of the bite force, I estimate the forces required to cut leaves. Consider a blade-like tool which exerts a force of magnitude F to make a cut of length dx through a thin sheet of thickness t. The work done, $\int F dx$, supplies the energy required to create the new

surface arising from the cut, $Gtdx$, where G is the energy associated with a unit area of surface; the cutting force then follows as $F_c \approx Gt$. This calculation provides a lower bound on the required force, because it neglects the influence of friction, tool geometry and sheet bending (e. g. Kamyab et al., 1998; J. G. Williams and Patel, 2016; B. Zhang et al., 2019). Onoda et al. (2011) used cutting tests to quantify a proxy for G, the work per unit fracture length to cut leaf lamina of known thickness, for about 1000 tropical plant species (Darvell et al., 1996; Onoda et al., 2011, I note that although *A. vollenweideri* is often referred to as a grass-cutting ant, workers also cut dicotyledonous leaves, see H. Fowler et al., 1986). On the basis of the simple mechanical model and these extensive experimental results, I estimate that the forces required to cut tropical leaves vary between 7 - 828 mN. The median required cutting force of 82 mN can be generated by a worker of about 5 mg (see Fig. 4.5), and I submit that this finding strongly suggests that the remarkable magnitude of bite forces in *A. vollenweideri* arises from the ecological need to cut leaves.

In order to contextualise the positive allometry of bite force, I next calculate the fraction of cuttable leaves as a function of worker size, both for allometric and hypothetically isometric workers (see Fig. 4.5). A direct comparison between two populations of workers which follow different scaling laws requires to specify the body mass at which the two scaling lines intersect. Do large workers bite relatively more strongly, or small workers relatively more weakly? This question cannot be answered *a priori*, and I thus refer to three biological arguments instead: First, the worker-size distribution in leaf-cutter ant colonies typically has a long right tail, i. e. the vast majority of foraging workers is relatively small (E. O. Wilson, 1953, 1980a, 1983b; Wetterer, 1999). Second, large workers are only produced in larger numbers once colonies exceed a critical size (E. O. Wilson, 1983b; Wetterer, 1999). Third, larger workers are more 'costly' than smaller workers. On the basis of these arguments, increasing the bite force capacity disproportionally may represent a strategy to minimise the cost associated with a unit increase in maximum bite force. A disproportionate decrease of bite forces, in contrast, appears to have no obvious biological benefit. Thus, small workers may represent a reasonable generalist 'starting point', and I choose a weight of 1 mg, at the transition between minims and medias (E. O. Wilson, 1980a, and Chapter 2), as intersection mass.

Viewed in this light, the positive allometry of bite force has substantial benefits for the colony for at least two reasons. First, the maximum bite force of an allometric worker with a body mass of 27 mg, at the upper end of forager sizes typically reported in *Atta* (Wetterer, 1990; Wetterer, 1994a,b; Röschard and Roces, 2003b; Evison and Ratnieks, 2007), exceeds that of an equally-sized isometric worker by a factor of two (see Fig. 4.5A). Provided that the data reported by Onoda et al. (2011) are representative, this difference increases the fraction of cuttable leaves from 94 % to almost 100 % (see Fig. 4.5B). This difference may seem small, but this perception is erroneous: A large isometric forager would need to be three times heavier to cut the same fraction of leaves. Second, the smallest worker that can cut the median leaf almost halves in mass between isometric and allometric workers (5 to 3 mg, see Fig. 4.5B). As the majority of workers are typically small (Wetterer, 1999), the positive allometry thus significantly increases the fraction of the colony that can partake in leaf-cutting: an allometric forager of 5 mg can cut up to 70 % of leaves, a whopping 20 % more than its isometric

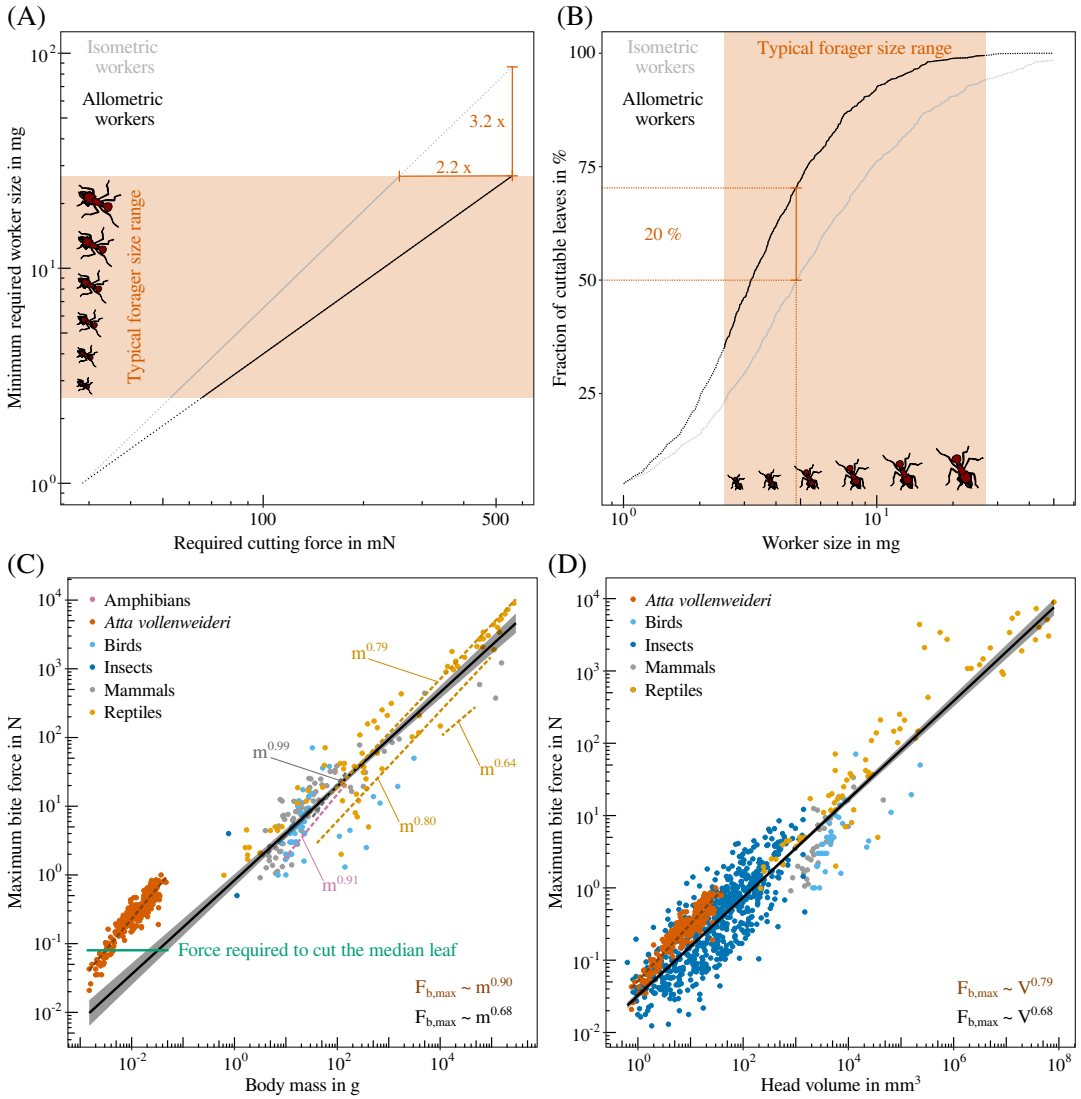


FIGURE 4.5: (**A**) I consider possible benefits of the positive allometry of bite force by calculating the minimum worker size which can generate a given force, both for measured positively allometric and hypothetical isometric workers. An isometric worker needs to be about three times larger to produce the same bite force as the largest allometric forager; typical *Atta vollenweideri* foragers range between 2.5 to 26.9 mg (Röschard and Roces, 2003b). (**B**) An allometric workforce increases the total fraction of cuttable leaves, estimated from measurements on 1000 tropical plant species (Onoda et al., 2011), from around 94 % to almost 100 %. A medium-sized forager of about 5 mg can cut 70 % of leaves; its isometric counterpart only 50 %. The positive allometry of bite forces thus likely increases harvesting speed, and provides flexibility in task allocation, so enhancing colony fitness. (**C**) Positive allometry of bite force has been reported in intraspecific studies for several taxa (dashed lines, see G. M. Erickson et al., 2003; Becerra et al., 2011; Marshall et al., 2012, 2014; Lappin et al., 2017, and Table 4.1). Across distantly related species and a large size range, however, bite forces scale with isometry [black line, $\text{mass}^{0.68}$, OLS 95 % CI: (0.65 | 0.72), R^2 = 0.86]; each circle represents the average maximum bite force for a single species (extracted from Goyens et al., 2014b; Weihmann et al., 2015a; Sakamoto et al., 2019). *A. vollenweideri* ants generate exceptionally large weight-specific bite forces, comparable to those of amniotes 20 times heavier. (**D**) Relative to their head volume, however, their bite forces are comparable to those of other insects (extracted from Rühr et al., 2022), and amniotes (Sakamoto et al., 2019), suggesting that leaf-cutter ants have a large weight-specific head volume. Across species, bite forces are isometric, $\text{head volume}^{0.68}$ [OLS 95 % CI: (0.66 | 0.70), R^2 = 0.87]. Within *A. vollenweideri*, however, bite force $\propto$ $\text{head volume}^{0.79}$ [OLS 95 % CI: (0.75 | 0.83), R^2 = 0.86], in excess of isometric predictions, due to a disproportionate increase in volume-specific physiological cross-sectional area of the mandible closer muscle (see Chapter 2).

counterpart. This substantial increase in the size range which can forage on a large number of plant species facilitates flexible task assignment, likely increases harvesting speed and overall influx of nutrients to the nest, and may thus be reasonably expected to enhance colony fitness.

In addition to the positive allometry of maximum bite force, my results revealed a significant decrease in opening angle at which fibres take their optimum length, θ_{opt}. I note that the last correction step, which led to this conclusion, is complex. In contrast to the first three corrections steps which are based on geometrical relations and thus have high predictive accuracy, it involves assumptions on muscle physiology, and neglects passive force-length effects due to muscle or connective tissue elasticity (see Chapter 3). In support of the validity of my angle correction and the resulting conclusion, three independent lines of evidence may be offered. First, the angle-corrected regression analysis explains a substantially larger share of the variation of bite force with mass (86 % vs 74 % for $|\mathbf{F}_{b,\theta}|$, see Fig. 4.4B). Second, the regression residuals are independent of opening angle [ANOVA: $F_{1,246}$ = 2.43, p = 0.12, see Fig. 4.4C], which does not hold without angle-correction [ANOVA: $F_{1,246}$ = 148, p < 0.001]. Third, the relationship between θ_{opt} and body mass remains significant even after removing the smallest and largest size classes, which contain fewer data points (see section 4.2), and are thus associated with higher uncertainty [OLS: slope = -0.08, 95 % CI: (-0.15 | -0.01), p < 0.05, R^2 = 0.44]. My result therefore appears statistically robust, and I next offer a cautious functional interpretation. Ant workers large or small may often forage on the same plant leaf. Although their size differs, the characteristic dimension of the leaf lamina – its thickness – is the same. Because cuts are typically initiated at the leaf-edge by drawing mandibles together like scissors, ants need to produce sufficiently large bite force at a gape width comparable to the leaf lamina thickness. For an ant of 3 mg, the strongest bites occur at a mandible gape of 0.1 mm, approximately half the median leaf thickness (Onoda et al., 2011). At 0.2 mm gape, the opening angle is only a few degrees larger and the force is almost identical ($\approx$ 99 %). If, however, this small ant had the same θ_{max} as the largest colony workers, the force at 0.2 mm would be 10 % less. I thus suggest that shifts in the optimal length such that the maximum bite force occurs at larger opening angles in small workers may represent an adaptive strategy to counter size-specific disadvantages when workers of different size forage on leaves with a similar thickness.

4.4.3 Positive allometry of bite force is common within, but rare across species

I discussed the mechanistic origin and ecological significance of the positive allometry of bite forces in *A. vollenweideri*. As a last step, I place my findings in a broader comparative and evolutionary context.

To this end, I compare both the scaling and magnitude of bite forces with two extensive datasets including close to 900 species, covering eight orders of magnitude in body mass and head volume (Sakamoto et al., 2019; Rühr et al., 2022). Regression analysis on $\log_{10}$-transformed bite force data for 203 amniote and two insect species against body mass (Goyens et al., 2014b; Weihmann et al., 2015a; Sakamoto et al., 2019), and for 139 amniote and 653 insect species against head volume (Sakamoto

TABLE 4.1: Scaling of maximum bite forces for intraspecific (or intrageneric ‡) scaling studies across various taxa. The statistical models used to characterise the scaling relationships include Ordinary Least Squares (OLS) and Reduced Major Axis (RMA) regressions performed on $\log_{10}$-transformed data; in three studies, a non-linear RMA regression on untransformed data was used instead (Marshall et al., 2012, 2014; Vassallo et al., 2016). The relevant morphological variables are body mass (m), or one of several characteristic lengths, L: manus length (ML), snout vent length (SVL), carapace length (CL), and body length (BL). Where possible, I selected body mass as key variable to facilitate comparison with this study. A range of scaling coefficients is given when more than one species (or genus ‡), intraspecific morphotypes or sexual dimorphism were studied. Significant deviations from isometric scaling, i ($m^{0.67}$, L^2) are indicated with a p for positive allometry or n for negative allometry. I calculated a $\log_{10}$-transformed bite force quotient (BFQ) based on the reported mass range and regression coefficients (see Heethoff and Norton, 2009; Meijden et al., 2012). Because the BFQ is based on isometry, studies that reported allometric scaling are characterised by a range of BFQs. Where regression coefficients for body mass were missing, I calculated the range of BFQ based on the reported mass and bite force ranges (labelled with $*$). Bite forces that were not measured at the most distal tip of the jaws, or for which the bite position was not explicitly reported, are labelled with a †; these data are biased and thus need to be compared with care (see main text).

Taxon	Statistical model	Scaling	Allometry	$\log_{10}$(BFQ)	Source
Ants	OLS	$m^{0.90}$	p	2.50 - 2.85	this study
Ants	RMA	$m^{0.97}$	p	2.44 - 2.90	this study
Birds ‡	RMA	$m^{0.76-0.88}$	i	0.62 - 1.22 $*$	Sustaita and Hertel, 2010
Crabs	not specified	$m^{0.82}$	p	2.66 - 2.94 †	Oka et al., 2016
Crabs ‡	OLS	$ML^{1.49}$	n	no mass reported	Palmer et al., 1999
Crocodylians	OLS	$m^{0.79}$	p	1.92 - 2.36 †	G. M. Erickson et al., 2003
Crocodylians	RMA	$m^{0.77-0.78}$	p	1.98 - 2.40 †	G. Erickson et al., 2014
Frogs	RMA	$m^{0.91}$	p	1.59 - 1.88	Lappin et al., 2017
Eels	not specified	$BL^{2.79-2.94}$	p	no mass reported †	De Meyer et al., 2018
Lizards ‡	RMA	$SVL^{3.83-4.60}$	p	1.27 - 2.34 $*$ †	Meyers et al., 2002
Lizards	RMA	$SVL^{2.65-3.37}$	p	2.10 - 2.67 $*$ †	Herrel and O'Reilly, 2006
Lizards	OLS	$m^{0.57-0.73}$	n, p	2.02 - 2.36 $*$	M. E. Jones et al., 2020
Piranhas	OLS	$BL^{2.30}$	p	2.37 - 2.47 $*$	Grubich et al., 2012
Ratfish	OLS	$BL^{2.34}$	i	2.07 $*$	Huber et al., 2008
Rodents	RMA	$m^{0.89-0.99}$	p	1.83 - 2.04	Becerra et al., 2011
Rodents	RMA	$m^{1.11}$	p	1.91 - 2.06 $*$	Becerra et al., 2013
Rodents	non-linear RMA	$m^{0.93-1.01}$	p	1.78 - 2.07	Vassallo et al., 2016
Rodents	OLS	$m^{0.83}$	p	1.78 - 2.06 $*$	Ginot et al., 2020
Snakes	OLS	$m^{0.28}$	n	0.71 - 1.14 †	Penning, 2017
Turtles	RMA	$CL^{1.73-2.23}$	n, i	1.52 - 2.53 $*$ †	Herrel and O'Reilly, 2006
Turtles	RMA	$m^{0.98}$	p	1.90 - 2.48 †	Pfaller et al., 2010
Turtles	non-linear RMA	$m^{0.80}$	p	1.40 - 1.85	Marshall et al., 2012
Turtles	non-linear RMA	$m^{0.64}$	i	1.33	Marshall et al., 2014

et al., 2019; Rühr et al., 2022) suggests isometry of bite forces [mass$^{0.68}$, OLS 95 % CI: (0.65 | 0.72), R^2 = 0.86; head volume$^{0.68}$, OLS 95 % CI: (0.66 | 0.70), R^2 = 0.87, see Fig. 4.5]. The intercepts of the regression, which reflect mass- and head-volume specific bite forces (with mass in g, volume in mm^3, and force in N), in turn are -0.08 [mass across species: OLS 95 % CI: (-0.17 | 0.01)], 1.17 [mass within *A. vollenweideri*: OLS 95 % CI: (1.07 | 1.26), see Fig. 4.5C], -1.49 [volume across species: OLS 95 % CI: (-1.53 | -1.44)], and -1.29 [volume within *A. vollenweideri*: OLS 95 % CI: (-1.33 | -1.25)]. Leaf-cutter ants thus appear exceptional in at least two aspects: Their bite forces grow with strong positive allometry, and their weight-specific bite forces are in substantial excess of that for the average amniote and insect, respectively (also see Chapter 3); the largest ants produce maximum bite forces comparable to that of amniote species at least 20 times heavier (see Fig. 4.5C), and I have argued above that such a remarkable magnitude of bite forces probably arises from the ecological need to cut tough plant matter. Notably, both the magnitude and the scaling of the bite force of leaf-cutter ants are less remarkable relative to head volume [V$^{0.79}$, OLS 95 % CI: (0.75 | 0.83), R^2 = 0.86, see Fig. 4.5D]. This discrepancy reflects the fact that a large share of the positive allometry of bite forces in leaf-cutter ants is achieved by a positive allometry of head volume (see Chapter 2), and that leaf-cutter ants, and perhaps insects in general, have relatively larger heads than vertebrates; indeed, the weight-specific head volume for *A. vollenweideri* is 671 ± 74 mm^3/g compared to 209 ± 134 mm^3/g for amniotes (see Fig. 4.5 and Sakamoto et al., 2019).

In the above argument, I have conflated evolutionary allometry involving different species, with static allometry involving individuals of the same species at identical ontogenetic stage (Pélabon et al., 2013). In order to analyse if the static positive allometry of bite forces in leaf-cutter ants is indeed exceptional, and to facilitate a more appropriate comparison of the magnitude of bite forces, I collated results from 22 intraspecific and intrageneric scaling studies on bite force across twelve taxonomic groups (including this study, see Table 4.1. I note that the majority of intraspecific scaling studies report ontogenetic instead of static scaling coefficients). For each study, I then calculated a $\log_{10}$-transformed 'bite force quotient', $\log_{10}(\text{BFQ}) = \log_{10}(\text{bite force}/\text{body mass}^{2/3})$ in N/kg$^{2/3}$ (Heethoff and Norton, 2009; Meijden et al., 2012) as a measure for weight-specific bite performance. Leaf-cutter ants have the highest $\log_{10}(\text{BFQ})$ apart from coconut crabs, for which bite force were measured at a favourable mechanical advantage (Oka et al., 2016, in contrast, I report bite forces for the maximum outlever and thus smallest mechanical advantage for a given mandibular opening angle).

I conclude that leaf-cutter ants are highly specialised to produce large bite forces: (i) they have large heads relative to their body mass compared to vertebrates; (ii) the volume occupation of mandible closer muscle in these heads and (iii) the geometry of the bite apparatus are close to putative theoretical optima (see Chapters 2 and 3; and (iv), the estimated maximum stress of the mandible closer muscle is among the highest ever measured (see Chapter 3).

In sharp contrast to the magnitude of bite force, the positive static allometry appears to be less remarkable: around 70 % of available intraspecific studies reported significant positive allometry of

bite forces, if often less pronounced (including one study that also reported negative allometry for other phenotypes of the same species, M. E. Jones et al., 2020)). Remarkably, and with the notable exception of bats and finches (Aguirre et al., 2002; Meij and Bout, 2004; Herrel et al., 2005; Senawi et al., 2015; Sakamoto et al., 2019), bite force studies involving different genera typically report isometric scaling (Huber et al., 2005; Sakamoto et al., 2019; Deeming, 2022, and see meta-analysis above), or even modest negative allometry (Claussen et al., 2008; Huber et al., 2009; Van Daele et al., 2009; Becerra et al., 2011, 2013; Hite et al., 2019). There thus appears to be a systematic difference between ontogenetic, static and evolutionary scaling of bite forces. To visualise this contrasting tendency, I superimpose a small selection of scaling relationships on the overall evolutionary slope (dashed lines in Fig. 4.5C). The ontogenetic, static and evolutionary allometry of bite forces appears as a weak instance of Simpson's paradox, where the slope of a regression line across many data points is substantially different from the slope obtained for subsets of the data – a result which appears to be common in biomechanical scaling studies (Schmidt-Nielsen and Knut, 1984; Peattie and Full, 2007; Labonte et al., 2016). Positive allometry of bite forces is likely associated with direct ecological advantages, related for example to the quantity and quality of accessible food sources (e. g. G. M. Erickson et al., 2003; Herrel and O'Reilly, 2006, this study). However, increased evolutionary rates of adaptive change in bite forces, required to drive departures from isometry, appear to be the exception rather than the norm, at least across amniotes (Sakamoto et al., 2019).

Four factors may contribute to this seeming discrepancy: First, intraspecific and intrageneric studies on bite performance may be biased toward taxa which may be reasonably expected to face strong ecological or behavioural demands on their bite forces, so increasing the probability of departures from isometry (also see Bonduriansky, 2007). Second, strong positive allometry across many decades of mass is challenging if not impossible to achieve without fundamental 're-design' (Gould, 1966); as an illustrative example, a hypothetical leaf-cutter ant with a body mass of 3 g would have a closer muscle with a volume that exceeds that of its head capsule. Third, in particular 'static' scaling studies may often be limited by comparatively narrow size ranges (e. g. Herrel et al., 2001; Hite et al., 2019), which increases the influence of biological variation and thus decreases the accuracy of the estimated allometric slope. Fourth, few of the available scaling studies accounted for potential size-specific biases in bite force measurements (see section 4.2), and may thus report under- or overestimates of the allometric slope. Ultimately, the differences between ontogenetic, static and evolutionary allometry of bite forces reflect species-specific needs, coupled with complex developmental, evolutionary and ecological constraints (e.g. Gould, 1966; R. J. Smith, 1984; LaBarbera, 1989; Bonduriansky, 2007; Egset et al., 2012; Pélabon et al., 2013; Voje and Hansen, 2013; Pélabon et al., 2014; Voje et al., 2014; Bolstad et al., 2015). Untangling the influence of these different factors constitutes an exciting avenue for comparative and evolutionary work across disparate taxa, and a large range of body sizes.

4.5 Conclusion and outlook

Bite forces in leaf-cutter ants scale with strong positive allometry, driven and accurately predicted by morphological and physiological adaptations of the bite apparatus. The positive allometry enables the colony to access an increased number of plant species, and is thus ecologically meaningful. My study adds strong quantitative evidence in support of the hypothesis that size-polymorphism and the associated variation in shape broadens a colony's access to food plants (E. O. Wilson, 1980a; Waller, 1989; Wetterer, 1999; Clark, 2006; Hölldobler and E. O. Wilson, 2010). However, I acknowledge that the exact relationship between worker size, food plants and cutting behaviour is complex, and is influenced by nest distance (Roces, 1990), mandibular wear (R. M. Schofield et al., 2011), and stridulation of the ant gaster, which can reduce force fluctuations during cutting (Tautz et al., 1995; Roces, 2022). To fully integrate the mechanical results of this study with foraging behaviour, direct measurements of cutting forces with differently-sized mandibles as well as behavioural assays with materials of varying mechanical properties are needed (see Chapter 6). I hope that such work will increase our understanding of the complex interactions between polymorphism, bite force allometry and foraging ecology in leaf-cutter ants.

5 Biomechanical development of the bite apparatus

I acknowledge the contributions of Richard Johnston, who conducted the μCT scans, Lara Meyer, who conducted the nanoindentation experiments including sample preparation, provided the manual thickness measurements for validation and helped with cuticle brightness measurements and tissue segmentation, Natalie Imirzian, who also helped with tissue segmentation, and Flavio Roces, who provided the ant colony.

Summary

Many social insects display age polyethism, where young adults stay inside the nest, and older adults forage. The mechanisms of this behavioural change involve genetic and physiological aspects, but the importance of biomechanical factors remains unclear. To investigate whether the mechanical demands of foraging effectively prevent young workers from partaking in foraging, I studied the biomechanical development of the bite apparatus in *Atta vollenweideri* leaf-cutter ants in the days after eclosion. Fully-matured foragers generate peak *in-vivo* bite forces of around 100 mN, more than one order of magnitude in excess of those measured for freshly-eclosed callows. This change in bite force was accompanied by a sixfold increase in the volume of the mandible closer muscle, and by a substantial increase of the flexural rigidity of the head capsule, driven by a significant increase in both average thickness and modulus of the head capsule cuticle. Callows are likely incapable of cutting most tropical leaves, because their muscles do not yet generate sufficiently large bite forces, and their head capsule is so compliant that large muscle forces may cause critical damage. I suggest that continued biomechanical development post eclosion may be a key factor in age polyethism in social insects where foraging is associated with high mechanical demands on the musculoskeletal system.

5.1 Introduction

Division of labour is thought to be a key innovation in social insects, as it may increase the ergonomic efficiency and thus fitness of the colony (Oster and E. O. Wilson, 1978). Numerous theories suggest possible explanations for the emergence and mechanisms of a division of labour beyond reproduction, with a particular focus on size- and age-related task preferences (e. g. E. O. Wilson, 1980b; Tofts, 1993; Robinson et al., 1994; Beshers and Fewell, 2001).

Across distantly related insect taxa, age-related task preferences, or age polyethism, has evolved in bees (Seeley, 1982; Robinson et al., 1989; Calderone, 1995; Z.-Y. Huang and Robinson, 1996), wasps (O'Donnell and Jeanne, 1993; Shorter and Tibbetts, 2009), ants (E. O. Wilson, 1976; E. O. Wilson, 1980a; Beshers and Traniello, 1996; Julian and Fewell, 2004; Thomas and Elgar, 2003; Seid and Traniello, 2006; Camargo et al., 2007; Muscedere et al., 2009; Vieira et al., 2010), and termites (Hinze and Leuthold, 1999): freshly-eclosed colony workers tend to stay inside the nest and attend to queen and brood, and only older workers engage in foraging tasks outside the nest (see Fig. 5.1). This behavioural transition typically occurs within the first weeks after eclosion (e. g. Seeley, 1982; Hinze and Leuthold, 1999; Seid and Traniello, 2006; Camargo et al., 2007), although the exact timeline is subject to variation based on genotype (Julian and Fewell, 2004) and colony size (Thomas and Elgar, 2003; Jeanson, 2019).

Because of its frequent emergence and ecological impact, age polyethism in social insects has received considerable attention from behavioural biologists (Z.-Y. Huang and Robinson, 1996; Thomas and Elgar, 2003; Julian and Fewell, 2004; Shorter and Tibbetts, 2009; Jeanson, 2019), ecologists (O'Donnell and Jeanne, 1993; Tofilski, 2002; Yanagihara et al., 2018), geneticists (C. Lucas et al., 2010; Ingram et al., 2016), neuroethologists (Seid and Traniello, 2006; Muscedere et al., 2011; Muscedere and Traniello, 2012), and physicists alike (R. M. Schofield et al., 2002, 2011), and numerous associated genetic and physiological processes have been identified. For example, the transition from within-nest to outside foraging tasks is linked to substantial changes in gene expression (Ben-Shahar et al., 2002; C. Lucas et al., 2010; Ingram et al., 2016), hormone levels (O'Donnell and Jeanne, 1993; Shorter and Tibbetts, 2009; Jeanson, 2019), the exocrine system (Z.-Y. Huang and Robinson, 1996), muscle chemistry (Roberts and Elekonich, 2005; Schippers et al., 2010; Skandalis et al., 2011), and brain physiology and size (Robinson, 1998; Muscedere and Traniello, 2012).

In fact, the physiological development following eclosion is hypothesised to be key in determining the ability of workers to partake in certain colony tasks (Robinson et al., 1994; Calderone, 1995; Seid and Traniello, 2006; Muscedere et al., 2009, 2011), suggesting an emergence of age polyethism based on the development and retention of behavioural capabilities (Seid and Traniello, 2006, but see Tofts, 1993; Beshers and Fewell, 2001).

However, another aspect that may also affect such capabilities has received considerably less attention: the biomechanical development of young colony workers after eclosion (R. M. Schofield et al., 2002, 2003, 2011; Muscedere et al., 2011). Biomechanical factors are likely relevant, because outside foraging tasks are associated with substantial mechanical demands: the cutting, masticating, piercing, sucking and transportation of substrates all require sufficiently large muscle forces and a robust skeleton to transmit these forces without taking damage. Here, I conduct a study of the biomechanical development of a musculoskeletal apparatus that is of particular importance in foraging, in an ant species where the mechanical demands on it are particularly strong: the head capsule of leaf-cutter ants.

Leaf-cutter ant foraging involves the cutting and carrying of leaf fragments from fresh vegetation

surrounding the nest (Wirth et al., 2003; Hölldobler and E. O. Wilson, 2010). To overcome the high mechanical demands of cutting, leaf-cutter ants generate excessively large weight-specific bite forces (see Chapter 4) at a metabolic scope close to that measured for insect flight (Roces and Lighton, 1995). The ability to partake in foraging depends on the worker's bite performance and the mechanical robustness of the head capsule. Previous work suggests that the musculoskeletal bite apparatus has not yet fully matured at the time of eclosion: tooth hardness of leaf-cutter ant mandibles increases nearly threefold in the days after eclosion, a development correlated with corresponding changes in zinc-concentration (R. M. Schofield et al., 2002); the cephalic muscles of *Pheidole* ants grow substantially post eclosion, suggesting age-related constraints on foraging ability based on muscle development (Muscedere et al., 2011).

This study builds up on this work by quantifying the biomechanical development of the musculoskeletal bite apparatus of *Atta vollenweideri* leaf-cutter ants; I investigated to what extent mechanical ability varies in the days following eclosion by (i) measuring peak bite forces with a custom-built force setup, (ii) quantifying the volume of the mandible closer muscle and the thickness of the head capsule using μCT imaging, and (iii), extracting the indentation modulus of the cuticle from nanoindentation experiments. By establishing a biomechanical paradigm to investigate age-related foraging, I hope to increase our understanding of the physical constraints that may contribute to age polyethism in insects.

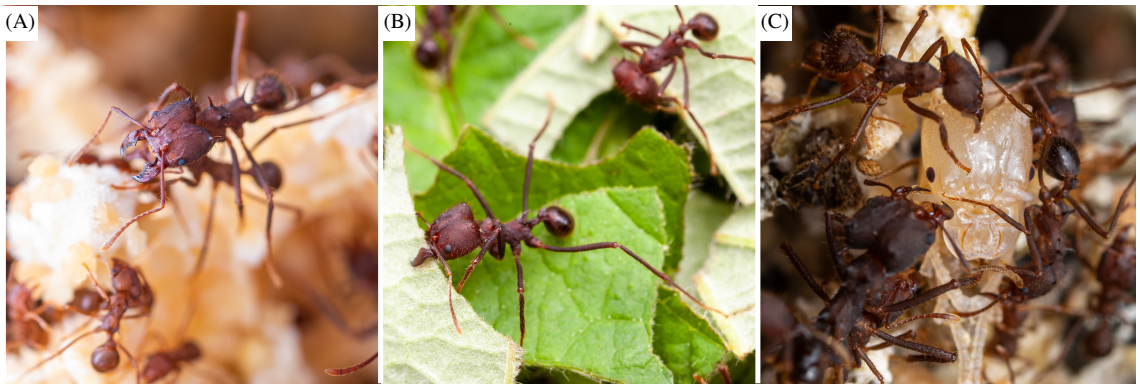


FIGURE 5.1: **(A)** Leaf-cutter ants harvest plant tissues from the nest surroundings to grow a subterranean fungus as crop. **(B)** Foraging tasks are only performed by workers exceeding a minimum age after eclosion, raising the question to what extent the mechanical demands of leaf-cutting drive this change in behaviour. **(C)** To address this question, I studied the biomechanical development of the musculoskeletal bite apparatus from freshly-eclosed callows to fully-matured foragers. Photo credit: Samuel T. Fabian.

5.2 Materials & methods

5.2.1 Study animals

I used workers from three *Atta vollenweideri* leaf-cutter ant colonies ('*E*', '*D*' and '*F*'), all founded and collected in Uruguay in 2014. The colonies were fed with bramble, cornflakes and honey water *ad libitum*, and kept under a 12 h:12 h light:dark cycle at 25°C and 50 % humidity in a climate chamber.

In order to minimise confounding effects due to worker size differences (see Chapter 2 and 4), I only collected small workers with a body mass between 3 and 7 mg, representing the lower end of observed forager sizes in *A. vollenweideri* (2.5-26.9 mg, see Röschard and Roces, 2003b). I collected 49 ants: 14 fully-darkened workers from the foraging area ($n_F = 14$), and 35 callows of varying cuticle brightness from the fungal gardens ($n_D = 7$, $n_E = 8$, $n_F = 20$). Callows were extracted by scooping fresh fungus from boxes that appeared to contain a lot of brood into a separate container, from which those ants with visibly brighter cuticle were taken. There was no significant difference in mean body mass between callows (4.5 ± 1.2 mg) and foragers (4.8 ± 1.2 mg; Wilcoxon rank sum test: W = 214.5, p = 0.51); I combined data from all three colonies as previous work demonstrated that bite forces do not differ across them (see Chapter 4).

5.2.2 Bite force measurements

In order to quantify bite performance, I measured the maximum bite force using a custom-built setup described in detail in Chapter 4. In brief, individual ants were held in front of two bite plates using insect tweezers (see Fig 5.2B). The ants then readily bit onto the two bite plates, both protruding from mechanically uncoupled beams. The first beam can rotate about a pivot and then pushes onto a capacitive force sensor, which is thus compressed when a force is applied to the bite plate. The second beam remains stationary, such that the distance between the two outer surfaces of both bite plates – the mandibular gape required to bite – is constant at 0.5 mm, or roughly a third of the average head width. Each measurement was terminated after at least five complete bite cycles or a total bite duration of more than 10 s. For the youngest and supposedly weakest callows, this condition was difficult to verify from the force trace alone as the peak bite forces were below 10 mN, equivalent to about twice the sensor noise (see section 5.3). For these ants (n = 11), I identified bites based on direct observations via a top-down camera, which filmed the ants during the experiment with 30 fps. After the measurement, all ants were weighed (AX304 Microbalance, 310 g x 0.1 mg, Mettler Toledo, Greifensee, Switzerland), and sacrificed by freezing.

From the recorded bite force traces, the maximum measured forces were extracted. However, these force maxima were still influenced by head orientation and bite location both on the mandible and bite plate. In order to remove the influence of these factors, I calculated the maximum bite force at an equivalent mandible outlever, the most distal end of the mandible, using the steps described in detail in Chapter 4. I did not correct for differences in mandibular opening angle as this requires assumptions on muscle physiology (see Chapter 4). However, the opening angles of callow and forager bites were almost identical, $78 \pm 6^\circ$ versus $77 \pm 5^\circ$ (Two sample t-test: $t_{47} = 0.63$, p = 0.53), so that any confounding effects are likely unsystematic. Bite forces of mature *A. vollenweideri* ants are maximal at an opening angle of about 60°; the forces measured here are about 15 % lower than this peak (see Chapter 4).

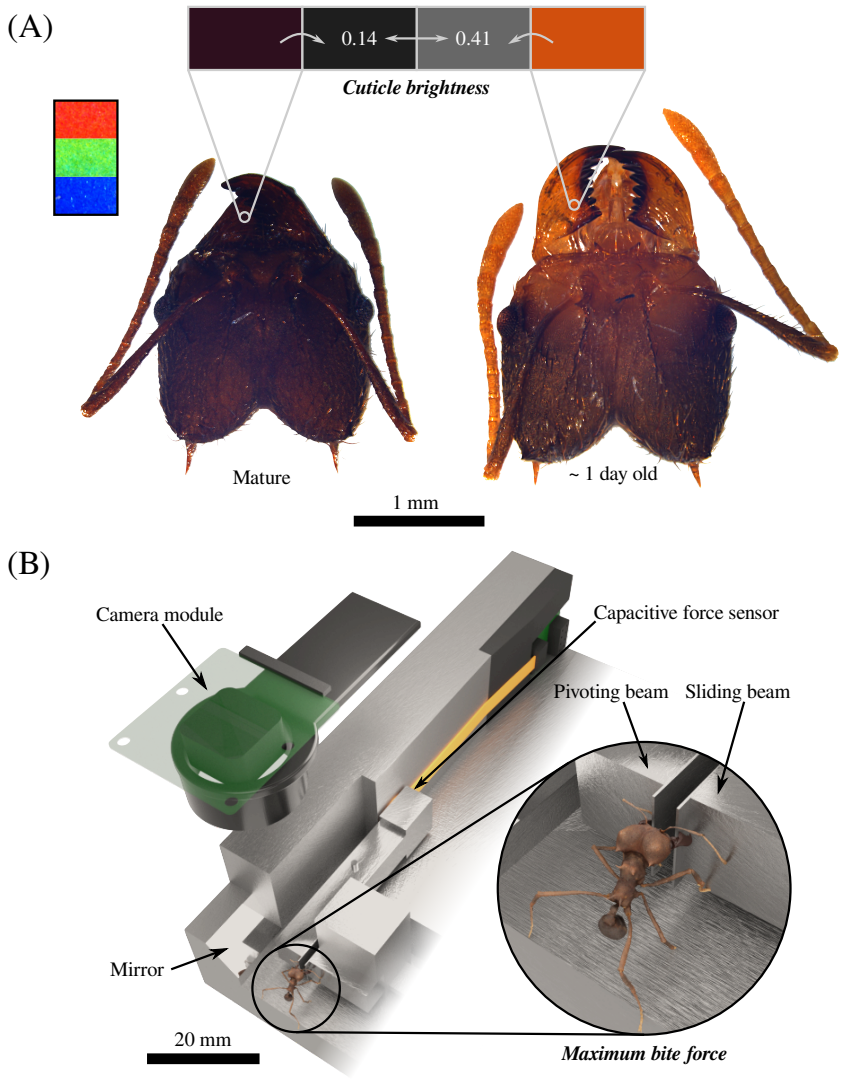


FIGURE 5.2: In order to study the biomechanical development of the musculoskeletal bite apparatus post eclosion, I extracted adult *Atta vollenweideri* leaf-cutter ants at different time points after eclosion from the foraging area and fungal gardens of the colony. I quantified *cuticle brightness*, *maximum bite force*, *indentation modulus*, *muscle volume* and *cuticle volume & thickness* (also see Fig. 5.3). **(A)** As proxy for age post eclosion, I measured the brightness of the mandible cuticle from standardised photographs, both for randomly selected ants, and for a smaller subset of ants of known age after eclosion. **(B)** I quantified bite performance with a custom-built force sensor (described in detail in Chapter 4; 3D model of biting ant created by Fabian Plum with the open-source photogrammetry platform 'scAnt', see Plum and Labonte, 2021).

5.2.3 Cuticle brightness

In order to approximate the age of the ants post eclosion, I measured cuticle brightness (see e. g. E. O. Wilson, 1976; R. M. Schofield et al., 2002; Seid and Traniello, 2006), which typically decreases after eclosion, in concert with cuticle sclerotisation (Politi et al., 2019). To make this link quantitative, I also extracted the cuticle brightness from a set of nine callows of known age post eclosion (also see Muscedere et al., 2011). To this end, late-stage pupae were taken from the fungal gardens and

placed in a separate container (≈15 x 8 x 5 cm) with a small amount of fungus and dozens of minims to maintain them. The pupae were checked daily, and as soon as the legs had unfolded, they were marked with paint (Edding 4000 paint marker, Edding AG, Ahrensburg, Germany), and sacrificed after one (n = 3, 4.1 ± 0.9 mg), three (n = 3, 4.1 ± 0.8 mg) or five further days in the container (n = 3, 4.5 ± 1.0 mg; the difference in body mass between these subsets was not significant, ANOVA: $F_{1,6}$ = 0.22, p = 0.81).

To quantify cuticle brightness, I photographed worker head capsules in the horizontal plane using a high-resolution light microscope equipped with an apochromatic lens (camera: DMC5400, microscope: Z6 Apo controlled via *LAS X*; Leica Microsystems GmbH, Wetzlar, Germany; see Fig. 5.2A). Heads were placed on white paper next to a printed RGB colour stripe, which served as a baseline to enable comparison between relative colour differences across photographs (see Fig. 5.2A). To minimise such differences, I used the same exposure time and colour profile in *LAS X*, and kept lighting conditions approximately constant, using the microscope-internal light source and two external LED lamps. From each image, the RGB values for a defined set of 'regions of interest' (ROIs) were extracted using the 'Color histogram' function in *Fiji* (Schindelin et al., 2012). Three rectangular ROIs were taken from the colour stripe – one of each colour, approximately spanning 200 x 150 pixels – and one circular ROI from a 'tooth-free' region of the mandible blade with a diameter of 30 pixels (see Fig 5.2A). The perceived colour of the mandible is likely affected by both pigmentation and variations in translucency of the cuticle due to local variations in thickness. To minimise confounding effects, I always measured cuticle brightness at locations where the left and right mandible did not overlap. I then calculated cuticle brightness from the RGB values as $b_{RGB} = (R+G+B)/(3 \cdot 255)$, equivalent to an unweighted greyscale conversion native to *Fiji*. Neither body mass nor the brightness of the colour stripe differed significantly between these monitored callows (n = 9) and all other workers (n = 49; body mass: Wilcoxon rank sum test: W = 197.5, p = 0.63; brightness: Wilcoxon rank sum test: W = 374, p = 0.18). However, I found a significant correlation between body mass and cuticle brightness across the ants used for bite experiments (Spearman's rank correlation: ρ_{47} = -0.38, p < 0.01), such that dark ants ($b_{RGB} < 0.20$) weighed 5.2 ± 1.2 mg, and bright ants ($b_{RGB} > 0.35$) weighed 4.2 ± 1.2 mg, approximately 20 % less. This effect may be attributed to size-dependent differences in mandible thickness, which resulted in age-independent differences in cuticle translucency and brightness. I, however, argue that any confounding effects of body mass are small in comparison to the effects of ageing and the associated development of the bite apparatus (see section 5.3).

5.2.4 Nanoindentation

To investigate if the material properties of the head capsule change, nanoindentation experiments were conducted. To this end, a subset of twelve ants was used (from the 49 biting ants), covering the range of observed cuticle brightness: eight callows (4.3 ± 1.2 mg) and four foragers (4.3 ± 1.2 mg; the difference in body mass was not significant, Two sample t-test: t_{10} = 0.03, p = 0.97). The samples were embedded in two-part epoxy (EPO-Set, MetPrep Ltd., Coventry, UK), so that the horizontal head plane faced upwards (see Fig. 5.3A). To facilitate head capsule alignment, an insect pin was

pierced into each head capsule prior to embedding. After curing for at least 6 h, the samples were ground (Saphir 250 A2-ECO, QATM, Mammelzen, Germany) using abrasive silicon-carbide paper of increasing grit numbers (400, 800, 1200, 2500, 4000) in single pressure mode at 25 N for 30, 90, 120, 180 and 180 s, respectively. All samples were then polished with 0.3 μm alumina and 0.06 μm colloidal silica suspensions, respectively (MetPrep Ltd., Coventry, UK), at 15 N for 120 s each.

Indentations were performed with a Hysitron TriboIndenter (Ti 950, Bruker Corporation, Billerica, MA, USA) and a Berkovich probe. Each sample was indented numerous times (19 ± 9) at three different regions of the head capsule where the closer muscle attaches (see red areas in Fig. 5.3A). The minimum distance between indents was approximately 20 μm, and from indents to cuticle edge $\approx$ 2 μm. A trapezoidal loading profile in closed-loop displacement control was used with a load time of 5 s, a peak displacement of 300 nm, a hold time of 20 s, and an unloading time of 5 s. The indentation modulus was extracted from the unloading curve using the native control software and Oliver-Pharr analysis (see Oliver and Pharr, 1992); the tip-area function of the Berkovich tip was calibrated with 100 indents on fused quartz, and confirmed on polycarbonate standards supplied by the manufacturer. All measurements were conducted at ambient conditions.

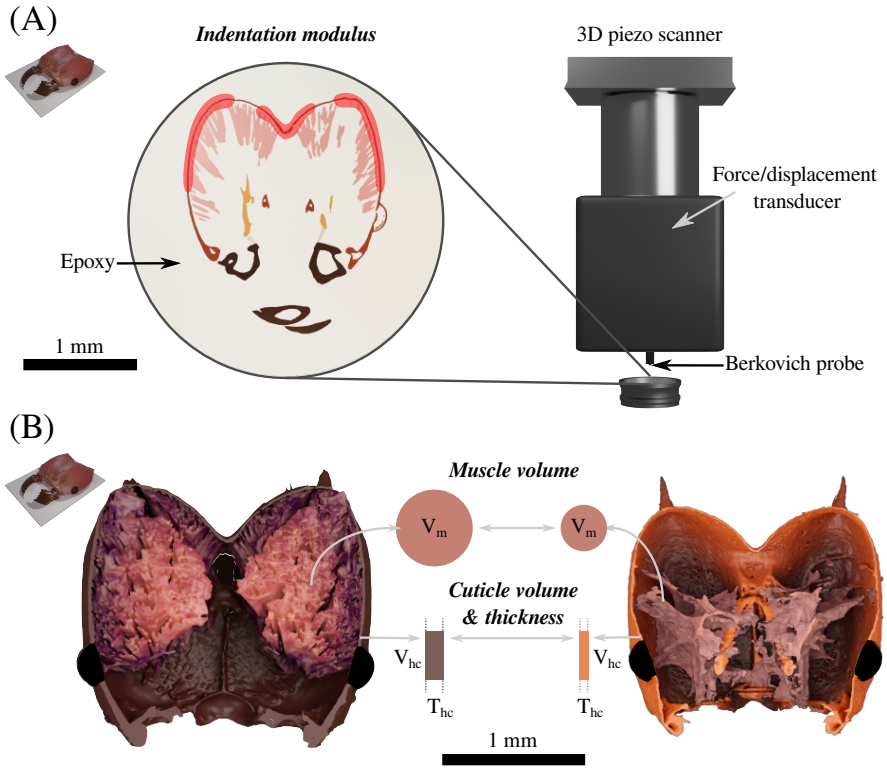


FIGURE 5.3: **(A)** In order to assess the change in structural rigidity of the head capsule, its indentation modulus was measured via nanoindentation experiments at several locations in the horizontal head plane (red areas), and the average head capsule thickness, T_{hc}, was extracted from μCT images **(B)**. From these images, I further extracted the volumes of the mandible closer muscle and head cuticle, V_m and V_{hc}, respectively.

5.2.5 Tomography and morphometric analysis

In order to quantify muscle volume and the thickness of the head capsule, an additional subset of ten ants was prepared for μCT imaging: seven callows (4.2 $\pm$ 1.3 mg) and three foragers (4.7 $\pm$ 1.5 mg); the difference in body mass was not significant (Two sample t-test: t_8 = -0.60, p = 0.56). For mature workers, the labrum and antennae were removed with forceps, and about five additional holes were pierced into the head capsule using insect pins to facilitate the fixative penetration. For the callows, only the antennae were removed, and the head capsule was otherwise left intact; this precaution was necessary to minimise deformation of the head capsule during manual manipulation (see section 5.3). All heads were fixed in paraformaldehyde solution (4 % in PBS, Thermo Fisher Scientific, Waltham, MA, USA) for 18 h, and subsequently dehydrated via storage in 70 %, 80 %, 90 % and 100 % ethanol for one hour each.

Prior to scanning, the samples were stained with 1 % iodine in ethanol for 48-168 hours (see Metscher, 2009), rinsed, and transferred to a pipette tip with 95 % ethanol. The samples were imaged via X-ray microscopy (XRM), using a lab-based Xradia Versa 520 (Carl Zeiss XRM Inc., Dublin, CA, USA; with a tube voltage of 70 kV, current of 85 μA, and exposure time of 500 ms), a CCD detector system with scintillator-coupled visible light optics, and a tungsten transmission target. A low energy filter was placed in the beam path (LE1, proprietary Carl Zeiss microscopy filter), and a total of 2401 projections were captured at a 4x lens magnification with 2x binning over a '180 degrees plus fan angle' range. The tomograms were reconstructed from 2D projections using a commercial software package (XMReconstructor, Carl Zeiss XRM Inc., Dublin, CA, USA), with a cone-beam reconstruction algorithm based on filtered back-projection, resulting in 8-bit greyscale image stacks with isotropic voxel sizes between 2.6 to 3.4 μm.

From the tomographic scans, the mandible closer muscle and head capsule were segmented in ITK-SNAP (v 3.6, Yushkevich et al., 2006), to then extract the respective tissue volumes (see Fig. 5.3B). The average cuticle thickness was obtained via the 'LocalThickness' function (boneJ plugin in *Fiji*, Domander et al., 2021), performed on the image stack of the head capsule segmentation. To quantify the error of the thickness measurement, I created an artificial 3D image of a hollow cylinder in Python (v 3.9.7, Van Rossum and Drake, 2009), with a uniform shell thickness of 10 px, within the range of average values extracted in this study (5-12 px). The estimated shell thickness was virtually uniform across the cylinder, and within $\approx$1 % of its true value. However, there may be a second source of error due to partial volume effects of the tomographic images; partial volume effects occur at the interfaces between two materials when a voxel is partially filled by both, resulting in an intermediate greyscale value (Withers et al., 2021). Such effects may be particularly problematic because the lowest measured cuticle thickness was only 5 px. During segmentation, I tried to avoid the 'smearing out' of tissue by excluding the voxels that had greyscale values closer to those of the tissue surroundings (also see Souza et al., 2005). However, this assessment is subjective and difficult to quantify. I hence offer a second argument in support of the accuracy of my measurements and the conclusions I draw from them: The head cross-sections used for nanoindentation were photographed with the microscope

and camera system internal to the Hysitron TriboIndenter. Cuticle thickness was then measured at 30 different locations across the sample (see red areas in Fig. 5.3A), as the length of the shortest line connecting both tissue boundaries. The extracted cuticle thickness of dark foragers exceeded that of the brightest callows ($b_{RGB} > 0.35$) by a factor of 2.3 (14.3 ± 2.9 μm vs 6.2 ± 1.9 μm), close to the ratio obtained from the segmented tomography scans (factor of 1.9, see section 5.3).

5.2.6 Statistical analysis

To test for significant correlation between cuticle brightness and the other experimental quantities, I performed Spearman's rank correlation tests to account for non-normality of brightness values (Shapiro-Wilk normality test: $W_{48} = 0.92$, $p < 0.01$). Due to methodological limitations, data for indentation modulus and cuticle thickness were unpaired and only available for a small subset of ants. To estimate both for all ants used in bite experiments, I characterised the relationship between indentation modulus, head capsule thickness and cuticle brightness via Ordinary Least Squares (OLS) regressions on $\log_{10}$-transformed data.

5.3 Results and discussion

In the days following eclosion, social insects often abstain from foraging tasks outside the nest, and instead exclusively engage in in-nest activities such as brood care (e. g. E. O. Wilson, 1980a; Seeley, 1982; Seid and Traniello, 2006). Although this 'age polyethism' is well established, it remains unclear why it occurs. From a biomechanical perspective, foraging requires the ability to generate and withstand substantial forces, be it for object grasping, carrying or mechanical processing. However, biomechanical traits are rarely studied in the context of age polyethism (but see R. M. Schofield et al., 2002; Muscedere et al., 2011; R. M. Schofield et al., 2011). To test if the mechanical demands of foraging limit the ability of young workers to partake in it, I quantified a set of key performance parameters of the musculoskeletal bite apparatus of *A. vollenweideri* leaf-cutter ants. Bite forces of fully-matured foragers exceeded those of freshly-eclosed callows by more than one order of magnitude. This variation may arise because the mandible closer muscle is not yet fully developed early after eclosion, or because the mechanical stability of the head capsule limits the maximum force that can be applied to it without collapsing. In the following paragraphs, I discuss the evidence of both hypotheses, and embed my findings in the context of age-related foraging in leaf-cutter ants.

5.3.1 Co-development of bite force and muscle post eclosion

One of the key performance metrics of the musculoskeletal apparatus is the maximum available bite force. Across workers with different cuticle brightness, maximum bite force varied by a factor of 13 from 102 ± 46 mN for dark foragers ($b_{RGB} = 0.17 \pm 0.03$) to only 8 ± 6 mN for the brightest callows ($b_{RGB} > 0.35$, see Fig. 5.4A), barely exceeding the sensor noise. The cuticle brightness, extracted for these ants, ranged from a minimum of 0.13 to a maximum of 0.52. For comparison, the cuticle brightness of the monitored ants decreased significantly from 0.37 ± 0.04 at one day to

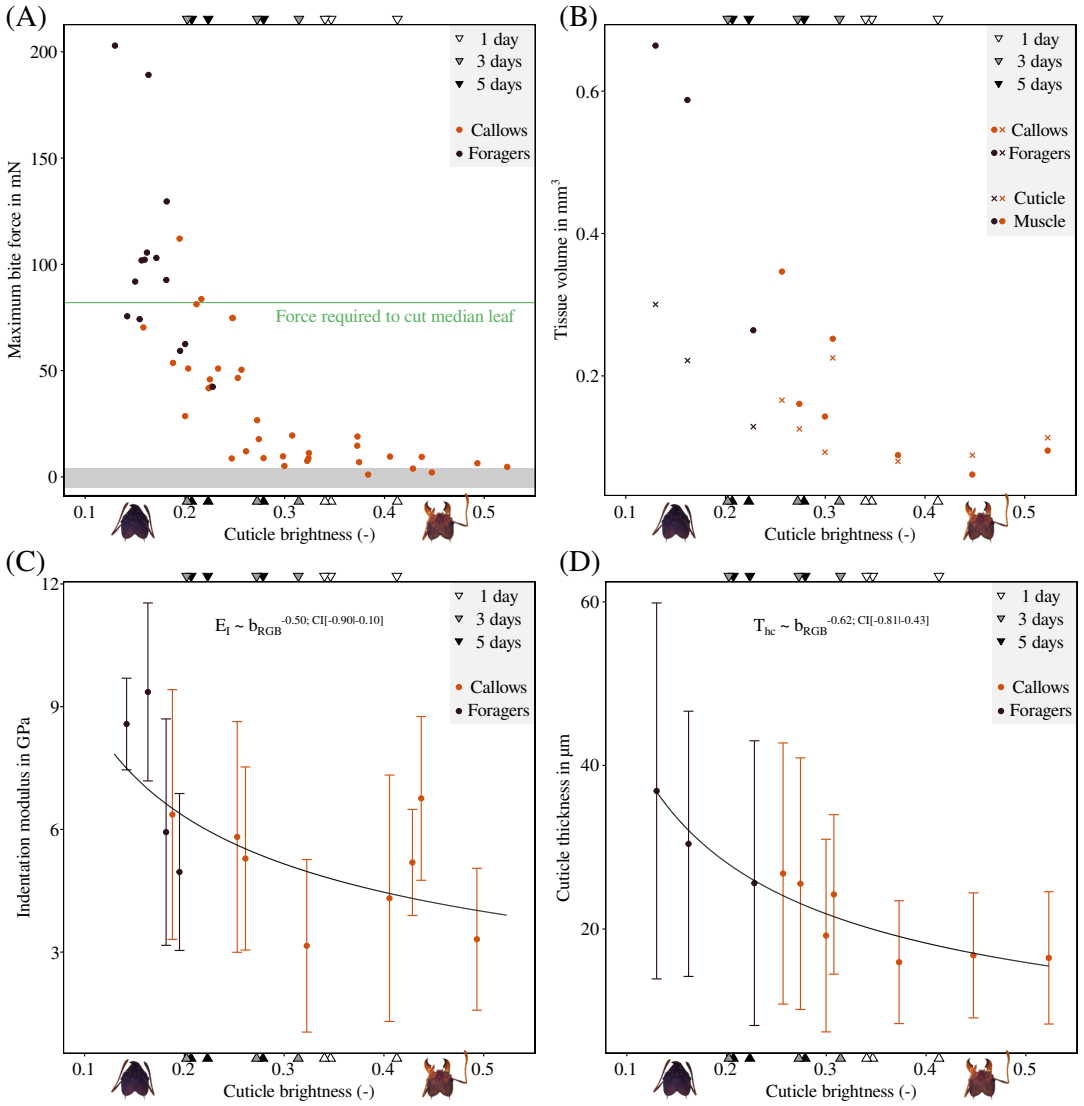


FIGURE 5.4: *Atta vollenweideri* leaf-cutter ant workers with varying cuticle brightness were extracted from the colony; workers with bright cuticle were extracted from the fungal gardens (callows), and those with dark cuticle from the foraging area (foragers). To link brightness to age, a set of nine late-stage pupae were photographed one, three or five days post eclosion (triangles). **(A)** Maximum bite force negatively correlates with cuticle brightness, and decreases steeply from a maximum of 200 mN for workers with dark cuticle to a minimum of less than 10 mN for bright callows, just in excess of sensor noise (shaded area, n = 49). The poor bite performance of callows likely constrains their ability to partake in foraging activities such as leaf-cutting; the force required to cut the median tropical leaf is about 80 mN, a factor of 10 larger than bite forces of callows (leaf data extracted from Onoda et al., 2011). **(B)** In order to investigate the origin of the variation in bite force, the total volume of the mandible closer muscle (circles), and of the head capsule cuticle (crosses) were extracted from segmented tomography scans. Muscle volume decreases significantly by a factor of six, and cuticle volume by a factor of two between fully-matured foragers and the brightest callows (n = 10). **(C)** To determine the flexural rigidity of the head capsule, both indentation modulus and thickness of the cuticle were measured. The indentation modulus, E_I, decreases significantly with cuticle brightness, b_{RGB}, by a factor of 1.5 (n = 12; Ordinary Least Squares (OLS) regression on $\log_{10}$-transformed data, slope: -0.50, 95% CI: [-0.90 | -0.10], R^2 = 0.43). **(D)** The average head capsule thickness, T_{hc}, decreases from $\approx$ 30 μm for foragers to $\approx$ 15 μm for the brightest callows (n = 10; OLS regression on $\log_{10}$-transformed data, slope: -0.62, 95% CI: [-0.81 | -0.43], R^2 = 0.87), suggesting that almost all variation in cuticle volume stems from changes in cuticle thickness.

0.24 ± 0.04 at five days post eclosion (ANOVA: $F_{1,6} = 6.84$, $p < 0.05$, see Fig. 5.4). These results suggest that the youngest biting callows were presumably younger than 24 h, and fully-darkened foragers were older than 5 days, which may be a conservative estimate given that closely-related *A. sexdens rubipilosa* ants spend 3-4 weeks in the callow phase (see R. M. Schofield et al., 2002).

The change in bite force is associated with a substantial increase in the volume of the mandible closer muscle; from bright callows ($b_{RGB} > 0.35$) to foragers, muscle volume increases by a factor of six from 0.08 ± 0.02 mm^3 to 0.51 ± 0.21 mm^3 (see Table 5.1 and Fig. 5.4B; volume data were combined for both head hemispheres). To put this change into perspective, the muscle volume of callows is about equal to that of fully-matured workers which are four times lighter (1.1 mg, see Chapter 2, and Fig. 5.5); a size that would typically not engage in leaf-cutting (Röschard and Roces, 2003b).

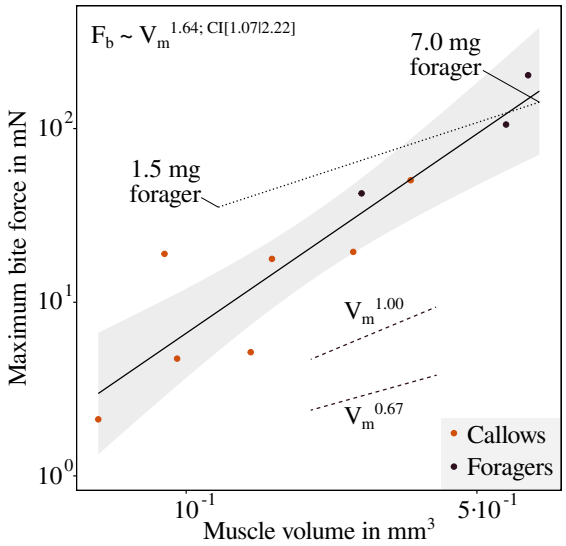


FIGURE 5.5: From callows to fully-darkened foragers of the same size, the maximum bite force increased with muscle volume as $F_b \propto {V_m}^{1.64}$ (OLS regression on $\log_{10}$-transformed data, 95% CI slope: [1.07 | 2.22], R^2 = 0.85). This positive allometry suggests that both muscle volume and volume-specific bite force increase substantially post eclosion. For comparison, a fully-matured worker of 1.5 mg with the same muscle volume and a third of the body weight produces four times higher bite forces (F_b was extracted for the same opening angle as this study, see Chapter 2 and 4).

The substantial increase in muscle volume raises the question to what extent body mass, too, may change during adult development. To test for such effects, I extracted a second size-metric from the tomographic scans, the distance between the mandibular joint centres (as defined in Chapter 2) – a metric that I considered unlikely to change with age. For callows, the joint distance was 1.13 ± 0.12 mm, not significantly different to that of foragers (1.20 ± 0.17 mm, Two sample t-test: $t_8 = -0.78$, $p = 0.46$). I hence assume that any change of body mass during maturation is negligible.

In order to assess to what extent the variation of bite force can be explained by changes in muscle volume, we first need a theoretical prediction for the scaling relationship between both. The basis for such a prediction is not obvious, because although the force of a muscle is typically proportional to its cross-sectional area (Josephson, 1975), it is unclear where exactly additional volume accumulates

TABLE 5.1: Results of Spearman's rank correlation on a set of biomechanical parameters paired with cuticle brightness, b_{RGB}. The degrees of freedom (Df = n-2), correlation coefficients (ρ) and p-values are provided for each test. All parameters apart from $\hat{\kappa}$ were significantly negatively correlated with cuticle brightness; $\hat{\kappa}$ represents a proxy for cuticle strain based on maximum bite force, and the flexural rigidity and thickness of the head capsule.

Parameter	Symbol	Df	ρ	P-value
Maximum bite force	F_b	47	-0.89	< 0.001
Muscle volume	V_m	8	-0.92	< 0.001
Cuticle volume	V_{hc}	8	-0.71	< 0.05
Cuticle thickness	T_{hc}	8	-0.94	< 0.001
Indentation modulus	E_I	10	-0.62	< 0.05
Cuticle 'deformation'	κ	47	-0.37	< 0.01
Cuticle 'strain'	$\hat{\kappa}$	47	0.02	= 0.89

during muscle development. Based on geometric similarity, the cross-sectional area grows proportional to $V_m^{0.67}$, which may provide a reasonable lower bound for the expected scaling relationship. For the upper bound, we may assume that muscle fibre length remains constant, so that all volume accumulates in the cross-section, and muscle force scales in direct proportion to volume; this may be a 'generous' upper bound as myofibrils typically grow both in width and in length during muscle maturation (Lemke and Schnorrer, 2017). Based on these assumptions, the expected scaling coefficient of bite force lies between two-thirds and one. I observed $F_b \propto V_m^{1.64}$, in substantial excess of both theoretical predictions (OLS regression on $\log_{10}$-transformed data, slope: 1.64, 95% CI: [1.07 | 2.22], R^2 = 0.85; see Fig. 5.5), suggesting that volume changes alone are insufficient to explain the increase of bite forces.

The mandible closer muscle in callow leaf-cutter ants is thus not only considerably smaller, but also has a reduced force capacity. Strikingly, this 'underperformance' was previously predicted by Muscedere et al. (2011), who studied the development of cephalic muscles in *Pheidole* ants post eclosion; they found that freshly-eclosed callows had muscle fibres that were substantially thinner (by a factor of up to three), had a non-uniform diameter, and lacked characteristic striation compared to mature ants (Muscedere et al., 2011). Although I was unable to identify the ultrastructure of the muscle from the tomographic scans, I also noticed further developmental differences in addition to changes in volume: Muscle fibres of callows were less distinctly separated and often detached from the head capsule (for more details, see Appendix D). The detachment of muscle is surprising because muscle attachment typically matures in the early steps of muscle morphogenesis, as shown in *Drosophila* (e. g. Lemke and Schnorrer, 2017; Luis and Schnorrer, 2021). To test if this effect arose as an artefact of freeze-thawing and sample preparation, another two callows were scanned (≈1 and 3 days old) that underwent the same protocol, but were not used in bite experiments (see Fig. D.1 in Appendix D). Muscle detachment was less severe in these ants, cautiously suggesting that (i) the bite

experiment may have caused some muscle fibre to detach, and (ii) muscle formation may have only just begun at the point of eclosion.

In fact, substantial muscle development after eclosion is common in insects: The cross-sectional area of beetle flight muscle (De Kort, 1990) and locust abdominal muscle (Rose et al., 2001) increases substantially. Flight muscles in bees display a sharp increase of enzyme activity in the first days after eclosion, suggesting biochemical adjustments (Roberts and Elekonich, 2005; Schippers et al., 2010; Skandalis et al., 2011). During metamorphosis in *Drosophila* flies and *Manduca* moths, the developing adult flight muscles initially lack fully-matured motor neurons required for muscle activation (e. g. Fernandes and Keshishian, 1998; Hughes and Salinas, 1999; Bayline et al., 2001). The 'underperformance' of muscle observed in this study, may hence be a result of the combined effects of anatomical, physiological, biochemical and neurological deficiencies. The exact magnitude of this performance gap is difficult to quantify as discussed above; a comparison to a smaller but fully-matured worker may be indicative nonetheless: A mature worker of 1.5 mg with the same muscle volume as a callow produces four times higher bite forces at a third of its body mass (see Fig. 5.5 and Chapter 2 and 4).

5.3.2 Flexural rigidity and the mechanical demands of the head capsule during biting

I have demonstrated that bite forces in callow leaf-cutter ants are strongly reduced, most likely due to incomplete muscle development. Next, I turn my attention to another biomechanical parameter that determines the ability to safely apply large bite forces: the mechanical stability of the head capsule. The ant head capsule is remarkably thin: even for mature ants, it has a thickness comparable to that of human hair (see Fig 5.4D). This thin head capsule has to resist substantial size-specific bite and muscle forces. A single muscle fibre with a diameter of 25-30 μm generates forces up to 0.70 mN, and ants of the considered weight have close to 1000 closer muscle fibres, resulting in a total force of $\approx$650 mN, more than ten thousand times their body weight (see Chapter 2 and 4). To estimate the structural stability of the head capsule, I consider the flexural rigidity, D, the relevant metric for thin plates deformed in bending (Young and Budynas, 2002):

$$D \propto E_I T_{hc}^3 \tag{5.1}$$

Here, E_I is the indentation modulus of the head capsule cuticle, and T_{hc} is its thickness.

E_I increased significantly with decreasing cuticle brightness ($p < 0.05$, see Table 5.1 and Fig. 5.4C; OLS regression slope: -0.50, 95% CI: [-0.90 | -0.10], R^2 = 0.43). For foragers, the indentation modulus was 7.2 ± 2.1 GPa, 1.5 times higher than for bright callows ($b_{RGB} > 0.35$), 4.9 ± 1.5 GPa; both values are well within the range of moduli reported for insect cuticle (0.4-30 GPa, see Vincent and Wegst, 2004; Labonte et al., 2017). The relative increase in modulus is consistent with previous work on insects: the bending modulus of locust tibiae increases approximately threefold during the growth phase following the final moult (Parle and D. Taylor, 2017), and the tooth hardness of leaf-cutter ant

mandibles increases by a factor of nearly three (R. M. Schofield et al., 2002), a development associated with increased zinc-concentration and possibly resistance to mandibular wear (also see R. M. Schofield et al., 2003). In some leaf-cutter ant species, a biomineral layer forms on the epicuticle a week after eclosion, resulting an a twofold increase in hardness (H. Li et al., 2020). The biomechanical development of insect cuticle is often linked to tanning and sclerotisation, a process associated with water loss and cross-linking of cuticle proteins with chitin (Wappner and Quesada-Allué, 1996; Vincent and Wegst, 2004; Politi et al., 2019). Indeed, cuticle hydration affects both indentation modulus and hardness (Vincent and Wegst, 2004; Klocke and Schmitz, 2011), and because the experiments in this study were conducted with small samples in ambient conditions, I likely overestimate the modulus, and underestimate its increase during post-eclosion development (see Fig. 3 in Labonte et al., 2017).

The head capsule thickness, T_{hc}, in turn increased significantly by a factor of two from 16.4 ± 0.4 μm for bright callows to 31.0 ± 5.7 μm for foragers ($p < 0.001$, see Table 5.1 and Fig. 5.4D; OLS regression slope: -0.62, 95% CI: [-0.81 | -0.43], R^2 = 0.87); this variation is comparable to the cuticle thickness range measured from the pronotum of other Myrmicine workers of similar head width ($\approx$1.7 mm, see Fig. 2 in C. Peeters et al., 2017). Notably, the increase in cuticle thickness appears to be non-uniform, indicated by the increasing standard deviation with decreasing cuticle brightness (see Fig. 5.4D): For bright callows ($b_{RGB} > 0.35$), the standard deviation is 7.8 ± 0.3 μm, significantly smaller than that of foragers, 18.9 ± 3.6 μm (Spearman's rank correlation: ρ_8 = -0.94, $p < 0.001$; this also holds for the coefficient of variation: ρ_8 = -0.70, $p < 0.05$). This result suggests a 'targeted' growth of cuticle during post-eclosion development, perhaps in regions most prone to deformation. Cuticle volume increases significantly, too, in almost direct proportion to cuticle thickness ($p < 0.05$, see Table 5.1 and Fig. 5.4B): Foragers have an average cuticle volume of 0.22 ± 0.09 mm^3, exceeding that of bright callows by a factor of 2.3 ($b_{RGB} > 0.35$, 0.09 ± 0.02 mm^3). Cuticle growth post eclosion has been reported for other insects such as e. g. locusts (Hepburn and Joffe, 1974; Parle and D. Taylor, 2017), grasshoppers (Neville, 1963), and moths (Hopkins and Kramer, 1992), and it is associated with the internal deposition of additional layers of endocuticle (Neville, 1963; Parle and D. Taylor, 2017). In the initial growth phase following the final moult, locusts deposit about 1.8μm of endocuticle per day (Parle and D. Taylor, 2017). Assuming that the age difference between foragers and bright callows is one week, the cuticle growth rate for leaf-cutter ants is about the same, 14.6 μm / 7 d $\approx$ 2 μm/d.

The combined effects of the changes in indentation modulus and cuticle thickness result in a drastic increase of the flexural rigidity with cuticle brightness (see Fig. 5.6A; to obtain a numerical value for D from Eq. 5.1, I used the proportionality factor $1/(12(1-0.3^2))$, see Young and Budynas, 2002). From the lightest to the darkest workers, the flexural rigidity increases by a staggering factor of 27, from 1.3 to 35.7 mN mm; I note that this result is based on interpolation via regression, and is hence affected by the associated uncertainties of the slope (see CIs in Fig. 5.4). The majority of this increase is driven by the change in cuticle thickness (factor of 13.4), which is cubed in Eq. 5.1, whereas the indentation modulus contributes linearly and thus has a much smaller effect (factor of 2.0). In order to demonstrate the effect of this difference in flexural rigidity, I calculated the expected deflection

for two plates of the same area, but of different thickness and moduli, approximated by T_{hc} and E_I, respectively, for a forager with a cuticle brightness of $b_{RGB} = 0.15$ and a callow with $b_{RGB} = 0.5$. Under the same load, equal to half of the maximum muscle stress extracted for closely-related *A. cephalotes* majors (Chapter 3), the resulting deflection of callow cuticle is 17 times higher than for dark cuticle; absolute values of deflection are estimated in Appendix D.

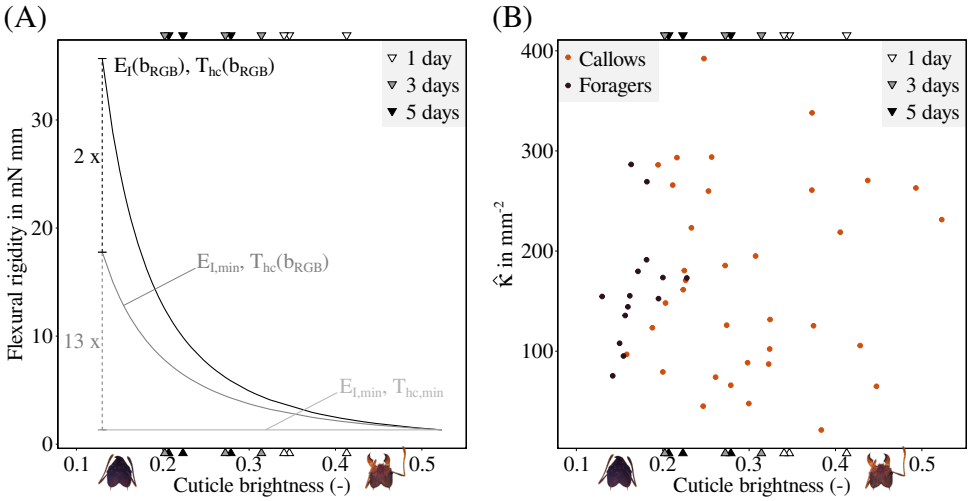


FIGURE 5.6: **(A)** The muscle development is accompanied by changes in cuticle thickness and indentation modulus, leading to an increase of the flexural rigidity of the head capsule, D, by a factor 27. The majority of this increase stems from an increase in cuticle thickness, T_{hc} (factor 13.4), due to the cubic dependency of D (see Eq. 5.1), whereas the indentation modulus, E_I, contributes only linearly (factor 2.0). The cuticle brightness of freshly-eclosed ants of known age is shown at the top and bottom abscissa for reference (triangles). **(B)** The ratio between maximum bite force and flexural rigidity normalised with cuticle thickness, $\hat{\kappa}$, serves as a proxy for cuticle strain. $\hat{\kappa}$ does not correlate significantly with cuticle brightness (p = 0.89, see Table 5.1), indicating an approximately constant mechanical demand on the head capsule during biting across the post eclosion development.

These results invite another hypothesis, why callows 'underperform' when biting, in addition to continued muscle growth and physiological development (see Fig. 5.5). Callows may 'choose' to bite with sub-maximal muscle force in order to avoid large deformations of the head capsule. I consider two possible constraints that may lead to permanent damages: (i) absolute deformation, relevant if the elastic deformation is sufficiently large to cause damage inside the head, e. g. by compressing soft tissues; and (ii), relative deformation, relevant if the stress in the cuticle exceeds its elastic limit, causing fissures or permanent deformation. First, I approximate the absolute cuticle deformation resulting from biting, κ, as ratio between maximum bite force and flexural rigidity. For foragers, $\kappa = 5.09 \pm 1.74\,\mathrm{mm}^{-1}$, 1.5 times higher than for bright callows $\kappa = 3.36 \pm 1.89\,\mathrm{mm}^{-1}$. This difference, although significant (p < 0.01, see Table 5.1), is remarkably small in comparison to the large variation in both bite force and flexural rigidity. Second, I estimate relative cuticle deformation or 'strain' as $\hat{\kappa} = \kappa / T_{hc}$. Strikingly, $\hat{\kappa}$ is not significantly correlated with cuticle brightness (p = 0.89, see Table 5.1 and Fig. 5.6B); it takes an average value of $170 \pm 85\,\mathrm{mm}^{-2}$. I stress that the numerical values of κ and $\hat{\kappa}$ do not translate to actual cuticle deformation and strain, respectively, but are approximately proportional to them; the counter-intuitive units arise from the square of a missing

length scale that causes the bending moment in the cuticle, which is likely proportional to the constant external head dimensions (also see Eq. D.1 in Appendix D).

Bite forces, muscle ultrastructure and volume, and head capsule rigidity all develop in the days following eclosion. Indeed, the increase of all extracted parameters with decreasing cuticle brightness follow a similar pattern, with a rapid increase in a narrow range of brightness values (see Fig. 5.4). This co-development results in an approximately constant mechanical strain on the head capsule cuticle associated with maximum bite force throughout the callow phase of the workers. Future work will need to address to what extent these changes are causally linked, as is observed in vertebrates (see e. g. Nowlan et al., 2008, 2012; Boselli et al., 2015).

5.3.3 Biomechanical limitations of foraging ability in leaf-cutter ants

I set out to investigate if the behavioural transition from within-nest to outside-foraging tasks may arise from variation in biomechanical performance. I have reported evidence for strong changes in bite force in the days following eclosion. Now, I address if these changes may explain why young callows do not forage. In leaf-cutter ants, foraging involves the cutting and carrying of leaf fragments from fresh vegetation surrounding the nest (Wirth et al., 2003). The ability of a forager to cut leaves depends on the ratio of two key forces: the maximum bite force, and the minimum force required to initiate and propagate a cut through leaf lamina and veins (F. Clissold, 2007). Based on published mechanical data for around 1000 tropical leaves, the expected cutting forces range between 7-828 mN, with a median of 82 mN (Onoda et al., 2011, and Chapter 4). Thus, the foragers used in this study would be able to cut approximately half of the measured tropical leaves, whereas bright callows could cut virtually none of them. But, foraging also involves the carrying of leaf fragments: A forager of 5 mg may carry fragments of around 15 mg, or three times its body weight (Rudolph and Loudon, 1986; Röschard and Roces, 2003b). This load may sound heavy, but the gravitational force that needs to be countered is only 0.15 mN, small even compared to the poor bite performance of callows. However, fragments cut from grasses may be as long as 30 mm (Röschard and Roces, 2003b), five times longer than the ants themselves (Moll et al., 2010), or 20 times their head length (see Chapter 2); carrying fragments of this length poses a difficult mechanical challenge, which requires continuous adjustments of the neck angle to maintain stability during walking, and likely involves large moments around the neck joint (Moll et al., 2010, 2013). Assuming that neck muscles are similarly underdeveloped early after eclosion, the ability to carry large fragments may be limited in young callows.

Our results suggest that the foraging ability of young workers is largely constrained by a poor bite performance based on underdeveloped muscles and a low mechanical stability of the head capsule. But, the mechanical constraints of age polyethism may continue beyond the time frame considered here: Foragers with worn mandibles may require more than twice the force to cut the same material than those with pristine mandibles (R. M. Schofield et al., 2011, and Chapter 6), and they are more

likely to carry leaves instead of cutting (R. M. Schofield et al., 2011); eventually, the oldest workers often switch to tasks related to waste disposal (Hart and Ratnieks, 2001; Camargo et al., 2007).

5.4 Conclusion and outlook

In the days following eclosion, the musculoskeletal bite apparatus of young leaf-cutter ants undergoes substantial biomechanical development: the maximum bite force, muscle volume, head capsule thickness and the cuticle-mechanical properties all increase substantially, from a point where bite forces would be too low to cut, and the head capsule too mechanically unstable to resist large muscle forces, to full biomechanical ability; leaf-cutter ant callows are not yet able to engage in foraging tasks involving cutting. My findings add further support to the hypothesis that age polyethism is largely dictated by developmental factors (e. g. Seid and Traniello, 2006; Muscedere et al., 2009), and suggests exciting avenues for future research on the co-dependency of muscle and cuticle development, which hints at an important role of mechanical stimuli, an area of research that has received considerable interest in vertebrates (e. g. Nowlan et al., 2008, 2012; Boselli et al., 2015), but less so in invertebrates (see e. g. Parle et al., 2017; Lemke and Schnorrer, 2017). Many tasks in colonies of social insects impose mechanical demands, and I thus hope that biomechanical analyses will help to increase our general understanding of age polyethism more broadly.

6 Scaling of mandibular cutting forces

I acknowledge the contributions of Liv Walthaus, who synthesised the polymer sheets, characterised their mechanical properties, and helped with the cutting force experiments.

Summary

Regardless of body size, many herbivores need to mechanically process plant tissue with their bite apparatus. The ability to do so is determined by two forces: the maximum available bite force, and the minimum required force for cutting. It remains unclear how the ratio of these forces varies across body sizes. The size-dependent ability to cut leaves is of particular importance to the ecology of leaf-cutter ants, which can vary vastly in body size. In combination with previously measured bite force data, I assessed the cutting ability of *Atta vollenweideri* ants. To this end, I measured the forces required to cut synthetic PDMS sheets with differently-sized mandibles, using a custom-built force setup. Cutting forces were independent of mandible size, but increased by a factor of two between callows with pristine mandibles and foragers with varying degrees of mandibular wear. Adverse effects of mandibular wear are thus likely more important than size-differences, suggesting that the ability to cut a given leaf is mainly determined by mandibular wear, the size-dependent capacity for bite force generation, and plant-mechanical properties. I argue that the main findings of this study can be extrapolated to plant materials, and speculate that mandibular wear may substantially limit the range of accessible plant tissues, not only for leaf-cutter ants, but for insect herbivores in general.

6.1 Introduction

Plant-feeding occurs at vastly different scales ranging from large bulk-feeding mammals to tiny cell-ingesting leaf miners (Sanson, 2006). Despite these differences in scale, all herbivores share the same basic task: they need to mechanically access the plant tissue; i. e. if they cannot tear, masticate, cut, pierce or drill the plant, they cannot feed on it. From a mechanical perspective, a necessary condition for plant-feeding is then given by the ratio of two key forces: the maximum available force, determined by the musculoskeletal apparatus, and the minimum required force to fracture the tissue (Sanson, 2006; F. Clissold, 2007).

It is difficult to assess *a priori* how this force ratio changes across animals of different sizes: Based on a simple scaling argument, the maximum available force may increase in proportion to body mass to the power of two-thirds (Alexander, 1985), which seemingly suggests that larger animals require a smaller fraction of their force capacity for plant-feeding. However, this conclusion is premature

as it neglects the second relevant force: the minimum force required for fracture. The scaling and magnitude of this force is more difficult to predict because it depends both on plant-mechanical properties (Vincent, 1990; P. W. Lucas et al., 2000; Sanson et al., 2001; Onoda et al., 2011; Hua et al., 2020), and on the geometry of the cutting, chewing or piercing 'tool' in question (P. W. Lucas, 2004; T. Atkins, 2009; R. M. Schofield et al., 2016; P. S. Anderson, 2018; Crofts et al., 2019; Gundiah and Jaddivada, 2020).

An organism where body size is a key parameter of the behavioural portfolio, in particular relating to herbivory, are leaf-cutter ants (E. O. Wilson, 1980a; Wirth et al., 2003; Hölldobler and E. O. Wilson, 2010). Leaf-cutter ant colonies consist of up to several million workers, which cover a large range of body sizes from less than a milligram to over 100 mg in some species (Weber, 1972; Wetterer, 1994a, 1995a; Wetterer, 1999); colony workers that typically partake in foraging tasks range between 1-30 mg (Wetterer, 1994b, 1995a; Röschard and Roces, 2003b).

Leaf-cutter ant foraging involves the cutting and transporting of leaf fragments from various plants in the colony surroundings (J. M. Cherrett, 1968, 1972; E. O. Wilson, 1980a; Wirth et al., 2003). Some aspects of foraging are known to be affected by worker size: e. g. larger ants cut and carry larger fragments (Roces, 1990; Wetterer, 1991a, 1994a; Burd, 1996), cut and carry at higher speeds (Rudolph and Loudon, 1986; Howard, 1988; Nichols-Orians and Schultz, 1989; Roces and Hölldobler, 1994; Burd, 1996; Röschard and Roces, 2002; R. M. Schofield et al., 2011), and forage on 'tougher' plants than smaller ants (J. M. Cherrett, 1972; E. O. Wilson, 1980a,b; Rudolph and Loudon, 1986; Nichols-Orians and Schultz, 1989; Nichols-Orians and Schultz, 1990; Wetterer, 1991a, 1994b).

In contrast to this strong observational evidence for size-effects in foraging, the biomechanical reasons for it remain poorly understood (but see Wetterer, 1991a; Paul and Gronenberg, 1999; R. M. Schofield et al., 2011). In order to assess the size-effects on the ability to leaf-cut, I previously measured the maximum available bite forces of *Atta vollenweideri* leaf-cutter ants (see Chapter 4). Peak forces increased with a strong positive allometry, $F_b \propto m^{0.90}$, in substantial excess of the isometric prediction, $F_b \propto m^{0.67}$. A large forager of 30 mg generates peak bite forces of about 600 mN, 12 times more than a small forager of 2 mg, $F_b \approx 50$ mN (see Chapter 4). As a result, large foragers are presumably able to cut a considerably larger fraction of tropical leaves (see Chapter 4 and Onoda et al., 2011). This conclusion, however, remains speculative without also quantifying the scaling of forces required for cutting. Based on geometric similarity, we may naively expect the cutting forces to vary approximately as $F_c \propto L_c \propto m^{0.33}$, increasing linearly with a characteristic length (Kamyab et al., 1998; R. M. Schofield et al., 2016; Schuldt et al., 2016). However, leaf-cutter ant mandibles vary not only in size across polymorphs, but also in shape (L. C. Silva et al., 2016, and N Imirzian, F Püffel and D Labonte, in preparation). It is thus prudent to directly measure mandibular cutting forces across sizes in order to establish a scaling relationship empirically. For this reason, I extracted differently-sized ant workers from the colony, isolated their mandibles, and measured mandibular cutting forces with a custom-built setup. Based on these measurements, I then assess the size-dependence of cutting ability in leaf-cutter ants based on bite force capacity and mandible 'sharpness', and discuss avenues

for future research emerging from these findings.

6.2 Materials & methods

6.2.1 Study animals

I extracted *A. vollenweidei* leaf-cutter ants from two colonies, founded and collected in Uruguay in 2014. The colonies were kept in a climate chamber (FitoClima 12.000 PH, Aralab, Rio de Mouro, Portugal) at 25 $^{\circ}C$ and 50 - 60 % relative humidity, with a 12/12 h light-dark cycle; they were fed with bramble, laurel, cornflakes and honey water *ad libitum* in a foraging arena that was connected to the main colony via PVC tubes ($\approx$ 30 cm to the closest fungus box with an inner tube diameter of 25 mm).

To quantify the effects of worker-size on cutting forces, I collected two sets of ants across the entire size-range, excluding the smallest workers, which typically do not cut leaves (body mass $<$1 mg E. O. Wilson, 1980a; Röschard and Roces, 2003b): First, I extracted a set of workers from the fungal garden that had either freshly eclosed, identified by their bright cuticle, or were still in the pupal stage (see R. M. Schofield et al., 2003, 2011). In the weeks following eclosion, callows remain inside the nest and abstain from foraging activities (E. O. Wilson, 1980a; Camargo et al., 2007). During this time, the bite apparatus undergoes a substantial biomechanical development; only after this development are workers fully capable of partaking in foraging tasks (see Chapter 5 and R. M. Schofield et al., 2002). The mandibles of these workers were thus expected to be 'pristine', which allowed us to test for the effects of mandible size on cutting force without confounding effects due to mandibular wear (see R. M. Schofield et al., 2011). To ensure the incorporation of zinc into the mandibular teeth was completed, I kept the callows alive until at least 72 h post eclosion (see R. M. Schofield et al., 2003, 2011); eclosion was defined as time point at which the legs had completely unfolded (also see R. M. Schofield et al., 2003). To monitor pupae and callows, I placed them in centrifuge tubes, which in turn were placed inside the foraging arena of the colony. The tubes contained small amounts of fungus, and had a 3D-printed PLA lid with holes too small for the collected workers to pass through, but large enough for minims to enter for pupal maintenance (see R. M. Schofield et al., 2011). This method was unsuitable for smaller ants, which would often manage to leave the tubes. Most smaller ants ($<$10 mg) were hence collected by transferring late-stage pupae into a completely separated container with sufficient amounts of fungus and numerous minims. As soon as an ant hatched, it was marked with a unique colour code (Edding 4000 paint marker, Edding AG, Ahrensburg, Germany) for identification (also see Pielström and Roces, 2013).

I next collected a set of differently-sized and fully-matured workers from the foraging arena. These workers had acquired the biomechanical ability to forage (see Chapter 5 and R. M. Schofield et al., 2002), and were thus likely to show signs of mandibular wear from cutting leaves (R. M. Schofield et al., 2011). Quantifying the mandibular cutting forces for these ants in addition to callows allowed us to investigate the effects of mandibular wear on cutting ability as a function of worker size.

6.2.2 Mandible preparation and wear determination

All ants were sacrificed by freezing, weighed to the nearest 0.1 mg (Explorer Analytical EX124, max. 120 g x 0.1 mg, OHAUS Corp., Parsippany, NJ, USA; body mass ranged between 1.8 to 46.4 mg), and decapitated using micro-scissors. The head capsules were split in half along the sagittal plane using a scalpel, and only the left head hemisphere was retained (see Fig. 6.1). Leaf-cutter ants show no preference between left and right mandible when cutting (Tautz et al., 1995), and their bite apparatus is bilaterally symmetric (see Chapter 2) I hence conjecture that there are no systematic differences between both sides. To facilitate sample mounting, I inserted insect pins into the head halves (size '2' for ants < 10 mg, size '4' for ants of 10 - 20 mg, and size '6' for ants > 20 mg). I then immobilised the interfaces between insect pin, head capsule and mandible base around the joint with two-component epoxy (Araldite Rapid, Huntsman Corp., The Woodlands, TX, USA) to minimise compliance of the mandible-head-pin complex (see Fig. 6.1).

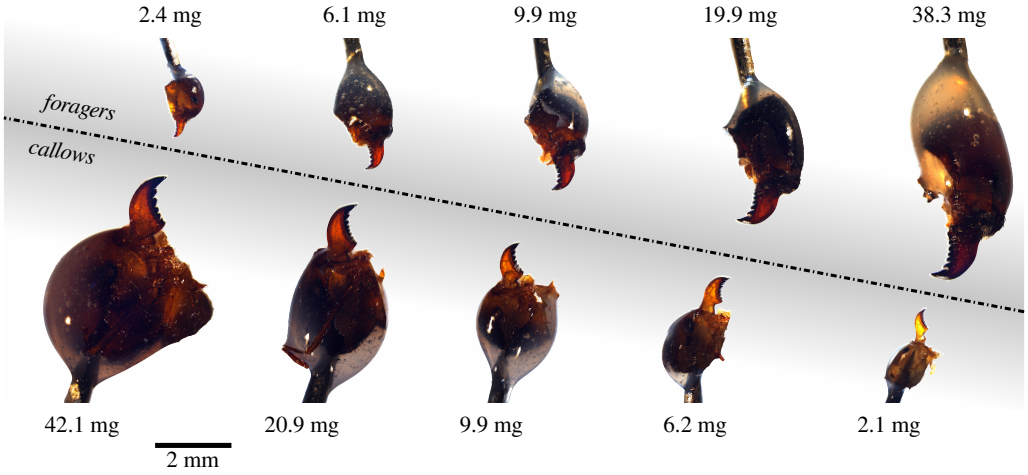


FIGURE 6.1: In order to measure mandibular cutting forces, *Atta vollenweideri* leaf-cutter ants across the size-range were extracted from the foraging arena and fungal garden of two colonies, and their mandibles were prepared for cutting experiments. Both foragers (with worn mandibles) and callows (with pristine mandibles) were used for the experiments to quantify the effects of both worker size and mandibular wear on cutting force.

In order to determine a proxy for the degree of mandibular wear, I photographed the mandibles with a camera mounted onto a light microscope (DMC5400 on Z6 Apo, Leica Microsystems GmbH, Wetzlar, Germany); the mandibles were aligned such that their dorsal surface was in focus. Numerous metrics for mandibular wear have been proposed in literature, including mandible length changes (Raupp, 1985; Dockter, 1993), shape changes of the mandibular cutting edge (Roitberg et al., 2005; M. Smith et al., 2007; Kvedaras et al., 2009), number of lost mandibular teeth (Oettler and Johnson, 2009), reduction in profile area of distal mandibular teeth (Kokko et al., 1993), and length changes of the mandibular teeth most relevant for cutting (R. M. Schofield et al., 2011; Kuřavová et al., 2014). All of these metrics are proxies with no direct established mechanistic link to cutting force. As such, their predictive value can only be assessed in correlation to direct cutting force measurements, and selecting any one of them is difficult to justify *a priori*. I chose a metric that has been demonstrated to be significantly correlated with cutting force in closely-related *A. cephalotes* ants, so enabling a direct

comparison (R. M. Schofield et al., 2011); however, I do not intend to imply that this metric is more or less suitable than any of the others. In accordance with R. M. Schofield et al. (2011), mandibular wear, W, was defined as:

$$W = (\Delta T_2 + \alpha \Delta T_1)/2 \tag{6.1}$$

ΔT_1 and ΔT_2 are the length differences between the most distal and second most distal tooth, respectively, and their expected pristine length. Pristine tooth length was obtained via regression analysis on measurements of callow mandibles (see Appendix E); α is a weighting factor, defined as ratio between the average length differences, $\alpha = \overline{\Delta T_2}/\overline{\Delta T_1}$ (for more details, see R. M. Schofield et al., 2011).

I measured the length of the mandible blade and the two most distal teeth from each photograph (for exact methodology, see Appendix E), and calculated wear as in Eq. 6.1. 17 out of 76 mandible length and ten teeth length measurements were impossible, because relevant parts of the mandible were obstructed by the head capsule.

6.2.3 Polymer synthesis and mechanical testing

In previous studies on mandibular cutting forces, leaf lamina and floral petals were used as cutting substrates (Tautz et al., 1995; R. M. Schofield et al., 2011). However, plant tissues are typically heterogeneous, of uneven thickness, and have mechanical properties that vary with hydration and tissue age (e. g. Choong, 1996; Spatz et al., 1999; Hayot et al., 2012; Hua et al., 2020; Cordoba-Barco et al., 2020). In order to minimise variation due to material inhomogeneities, I hence used well-defined PDMS sheets as cutting substrate. Such 'synthetic leaves' can be rendered attractive to leaf-cutter ants by adding food odours (e. g. Roces, 1990; Roces and Lighton, 1995; Arenas and Roces, 2018, and own observations); the quantitative predictions resulting from this study may hence be tested in future experiments on live ants (see 6.4).

The PDMS sheets were synthesised based on a 4:1 (silicon base: curing agent) mixing ratio (SYLGARD 184, Dow Inc., Midland, MI, USA). The mixed but uncured PDMS was sandwiched between two salinised glass plates, separated by feeler gauges ($200 \pm 6\,\mu$m, Precision Brand, Downers Grove, IL, USA; see Fig. 6.2B), and pre-cured at 100°C for two hours. The PDMS 'sandwich' was then cooled to room temperature, slowly peeled from the glass plates, placed on aluminium foil, and fully cured at 165°C for 48 hours (Seghir and Arscott, 2015).

To mechanically characterise the PDMS sheets, pure shear tearing and uniaxial tension tests were conducted with a universal tension and compression system (Multitest5-xt, Mecmesin Ltd., Slinfold, UK; using a 10 N load cell and Mec277 double-action vice grips with diamond jaws). Two rectangular samples from each of eight individual sheets were prepared for pure shear tearing; in one of the two samples, a notch of 3 mm length was introduced at the centre of the short side (see Fig. 6.2 for dimensions). Both samples were tested at a strain rate of 0.0067 s^{-1} to approximate quasi-static

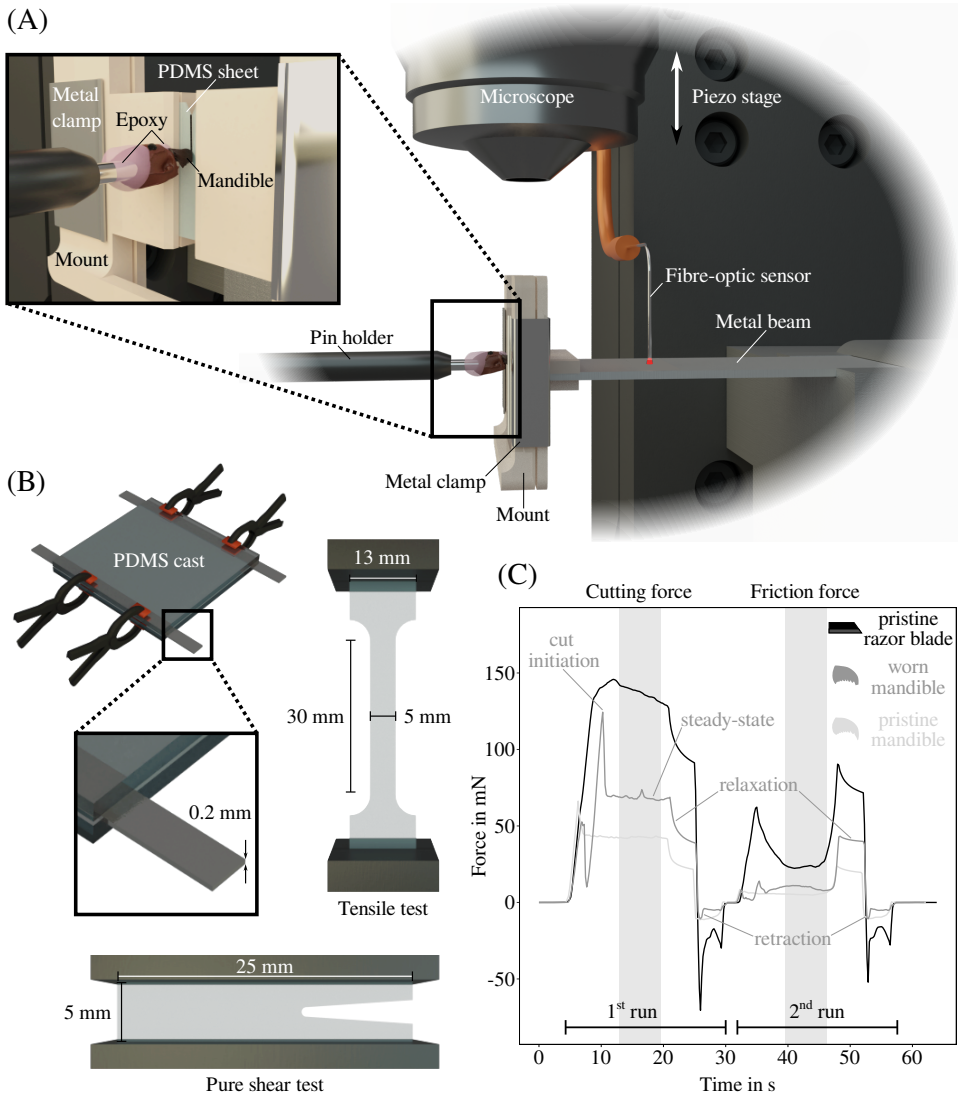


FIGURE 6.2: **(A)** To quantify the effects of worker size and mandibular wear on cutting force, I measured cutting forces using a custom-built setup based on a fibre-optic displacement sensor and a bending beam, both connected to a piezo motor stage. The cutting substrate was mounted at the free end of the beam, and the mandible was positioned above the substrate. The setup was moved vertically against the mandible, causing the substrate to be cut and the beam to deflect (see Appendix E for calibration details). **(B)** As cutting substrate, I used PDMS sheets of $\approx 200\ \mu$m thickness, mechanically characterised via pure shear and tensile tests following established protocols (see section 6.2.3). **(C)** After an initial loading phase, the forces peaked at cut initiation and then dropped to an approximately constant value. After this 'steady-state' phase, the forces dropped again when the motor stopped and became negative as the setup was moved back to its original position. A second run through the cut was performed to extract the friction between mandible blade and the cut PDMS. I extracted the drift-corrected average cutting force and the corresponding friction across 2 mm cutting distance (shaded areas) for further analysis.

loading conditions. From the notched sample, the critical displacement at rupture was identified; the force-distance curve of the unnotched sample was then integrated from zero to this critical displacement to obtain the work done by the applied load. Fracture toughness was calculated as this work divided by sample width and thickness (for more details, see J.-Y. Sun et al., 2012; B. Zhang et al., 2019); on average, the fracture toughness was $G_c = 98 \pm 7\,\mathrm{J/m^2}$.

Next, uniaxial tension tests at 0.5 mm/s motor speed were conducted with two 'dog-bone' samples cut from each sheet according to ISO standards (ISO37 and ISO5893, see Fig. 6.2). The Young's modulus was extracted from the loading region of the stress-strain curve via linear regression between 0-10 % strain (see Palchesko et al., 2012; Creton and Ciccotti, 2016); on average, the Young's modulus was $E = 4.1 \pm 0.3\,\mathrm{MPa}$. Sheet thickness was measured at six random locations across the sheet with a digital micrometer (max. 25 mm x 0.001 mm, Mitutoyo Corp., Kawasaki, Japan); on average, sheet thickness was $215 \pm 8\,\mu\mathrm{m}$.

6.2.4 Cutting force setup

To measure mandibular cutting forces, a custom-built setup was designed based on a fibre-optic displacement sensor (μDMS-RC32 controlled via DMS Control v 3.015, Philtec Inc. Annapolis, MD, USA; linear range of 2.5 mm, recording at 81.4 Hz at 30° and 50 % transmitted optical power). The sensor was held in place by a custom-built holder, mounted on two micromanipulators to control its orientation, and attached to a piezo motor stage (M-404.6PD controlled via PIMikroMove v 2.33.3.0, Physik Instrumente GmbH & Co. KG, Karlsruhe, Germany; see Fig. 6.2A). The sensor was placed above a bending beam made from stainless steel and clamped on one side, with a thickness of 0.35 mm, a width of 10.4 mm, and a free length of 28.7 mm, such that the sensor tip was about $400\,\mu$m above the beam surface (see Labonte and Federle, 2015, for a similar setup). At the free end of the beam, a 3D printed mount was attached; this mount held the PDMS sheets during the experiments, clamped in place by two metal clips on either side (Supaclip 40, Rapesco Office Products PLC, Sevenoaks, UK). At the centre of the mount, there was a 'free' cutting region (1.5 mm wide and 8 mm long), over which the mandibles and razorblades were positioned (see Fig. 6.2A).

I calibrated the sensor with a series of ten calibration weights ranging between 10-245 mN (Kern & Sohn GmbH, Balingen, Germany), covering the range of observed mandibular cutting forces (19 - 172 mN). Weights were suspended from the mount in increasing order, and at the lever arm at which cutting forces were applied. For each calibration weight, I averaged the sensor output across 5 s after initial force fluctuations had faded (see Fig. E.2 in Appendix E). To account for sensor drift, the sensor output was extracted for the unloaded beam at the beginning and end of the measurement, and a linear drift correction was implemented; sensor drift, however, was generally small, ≈ 0.01 mN/s, or 6 mN and thus less than 5 % of the smallest cutting force over the duration of a typical measurement of 60 s. From simple beam theory, the relationship between applied force and beam deflection should be linear for small deflections. I indeed observed linearity for calibration forces < 150 mN; for forces

exceeding 150 mN, however, the sensor distance was systematically 'sub-linear', suggesting deflections sufficiently large to invalidate the use of the small angle approximation. I thus used a quadratic regression model to characterise the relationship between force and distance, which accounted for more than 99 % of the variation, and yielded a lower Akaike Information Criterion compared to a linear or cubic model ($AIC_{linear} = 91.7$, $AIC_{quadratic} = 59.6$, $AIC_{cubic} = 61.6$; see Fig. E.2 in Appendix E).

6.2.5 Experimental protocol

I mounted the mandibles individually onto a pin holder, which was connected to a 3D micromanipulator. The mandibles were positioned using a top-down microscope such that the dorso-ventral head axis was approximately horizontal, the mandibular teeth were roughly perpendicular to the PDMS sheet, and the most distal tooth tip just about extended over the sheet (see R. M. Schofield et al., 2011, and Fig. 6.2A).

I cut a small wedge into all PDMS sheets ($\approx 30^{\circ}$ and 1.5 mm deep) to facilitate the cut initiation by reducing effects of sheet bending and buckling (see Lake and Yeoh, 1978; R. M. Schofield et al., 2011; B. Zhang et al., 2019). The unstretched sheets were placed individually between the two components of the polymer mount, and metal clips were slid onto the mount using the clip dispenser provided by the manufacturer, such that both clamps were approximately parallel and 6 mm away from the mount centre (see Fig. 6.2A); this procedure ensured that the clamping conditions were kept approximately constant across measurements.

I then moved the sheet toward the mandible by incrementally moving the motor stage upwards until the tip of the pre-cut wedge was about to contact the mandibular cutting edge. The sensor recording was started, and the PDMS sheet was moved vertically against the mandible blade, akin to the 'blade-like' cutting behaviour observed in 'freely cutting' leaf-cutter ants (see Tautz et al., 1995; R. M. Schofield et al., 2011). The motor moved at a constant speed of 0.3 mm/s, at the upper end of cutting speeds observed during foraging (≈0.02 - 0.30 mm/s, see J. M. Cherrett, 1972; Nichols-Orians and Schultz, 1989; Roces and Hölldobler, 1994; Roces and Lighton, 1995; Tautz et al., 1995; Burd, 1996; R. M. Schofield et al., 2011), and over a total distance of 5 mm; the beam deflected by around 100 μm for a medium cutting force of 65 mN, so that the corresponding displacement of the sheet-holding mount was about 4.9 mm (see Appendix E figure on sensor calibration). The sheet was subsequently retracted to its original position, and a second run was initiated in order to extract the force due to friction and elastic deformation of the thin sheet (henceforth referred to as friction force, see e. g. A. G. Atkins and Mai, 1979; McCarthy et al., 2007; T. Atkins, 2009; Schuldt et al., 2016). After a force peak at cut initiation, the cutting forces remained approximately constant until the motor stopped, and forces decreased (see Fig. 6.2C). I extracted the drift-corrected steady-state cutting force averaged across 2 mm following the initial peak; the corresponding friction forces were extracted from the second run at the same motor positions, and averaged across the same distance (see Fig. 6.2C).

The cutting speeds observed for leaf-cutter ants typically vary with forager size; larger ants cut more quickly than smaller ants (Nichols-Orians and Schultz, 1989; Roces and Hölldobler, 1994; R. M. Schofield et al., 2011). To quantify the effects of speed on cutting force, I performed a series of measurements with a single individual (forager with a body mass of 19.9 mg) at 0.1 mm/s, 0.2 mm/s and 0.3 mm/s. Three repetitions were done per speed without remounting the mandible between measurements to reduce confounding effects due to small variations in mandible blade orientation. Variation due to remounting was quantified by measuring cutting forces of one small (5.4 mg) and one large forager (38.4 mg) at a constant cutting speed of 0.3 mm/s. Both samples were mounted three times onto the pin holder, and cutting experiments were performed three times per mount.

Mounting had no significant effect on cutting force (Analysis of Variance (ANOVA), small worker: $F_{2,6}$ = 4.43, p = 0.07; ANOVA, large worker: $F_{2,6}$ = 0.26, p = 0.71); I hence pooled the nine measurements per mandible and calculated the coefficient of variation, CV, for each: $CV_{\text{small}} = 0.10$ and $CV_{\text{large}} = 0.03$ (see Fig. 6.3B). The relative force variation was thus three times larger for the smaller mandible, suggesting that consistent mandible alignment was easier for larger mandibles. However, even for the smaller mandible, the force variation was small in comparison to the inter-individual variation across all foragers, $CV_{\text{foragers}} = 0.52$ (see section 6.3). I thus performed only a single measurement, from one individual mount per specimen, unless otherwise indicated.

To contextualise our results based on *biological* ant mandibles and *synthetic* PDMS sheets, I performed two additional experiments. First, I measured cutting forces of pristine razor blades (10050-00, Fine Science Tools, Foster City, CA, USA; 0.1 mm thickness), broken into small fragments ($\approx$1 mm wide and 5 mm long) with a clamping tool to reduce the contact area between blade and the PDMS sheet (n = 6). Second, I performed cutting experiments with mandibles on a biological substrate, the leaf lamina of Japanese laurel, *Aucuba japonica*; the colonies were regularly fed with these leaves, and the lamina appeared comparatively homogeneous. Laurel leaves were cut from the plant on the day of the experiment, and kept hydrated with a wet tissue wrapped around the stem between collection and measurement. To reduce variation due to material inhomogeneities, I cut all laurel samples from the same leaf, from a region close to the mid-vein; leaf samples were then mounted such that the cut ran perpendicular to the mid-vein. I used mandibles of six ants, three foragers (body mass 6.8 - 38.8 mg) and three callows (body mass 6.2 - 42.1 mg).

Measurements were considered invalid and thus repeated when at least one of the following criteria was met: (i) the head capsule was visibly in contact with the clamp or the cutting substrates; this occurred when the head capsule was positioned very close to the clamp and the PDMS sheet buckled; (ii), the mandible slipped out of the cut; (iii), the steady-state phase was too short to extract a meaningful cutting force (< 2 mm); (iv), the epoxy fixation of the joint failed, leading to mandible rotation; in these cases, the samples were re-glued and used again; or (v), the sample slipped out of the pin holder as observed occasionally for measurements involving high cutting force as on laurel (see section 6.3).

6.2.6 Data curation and statistical analysis

I excluded a total of four (out of 46) callows and five (out of 39) foragers, because optical inspection of the mandible suggested that small amounts of epoxy contaminated the mandibular teeth, and cleaning attempts failed or caused visible damage. Additionally, I excluded three (out of six) razor blade measurements, because the cutting forces exceeded the calibration range (> 245 mN).

Extraction of the average cutting and friction force from the raw data was done in python (v 3.9.7, Van Rossum and Drake, 2009), and all statistical analyses were conducted in R (v 4.1.1, R Core Team, 2022). To characterise the relationship between the extracted forces, body mass, and the two experimental groups (foragers vs callows), I used Analysis of Covariance (ANCOVA) with Type III sums of squares (see Field et al., 2012). In addition, I performed Ordinary Least Squares (OLS) regressions to characterise the scaling relationships within the experimental groups. If not stated otherwise, I performed these analyses on $\log_{10}$-transformed data, and report other results as mean $\pm$ standard deviation.

6.3 Results

6.3.1 Effects of cutting speed

The cutting speeds observed during natural foraging typically depend on both worker size and leaf-mechanical properties; larger ants cut faster than smaller ants, and 'tougher' leaves are cut more slowly than 'tender' leaves (Nichols-Orians and Schultz, 1989; Roces and Hölldobler, 1994; R. M. Schofield et al., 2011). I quantified the interaction between speed and cutting force on synthetic PDMS sheets: Cutting forces increased significantly with speed (ANOVA: $F_{1,7}$ = 33.0, p < 0.001) from 29 ± 2 mN at 0.1 mm/s to 36 ± 1 mN at 0.3 mm/s (Two Sample t-tests: 0.1 vs 0.2 mm/s, t_4 = -2.08, p = 0.11; 0.2 vs 0.3 mm/s, t_4 = -2.94, p < 0.05; 0.1 vs 0.3 mm/s, t_4 = -6.66, p < 0.01; see Fig. 6.3A). Cutting forces thus increased by 20 % for a threefold increase in speed.

6.3.2 Cutting forces are independent of mandible size

Across differently-sized callows and foragers, cutting forces, F_c, were independent of body mass (ANCOVA: $F_{1,72}$ = 0.97, p = 0.33), but depended significantly on the experimental group ($F_{1,72}$ = 21.2, p < 0.001; see Fig. 6.4A). However, these main effects must be interpreted with caution as the interaction term was significant ($F_{1,72}$ = 4.42, p < 0.05, see Field et al., 2012), suggesting that the relationship between cutting force and body mass differs between the experimental groups. Indeed, within callows, cutting forces tended to increase with body mass, but slightly decreased within foragers; although both regression results are not significant ($p \geq 0.11$, see Table 6.1).

On average, cutting forces of foragers exceeded those of callows by a factor of two, 64 ± 33 mN vs 31 ± 7 mN, respectively. Notably, the coefficient of variation was considerably larger for foragers compared to callows, $CV_{\text{foragers}} = 0.52$ and $CV_{\text{callows}} = 0.23$, suggesting that both relative

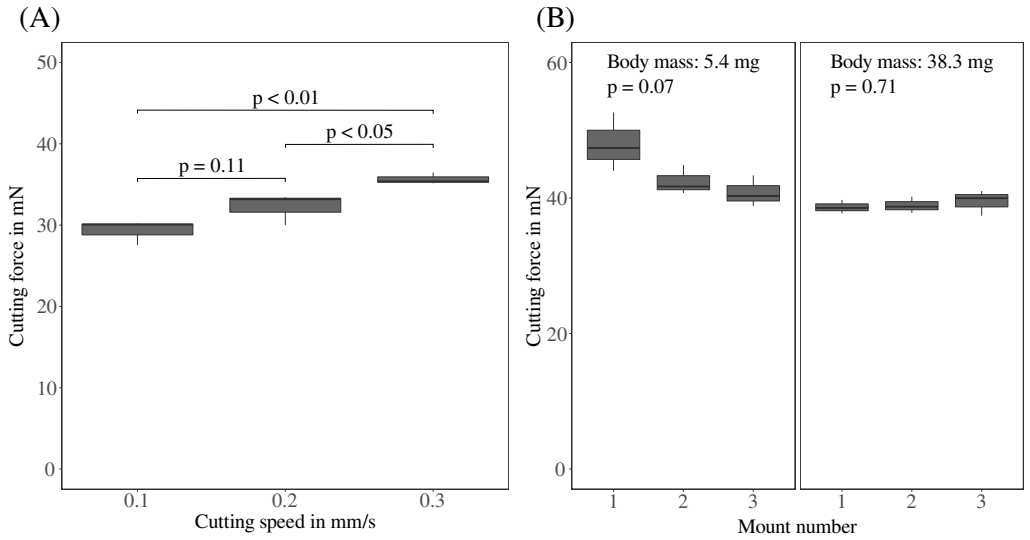


FIGURE 6.3: **(A)** To quantify the effects of cutting speed on mandibular cutting forces, a single forager (body mass 19.9 mg) was tested at 0.1, 0.2 and 0.3 mm/s for three repetitions each. The forces increased significantly with speed from a mean of 29 to 36 mN (or about 20 %; see main text for statistics). Although significant, this increase is small compared to the overall variation across callow and forager mandibles (19 - 172 mN), and thus perhaps of limited biological significance. **(B)** Similarly, the variation from mounting was small in comparison to inter-individual variation, as indicated by the coefficient of variation, CV: $CV_{\text{small}} = 0.10$, $CV_{\text{large}} = 0.03$, $CV_{\text{foragers}} = 0.52$. Notably, the relative cutting force variation was larger for the smaller ant, CVsmall > CVlarge, suggesting that consistent mandible alignment was easier for larger mandibles.

and absolute force variation was larger among foragers. Despite these differences, the magnitude of cutting force extracted for both groups was small in comparison to that of pristine razor blades, 124 ± 46 mN, with a minimum measured cutting force of 72 mN (see Fig. 6.4A; Wilcoxon rank sum test, forager mandibles vs razor blades: W = 12, p < 0.05; callow mandibles vs razor blades: W = 0, p < 0.001).

TABLE 6.1: Results of Ordinary Least Squares regressions describing the relationship between cutting force, F_c, friction force, F_f, 'frictionless' net cutting force, F_{nc}, and mandibular wear, W, with body mass in mg. All regressions were performed on $\log_{10}$-transformed values, apart from mandibular wear which contained negative values; this regression was done on semi-$\log_{10}$-transformed data instead. 95 % confidence intervals are provided in parentheses.

Quantity	Unit	Group	Elevation	Slope	R^2
F_c	mN	Foragers	1.90 (1.69, 2.11)	-0.15 (-0.35, 0.06)	0.06
F_c	mN	Callows	1.41 (1.33, 1.50)	0.07 (-0.02, 0.15)	0.06
F_f	mN	Foragers	0.74 (0.51, 0.98)	-0.14 (-0.37, 0.08)	0.05
F_f	mN	Callows	0.65 (0.42, 0.88)	-0.05 (-0.27, 0.16)	0.01
F_{nc}	mN	Foragers	1.85 (1.62, 2.07)	-0.13 (-0.35, 0.08)	0.05
F_{nc}	mN	Callows	1.32 (1.23, 1.41)	0.09 (0.01, 0.17)	0.11
W	μm	Foragers	13.43 (1.75, 25.10)	-6.02 (-17.19, 5.16)	0.05

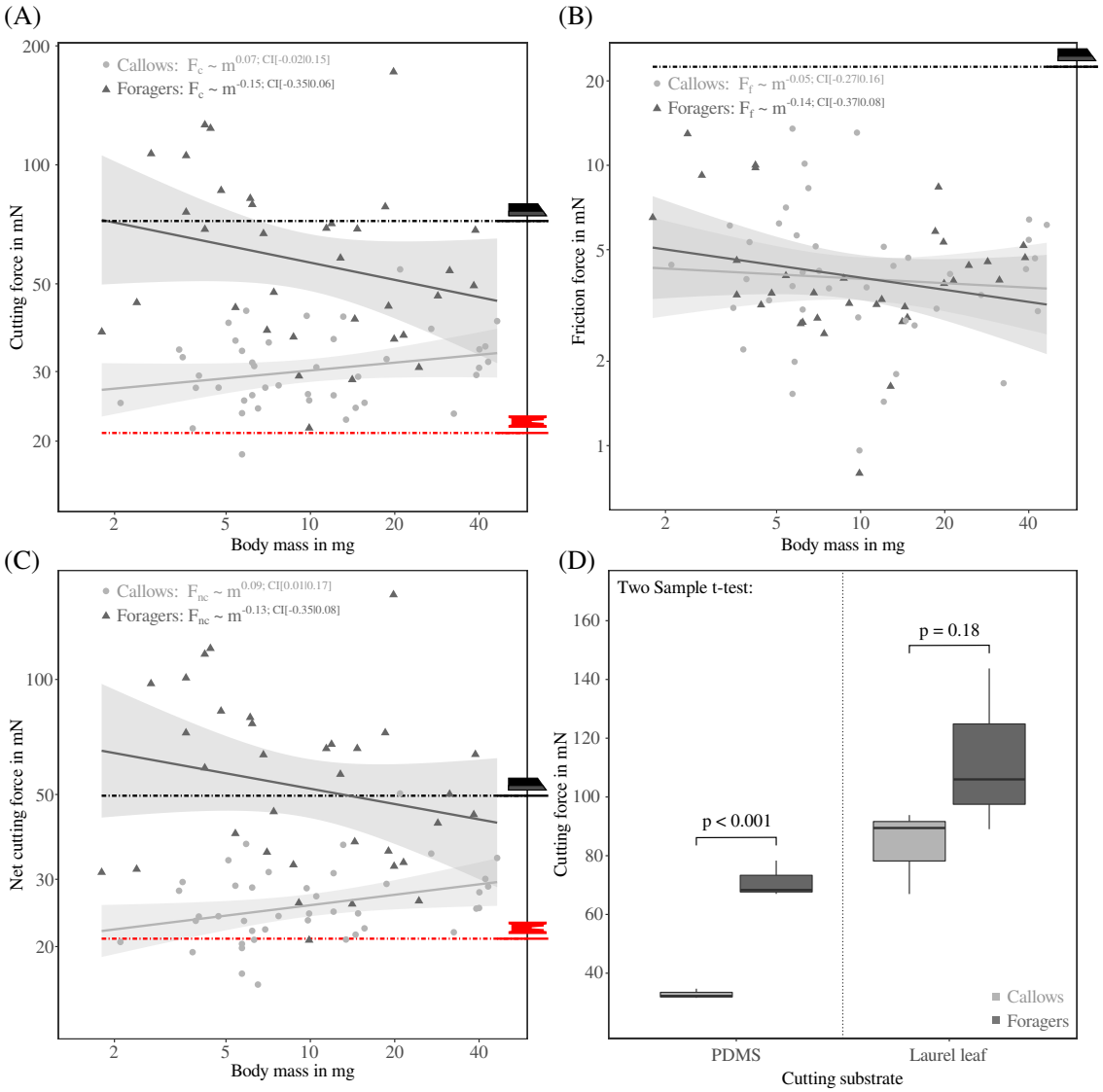


FIGURE 6.4: **(A)** Leaf-cutting is performed by workers spanning an order of magnitude in body mass. To assess how cutting ability is affected by mandible size, I measured mandibular cutting forces across almost the entire size-range (body mass, m, 1.8 to 46.4 mg), and for two experimental groups: callows with pristine mandibles, and workers from the foraging arena with mandibles of varying degrees of mandibular wear. Cutting forces, F_c, were independent of body mass for both experimental groups (see main text for statistics), but twice as high for foragers compared to callows. On average, cutting forces of both groups were smaller than those from pristine razor blades, 124 ± 46 mN, with a minimum force of 72 mN (black dashed lines). **(B)** Friction forces, F_f, were about 5 ± 3 mN for both groups independent of body mass, and significantly smaller than for razor blades. The relative frictional component of the total cutting force was about 10 % for mandibles. **(C)** Net cutting forces, F_{nc}, were not significantly affected by body mass in foragers. For callows, however, F_{nc} increased significantly in proportion to $m^{0.09}$, from values close to a theoretical minimum based on pure shear tearing tests to values closer to those obtained from foragers. **(D)** To test if the difference in cutting force between callows and foragers is also present when using a biological substrate, cutting experiments on *Aucuba japonica* leaf lamina were performed using mandibles from a selection of six representative ants (three forager and three callows across the size-range). The absolute difference in cutting force between callows and foragers was 30 mN, similar to the results obtained for PDMS sheets (38 mN); this difference, however, was not significant.

Across all ant mandibles, friction forces, F_f, were 5 ± 3 mN with neither significant differences between experimental groups, nor significant size-effects (ANCOVA, experimental group: $F_{1,72} = 0.34$, $p = 0.56$; body mass: $F_{1,72} = 0.25$, $p = 0.62$; see Fig. 6.4B and Table 6.1). Because callow mandibles required less cutting force, the relative frictional component was significantly higher for callows: friction accounted for about 15 ± 8 %, as opposed to 8 ± 6 %, of the total cutting force (ANCOVA: $F_{1,72} = 5.98$, $p < 0.05$). Frictional forces of razor blades were 27 ± 8 mN, or 24 ± 7 % of the cutting forces, significantly larger both in relative and absolute terms than for callow and forager mandibles (see Fig. 6.4B; Wilcoxon rank sum test, forager mandibles vs razor blades, absolute: $W = 0$, $p < 0.001$; relative: $W = 3$, $p < 0.01$; callow mandibles vs razor blades, absolute: $W = 0$, $p < 0.001$, relative: $W = 19$, $p < 0.05$).

Due to constant friction forces for ant mandibles, the scaling relationship of 'frictionless' net cutting force, $F_{nc} = F_c - F_f$, essentially mirrors the results obtained for total cutting force (see Fig. 6.4C). Net cutting forces were independent of body mass (ANCOVA: $F_{1,72} = 1.64$, $p = 0.20$), but depended significantly on experimental group ($F_{1,72} = 22.6$, $p < 0.001$), with a significant interaction ($F_{1,72} = 4.46$, $p < 0.05$). Within foragers, F_{nc} tended to decrease with size, but not significantly ($p = 0.22$, see Table 6.1); on average, F_{nc} was 59 ± 32 mN, similar to the minimum force obtained for razor blades (50 mN). Within callows, however, F_{nc} increased significantly with worker size ($p < 0.05$, see Table 6.1), at the lower end approaching the minimum cutting forces predicted from tearing experiments (see Fig. 6.4C and section 6.4).

To test if the observed difference in mandibular cutting force between callows and foragers is also present when using biological substrates, I measured cutting forces for a small subset of both age groups with laurel leaf lamina as cutting substrate. The mandibular cutting forces of foragers were 113 ± 28 mN, exceeding those of callows (83 ± 14 mN) by approximately 30 mN (see Fig. 6.4D); however, this difference was not significant (Two Sample t-test: $t_4 = -1.62$, $p = 0.18$). The average frictional component was 13 ± 8 %, pooled for all ants. For the same set of ants, the difference in cutting force on PDMS was significant, and similar in magnitude (foragers: 71 ± 6 mN, callows: 33 ± 2 mN; Two Sample t-test: $t_4 = -10.37$, $p < 0.001$).

6.3.3 Cutting forces increase significantly with mandibular wear

Frequent plant-cutting or chewing can cause substantial wear (Raupp, 1985; Roitberg et al., 2005; Depieri et al., 2010; R. M. Schofield et al., 2011). To test to what extent mandibular wear can explain variations in cutting force, I calculated a wear index based on changes in distal tooth length (see Eq. 6.1, R. M. Schofield et al., 2011). Mandibular wear of foragers was $8 \pm 10\,\mu$m, independent of body mass (ANOVA on semi-$\log_{10}$-transformed data: $F_{1,22} = 1.25$, $p = 0.28$; see Table 6.1 and Fig. 6.5A). This size-independence suggests that smaller ants lost a larger proportion of their teeth to wear. Indeed, the mandibular wear index, normalised with the pristine length of the most distal tooth, decreased significantly with size (ANOVA on semi-$\log_{10}$-transformed data: $F_{1,22} = 5.41$, $p < 0.05$). The wear index explained about one third of the variation of cutting force, which increased

significantly with wear at a rate of 2.09 mN/μm OLS regression on untransformed data: 95 % CI of slope (0.76 | 3.43), p < 0.01, R^2 = 0.33; see Fig. 6.5B).

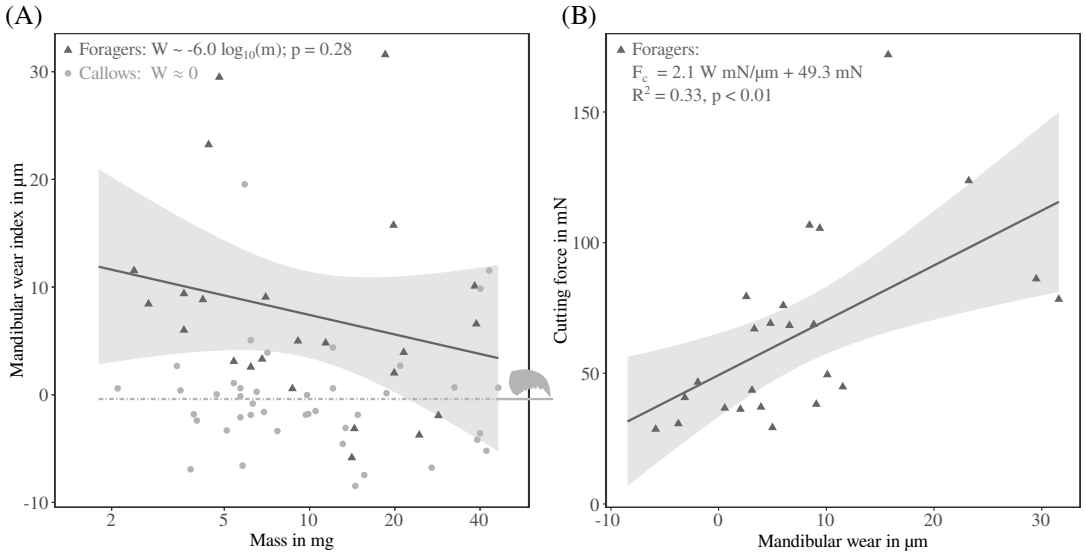


FIGURE 6.5: **(A)** I calculated a mandibular wear index based on length changes of the two most distal teeth (see R. M. Schofield et al., 2011, and Eq. 6.1 in the main text). In foragers, mandibular wear was $8 \pm 10\,\mu$m, independent of worker size, and by definition, centred around zero for callows ($0 \pm 5\,\mu$m). **(B)** Mandibular cutting forces increased significantly with this metric of wear (Ordinary Least Squares regression on forager data: slope = 2.09, 95 % CI (0.76 | 3.43)). This wear metric is easily obtained, but it has small predictive power on this dataset, explaining less than 50 % of the observed variation in cutting force.

6.4 Discussion

Leaf-cutter ant foragers vary both in size and shape (E. O. Wilson, 1953; Feener et al., 1988; Wetterer, 1991a; L. C. Silva et al., 2016, and see Chapter 2), rendering simple scaling arguments on size-dependent cutting ability difficult. I have previously shown that larger foragers can generate disproportionally large bite forces due to distinct morphological adaptations to the musculoskeletal bite apparatus (see Chapter 2 and 4), but how do cutting forces scale across sizes?

Based on experiments using synthetic PDMS sheets as cutting substrate, the cutting forces of both callows and foragers were size-invariant. After removing effects of friction, the net cutting forces of callows showed a small but significant size-effect, $F_{nc} \propto m^{0.09}$, whereas the scaling coefficient obtained for foragers remained not significantly different from zero. In the following paragraphs, I will (i) discuss the mechanical foundation of these results, (ii) discuss their implications on size-related cutting ability, and (iii), provide an outlook for future studies on the mechanics of cutting in leaf-cutter ants.

6.4.1 Cutting mechanics and mandible 'sharpness'

In essence, cutting is a process resulting in the formation of new surfaces (T. Atkins, 2009; J. G. Williams and Patel, 2016). In order to advance a cut by a length dx, the external work supplied via

the cutting tool, $F_c\,dx$, needs to be at least as large as the energy required to create the new surface area resulting from the cut (Wang, 1996; J. G. Williams and Patel, 2016):

$$F_c\,dx \geq G_c\,t\,dx \tag{6.2}$$

where G_c is the fracture toughness of the material, and t is its thickness. A lower bound for cutting force is thus $F_{c,min} = G_c\,t$ (Kamyab et al., 1998; J. G. Williams and Patel, 2016). The minimum required cutting force for PDMS is $F_{c,min} \approx 21\,mN$, based on the fracture toughness extracted from pure shear tearing tests and the sheet thickness measurements (see section 6.2 and red lines in Fig. 6.4). Based on this energy-based criterion, the 'naive' expectation would be that cutting forces are independent of mandible size. And indeed, cutting forces within both experimental groups are size-invariant, and for callows, they are remarkably close to this minimum, ≈30 mN (see section 6.3). However, cutting forces of forager mandibles were 3.5 times higher than $F_{c,min}$, suggesting that the fracture criterion, defined by Eq. 6.2, cannot fully explain the magnitude of cutting force (Griffith, 1921; T. Atkins, 2009; J. G. Williams, 2015a; J. G. Williams and Patel, 2016). Friction forces make up only a small fraction of the total cutting force in both groups, and thus cannot explain this discrepancy either (see Fig. 6.4); the observed difference in mandibular wear between callows and foragers may thus affect mandible 'sharpness' and thus cause an increase in cutting force. But what exactly is mandible 'sharpness' and how does it relate to cutting forces?

There is no universally agreed definition of 'sharpness' (see Reilly et al., 2004; McCarthy et al., 2007, 2010; Schuldt et al., 2013, 2016; P. S. Anderson, 2018; Crofts and P. Anderson, 2018; Crofts et al., 2019; B. Zhang and P. S. Anderson, 2022), but it is often associated with a characteristic length scale such as the blade tip radius of the cutting tool (e. g. Reilly et al., 2004; T. Atkins, 2009; B. Zhang et al., 2019). A more general definition may be given by the ratio between cutting force and minimum required force, $F_c/F_{c,min}$ (see Eq. 6.2). A tool is then 'sharp', when $F_c/F_{c,min} \approx 1$, and 'blunt' when cutting forces far exceed the minimum possible force, $F_c/F_{c,min} \gg 1$. Tool 'sharpness' then depends both on the geometry of the cutting tool and on the fracture properties of material, which are typically associated with a characteristic length scale (Kountanya and Endres, 2004; T. Atkins, 2009; Creton and Ciccotti, 2016; B. Zhang et al., 2019; B. Zhang and Hutchens, 2021).

For fracture in soft materials, an important length scale is determined by the ratio between fracture toughness and Young's modulus, G_c/E (Creton and Ciccotti, 2016). For the cutting substrate used in this study, $G_c/E \approx 24\,\mu$m, of the same order of magnitude as values reported for PDMS with different mixing ratios ($\approx 100\,\mu$m, see B. Zhang et al., 2019). This length appears large in comparison to the tip radius of pristine and worn mandibles, ≈ 50 nm and $\approx 10\,\mu$m, respectively, measured for *A. cephalotes* ant workers (R. M. Schofield et al., 2011), suggesting that processes at other length scales may determine fracture in PDMS (also see B. Zhang et al., 2019; B. Zhang and Hutchens, 2021).

The governing mechanisms for fracture in soft solids are not yet fully understood, even for materials that are comparatively well characterised such as PDMS (B. Zhang et al., 2019; B. Zhang and

Hutchens, 2021). For heterogeneous plant materials with species-, tissue-, age-, hydration- and time-dependent material properties (e. g. Choong, 1996; Spatz et al., 1999; Onoda et al., 2011; Hayot et al., 2012; Hua et al., 2020; Cordoba-Barco et al., 2020), any quantitative predictions on the relevant length scale and 'sharpness' threshold appear even further out of reach, if not practically impossible. Direct cutting force measurements appear attractive in order to characterise the 'sharpness' of insect mandibles as they provide a clear, and biologically meaningful metric. Pristine mandibles of callow workers are exceedingly 'sharp', and even mandibles with moderate levels of mandibular wear require similar forces to the 'sharpest' pristine razor blade (see section 6.3); these results likely represents a morphological adaptation to the high mechanical demands of leaf-cutting (also see R. M. Schofield et al., 2002, 2011; Onoda et al., 2011).

6.4.2 Mandibular wear and size-related cutting ability

I have discussed the mechanical basis for mandibular cutting forces, now I turn my attention to the biological implications resulting from them. It is not possible to directly extrapolate the results obtained for PDMS to *all* plant materials. For example, it is conceivable that some plant tissues have fracture properties, which render even the most worn forager mandibles 'sharp', because the relevant length scale of the material exceeds that of the mandibular cutting blade (see Kountanya and Endres, 2004; B. Zhang et al., 2019). However, I argue that it is unlikely that all or even most plant tissues are 'insensitive' to variation in mandibular wear, because of the following three reasons: First, the average cutting force required for forager mandibles to cut laurel leaf lamina was 30 mN higher than for callow mandibles (see Fig. 6.4D; although this difference was not significant); similarly, R. M. Schofield et al. (2011) measured cutting forces twice as high for worn mandibles compared to pristine mandibles of *A. cephalotes* worker on *Prunus lusitanica* leaves. Second, leaf-cutter ants with worn mandibles cut at significantly lower speeds, suggesting adverse effects on cutting ability (R. M. Schofield et al., 2011); a similar observation was made for leaf beetles which not only consumed leaves more slowly, but also produced fewer eggs (Raupp, 1985). Third, leaf-cutter ants with worn mandibles are more likely to carry than to cut leaves (R. M. Schofield et al., 2011), and the oldest colony workers may switch to mechanically less demanding tasks such as waste disposal (Hart and Ratnieks, 2001; Camargo et al., 2007). I hence conjecture that mandibular wear plays an important role for the ability to cut leaves not only for leaf-cutter ants, but likely for other insect herbivores as well.

My results suggest that cutting forces are independent of mandible size. This finding appears remarkable given the large range of tested worker sizes (factor of ≈ 30 in body mass), and the associated changes in mandible dimensions; the mandible blade length varies by a factor of about $30^{0.31} \approx 3$ across the size-range (see regression results in Table E.1 in Appendix E). The size-independence of cutting forces for callow mandibles suggests that the important length scale for cutting either varies only little across sizes (and perhaps scales with negative allometry) or was generally below a relevant threshold for PDMS. Although the scaling coefficients for both callows and foragers were not significantly different from zero (see Fig. 6.4A and Table 6.1), they were significantly different from each other ($p < 0.05$, see ANCOVA results). Smaller ants may thus be more affected by mandibular wear

(also see R. M. Schofield et al., 2016). Indeed, the wear index normalised with tooth length decreased significantly with size ($p < 0.05$, see section 6.3). Similarly, R. M. Schofield et al. (2011) found that the second most distal tooth was more worn in smaller ants.

The relationship between cutting force and wear index was significant ($p < 0.01$, see section 6.3), with a similar slope than observed for *A. cephalotes*, 2.1 vs 3.7 mN/μm, respectively (R. M. Schofield et al., 2011). However, only one-third of the force variation was explained by the index (see Fig. 6.5B). Some of the remaining variation may be attributed to methodology, but these effects were likely minor (see Fig. 6.3B and 6.2). A more predictive index may be the blade tip radius, measured in the mandible cross-section (see R. M. Schofield et al., 2011, 2016); obtaining this index, however, involves electron microscopy, and may thus be less applicable to large sample sizes (see R. M. Schofield et al., 2011).

The ability to cut leaves depends on both wear-dependent cutting forces and size-dependent bite forces. Next, I assess the relative importance of bite force and mandibular wear on the ability to cut. Across the size-range of leaf-cutting workers the maximum bite force varies by a factor of about 12, $(30/2)^{0.90} \approx 12$. Across small workers with a body mass of 4-6 mg, cutting forces ranged between 19-126 mN (n = 14), a factor of almost 7. To compensate for this increase in cutting force with an equivalent increase in bite force, a small worker needed to be about 8 times heavier, $7^{1/0.90} \approx 8$. Notably, across large workers (body mass > 30 mg), cutting forces varied by a factor of only three, 23-68 mN (n = 10), which still requires a threefold increase in body mass; the difference between size groups is in line with the notion that smaller ants may be more affected by mandibular wear.

I have demonstrated that for the same level of wear, the ability to cut a given substrate is mainly determined by bite force, which strongly favours larger workers. The common observation that larger foragers cut at higher speeds may thus result from the fact that they use a smaller fraction of their available muscle force capacity, which may allow them to contract muscle at higher speeds, in addition to expected changes from fibre length differences (Hill, 1938; A. Gordon et al., 1966; Josephson, 1975). The effects of speed on cutting forces are difficult to predict quantitatively as they depend on the tissue-specific viscoelastic properties of the plant (e. g. see Spatz et al., 1999; Hayot et al., 2012; Cordoba-Barco et al., 2020). Our results, however, suggest that they may be small: A threefold increase in cutting speed resulted in a comparatively small increase in cutting force of only 20 % (also see B. Zhang et al., 2019, and Fig. 6.3A).

I acknowledge that the cutting behaviour of leaf-cutter ants is far more complex than what I replicated in the experiment: For example, the mandibles rotate instead of translating linearly; neck muscles may be used to change head and mandible orientation during cutting, and perhaps even directly contribute to cut propagation; and the section of the mandible blade used for cutting may be adjusted to account for local differences in mandible 'sharpness', or to dynamically alter the effective mechanical advantage of the mandible lever system. Despite these differences, two arguments suggest that my experiments are informative: Cutting forces of pristine mandibles were close to a theoretical minimum for PDMS; and although more complex mandible motion may decrease cutting forces in some cases (Reyssat et al., 2012; Y. Liu et al., 2021), out-of-plane forces applied to thin sheets likely

result in sheet bending instead of concentrating tensile stresses, leading instead to an increase in cutting forces. Because leaf-cutter ants already need to show exceptional morphological and physiological adaptations to be able to produce bite forces sufficient to cut leaves (see Chapters 3 and 4), it is biologically implausible and physically impossible that forces during 'free cutting' are substantially amplified over the minimum force dictated by leaf toughness. I thus argue that the basic mechanical interaction between mandible and substrate remains the same, and that the general conclusions from this study are applicable to 'real world' foraging scenarios (also see Tautz et al., 1995; R. M. Schofield et al., 2011).

6.5 Conclusions and outlook

The ability to cut leaves involves complex interactions between worker size, bite force capacity, wear-dependent cutting forces, plant-material properties and adaptive cutting behaviour. I tried to untangle this complexity, by removing the confounding effects of material heterogeneity and non-linear mandible motion, and studied the effects of worker size across two experimental groups with varying levels of mandibular wear. Although smaller ants may experience a larger increase in cutting force from pristine to worn mandibles, cutting forces were still largely size-independent. The ability to cut leaves is thus mostly affected by size-dependent bite forces, plant-material properties, and mandibular wear (see Chapter 4); the effects of wear can be substantial, and may often limit the range of accessible plant tissues, which likely applies to other insect herbivores as well.

A natural extension to this work would be to use other materials as cutting substrate: Using a range of relevant plant materials could serve as a basis to assess the biological importance of mandible geometry more broadly; using other synthetic materials with well-defined properties could help to characterise mandibles as cutting tools more generally. A careful inspection of the mandibular cutting blade, in combination with mandible abrasion experiments, could yield important insights into the mechanisms of wear resistance in insects (see R. M. Schofield et al., 2002; Reynolds et al., 2009). I hope that the findings of this study, and the future work they may inform, will help to increase our understanding of size-specific foraging preferences in leaf-cutter ants, and more generally, highlight the importance of biomechanical factors in the herbivory of insects.

7 Concluding remarks

Insects use their bite apparatus to retrieve and process food, dig tunnels, fight over mating partners, and even to escape predators. In some cases, these ecological factors have driven the evolution of rather extreme mandible and head shapes, and ingenious biomechanical mechanisms: Male stag beetles use their elongated mandibles to throw and chase away mating rivals (Goyens et al., 2015); antlion larvae create cone-shaped pits as traps by skilfully flicking sand grains from the bottom of the digging groove (J. R. Lucas, 1982); trap-jaw ants store elastic potential energy in cuticle to launch powerful strikes against prey and to flick themselves off the ground (Patek et al., 2006).

In this thesis, I investigated the bite apparatus of leaf-cutter ants, a true master of herbivory, and a notorious pest species in the Neotropics that occupies another niche of extreme shapes: leaf-cutter ants possess razor-sharp mandibles driven by enormous closer muscles, which enable them to cut most tropical leaves. In the following paragraphs, I will describe the biomechanical mechanisms driving this ability and how it varies with size and age of the ants, synthesised from all experimental chapters, and provide a broad outlook for future research in this field.

The ability to cut leaves depends on the ratio of two key forces: the maximum available bite force and the minimum required cutting force. Bite forces are determined by the size, arrangement and maximum stress of the mandible closer muscle, and the mechanical advantage of the force transmission system. Leaf-cutter ant workers vary by more than one order of magnitude in body mass, and maximum bite forces increase with strong positive allometry: Large ants produce peak bite forces two times larger than predicted from isometry; to generate the same maximum bite force, isometric workers needed to be three times larger than the largest workers in the colony. This positive allometry thus likely saves the colony 'production' costs associated with excessively large workers.

The positive allometry of bite force is mainly achieved by a disproportionate increase in muscle volume in combination with an isometric growth of muscle fibre length. As a result, the physiological cross-sectional area of the mandible closer muscle, which defines muscle force capacity, increases with strong positive allometry. The resulting increase in apodeme force is only slightly attenuated by changes to the fibre pennation angle. This seeming decrease of bite force capacity, however, reverses when changes to the internal muscle attachment area are taken into account, so that the effects of pennation angle changes may still lead to an overall increase in bite force capacity. The mechanical advantage of the mandible lever system increases by about 20 % across the size-range, achieved by a disproportionate increase in effective inlever. An even stronger allometry of inlever length is likely constrained by muscle fibre strain; to maintain an approximately constant mandibular opening range, the scaling coefficients of fibre length and effective inlever need to be similar for a given

maximum strain. Maximum muscle stress appears to be approximately size-invariant, so that the scaling of bite forces can be accurately predicted from the morphology of the bite apparatus alone.

Most bite force determinants vary with mandibular opening angle, so that bite forces, too, are a function of opening angle. For leaf-cutter ant majors, bite forces peak at comparatively small opening angles, at a mandible gape most relevant for leaf-cutting, and decrease to only one-fifth of the maximum at large angles. For smaller ants, this force peak occurs at significantly larger opening angles, which may reflect a size-dependent physiological adaptation driven by the need to cut leaves with a thickness that takes up a larger fraction of the maximum possible mandible gape. The variation of bite force with opening angle is mainly driven by changes in muscle stress and mechanical advantage, whereas fibre pennation angle has only minor effects. The opening angle-dependent variation of mechanical advantage is determined by the alignment between apodeme force vector and mandible inlever. This alignment, defined by the apodeme angle, is optimum at small opening angles and deviates from this optimum at larger opening angles. Compared to the pennation angle, the apodeme angle is a much more versatile 'design' parameter to modulate the opening angle at which bite forces peak: Minor changes to the mandible shape would suffice to change the apodeme angle and thus shift the opening angle at which the effective inlever takes its maximum. In contrast, the pennation angle is always maximum for small opening angles and decreases monotonously with increase opening angle.

Although the immediate effects of the pennation angle on bite force seem small and strongly constrained, fibre pennation enables 'displacement' gearing, which reduces the fibre strain required to cover the same range of opening angles. This reduction is of particular importance because muscle stress can decay steeply with fibre strain. In fact, the majority of the decrease in bite force with opening angle is attributed to changes in muscle stress, which drops substantially at large opening angles. This adverse effect of fibre strain is less pronounced in directly-attached muscle fibres compared to those that attach to the apodeme via thin filaments; directly-attached fibres are generally longer, so shorten relatively less across the opening range. However, the number of directly-attached fibres is likely limited by the need to provide sufficient muscle attachment area to the apodeme. In fact, filament-attachment and the associated increase of internal attachment radius enable leaf-cutter ants to fill the confined space of their head capsules almost optimally with mandible closer muscle. For a given external geometry and the approximately radial arrangement of muscle fibres around the apodeme, there exists a trade-off between muscle fibre length, which determines maximum displacement, and cross-sectional area, which determines maximum force. Workers of all sizes have a muscle fibre arrangement that is close to maximising volume occupancy (based on the product between both) and thus work capacity of the muscle. However, larger ants display a shift in muscle investment towards a force-optimised arrangement; the size-specific physiological cross-sectional area increases by more than 50 % with only minor changes to relative muscle volume. The remaining disproportionate increase in physiological cross-sectional area is enabled by an increased muscle volume, accommodated by disproportionally larger head capsules.

I assessed the effects of these morphological adaptations and the associated allometry of bite force on the ability to cut leaves: Based on published leaf-mechanical data (Onoda et al., 2011), the largest foragers can cut almost all measured tropical leaves, and a comparatively small forager of 5 mg can still cut 70 % of leaves, 20 % more than a same-sized isometric worker could do. The allometry of bite force thus substantially increases the worker size-range that can forage on a large number of plant species, which likely facilitates flexible task assignment during foraging. However, this analysis neglects the effects of mandible 'sharpness' on the force required to propagate a cut through leaf tissue, which may increase with size, too. Based on cutting experiments on homogenous, 'synthetic leaves', the cutting forces of pristine mandibles from recently-eclosed callows were size-invariant, suggesting that geometric differences of the cutting edge do not affect the cutting forces for some substrates. The same experiment on fully-matured foragers confirmed this size-independency; however, average cutting forces were about twice as high compared to callows, indicating adverse effects on cutting ability due to mandibular wear. This result seemingly suggests that freshly-eclosed workers would be most suitable to perform leaf-cutting tasks. However, this conclusion is premature as it neglects other biomechanical factors relevant for cutting such as the musculoskeletal development of the bite apparatus and associated changes in bite performance.

Bite forces increase by an order of magnitude between freshly-eclosed callows and fully-matured foragers. This development is associated with substantial changes to the size and structure of the mandible closer muscle, as well as with a considerable increase of the mechanical stability of the head capsule. As a consequence, young callows have insufficiently developed closer muscles to produce the bite forces required for cutting most leaves, and a head capsule that lacks the rigidity required to withstand the hypothetical forces of a fully-developed muscle. In contrast, fully-matured foragers have acquired full biomechanical ability for leaf-cutting, capable of generating among the highest weight-specific bite forces ever reported for any animal, and exceeding a theoretically predicted upper limit of bite force by a staggering factor of five (Alexander, 1985). The specialisation to produce excessively large weight-specific bite forces is likely driven by the need to cut leaves; leaf-cutter ants may cut the same leaves lowland tapirs feed on, but they weigh up to 100 million times less (200 kg vs 2 mg). The results of this thesis suggest five key mechanisms that enable this specialisation for cutting: First, the weight-specific head volume exceeds those of the average amniote by a factor of almost four. Second, most of these heads are filled by mandible closer muscle (about 80 %). Third, the geometry of the musculoskeletal bite apparatus is almost optimum for generating largest possible forces across a relevant range of opening angles. Fourth, the maximum muscle stress of the mandible closer muscle is among the highest ever reported for arthropod muscle. And fifth, the mandibular cutting forces of most workers (even those from the foraging area) are smaller than those of unused razor blades, suggesting geometric adaptations of the mandibular cutting blade.

In this thesis, I provided an analysis of the leaf-cutter ant bite apparatus, and I demonstrated that the rare ability to feed on a broad spectrum of plant materials necessitates an extraordinary specialisation of the bite apparatus. Assessing the degree of specialisation to perform any task is difficult as it requires clear boundary conditions and the comparison to theoretical optima. The boundary conditions of herbivory in insects are defined by the general anatomy of the bite apparatus, and the basic physical interactions during plant-feeding. Combining both allowed me to derive theoretical optima for musculoskeletal geometry from first principles. I developed and deployed a set of novel approaches, models, and experimental designs to isolate key parameters of morphological, physiological and biomechanical specialisation separately, and so established a biomechanical paradigm for plant-feeding in insects. I hope that the quantitative assessment of insect biting and cutting ability, enabled by this work, will inform future research on insect functional morphology, ecology and evolution.

I have argued that key ideas of my thesis likely transcend to other insect herbivores, which are typically equipped with similar head structures and which face the same basic task to mechanically process plants. This thesis may thus also be informative for future research on crop protection, with the ultimate aim to grow plants with a strong natural resistance against insect pests. Increased leaf toughness and abrasiveness appear to be promising traits to select for, as they can restrict the fraction of insects which can feed on them to only the strongest. Leaf-cutter ants appear to be particularly specialised for herbivory, but even they likely operate close to maximum muscle activation when encountering tough leaves. In combination with an increase in cutting force due to mandibular wear, the ability of insect herbivores to plant-feed may be drastically reduced.

Future studies based on this work may involve the biomechanical characterisation of other key insect pests, quantifying the relative effort and degree of specialisation for plant-feeding. Some of the most hazardous insect pests such as the Colorado potato beetle, European corn borer, and brown plant hopper, are specialised to feed on a small set of plants. If such pests operated close to maximum effort, small changes in toughness may suffice to render the plants inedible. If, additionally, the insects already possess a bite apparatus which generates close to maximum size-specific bite forces, more substantial changes to the musculoskeletal system may be required to meet the increased demands for feeding, but with larger evolutionary constraints.

I synthesised and discussed the key findings of my thesis and outlined general directions of future research which may be of larger societal and economic interest. Next, I will turn my attention to some of the limitations of my work, and present other exciting avenues that lie beyond the scope of this thesis.

I explored some aspects of the spatial constraints imposed by the insect exoskeleton. However, this analysis was largely limited to a given outer geometry. A more general investigation of the 'design space' span by the various external and internal parameters of the insect head capsule may yield further insights into the functional morphology of the insect bite apparatus. Particularly interesting for further investigation may be the filament-attachment of muscle fibres, which determines the

maximum 'packing density' of muscle and controls the relationship between apodeme displacement, pennation angle, muscle contraction and average apodeme force.

There is remarkably little known about insect bite performance in general, and especially with regard to variation based on the mandibular opening angle (Goyens et al., 2014b; Weihmann et al., 2015a). I demonstrated that bite force measurements in combination with the biomechanical analysis of the musculoskeletal apparatus allows researchers to extract the force-length properties of insect muscle, and to assess the degree of specialisation to generate maximum forces across a relevant mandibular opening range. More studies across the insect tree of life including species with different dietary demands would enable a comparative analysis of the morphology and physiology of the insect bite apparatus.

In order to assess the cutting ability of differently-sized leaf-cutter ant workers, I measured mandibular cutting forces using a polymer with well-defined material properties. A natural extension to this work would be to change the structural and mechanical properties of the polymer and explore the applicability of fracture-mechanical theory when using insect mandibles as cutting tools. Such analyses would also benefit from a more detailed characterisation of the mandibular cutting edge with a particular focus on the mandible cross-section. The existing literature on mandibular wear contains little quantitative data on the abrasiveness of natural substrates on insect cuticle (but see Raupp, 1985; Roitberg et al., 2005; Depieri et al., 2010). Cutting experiments using silicon-enriched plant leaves may provide a quantitative link between cutting substrate and the mandible abrasion per unit cut length. The results of such experiments, again, may inform breeding criteria to ultimately enhance crop protection.

In my PhD, I mainly focussed on forces and the parameters that determine them. However, insect herbivory is also constrained by the energetics of cutting. Leaf-cutting belongs to the energetically most demanding activities performed by insects, but only one study has actually quantified its metabolic costs (Roces and Lighton, 1995). A detailed study of the metabolic rates associated with cutting substrates of varying mechanical properties could yield insights into the relationship between worker size, cutting speed, and muscle limitations due to power or force output. Such work is necessary to assess the ergonomic efficiency of foraging in leaf-cutter ants.

Lastly, I performed all my experiments on singular individuals that I extracted from the colony; this procedure allowed me to quantify worker size- and age-dependent differences of the musculoskeletal bite apparatus. Future studies can add on to this work by performing experiments at the whole colony level; the predictions on cutting ability resulting from this thesis could be tested in foraging assays using 'synthetic leaves' with known material properties.

I hope that the results presented in this thesis will help to explain some of the multitudinous factors that have driven the evolution of the insect bite apparatus, will serve as a guide for future comparative studies on insect bite and cutting forces and their dependency on body size, will ultimately help to select suitable breeding criteria for enhanced crop protection against insect pests, and will increase our understanding of the complex ecology of leaf-cutter ant colonies. And here, I finish my thesis with a quote from Edward Osbourne Wilson, whose contributions to the field of myrmecology have inspired this work and set the stage for many insightful ecological studies on leaf-cutter ants; I hope it was an interesting read.

If all mankind were to disappear, the world would regenerate back to the rich state of equilibrium that existed ten thousand years ago. If insects were to vanish, the environment would collapse into chaos.

A Morphological determinants of bite force capacity

A.1 Tomography

All scans were conducted with a parallel polychromatic X-ray beam produced by a 1.5 T bending magnet. The beam was spectrally filtered by 0.7 mm aluminum. A fast indirect detector system was employed, consisting of a 12 μm LSO:Tb scintillator (Cecilia et al., 2011) and a diffraction limited optical microscope (Optique Peter) (Douissard et al., 2012), coupled with a 12 bit pco.dimax high speed camera with 2016 x 2016 pixels. Scans were done by taking 3,000 projections at 70 fps over an angular range of 180°. Depending on their sizes, the heads were scanned with optical magnifications of either 5x or 10x, resulting in effective pixel sizes of 2.44 μm and 1.22 μm, respectively. The control system 'concert' (Vogelgesang et al., 2016) was employed for automated data acquisition and online reconstruction of tomographic slices for data quality assurance during the measurement campaign. Data processing included flat field correction and phase retrieval of the projections based on the transport of intensity equation (Paganin et al., 2002). The execution of the pipelines, including tomographic reconstruction, was performed by the UFO framework (Vogelgesang et al., 2012).

A.2 Fibre-tracking algorithm

A custom-written algorithm was used to determine the number of muscle fibres, their length and orientation. Inspired by commercial software such as 'Amira XTracing' or 'Avizo XFiber' (Thermo Fisher Scientific Inc., Waltham, Massachusetts, USA), individual fibres were grown from 'seed points' (see Sullivan et al., 2019; Sartori and Stark, 2021), placed at the origin of individual muscle fibres on the head capsule. Fibre origins were identified through a series of three steps in 'Fiji' (see Fig. A.1):

First, the segmented head capsule was dilated by a factor proportional to the average muscle fibre thickness (Fig. A.1 D). The number of dilation iterations n_{dil} was defined as a constant proportion of the fibre diameter extracted from manual measurements, and was interpolated across the size range using a linear regression on $\log_{10}$-transformed data. Visual inspection suggested that a dilation equal to two-thirds of the diameter in pixels resulted in intersections sufficiently large to be clearly identified as individual muscle fibres, and small enough to prevent fibre merging (see Fig. A.1 B).

Second, the intersections between dilated head capsule and muscle tissue were extracted (see Fig. A.1 B & E).

Third, the number of distinct intersections, exceeding a minimum volume, and their centres-of-mass were calculated via a 3D particle analysis. The xyz coordinates of the centres-of-mass were used as the origins of these fibres (Fig. A.1 F).

Starting from these seed points, I estimated both the length and orientation of the muscle fibres via an iterative 'fibre-tracking' process. This process takes advantage of the fact that muscle fibres in insects are approximately straight lines. Each fibre seed point was assigned an initial orientation, equivalent to the shortest line between the seed point and the centre-of-mass of the apodeme (Fig. A.1 F). Each seed was then grown along this orientation pixel by pixel, until unsegmented tissue was reached. To account for irregularities in fibre morphology and segmentation, a small number of unsegmented pixels was allowed to be crossed. This number was calculated as $n_{cancel} = (s_{min} - n_{dil})/2$, where s_{min} represents the average minimum pixel distance between individual seed points. This cancel criterion accounts for variation in both fibre diameter and density, and usually equalled about four pixels. Occasionally, the seed point itself was unsegmented, leading to 'zero-length' fibres. In these cases, a new seed point was selected at random from within the bounding box of the same particle. If a fibre could be grown to a length at least two times n_{dil}, the seed point was considered acceptable.

As the concluding step of each algorithmic iteration, the quality of the grown fibre was assessed by dividing its length with the variation in greyscale value along its length, calculated from unsegmented CT data. If the fibre was long, located within a single muscle fibre and crossed few small unsegmented gaps, the variation in greyscale was small and the quality metric large. If, in contrast, it was short, crossed numerous unsegmented gaps and included tissue from several muscle fibres, the greyscale variation was large and the quality metric small. Hence, the algorithm favoured long and homogenous segments.

This process was conducted once for the initial orientation, and was then repeated 2000 times for orientations chosen at random from a 'search cone' defined with respect to the fibre which has the highest quality metric. This search cone was created by rotating the cone's centre line around all three coordinate axes by angles taken from a population of angles normally-distributed around zero degrees. The standard deviation of this normal distribution was set to 10 ° for the first iteration and was subsequently linearly decreased with increasing number of iterations to a minimum of 0.1 ° (see Fig. A.1). If the quality metric of the current iteration had increased compared to the previous 'best guess', the orientation of the search cone was updated. Otherwise, the next iteration was conducted along an orientation chosen at random from the previous search cone.

The number of iterations per fibre was determined by preliminary measurements using a subset of ten fibres from one closer muscle tissue. Each fibre was tracked for a number of iterations ranging between 20 and 20,000, and fibre length and pennation angle were extracted (fibre length was measured as the number of segmented pixels along the fibre orientation multiplied with the scan resolution). This process was repeated 50 times for each fibre in order to quantify the repeatability of the outcome. After 2000 iterations the average fibre length was less than 1 % shorter compared to the maximum extracted at 20,000 iterations, and the average standard deviation of the pennation

angles dropped to 3.6 °, less than twice the minimum error set by the intrinsic limit of the method (see Fig. A.1). Hence, a number of 2000 iterations was regarded sufficiently large to yield reliable results while keeping the computational effort manageable.

Fibres with aspect ratios below two were removed from the dataset as such short fibres were not observed in the CT-scans, and hence likely reflect incorrectly identified seed points (see Chapter 2). Fibre length was measured as the total number of segmented pixels between the fibre seed point and point of fibre termination. This calculation does not account for a small part of the fibre between seed point and head capsule, approximately equal to half the number of dilation steps. To correct for this systematic error, another fibre was grown from the seed point in the opposite direction but along the final fibre orientation, until unsegmented tissue was reached. The length of this fibre segment was then added to the fibre length.

In order to validate the fibre-tracking algorithm, a subset of 40 opener and closer muscle fibres were manually analysed for seven ants across the entire size spectrum (278 in total – the opener muscle tissue of the smallest ant had only 18 suitable fibres). Individual fibres were identified using the results of preliminary 3D particle analysis on the muscle intersections in Fiji. Fibres were selected for tracking when distinctly visible in both CT-scan and segmentation image. The locations of the fibre centres at origin and insertion to the apodeme were extracted, and fibre length and orientation were calculated (see Chapter 2).

A.3 Cuticle saving via filament-attachment

I estimated the material volume saved by filament-attachment as follows: The total volume of filament is $V_{fil} = n_f A_{fil} L_{fil}$, where n_f is the number of filament-attached fibres, L_{fil} the average filament length (estimated from internal head dimensions), and A_{fil} their cross-sectional area (calculated assuming that the cross-section approximates a circle of diameter d). Filaments were too thin to be reliably segmented, but visual inspection of the CT scans suggested that $d \approx 4\,\mu m$ with little variation within and across specimens (also see Gronenberg et al., 1997). As almost all muscle fibres in *A. vollenweideri* were attached via filaments, the amount of internal cuticle required for filament-attached fibres then equals the sum of V_{fil} and the apodeme volume V_{apo}. In contrast, the amount of internal cuticle required for direct attachment is equal to the entire internal volume V_{int}. The difference between these volumes, the volume saved through filament-attachment for both head halves is $V_{saved} = 2(V_{int} - (V_{fil} + V_{apo}))$, which was approximately equal to the cuticle volume of the entire head capsule. Hence, filament-attachment substantially reduces the required cuticle tissue, and might be a light-weight strategy to satisfy the excessive demand of fibre attachment area.

A.4 Area coverage of apodeme

Because the majority of muscle fibre attach to the apodeme via filaments, the required surface area is dominated by the relatively small cross-section of the filaments. I estimated the area fraction covered

as $(n_f A_{fil} + n_d A_f)/(sin(\phi) A_{apo,s})$, where $A_{apo,s}$ is the apodeme surface area, and n_d corresponds to the number of directly-attached fibres.

A.5 Estimation of A_{apo} and σ_{apo}

The maximum force is experienced by the anterior parts of the apodeme cross-section. Accordingly, the cross-sectional area of the apodeme is largest close to mandible insertion and decreases towards its posterior end (see Paul, 2001). In order to identify the location of maximum stress, an assumption on the increase of force with apodeme length is required. The simplest plausible assumption is that the number of fibres increases along the length of the apodeme in proportion to the apodeme perimeter. The predicted increase in force is larger than the increase in cross-sectional area, so that the highest stresses is expected at the anterior end of the apodeme, where the cross-sectional area is maximal. Maximum cross-sectional area scales with strong positive allometry $A_{apo} \propto m^{0.89}$ [95 % CI: (0.83 | 0.95), see Fig. 2.6A], similar to the increase of maximum load along the apodeme, which scales proportional to $A_{phys} cos(\phi) \propto m^{0.84}$. A similar conclusion holds if the average cross-sectional area is used instead, $\hat{A}_{apo} \propto m^{0.91}$ [95 % CI: (0.85 | 0.97)].

In order to estimate the approximate tensile strength of the apodeme, I note that its density appears similar to that of the head capsule, which has a modulus of the order of 6 GPa (see Chapter 5). The strength may then be estimated as approximately 1/60 of the modulus (Labonte et al., 2017), i. e. $\sigma_{apo} = 100$ MPa. Alternatively, I may consider available estimates on the longitudinal tensile strength of insect cuticle which is approximately 94 MPa (Jensen and Weis-Fogh, 1962), or the tensile strength of the leg extensor apodeme in locusts, which is 600 MPa (Bennet-Clark, 1975). These estimates change the conclusion on the numerical value of the safety factor, but do not affect the conclusion that the apodeme strength is at least a hundred times larger than the muscle stress.

A.6 A simple geometric model of the ant head capsule

I model the shape of each half of the head capsule as a cylinder with radius R and height $h = f_h R$ (with $f_h \geq 0$). This cylinder is terminated with a spherical cap, also with radius R, at its posterior end. The internal attachment area, in turn, is defined by a cylindrical part with equal height h, but radius $r = f_r R$ for the cylindrical section and the spherical cap (with $0 \leq f_r \leq 1$. The external volume is $V_{ext} = \pi R^2 h + 2/3 \pi R^3$, the internal attachment area is $A_{int} = 2\pi r\,(h + r)$, and the volume available for muscle fibres is $V_m = A_{int}\,(R - r)$. It is crucial to note that this volume is not equal to the difference between external and internal volume, because the internal and external areas are not equal. A_{phys} can be estimated as $A_{phys} \approx \sin\phi A_{int}$. The maximum surface-to-volume ratio of the muscle is then:

$$\frac{A_{phys}}{V_m} = \frac{\sin\phi A_{int}}{A_{int}\,(R - r)} = \frac{\sin\phi}{R\left(1 - \frac{r}{R}\right)} = \frac{\sin\phi}{R\,(1 - f_r)} \tag{A.1}$$

which is Eq. 2.2 in the main manuscript. The fraction of the available volume occupied by muscle is:

$$\frac{V_m}{V_{ext}} = \eta = \frac{2\pi r\,(h+r)\,(R-r)}{\pi R^2 h + 2/3\pi R^3} \tag{A.2}$$

Introducing $r/R = f_r$ and $h/R = f_h$ yields Eq. 2.3 in the main manuscript:

$$\frac{V_m}{V_{ext}} = \eta = \frac{f_r^2\,(1-f_r) + f_h f_r\,(1-f_r)}{1/3 + f_h/2} \tag{A.3}$$

In the domain $0 < f_r < 1 \wedge f_h \geq 0$, this function takes a maximum value:

$$f_r = \frac{1}{3}(\sqrt{f_h^2 + f_h + 1} + 1 - f_h) \tag{A.4}$$

The value for f_r which maximise η is thus at most $2/3$ (for $f_h = 0$), and then monotonously decays towards an asymptotic minimum value of $f_r = 0.5$ as $f_h \to \infty$. These two limiting cases set an lower and upper bound for $0.44 < \eta_{max} < 0.5$, which can be shown formally be inserting Eq.A.4 in Eq. A.3; the derivative of this function with respect to f_h is positive for all $f_h > 0$. The two bounds for η may be understood by recognising that these limits correspond to two 'extreme' shapes of a high-aspect ratio cylinder ($h >> r$) and a hemisphere ($h = 0$).

TABLE A.1: Results of standardised major axis regressions describing the relationship of $\log_{10}$-transformed determinants of bite force capacity A_{eff}, internal and external head dimensions with $\log_{10}$(body mass in mg). 95 % confidence intervals are provided in parentheses.

Quantity	Unit	Elevation	Slope	R^2
A_{eff}	mm^2	-1.5 (-1.57, -1.43)	0.89 (0.82, 0.96)	0.99
V_m	mm^3	-1.43 (-1.53, -1.34)	1.16 (1.07, 1.26)	0.98
L_f	μm	2.39 (2.35, 2.44)	0.3 (0.26, 0.35)	0.96
A_{phys}	mm^2	-0.83 (-0.9, -0.76)	0.86 (0.8, 0.93)	0.99
cosϕ	(-)	-0.09 (-0.1, -0.07)	-0.03 (-0.05, -0.02)	0.49
MA	(-)	-0.58 (-0.61, -0.55)	0.06 (0.04, 0.1)	0.54
$\lvert\mathbf{L}_{i,eff}\rvert$	mm	-0.76 (-0.79, -0.72)	0.39 (0.36, 0.42)	0.98
$\lvert\mathbf{L}_{o,eff,p}\rvert$	mm	-0.43 (-0.46, -0.4)	0.36 (0.33, 0.38)	0.99
$\lvert\mathbf{L}_{o,eff,d}\rvert$	mm	-0.19 (-0.21, -0.16)	0.34 (0.32, 0.36)	0.99
V_h	mm^3	-0.57 (-0.63, -0.5)	1.15 (1.09, 1.22)	0.99
W_h	mm	-0.02 (-0.04, 0)	0.4 (0.38, 0.43)	0.99
H_h	mm	-0.23 (-0.25, -0.21)	0.38 (0.36, 0.4)	0.99
L_h	mm	-0.08 (-0.11, -0.05)	0.37 (0.34, 0.4)	0.98
A_{apo}	mm^2	-2.71 (-2.78, -2.65)	0.9 (0.84, 0.96)	0.99

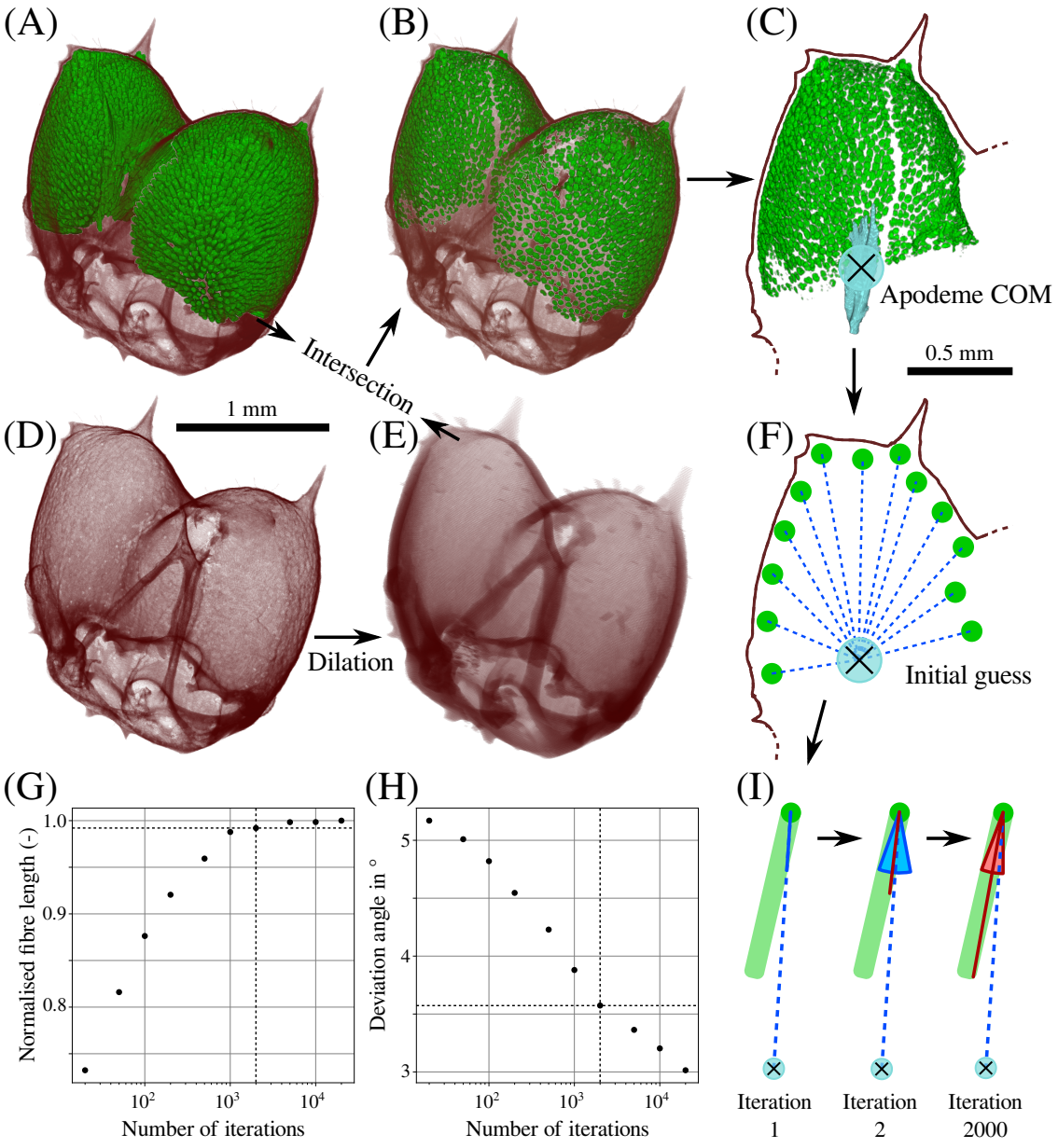


FIGURE A.1: I extracted the length and pennation angle of every fibre of the closer muscle with a custom-written tracking algorithm. The head capsule segmentation (**D**) was dilated, and the intersection (**B**) between dilated head capsule (**E**) and closer muscle (**A**) was calculated, resulting in spatially distinct fibre seeds. The apodeme centre-of-mass (COM) was calculated (**C**), and the lines connecting fibre seeds and apodeme COM were selected as initial fibre orientations (**F**). This 'initial guess' was then refined through an iterative optimisation process (**I**), favouring long and homogenous fibre segments. For error estimation, fibre length and pennation angle were extracted for a subset of fibres, revealing that fibre length increases only little (**G**), and pennation angle showed small variation for repeated measurements (**H**), after 2000 iterations of the optimisation algorithm.

B Relationship between bite force and mandibular opening angle

B.1 Model derivations

As the mandible opens and closes, the apodeme displaces along its main axis by an amount Δ with respect to a reference position. I assume the muscle expansion perpendicular to the apodeme main axis to remain constant (i. e. the head capsule to be rigid), so that the muscle fibres rotate around their origins at the head capsule (see Benninghoff and Rollhäuser, 1952, and Fig. 3.1D in Chapter 3). As a consequence, a fibre with a total length $L_{t,0}$ at a pennation angle ϕ_0 shortens to a length L_t at an angle ϕ, where the expansion of the fibre along the lateral axis remains constant as $\sin\phi_0 L_{t,0}$. The fibre expansion along the apodeme main axis, however, decreases from $\cos\phi_0 L_{t,0}$ to $\cos\phi_0 L_{t,0-\Delta}$. As a result, the pennation angle ϕ changes as:

$$\phi(\theta) = \arctan\left(\frac{\sin\phi_0}{\cos\phi_0 - \Delta(\theta)/L_{t,0}}\right) \tag{B.1}$$

equivalent to Eq. 3.4 in Chapter 3. For directly-attached fibres, the fibre length is equal to the total length, $L_d = L_t$, and follows directly from the Pythagorean theorem:

$$L_d(\theta) = \sqrt{[\cos\phi_0 L_{d,0} - \Delta(\theta)]^2 + [\sin\phi_0 L_{d,0}]^2} \tag{B.2}$$

equivalent to Eq. 3.6 in Chapter 3. For filament-attached fibres, the fibre length is equal to the total length minus filament length, $L_f = L_t - L_{fil}$; the relationship between fibre length and apodeme displacement is hence modified, as:

$$L_f(\theta) = \sqrt{\begin{matrix}[\cos\phi_0(L_{f,0} + L_{fil}) - \Delta(\theta)]^2 \\ + [\sin\phi_0(L_{f,0} + L_{fil})]^2\end{matrix}} - L_{fil} \tag{B.3}$$

equivalent to Eq. 3.7 in Chapter 3. Key here is that the fraction of the total length occupied by the filament is of a constant length. As a result, the fibre strain for a given Δ is larger for filament-attached fibres compared to directly-attached fibres of the same total length.

The magnitude of bite force $|\mathbf{F}_b|$ was derived as a function of mandibular opening angle (see Eq. 3.1), because this relationship is biologically relevant, and it allows me to compare my results to existing literature (e. g. Dumont and Herrel, 2003; Goyens et al., 2014b; Weihmann et al., 2015a). $|\mathbf{F}_b|$ can, however, also be expressed as a function of fibre stretch, in accordance with the causal relationship:

$$|\mathbf{F}_b|(\lambda) = \sigma(\lambda) A_{phys} \cos[\phi(\lambda)] MA(\lambda) \tag{B.4}$$

The change of muscle stress follows directly as:

$$\sigma(\lambda) = \sigma_{max} e^{-\beta(1-\lambda)^2} \tag{B.5}$$

The fibre length is equal to the product between λ and the optimum fibre length L_{opt}. Consider two fibres, one directly- and one filament-attached, of the same total length. If the apodeme displaces to the same Δ, their pennation angles change both as defined in Eq. 3.4 in Chapter 3. If both fibres shorten to the same stretch ratio, however, their change in pennation angle differs. For directly-attached fibres, ϕ_d is determined by a reference pennation angle ϕ_0 at a fibre length $L_{d,0} = \lambda_0 L_{opt}$ and λ. In analogy to the previous derivation of $\phi(\theta)$, the lateral expansion of the fibre is assumed to be constant, $\sin \phi_d \lambda L_{opt} = \sin \phi_0 \lambda_0 L_{opt}$, resulting in:

$$\phi_d(\lambda) = \arcsin\left(\frac{\sin \phi_0 \lambda_0 L_{opt}}{\lambda L_{opt}}\right) \tag{B.6}$$

Correspondingly, the pennation angle for filament-attached fibres changes as:

$$\phi_f(\lambda) = \arcsin\left(\frac{\sin \phi_0 (\lambda_0 L_{opt} + L_{fil})}{\lambda L_{opt} + L_{fil}}\right) \tag{B.7}$$

For simplicity, the relationship between apodeme displacement and effective inlever with λ will be derived for directly-attached fibre only. The corresponding relationship for filament-attached fibres, however, follows the same geometric relations.

The apodeme displacement Δ increases with a decrease of fibre expansion along the apodeme main axis as:

$$\Delta(\lambda) = \cos \phi_0 \lambda_0 L_{opt} - \cos[\phi(\lambda)] \lambda L_{opt} \tag{B.8}$$

The effective inlever is determined by the length of the inlever projection onto the plane of rotation, $|\hat{\mathbf{R}} \times \mathbf{L}_i|$, the fraction of the apodeme main axis that lies in this plane $|\hat{\mathbf{R}} \times \hat{\mathbf{A}}|$, and the starting configuration between inlever and apodeme, characterised by the apodeme angle γ_0 measured at a reference stretch ratio λ_0 (see Fig. 3.1E in Chapter 3). At λ_0, the effective inlever is equal

to $\sin(\gamma_0)|\hat{\mathbf{R}} \times \mathbf{L}_i||\hat{\mathbf{R}} \times \hat{\mathbf{A}}|$, equivalent to Eq. 3.2 in Chapter 3. Following the Pythagorean theorem, this length can also be expressed as $\sqrt{|\hat{\mathbf{R}} \times \mathbf{L}_i|^2 - [\cos(\gamma_0)|\hat{\mathbf{R}} \times \mathbf{L}_i|]^2}|\hat{\mathbf{R}} \times \hat{\mathbf{A}}|$, where the term $\cos(\gamma_0)|\hat{\mathbf{R}} \times \mathbf{L}_i|$ captures the expansion of the inlever along the apodeme main axis in the plane of rotation. This expansion decreases as Δ increases, attenuated by the misalignment between apodeme main axis and rotational plane. As a result, the effective inlever varies with λ as:

$$|\mathbf{L}_{i,eff}(\lambda)| = \sqrt{|\hat{\mathbf{R}} \times \mathbf{L}_i|^2 - [\cos(\gamma_0)|\hat{\mathbf{R}} \times \mathbf{L}_i| - \Delta(\lambda)|\hat{\mathbf{R}} \times \hat{\mathbf{A}}|]^2}|\hat{\mathbf{R}} \times \hat{\mathbf{A}}| \tag{B.9}$$

B.2 Filament strain, head deformation and ligament rotation

I made three assumptions on the mechanical properties of the bite apparatus. First, I assumed that filament strain during muscle contraction is negligible. In order to estimate filament strain, I invoke Hooke's law, $\epsilon = \sigma_{fil}/E_{fil}$, where σ_{fil} is equal to the maximum muscle stress times the ratio between the cross-sectional areas of fibre and filament. The fibre cross-sectional area was extracted from the scans described in this study, the filament cross-sectional area was estimated from synchrotron-based scans with a higher resolution performed on *Atta vollenweideri* majors, described in detail in Chapter 2. The Young's modulus of the filaments E_{fil} was assumed to be equal to that of the head capsule (≈ 6 GPa, see Chapter 5), because their density appeared to be similar in the tomographic scans. Based on these assumptions, $\epsilon \approx 1.5\,\%$. I hence predict any filament length changes across mandibular opening angles to be negligible. This prediction is supported by the observation that filament length, extracted from the tomographic scans, is independent of opening angle [LMM with random intercepts and opening angle as fixed effect: $\chi^2_1 = 0.32$, p = 0.58].

Second, I assumed that the head capsule is rigid, so that the expansion of the muscle perpendicular to the apodeme main axis remains constant. In support of this assumption, head width approximated as twice the distance of the eye to the sagittal plane was independent of opening angle [LMM with random intercepts and opening angle as fixed effect: $\chi^2_1 = 0.35$, p = 0.56]. In contrast, head length decreased significantly with opening angle, but by less than 1μm per degree [LMM: $\chi^2_1 = 4.88$, p < 0.05], amounting to a total change of only $\approx 2\,\%$ across the opening range. I consider these effects small enough to be negligible.

Third, I hypothesised that the apodeme displaces only along its main axis, and that the lateral displacement, imposed by the rotation of the mandible, is bridged by the apodeme ligament. This hypothesis is supported by two observations. First, the apodeme indeed displaces only slightly along the lateral axis; the lateral projection distances of the apodeme centres-of-masses to the axis of apodeme motion never exceed 20 % of the expected lateral displacement from mandible rotation. Second, the lateral expansion of the ligament changes significantly with the sine of the apodeme angle [LMM with random intercepts and $\sin\gamma$ as fixed effect: $\chi^2_1 = 7.05$, p < 0.01], accounting for around two-thirds of the expected lateral displacement. The missing third may be attributed to the biological variation between samples. I also hypothesised that any displacement of the apodeme outside the

plane of rotation would be enabled by the ligament. Since the apodeme main axis and the rotational axis are basically perpendicular to each other, $|\hat{\mathbf{R}} \times \hat{\mathbf{A}}| \approx 1$, the associated out-of-plane displacement is indeed small.

B.3 Bite force extraction for 2D sensors

Bite forces are typically measured with 1D or 2D sensors. The force components that are not measured need to be inferred from geometry. For 1D sensors, the key geometric parameter to extract the magnitude of the bite force $|\mathbf{F}_b|$ is the angle between bite force vector and the sensitive axis (see Eq. 3.8 in Chapter 3). For 2D sensors, $|\mathbf{F}_b|$ is determined by the angle α between the bite force vector and the insensitive axis ($\mathbf{F}_{m,1} \times \mathbf{F}_{m,2}$). The orientation of the bite force vector depends on the orientations of the mandible outlever $\mathbf{L}_o$ and the joint rotational axis $\hat{\mathbf{R}}$, as described in Chapter 3. The magnitude of the measured forces is equal to the components of $\mathbf{F}_b$ that are perpendicular to the insensitive axis; this relationship is characterised by the sine of α, i. e. the cross product between $\mathbf{F}_b$ and $\mathbf{F}_{m,1} \times \mathbf{F}_{m,2}$, as:

$$|\mathbf{F}_b| = \frac{|\mathbf{F}_{m,1}| + |\mathbf{F}_{m,2}|}{\sin \alpha} = \frac{(|\mathbf{F}_{m,1}| + |\mathbf{F}_{m,2}|)|\mathbf{L}_o \times \hat{\mathbf{R}}||\mathbf{F}_{m,1} \times \mathbf{F}_{m,2}|}{|(\mathbf{L}_o \times \hat{\mathbf{R}}) \times (\mathbf{F}_{m,1} \times \mathbf{F}_{m,2})|} \tag{B.10}$$

B.4 Ant preparation for tomography

In order to characterise the morphological determinants of bite force, tomographic scans of ant heads were conducted across a maximum range of opening angles. To control mandibular opening, I built a 3D-printed device to restrain the ants after collection (see Fig. B.1A). PLA rods of varying diameter were placed asymmetrically between the mandibles of the clamped ant to achieve different opening angles between left and right head hemisphere. The rods were inserted into a cylindrical cavity in the device to ensure they remain in place. Subsequently, the ants were sacrificed by freezing, and their soft tissues were fixated and stained. To avoid posthumous mandible closure, the rods remained between the mandibles, but were truncated prior to scanning.

The samples were imaged with an X-ray microscope using a CCD detector system with scintillator-coupled visible light optics, and tungsten transmission target. An X-ray tube voltage of 70 kV was used, and a tube current of 85 µA, with an exposure of between 1000 - 2000 ms, and a total of 1601 projections captured over a '180 degrees plus fan angle' range . An objective lens giving an optical magnification of 0.4 x was selected with binning set to 2, producing isotropic voxels of 6.5 - 7.1 μm. A low energy filter was placed in the beam path (LE1 – proprietary Carl Zeiss microscopy filter). The tomograms were reconstructed as 16-bit from 2D projections using a Zeiss commercial software package (XMReconstructor, Carl Zeiss), a cone-beam reconstruction algorithm based on filtered back-projection. XMReconstructor was also used to produce 2D greyscale slices for subsequent analysis.

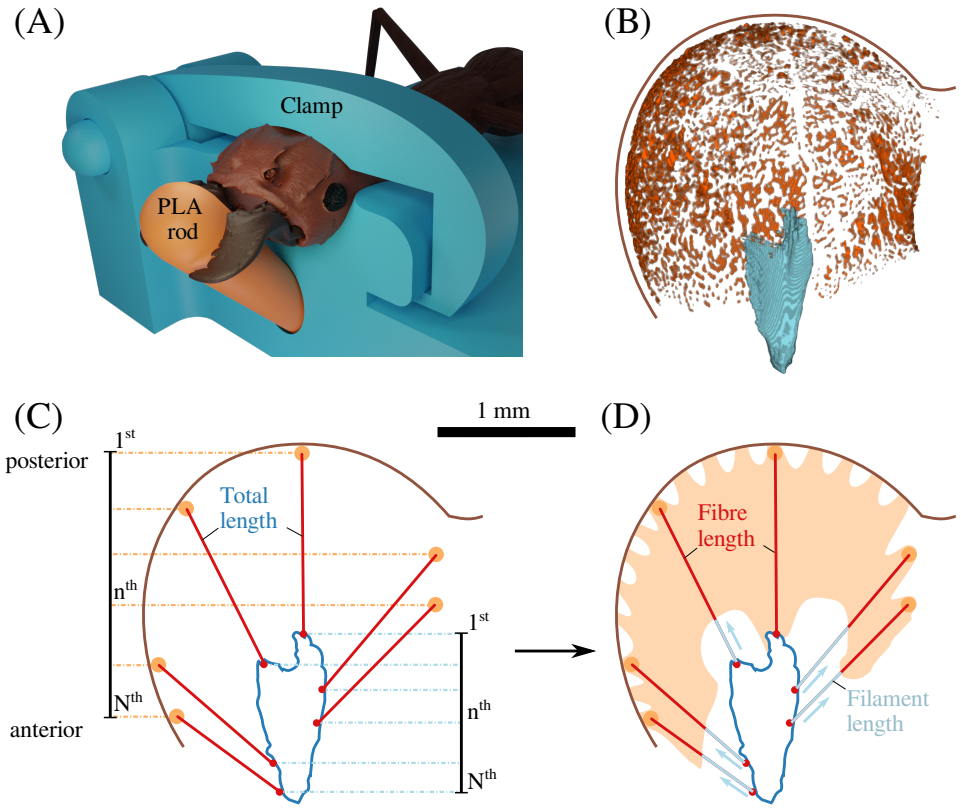


FIGURE B.1: (**A**) To link the measured bite forces to the morphology of the bite apparatus, tomographic scans of the heads were performed. Prior to scanning, the ants were clamped using a custom-built device; they were given PLA rods of varying thickness to bite onto. The rods prevented the mandibles from closing after death. (**B**) To extract muscle fibre length and orientation from the segmented scans, a three-step analysis was conducted. First, the fibre attachments to the head capsule were identified. (**C**) Second, according to their anterior-posterior position, these fibre attachments (N in total) were connected to the apodeme surface. (**D**) Third, from the apodeme surface, filaments were grown towards the fibre attachments until reaching muscle tissue. Fibre length was calculated as the difference between the projected total length and filament length.

B.5 Sensor calibration and bite force measurement

The sensor was calibrated by suspending calibration weights from the bite plate of the pivoting lever (see Chapter 4 for more details). Twelve weights between 10 and 150 g were used for calibration, exceeding the range of measured bite forces (109 - 1172 mN). Each weight was suspended five times, and the average sensor output over $\approx$ 2 s was extracted. A third degree polynomial was used to characterise the relationship between sensor output and force ($R^2 = 0.995$, see Fig. B.2A). Once calibrated, the sensor was used to measure ant bite forces (see Fig. B.2B). From each force, the maximum bite force was extracted for further analysis, as described in Chapter 3.

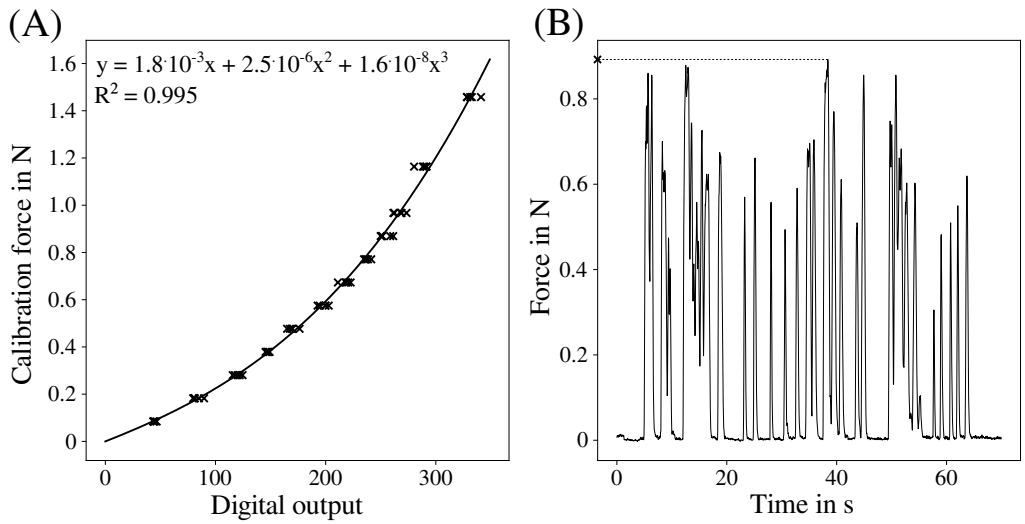


FIGURE B.2: (**A**) A force sensor was calibrated to measure bite forces of leaf-cutter ants at varying mandibular opening angles. To this end, calibration weights exceeding the range of measured forces were suspended from the sensitive bite plate of the force sensor. The relationship between calibration forces and digital output was characterised using a third-degree polynomial. (**B**) Bite forces were recorded until at least five bite cycles were completed. To compare bite force across different opening angles, the maximum measured force was extracted from each force trace.

B.6 Passive joint forces enabled by the opener muscle

Bite forces were measured across a large range of mandibular opening angles and the maximum stress, the shape parameter β and the optimum fibre length were extracted (see Fig 3.6A in Chapter 3). The general shape of the decrease in bite force with opening angle described by the model matches well with the measurements. For large opening angles $\geq 95°$, however, the model appears to underestimate the measured forces by $\approx$ 50 to 150 mN. This difference might be attributed to passive joint forces (see Weihmann et al., 2015a); elastic elements in and around the joint can act as a spring loaded by the mandible opener muscle. In order to estimate the magnitude of such joint forces, I calculated the maximum mandible opening force in analogy to Eq. 3.1 in Chapter 3. The maximum stress was assumed to be the same as for the closer muscle, the physiological cross-sectional area and pennation angles were estimated using results extracted from scans of *A. vollenweideri* majors

(see Chapter 2); the effective inlever was extracted from the scans used in this study. I estimate the maximum mandibular opening force to be around 50 mN, partially bridging the mismatch between model and measurement; the opener muscle may thus indirectly contribute to an increase in bite force at large opening angles.

C Scaling of maximum bite forces

C.1 Effects of bite plate deflection during biting

During bite force measurements, maximum forces of around $F = 1\,\mathrm{N}$ were applied onto the bite plates. I estimate the magnitude of plate deflection caused by these forces, δ_{max}, by invoking a result from simple beam theory: $\delta_{max} = FL^3/EHT^3$, where L is the protruding length of the bite plate (1 mm), H its height (6 mm), and T its thickness ($\approx$ 0.15 mm). Using a typical Young's modulus for stainless steel ($E \approx 200\,\mathrm{GPa}$), the deflection is at most $\delta_{max} = 0.0002\,\mathrm{mm}$. I hence neglected any effects of plate deflection.

C.2 Force sensor circuit and user interface

A custom-built force set-up was developed to measure bite forces of ants and other small insects. The bite forces were measured using a capacitive force sensor, connected to a raspberry pi via I^2C board (see Fig. C.1A). The pi is also connected to a stepper motor via driver board, to adjust the distance between two bite plates, a camera module to record the bite experiments simultaneously to the sensor readings, and a LCD touchscreen (see Fig. C.1B). A user interface, written in Python (v 3.5) enables the operator to calibrate the force sensor, start and stop the force and video recordings, set the current sensor reading to zero, display live outputs of force sensor and camera, save the measurements, and to adjust the plate distance.

C.3 Projection of the mandibular joint rotational axis

I determined the mandibular joint axis of rotation $\hat{\mathbf{R}}$ via kinematics analysis of the mandible motion [V Kang, F Püffel and D Labonte, in preparation]. I assumed that the relative orientation of $\hat{\mathbf{R}}$ to the head coordinate system of the scans, defined in Chapter 2, is size-invariant. However, the relative position of $\hat{\mathbf{R}}$ with respect to the head coordinate system defined for biting ants, may differ, because it is difficult to find the same key locations for all bite force recordings. I thus defined a second coordinate system based on the coordinates of the mandible joint and the two distinct head spikes (see Chapter 4). To quantify the variation of $\hat{\mathbf{R}}$ due to difference in spike location across sizes, $\hat{\mathbf{R}}$ was projected from the scan coordinate system to the spike-based coordinate systems of all scans. The angular difference between the projections of $\hat{\mathbf{R}}$ and their mean was small, $4 \pm 1^\circ$ with no significant size effect (Pearson's correlation coefficient: r_{11} = 0.46, P = 0.12). I hence selected the mean orientation of $\hat{\mathbf{R}}$ with respect to the head spikes for all sizes for the bite video analysis.

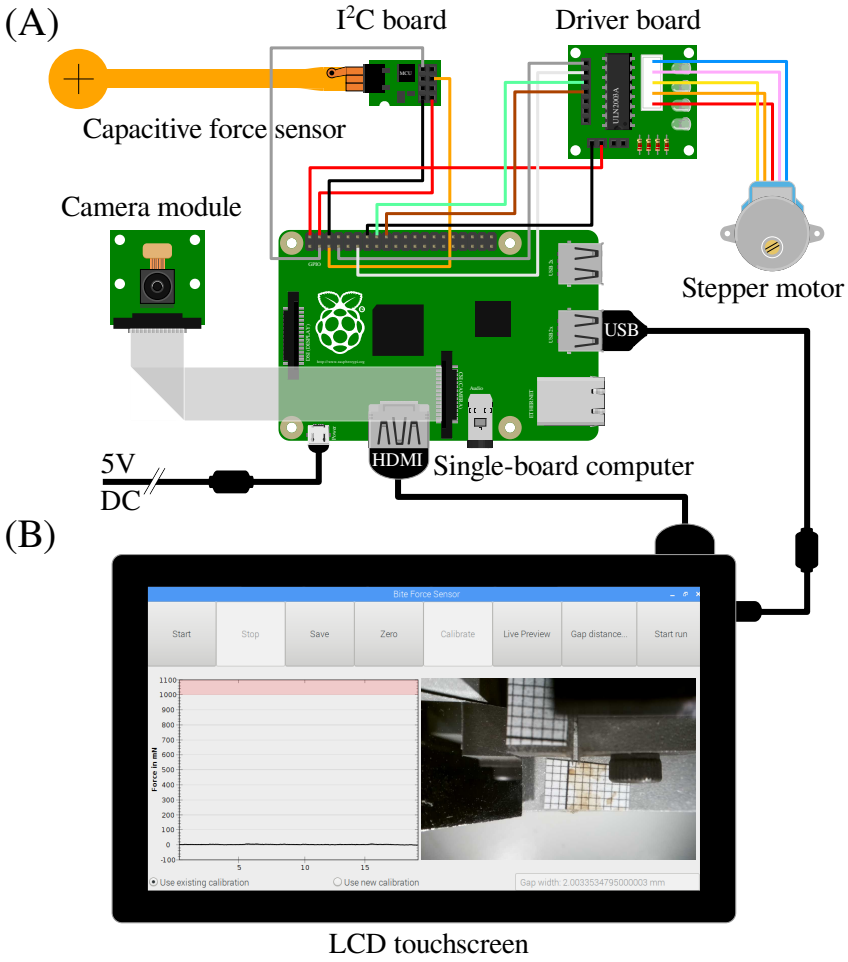


FIGURE C.1: (**A**) I developed a force set-up to accurately measure bite forces of small insect. Bite forces were measured by compressing a capacitive force sensor, sampled at 33 Hz (for more details, see Chapter 4). The sensor is connected to a raspberry pi via an I^{2}C board. The pi, powered at 5 V DC, is also connected to a stepper motor via driver board, a camera module, and a LCD touchscreen. (**B**) A user interface, written in Python (v 3.5), enables the experimenter to calibrate the force sensor, start and stop the force and video recordings, set current force readings to zero, show live readings of forces and camera output, save measurements, and move the stepper motor.

C.4 Filament length

The length of the filaments L_{fil} connecting muscle fibres and apodeme determines the relationship between muscle fibre length and mandibular opening angle, as detailed in Chapter 3. I estimated L_{fil} as the difference between the internal radius and apodeme radius, $L_{fil} = r_i - r_{apo}$. The internal radius represents the effective radius of attachment; the apodeme radius was defined as the equivalent radius of the apodeme cross-sectional area, assuming a circular shape, (see Chapter 2 for an exact definition).

TABLE C.1: Results of reduced major axis regressions describing the relationship of bite force with body mass and head volume (labelled with $*$), respectively, on $\log_{10}$-transformed data. 95 % confidence intervals are provided in parentheses.

Description	Units	Elevation	Slope	R^2
Morphological prediction	mN, mg	1.41 (1.31, 1.51)	0.93 (0.84, 0.1.03)	0.98
Fully-corrected measurement	mN, mg	1.38 (1.34, 1.43)	0.97 (0.93, 1.02)	0.86
Angle-uncorrected measurement	mN, mg	1.12 (1.05, 1.19)	0.99 (0.93, 1.06)	0.74
Raw measurement	mN, mg	1.33 (1.27, 1.39)	0.91 (0.86, 0.97)	0.75
Fully-corrected measurement $*$	N, mm^3	-1.34 (-1.38, -1.30)	0.85 (0.81, 0.89)	0.86
Meta-analysis	N, g	-0.18 (-0.27, -0.09)	0.74 (0.70, 0.77)	0.86
Meta-analysis $*$	N, mm^3	-1.59 (-1.63, -1.54)	0.91 (0.86, 0.97)	0.87

TABLE C.2: Results of reduced major axis regressions describing the relationship of mandibular opening angle in degrees, (i) at which muscle fibre length is optimum, θ_{opt}, and (ii) at which bite forces are maximum, θ_{max}, with body mass in mg on $\log_{10}$-transformed data. 95 % confidence intervals are provided in parentheses.

Quantity	Elevation	Slope	R^2
θ_{opt}	1.89 (1.83, 1.95)	-0.13 (-0.19, -0.08)	0.56
θ_{max}	1.83 (1.79, 1.87)	-0.08 (-0.12, -0.05)	0.59

D Biomechanical development of the bite apparatus

D.1 Further notable differences between callows and foragers

In addition to the quantitative differences detailed in the main text, I noticed a number of qualitative differences between callows and foragers: The mandibles of callow ants sometimes remained partially open after sacrificing them by freezing, whereas foragers always had their mandibles maximally closed; this difference presumably reflects differences in muscle development. During dissection, callow head capsules were noticeably 'squishy', and considerable amounts of watery liquid were expelled upon deformation (also see Chapter 5). When examined under the microscope, the mandible closer muscle of matured foragers appeared to fill the majority of the head capsule, whereas callows had much smaller muscles; consistent with μCT data (see Fig. D.1).

D.2 Plate model

We estimate the deformation of the head capsule caused by muscle contraction using a simple mechanical model. I model the head capsule as a plate of area, $A = H_w/4 \cdot H_h/2$, where head width, H_w and head height, H_h, were extracted for a 4.2 mg *Atta vollenweideri* ant (see Fig. D.2 and Chapter 2). The thickness of the plate is set equal to the average local thickness of the head capsule, T_{hc}, and the modulus is approximated as E_I (both measured in this study, see Chapter 5). For simplicity, I assume a quadratic shape of the plate with a side length of $a = \sqrt{A}$, clamped along all sides. In fully-matured leaf-cutter ants, the closer muscle attaches to the internal side of the head capsule with a maximum theoretical density of 50 % (assuming a cylindrical shape, see Chapter 2). At full muscle activation, the area load on the plate is thus equal to half of the maximum muscle stress, $\sigma = \sigma_m/2$ (σ_m = 1.16 MPa, extracted for *A. cephalotes* majors in Chapter 3). From plate theory, the associated maximum deflection then follows as:

$$w = \alpha\sigma\frac{a^4}{E_I T_{hc}^3} \tag{D.1}$$

where the geometry factor is $\alpha = 0.0138$ for square plates (Young and Budynas, 2002). For a forager with a cuticle brightness of 0.15, $E_I = 7.3$ GPa and $T_{hc} = 34\,\mu$m, so that the maximum deflection is 1.4 μm or 4 % of the cuticle thickness. For a callow with a cuticle brightness of 0.50, $E_I = 4.0$ GPa

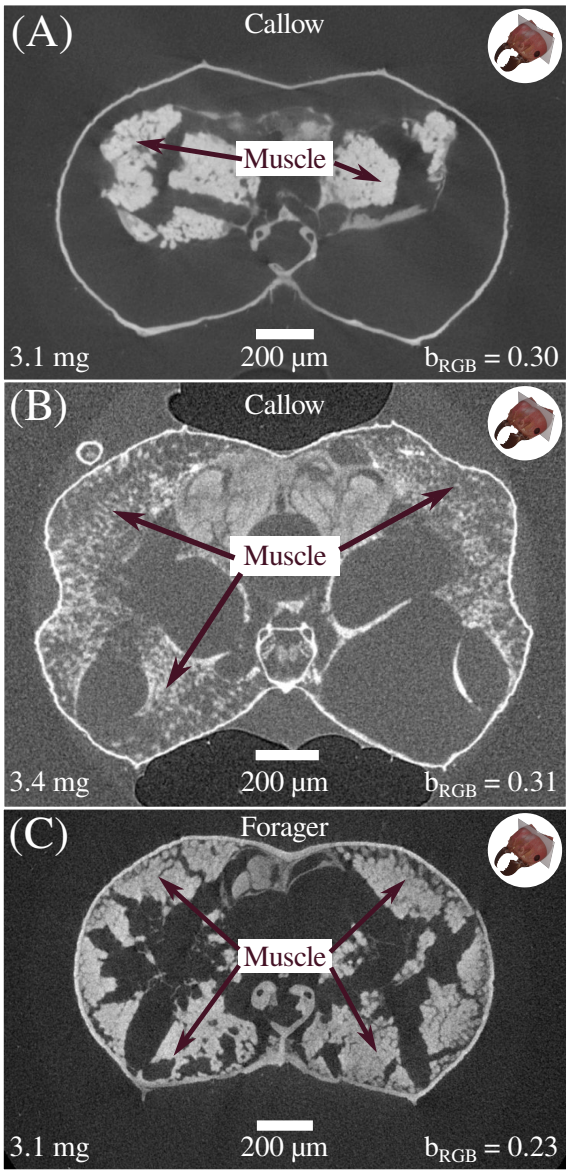


FIGURE D.1: Prior to μCT imaging, *Atta vollenweideri* leaf-cutter ants of varying cuticle brightness, b_{RGB}, were used for bite experiments, sacrificed by freezing, photographed and prepared for scanning. **(A)** I observed that the closer muscle tissue of callows that were used in bite experiments was often detached from the inner surface of the head capsule. **(B)** To test if this observation was an artefact of repeated freeze-thawing, another two callows were scanned that underwent the same treatment before tomography, but were not used in bite experiments; muscle fibres of these ants showed less detachment from the head capsule. **(C)** In fully-matured foragers that bit, muscle detachment was not observed.

and $T_{hc} = 16\,\mu$m, the deflection is 24.0 μm, equivalent to 150 % of the cuticle thickness. I hence argue that the deflection of the head capsule during muscle contraction is likely within the elastic limit for matured foragers, whereas it may cause critical damage for callows exposed to the same hypothetical muscle force. Assuming a much smaller area load of $\sigma = \sigma_m/26$, equivalent to the observed difference in bite force between foragers and bright callows, the deflection is only 1.8 μm for callows, or 12 % of the cuticle thickness.

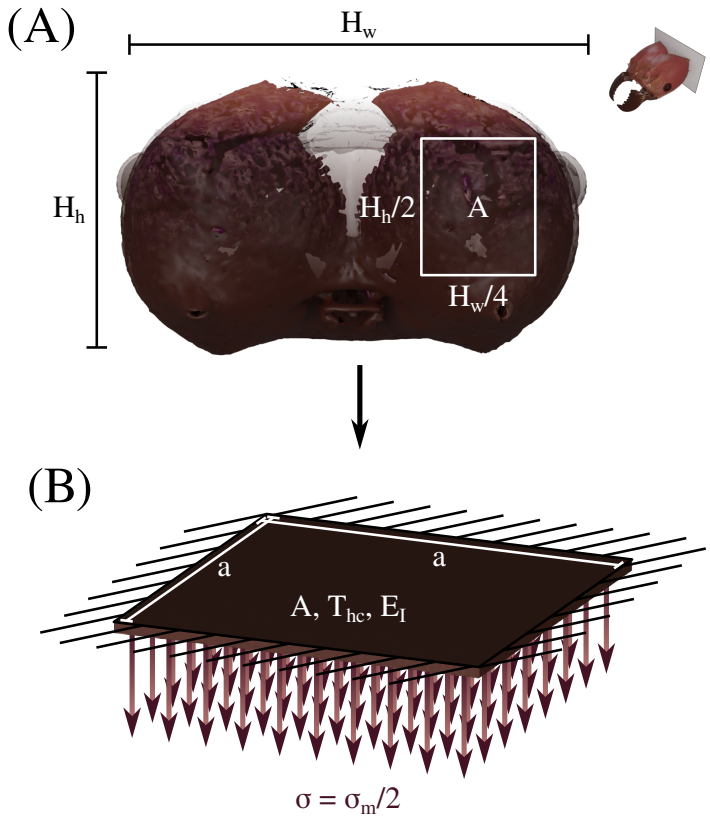


FIGURE D.2: **(A)** In order to illustrate the effects of cuticle maturation on head capsule deformation, I modelled the head capsule as a square plate with an area, $A = H_w/4 \cdot H_h/2$, where head width and height, H_w and H_h, respectively, were extracted for a 4.2 mg *A. vollenweideri* ant (see Chapter 2), a side length $a = \sqrt{A}$, a thickness, T_{hc}, and a modulus, E_I. **(B)** The plate was clamped at all sides, and a uniform area load, equal to half of the maximum muscle stress, σ_m, extracted for closely-related *A. cephalotes* majors (see Chapter 3), was applied. For the same load case, the resulting maximum deflection for a bright callow would be 24.0 μm or 1.5 times the cuticle thickness, 17 times higher than for a mature forager. In other words, if callows generated bite forces as large as those of fully-matured foragers, their head capsule would deform considerably, potentially resulting in permanent damage.

E Scaling of mandibular cutting forces

E.1 Tooth length measurements and wear determination

In order to estimate mandibular wear, I extracted the lengths of the most distal tooth, T_1, and second most distal tooth, T_2, of the mandible blade from photographic images, following Schofield et al. (see Fig. E.1 and R. M. Schofield et al., 2011). Tooth length was measured perpendicular to the line connecting the most distal tooth gap, also called 'V-blade', and the most proximal tooth gap; the length of this line determined the mandible blade length, L_{mb}. To establish the relationship between L_{mb}, T_1, and T_2 with body mass, I performed OLS regressions on $\log_{10}$-transformed values (see Table E.1 and Fig. E.1C). Based on the regression results obtained for the pristine teeth of callows, I calculated tooth length differences and mandibular wear (see Eq. 6.1 in Chapter 6). Notably, all length parameters were close to isometric scaling, $m^{0.33}$, apart from T_2 for pristine callow mandibles, which was proportional to $m^{0.12}$ (see Table E.1); this result suggests changes in mandible blade curvature across sizes (see L. C. Silva et al., 2016, and N Imirzian, F Püffel and D Labonte, in preparation).

Table E.1: Results of Ordinary Least Squares regressions describing the relationship between various mandible dimensions in μm and body mass in mg. All regressions were performed on $\log_{10}$-transformed data; 95 % confidence intervals are shown in parentheses.

Quantity	Group	Elevation	Slope	R^2
L_{mb}	Foragers	2.63 (2.62, 2.65)	0.31 (0.30, 0.33)	0.99
L_{mb}	Callows	2.66 (2.64, 2.68)	0.29 (0.27, 0.31)	0.96
T_1	Foragers	1.95 (1.76, 2.14)	0.38 (0.20, 0.56)	0.47
T_1	Callows	2.12 (2.08, 2.15)	0.32 (0.29, 0.35)	0.92
T_2	Foragers	1.50 (1.32, 1.68)	0.25 (0.08, 0.42)	0.30
T_2	Callows	1.70 (1.64, 1.77)	0.12 (0.06, 0.18)	0.28

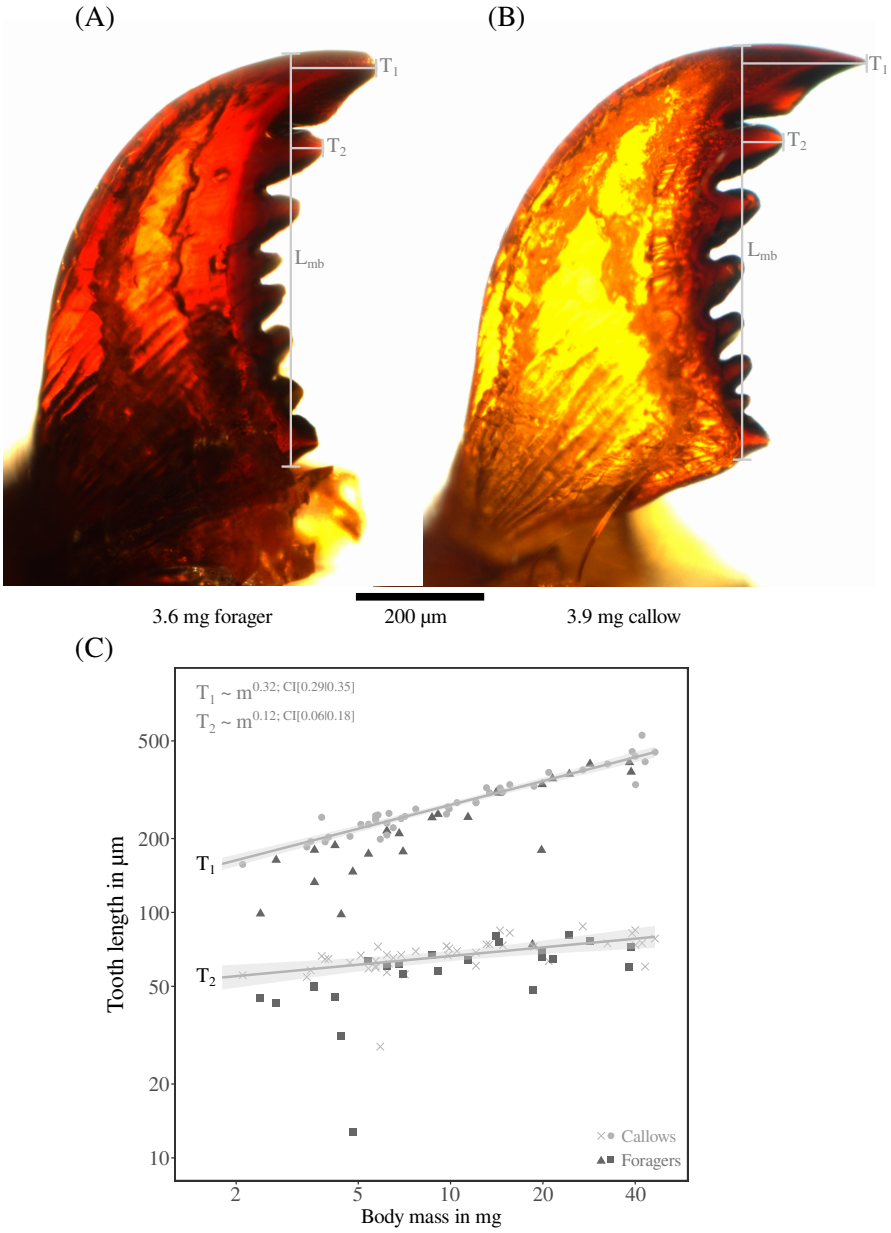


FIGURE E.1: **(A - B)** From both callows and foragers, I measured the length of the mandibular blade, L_{mb}, as the length of the line across the blade that passes through the most distal and most proximal tooth 'valleys'; tooth length was measured perpendicular to that line (see R. M. Schofield et al., 2011). I calculated mandibular wear based on the length of the two most distal teeth, T_1 and T_2, relative to their expected pristine length extracted via regression analysis on the callows (see R. M. Schofield et al., 2011, and results). **(C)** The pristine length of the most distal tooth increased as expected from isometry; the pristine length of the second most distal tooth increased with negative allometry (see Table E.1)

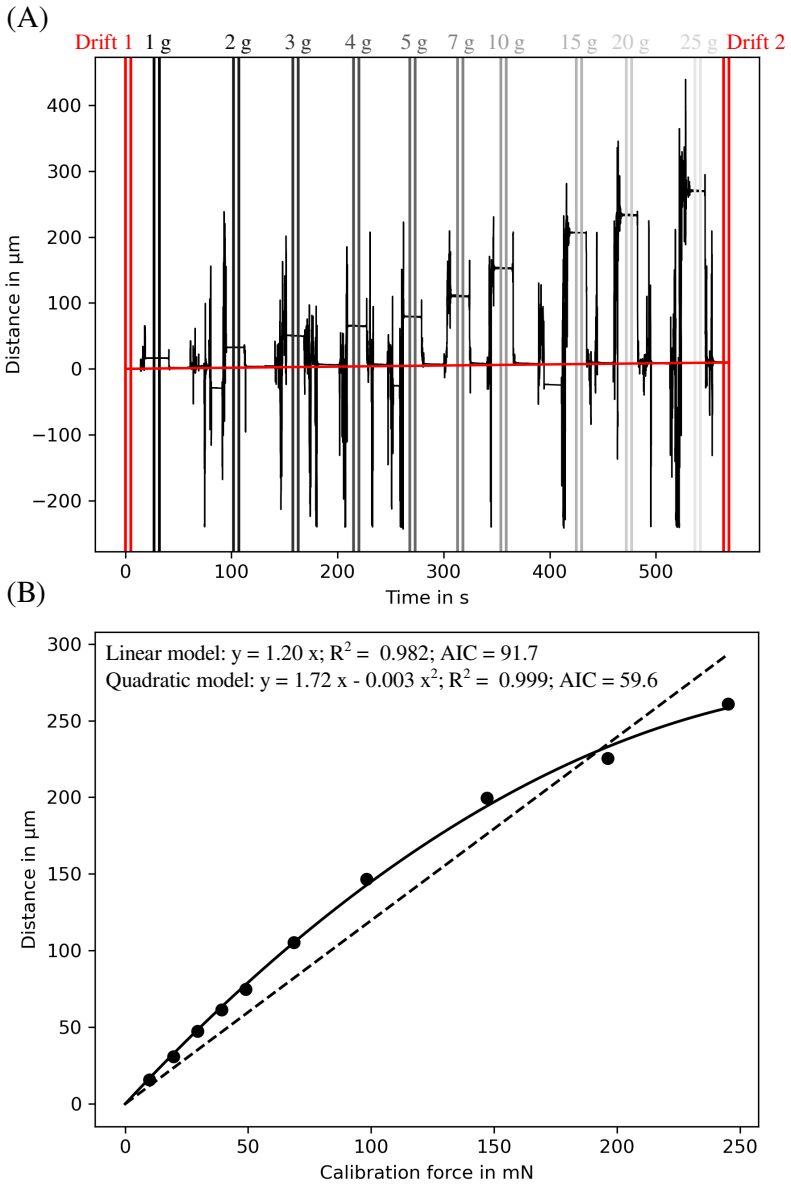


FIGURE E.2: **(A)** To calibrate the force sensor, I suspended a series of calibration weights from the free end of the bending beam (see Chapter 6). From the distance-time curve, I extracted the average distance across 5 s for each weight, and implemented a linear drift correction (red line). **(B)** I tested two regression models to characterise the relationship between distance and calibration force; the quadratic model yielded a lower Akaike Information Criterion and was hence preferred over the linear model.

F Permissions for republication

The contents of Chapters 2, 3, 4 and 5 were previously published as preprints on *bioRxiv* under the Creative Commons Attribution License (CC-BY 4.0). Chapter 2 was published in the *Journal of the Royal Society Interface* (Püffel et al., 2021), and is here republished with permission of the Royal Society; permission conveyed through Copyright Clearance Center, Inc. Chapter 3 was published in *Royal Society Open Science* under the Creative Commons Attribution License (CC-BY 4.0) (Püffel et al., 2023a).

In Chapter 1, Fig. 1.2 was adapted from Chapman (1995), and is republished with permission of *Springer*, from **Regulatory mechanisms in insect feeding, Chapman, R.F., de Boer, G., 1995**; permission conveyed through Copyright Clearance Center, Inc. Fig. 1.3 was taken from Wirth et al. (2003), and is republished with permission of *Springer*, from **Herbivory of Leaf-Cutting Ants: A Case Study on *Atta colombica* in the Tropical Rainforest of Panama, Wirth, R., Herz, H., Ryel, R.J., Beyschlag, W., Hölldobler, B., 2003**; permission conveyed through Copyright Clearance Center, Inc. Fig. 1.5 was adapted from Wetterer (1999), and is republished in accordance with the BOAI definition of open access as stated by the publishing journal *Sociobiology*.

Bibliography

Abraham, V. A. et al. (1998). "An integrated management approach for the red palm weevil *Rhynchophorus ferrugineus* Oliv. a key pest of date palm in the Middle East". In: *Journal of Agricultural and Marine Sciences* 3.1, pp. 77–83.

Agrawal, A. A. and K. Konno (2009). "Latex: a model for understanding mechanisms, ecology, and evolution of plant defense against herbivory". In: *Annual Review of Ecology, Evolution, and Systematics* 40, pp. 311–331.

Aguirre, L. F. et al. (2002). "Ecomorphological analysis of trophic niche partitioning in a tropical savannah bat community". In: *Proceedings of the Royal Society of London. Series B: Biological Sciences* 269.1497, pp. 1271–1278.

Ahn, A. N., K. Meijer, and R. J. Full (2006). "In situ muscle power differs without varying in vitro mechanical properties in two insect leg muscles innervated by the same motor neuron". In: *Journal of Experimental Biology* 209.17, pp. 3370–3382.

Alexander, R. M. (1985). "The maximum forces exerted by animals". In: *Journal of Experimental Biology* 115.1, pp. 231–238.

Alexander, R. M. (1969). "Mechanics of the feeding action of a cyprinid fish". In: *Journal of Zoology* 159.1, pp. 1–15.

Anderson, P. S. (2018). "Making a point: shared mechanics underlying the diversity of biological puncture". In: *Journal of Experimental Biology* 221.22, jeb187294.

Anderson, R. A., L. D. McBrayer, and A. Herrel (2008). "Bite force in vertebrates: opportunities and caveats for use of a nonpareil whole-animal performance measure". In: *Biological Journal of the Linnean Society* 93.4, pp. 709–720.

April, E. W. and P. W. Brandt (1973). "The Myofilament Lattice: Studies on Isolated Fibers: III. The effect of myofilament spacing upon tension". In: *The Journal of General Physiology* 61.4, pp. 490–508.

Arenas, A. and F. Roces (2018). "Appetitive and aversive learning of plants odors inside different nest compartments by foraging leaf-cutting ants". In: *Journal of Insect Physiology* 109, pp. 85–92.

Arganda, S. et al. (2020). "The neuroplasticity of division of labor: worker polymorphism, compound eye structure and brain organization in the leafcutter ant *Atta cephalotes*". In: *Journal of Comparative Physiology A* 206, pp. 651–662.

Atkins, A. G. and Y. W. Mai (1979). "On the guillotining of materials". In: *Journal of Materials Science* 14.11, pp. 2747–2754.

Atkins, T. (2009). *The Science and Engineering of Cutting: The Mechanics and Processes of Separating, Scratching and Puncturing Biomaterials, Metals and Non-metals*. Oxford, UK: Butterworth-Heinemann.

Azizi, E. (2014). "Locomotor function shapes the passive mechanical properties and operating lengths of muscle". In: *Proceedings of the Royal Society B: Biological Sciences* 281.1783, p. 20132914.

Azizi, E. et al. (2017). "Resistance to radial expansion limits muscle strain and work". In: *Biomechanics and Modeling in Mechanobiology* 16.5, pp. 1633–1643.

Azizi, E., E. L. Brainerd, and T. J. Roberts (2008). "Variable gearing in pennate muscles". In: *Proceedings of the National Academy of Sciences* 105.5, pp. 1745–1750.

Baker, G., L. H. Jones, and I. D. Wardrop (1959). "Cause of Wear in Sheeps' Teeth". In: *Nature* 184, pp. 1583–1584.

Barbosa, P., D. Berry, and C. K. Kary (2015). *Insect histology: Practical laboratory techniques*. John Wiley & Sons.

Barrer, P. and J. M. Cherrett (1972). "Some factors affecting the site and pattern of leaf-cutting activity in the ant *Atta cephalotes* L." In: *Physiological Entomology* 47, pp. 15–27.

Battisti, D. S. and R. L. Naylor (2009). "Historical warnings of future food insecurity with unprecedented seasonal heat". In: *Science* 323, pp. 240–244.

Bayline, R. J., C. Duch, and R. B. Levine (2001). "Nerve-muscle interactions regulate motor terminal growth and myoblast distribution during muscle development". In: *Developmental Biology* 231.2, pp. 348–363.

Becerra, F., A. Casinos, and A. I. Vassallo (2013). "Biting performance and skull biomechanics of a chisel tooth digging rodent (*Ctenomys tuconax*; Caviomorpha; Octodontoidea)". In: *Journal of Experimental Zoology Part A: Ecological Genetics and Physiology* 319.2, pp. 74–85.

Becerra, F. et al. (2011). "Bite force and jaw biomechanics in the subterranean rodent Talas tuco-tuco (*Ctenomys talarum*)(Caviomorpha: Octodontoidea)". In: *Canadian Journal of Zoology* 89.4, pp. 334–342.

Ben-Shahar, Y. et al. (2002). "Influence of gene action across different time scales on behavior". In: *Science* 296, pp. 741–44.

Bennet-Clark, H. (1975). "The energetics of the jump of the locust *Schistocerca gregaria*". In: *Journal of Experimental Biology* 63.1, pp. 53–83.

Benninghoff, A. and H. Rollhäuser (1952). "Zur inneren Mechanik des gefiederten Muskels". In: *Pflüger's Archiv für die gesamte Physiologie des Menschen und der Tiere* 254.6, pp. 527–548.

Beran, F. and G. Petschenka (2022). "Sequestration of Plant Defense Compounds by Insects: From Mechanisms to Insect–Plant Coevolution". In: *Annual Review of Entomology* 67, pp. 163–180.

Bernays, E. A. (1998). "Evolution of feeding behaviour in insect herbivores". In: *Bioscience, JSTOR* 48, pp. 35–44.

– (1986). "Diet-induced head allometry among foliage-chewing insects and its importance for graminivores". In: *Science* 231.4737, pp. 495–497.

Bernays, E. A. (1991). "Evolution of insect morphology in relation to plants". In: *Philosophical Transactions of the Royal Society of London. Series B: Biological Sciences* 333.1267, pp. 257–264.

Beshers, S. N. and J. H. Fewell (2001). "Models of division of labor in social insects". In: *Annual Review of Entomology* 46.1, pp. 413–440.

Beshers, S. N. and J. F. Traniello (1996). "Polyethism and the adaptiveness of worker size variation in the attine ant *Trachymyrmex septentrionalis*". In: *Journal of Insect Behavior* 9.1, pp. 61–83.

Blanke, A. (2019). "The Early Evolution of Biting–Chewing Performance in Hexapoda". In: *Insect Mouthparts*. Ed. by H. W. Krenn. Springer, pp. 175–202.

Blanke, A. et al. (2012). "Revival of Palaeoptera—head characters support a monophyletic origin of Odonata and Ephemeroptera (Insecta)". In: *Cladistics* 28.6, pp. 560–581.

Blanke, A. et al. (2015). "Mandibles with two joints evolved much earlier in the history of insects: dicondyly is a synapomorphy of bristletails, silverfish and winged insects". In: *Systematic Entomology* 40.2, pp. 357–364.

Blanke, A. et al. (2017). "Computational biomechanics changes our view on insect head evolution". In: *Proceedings of the Royal Society B: Biological Sciences* 284.1848, p. 20162412.

Block, J. D. and S. Rebach (1998). "Correlates of claw strength in the rock crab, *Cancer irroratus* (Decapoda, Brachyura)". In: *Crustaceana* 71.4, pp. 468–473.

Blundon, J. A. (1988). "Morphology and muscle stress of chelae of temperate and tropical stone crabs *Menippe mercenaria*". In: *Journal of Zoology* 215.4, pp. 663–673.

Bolstad, G. H. et al. (2015). "Complex constraints on allometry revealed by artificial selection on the wing of *Drosophila melanogaster*". In: *Proceedings of the National Academy of Sciences* 112.43, pp. 13284–13289.

Bomphrey, R. J. et al. (2016). "Flight of the dragonflies and damselflies". In: *Philosophical Transactions of the Royal Society B: Biological Sciences* 371.1704, p. 20150389.

Bonduriansky, R. (2007). "Sexual selection and allometry: a critical reappraisal of the evidence and ideas". In: *Evolution: International Journal of Organic Evolution* 61.4, pp. 838–849.

Booher, D. B. et al. (2021). "Functional innovation promotes diversification of form in the evolution of an ultrafast trap-jaw mechanism in ants". In: *Public Library of Science Biology* 19.3, e3001031.

Borel, B. (2017). "When the pesticides run out". In: *Nature* 543, pp. 302–304.

Boselli, F., J. B. Freund, and J. Vermot (2015). "Blood flow mechanics in cardiovascular development". In: *Cellular and Molecular Life Sciences* 72.13, pp. 2545–2559.

Brainerd, E. L. and E. Azizi (2005). "Muscle fiber angle, segment bulging and architectural gear ratio in segmented musculature". In: *Journal of Experimental Biology* 208.17, pp. 3249–3261.

Burd, M. (1995). "Variable Load Size-Ant Size Matching in Leaf-Cutting Ants, *Atta colombica* (Hymenoptera: Formicidae)". In: *Journal of Insect Behavior* 8.5, pp. 715–722.

– (1996). "Foraging performance by *Atta colombica*, a leaf-cutter ant". In: *The American Naturlist* 148.4, pp. 597–612.

– (2000a). "Body size effects on locomotion and load carriage in the highly polymorphic leaf-cutting ants *Atta colombica* and *Atta cephalotes*". In: *Behavioral Ecology* 11.2, pp. 125–131.

Burd, M. (2000b). "Foraging behaviour of *Atta cephalotes* (leaf-cutting ants): an examination of two predictions for load selection". In: *Animal Behaviour* 60, pp. 781–788.

– (2001). "Leaf tissue transport as a function of loading ratio in the leaf-cutting ant *Atta cephalotes*". In: *Ecological Entomology* 26, pp. 551–556.

Burd, M. and J. J. Howard (2005). "Central-place foraging continues beyond the nest entrance: the underground performance of leaf-cutting ants". In: *Animal Behaviour* 70, pp. 737–744.

Burrows, M. (2006). "Jumping performance of froghopper insects". In: *Journal of Experimental Biology* 209.23, pp. 4607–4621.

Burrows, M. and G. Sutton (2013). "Interacting gears synchronize propulsive leg movements in a jumping insect". In: *Science* 341.6151, pp. 1254–1256.

Bywater, C., M. Angilletta Jr, and R. Wilson (2008). "Weapon size is a reliable indicator of strength and social dominance in female slender crayfish (*Cherax dispar*)". In: *Functional Ecology* 22.2, pp. 311–316.

Calderone, N. W. (1995). "Temporal division of labor in the honey bee, Apis mellifera A developmental process or the result of environmental influences?" In: *Canadian Journal of Zoology* 73.8, pp. 1410–1416.

Camargo, R. et al. (2007). "Age polyethism in the leaf-cutting ant *Acromyrmex subterraneus brunneus* Forel, 1911 (Hym., Formicidae)". In: *Journal of Applied Entomology* 131.2, pp. 139–145.

Cao, F. et al. (2014). "A biological micro actuator: graded and closed-loop control of insect leg motion by electrical stimulation of muscles". In: *Public Library of Science One* 9.8, e105389.

Carroll, C. R. and C. A. Hoffman (1980). "Chemical feeding deterrent mobilized in response to insect herbivory and counteradaptation by *Epilachna tredecimnotata*". In: *Science* 209, pp. 414–416.

Cecilia, A. et al. (2011). "LPE grown LSO: Tb scintillator films for high-resolution X-ray imaging applications at synchrotron light sources". In: *Nuclear Instruments and Methods in Physics Research Section A: Accelerators, Spectrometers, Detectors and Associated Equipment* 648, S321–S323.

Chapman, R. (1995). "Mechanics of food handling by chewing insects". In: *Regulatory mechanisms in insect feeding*. Ed. by R. F. Chapman and G. de Boer. Springer, pp. 3–31.

Chapple, W. D. (1983). "Mechanical responses of a crustacean slow muscle". In: *Journal of Experimental Biology* 107.1, pp. 367–383.

Cherrett, J. M. (1968). "The foraging behaviour of *Atta cephalotes* L. (Hymenoptera, Formicidae)". In: *Journal of Animal Ecology* 37.2, pp. 387–403.

– (1972). "Some Factors Involved in the Selection of Vegetable Substrate by *Atta cephalotes* (L.) (Hymenoptera: Formicidae) in Tropical Rain Forest". In: *Journal of Animal Ecology* 41.3, pp. 647–660.

Choo, H. Y. et al. (2016). "Electrical stimulation of coleopteran muscle for initiating flight". In: *Public Library of Science One* 11.4, e0151808.

Choong, M. F. (1996). "What makes a leaf tough and how this affects the pattern of *Castanopsis fissa* leaf consumption by caterpillars". In: *Functional Ecology* 10.5, pp. 668–674.

Clark, E. (2006). "Dynamic matching of forager size to resources in the continuously polymorphic leaf-cutter ant, *Atta colombica* (Hymenoptera, Formicidae)". In: *Ecological Entomology* 31, pp. 629–635.

Claussen, D. L. et al. (2008). "Pinching forces in crayfish and fiddler crabs, and comparisons with the closing forces of other animals". In: *Journal of Comparative Physiology B* 178.3, pp. 333–342.

Clissold, F. J. et al. (2009). "Grass vs. net income: how plant toughness affects performance of an insect herbivore". In: *Ecology* 90, pp. 3393–3405.

Clissold, F. (2007). "The Biomechanics of Chewing and Plant Fracture: Mechanisms and Implications". In: *Advances in Insect Physiology* 34.

Coley, P. and J. A. Barone (1996). "Herbivory and plant defenses in tropical forests". In: *Annual Review of Ecology, Evolution, and Systematics* 27, pp. 305–335.

Coley, P. D. (1983). "Herbivory and defensive characteristics of tree species in a lowland tropical forest". In: *Ecological Monographs* 53.2, pp. 209–234.

Combes, S. A. et al. (2013). "Capture success and efficiency of dragonflies pursuing different types of prey". In: *Integrative and Comparative Biology* 53.5, pp. 787–798.

Cordoba-Barco, G., F. Casanova, and J. L. Ealo (2020). "Determination of poro-viscoelastic properties of vegetal tissues as a function of moisture content by means of stress relaxation tests". In: *Rheologica Acta* 59.4, pp. 201–208.

Costa, A. N. et al. (2008). "Do herbivores exert top-down effects in Neotropical savannas? Estimates of biomass consumption by leaf-cutter ants". In: *Journal of Vegetation Science* 19.6, pp. 849–854.

Crespo-Pérez, V. et al. (2020). "The importance of insects on land and in water: a tropical view". In: *Current Opinion in Insect Science* 40, pp. 31–38.

Creton, C. and M. Ciccotti (2016). "Fracture and adhesion of soft materials: a review". In: *Reports on Progress in Physics* 79.4, p. 046601.

Crofts, S. and P. Anderson (2018). "The influence of cactus spine surface structure on puncture performance and anchoring ability is tuned for ecology". In: *Proceedings of the Royal Society B* 285.1891, p. 20182280.

Crofts, S. et al. (2019). "How do morphological sharpness measures relate to puncture performance in viperid snake fangs?" In: *Biology Letters* 15.4, p. 20180905.

Currie, C. R. (2001). "Prevalence and impact of a virulent parasite on a tripartite mutualism". In: *Oecologia* 128, pp. 99–106.

Currie, C. R., U. G. Mueller, and D. Malloch (1999). "The agricultural pathology of ant fungus gardens". In: *Proceedings of the National Academy of Sciences of the U.S.A* 96, pp. 7998–8002.

Daly, D. C. et al. (2009). "A pulsed UWB receiver SoC for insect motion control". In: *IEEE Journal of solid-state circuits* 45.1, pp. 153–166.

Darvell, B. et al. (1996). "A portable fracture toughness tester for biological materials". In: *Measurement Science and Technology* 7.6, p. 954.

David, S. et al. (2016a). "Musculoskeletal modelling of the dragonfly mandible system as an aid to understanding the role of single muscles in an evolutionary context". In: *Journal of Experimental Biology* 219, pp. 1041–1049.

– (2016b). "Musculoskeletal modelling under an evolutionary perspective: deciphering the role of single muscle regions in closely related insects". In: *Journal of The Royal Society Interface* 13.

De Kort, C. (1990). "Thirty-five years of diapause research with the Colorado potato beetle". In: *Entomologia Experimentalis et Applicata* 56.1, pp. 1–13.

De Meyer, J. et al. (2018). "Broader head, stronger bite: *In vivo* bite forces in European eel *Anguilla anguilla*". In: *Journal of Fish Biology* 92.1, pp. 268–273.

Deeming, D. (2022). "Inter-relationships among body mass, body dimensions, jaw musculature and bite force in reptiles". In: *Journal of Zoology*, pp. 1–11.

Depieri, R. A., F. Siqueira, and A. R. Panizzi (2010). "Aging and food source effects on mandibular stylets teeth wear of phytophagous stink bug (Heteroptera: Pentatomidae)". In: *Neotropical Entomology* 39.6, pp. 952–956.

Dessem, D. and R. E. Druzinsky (1992). "Jaw-muscle activity in ferrets, *Mustela putorius furo*". In: *Journal of Morphology* 213.2, pp. 275–286.

Deutsch, C. A. et al. (2018). "Increase in crop losses to insect pests in a warming climate". In: *Science* 361, pp. 916–919.

Dhaliwal, G., V. Jindal, and A. Dhawan (2010). "Insect pest problems and crop losses: changing trends". In: *Indian Journal of Ecology* 37.1, pp. 1–7.

Di Giulio, A., M. Muzzi, and R. Romani (2015). "Functional anatomy of the explosive defensive system of bombardier beetles (Coleoptera, Carabidae, Brachininae)". In: *Arthropod Structure & Development* 44.5, pp. 468–490.

Dockter, D. E. (1993). "Developmental changes and wear of larval mandibles in *Heterocampa guttivitta* and *H. subrotata* (Notodontidae)". In: *Journal of the Lepidopterists' Society* 47.1, pp. 32–48.

Domander, R., A. A. Felder, and M. Doube (2021). "BoneJ2 - refactoring established research software". In: *Wellcome Open Research* 6.37.

Douglas, A. E. (2018). "Strategies for enhanced crop resistance to insect pests". In: *Annual Review of Plant Biology* 69, pp. 637–660.

Douissard, P.-A. et al. (2012). "A versatile indirect detector design for hard X-ray microimaging". In: *Journal of Instrumentation* 7.09, P09016.

Dumont, E. R. and A. Herrel (2003). "The effects of gape angle and bite point on bite force in bats". In: *Journal of Experimental Biology* 206.13, pp. 2117–2123.

Dussutour, A. et al. (2008). "Individual and collective problem-solving in a foraging context in the leaf-cutting ant *Atta colombica*". In: *Animal cognition* 12, pp. 21–30.

Egset, C. K. et al. (2012). "Artificial selection on allometry: change in elevation but not slope". In: *Journal of Evolutionary Biology* 25.5, pp. 938–948.

Ehrlich, P. R. and P. H. Raven (1964). "Butterflies and plants: a study in coevolution". In: *Evolution* 18, pp. 568–608.

Elner, R. W. and A. Campbell (1981). "Force, function and mechanical advantage in the chelae of the American lobster *Homarus americanus* (Decapoda: Crustacea)". In: *Journal of Zoology* 193.2, pp. 269–286.

Erickson, G. et al. (2014). "A comparative analysis of ontogenetic bite-force scaling among Crocodylia". In: *Journal of Zoology* 292.1, pp. 48–55.

Erickson, G. M., A. K. Lappin, and K. A. Vliet (2003). "The ontogeny of bite-force performance in American alligator (*Alligator mississippiensis*)". In: *Journal of Zoology* 260.3, pp. 317–327.

Erickson, G. M. et al. (1996). "Bite-force estimation for Tyrannosaurus rex from tooth-marked bones". In: *Nature* 382.6593, pp. 706–708.

Evison, S. E. and F. L. Ratnieks (2007). "New role for majors in *Atta* leafcutter ants". In: *Ecological Entomology* 32.5, pp. 451–454.

Fabian, J. M. et al. (2019). "Properties of predictive gain modulation in a dragonfly visual neuron". In: *Journal of Experimental Biology* 222.17, jeb207316.

Farji-Brener, A. G. (2001). "Why are leaf-cutting ants more common in secondary forest than in old-growth tropical forests? An evaluation of the palatable forage hypothesis". In: *Oikos* 92.1, pp. 169–177.

Farji-Brener, A. G. and Y. Sasal (2003). "Is dump material an effective small-scale deterrent to herbivory by leaf-cutting ants?" In: *Ecoscience* 10.2, pp. 151–154.

Federle, W., K. Rohrseitz, and B. Hölldobler (2000). "Attachment forces of ants measured with a centrifucge: better 'wax-runners' have a poorer attachment to a smooth surface". In: *The Journal of Experimental Biology* 203, pp. 505–512.

Federle, W. et al. (1997). "Slippery ant-plants and skilful climbers: selection and protection of specific ant partners by epicuticular wax blooms in *Macaranga* (Euphorbiaceae)". In: *Oecologia* 112, pp. 217–224.

Feener, D. H., J. R. Lighton, and G. A. Bartholomew (1988). "Curvilinear allometry, energetics and foraging ecology: a comparison of leaf-cutting ants and army ants". In: *Functional Ecology* 2.4, pp. 509–520.

Fernandes, J. J. and H. Keshishian (1998). "Nerve-muscle interactions during flight muscle development in *Drosophila*". In: *Development* 125.9, pp. 1769–1779.

Field, A., J. Miles, and Z. Field (2012). "Discovering Statistics Using R". In: *Great Britain: Sage Publications, Ltd*.

Folgarait, P. J. et al. (1996). "Leaf-cutting ant preferences for five native tropical plantation tree species growing under different light conditions". In: *Entomologia Experimentalis et Applicata* 80.3, pp. 521–530.

Forister, M. L. et al. (2015). "The global distribution of diet breadth in insect herbivores". In: *Proceedings of the National Academy of Sciences* 112.2, pp. 442–447.

Fowler, H. G. et al. (1989). "A pest is a pest is a pest? The dilemma of neotropical leaf-cutting ants keystone taxa of natural ecosystems". In: *Enviromental Management* 13, pp. 671–675.

Fowler, H. et al. (1986). "Economics of grass-cutting ants". In: *Fire ants and leaf-cutting ants*. CRC Press, pp. 18–35.

Freeman, P. W. and C. A. Lemen (2008). "Measuring bite force in small mammals with a piezo-resistive sensor". In: *Journal of Mammalogy* 89.2, pp. 513–517.

– (2010). "Simple predictors of bite force in bats: the good, the better and the better still". In: *Journal of Zoology* 282.4, pp. 284–290.

Full, R. and A. Ahn (1995). "Static forces and moments generated in the insect leg: comparison of a three-dimensional musculo-skeletal computer model with experimental measurements". In: *The journal of Experimental Biology* 198.6, pp. 1285–1298.

Fürstenberg-Hägg, J., M. Zagrobelny, and S. Bak (2013). "Plant defense against insect herbivores". In: *International Journal of Molecular Sciences* 14, pp. 10242–10297. ISSN: 1422-0067.

Futuyma, D. J. and A. A. Agrawal (2009). "Macroevolution and the biological diversity of plants and herbivores". In: *Proceedings of the National Academy of Sciences of the U.S.A* 106.43, pp. 18054–18061.

Garrett, R. W. et al. (2016). "Leaf processing behaviour in *Atta* leafcutter ants: 90% of leaf cutting takes place inside the nest, and ants select pieces that require less cutting". In: *Royal Society Open Science* 3.150111, pp. 1–12.

Gayon, J. (2000). "History of the concept of allometry". In: *American Zoologist* 40.5, pp. 748–758.

Gidmark, N. J. et al. (2013). "Bite force is limited by the force–length relationship of skeletal muscle in black carp, *Mylopharyngodon piceus*". In: *Biology Letters* 9.2, p. 20121181.

Ginot, S. et al. (2020). "Decoupled ontogeny of *in vivo* bite force and mandible morphology reveals effects of weaning and sexual maturation in mice". In: *Biological Journal of the Linnean Society* 129.3, pp. 558–569.

Giron, D. et al. (2018). "Promises and challenges in insect - plant interactions". In: *Entomologia Experimentalis et Applicata* 166.5, pp. 319–343.

Gordon, A., A. F. Huxley, and F. Julian (1966). "The variation in isometric tension with sarcomere length in vertebrate muscle fibres". In: *The Journal of Physiology* 184.1, pp. 170–192.

Gordon, D. M. (2016). "From division of labor to the collective behavior of social insects". In: *Behavioral Ecology and Sociobiology* 70.7, pp. 1101–1108.

Gould, S. J. (1966). "Allometry and size in ontogeny and phylogeny". In: *Biological reviews* 41.4, pp. 587–638.

Govind, C. and J. A. Blundon (1985). "Form and function of the asymmetric chelae in blue crabs with normal and reversed handedness". In: *The Biological Bulletin* 168.2, pp. 321–331.

Goyens, J., J. Dirckx, and P. Aerts (2015). "Stag beetle battle behavior and its associated anatomical adaptations". In: *Journal of Insect Behavior* 28.3, pp. 227–244.

Goyens, J. et al. (2014a). "Finite-element modelling reveals force modulation of jaw adductors in stag beetles". In: *Journal of the Royal Society Interface* 11.101, p. 20140908.

Goyens, J. et al. (2014b). "Biomechanical determinants of bite force dimorphism in *Cyclommatus metallifer* stag beetles". In: *Journal of Experimental Biology* 217, pp. 1065–1071.

Griffith, A. A. (1921). "VI. The phenomena of rupture and flow in solids". In: *Philosophical transactions of the royal society of london. Series A, containing papers of a mathematical or physical character* 221.582-593, pp. 163–198.

Groh, C. et al. (2014). "Density of mushroom body synaptic complexes limits intraspecies brain miniaturization in highly polymorphic leaf-cutting ant workers". In: *Proceedings of the Royal Society B: Biological Sciences* 281.1785, p. 20140432.

Gronenberg, W. (1995). "The fast mandible strike in the trap-jaw ant *Odontomachus*: I. Temporal properties and morphological characteristics". In: *Journal of Comparative Physiology A* 176, pp. 391–398.

– (1996). "Fast actions in small animals: springs and click mechanisms". In: *Journal of Comparative Physiology A* 178.6, pp. 727–734.

Gronenberg, W. et al. (1997). "Mandible muscle fibers in ants: fast or powerful?" In: *Cell & Tissue Research* 289, pp. 347–361.

Gronenberg, W. (2008). "Structure and function of ant (Hymenoptera: Formicidae) brains: strength in numbers". In: *Myrmecological News* 11, pp. 25–36.

Gronenberg, W., B. Hölldobler, and G. D. Alpert (1998a). "Jaws that snap: control of mandible movements in the ant *Mystrium*". In: *Journal of Insect Physiology* 44.3-4, pp. 241–253.

Gronenberg, W. et al. (1998b). "Trap-jaws revisited: the mandible mechanism of the ant *Acanthognathus*". In: *Physiological Entomology* 23.3, pp. 227–240.

Grubich, J. R. et al. (2012). "Mega-bites: extreme jaw forces of living and extinct piranhas (Serrasalmidae)". In: *Scientific Reports* 2.1, pp. 1–9.

Gundiah, N. and S. Jaddivada (2020). "Making the cut: mechanics of cutting and steering of insect probes". In: *Current Opinion in Insect Science* 42, pp. 84–89.

Guschlbauer, C., H. Scharstein, and A. Büschges (2007). "The extensor tibiae muscle of the stick insect: biomechanical properties of an insect walking leg muscle". In: *Journal of Experimental Biology* 210.6, pp. 1092–1108.

Habegger, M. L. et al. (2012). "Feeding biomechanics and theoretical calculations of bite force in bull sharks (*Carcharhinus leucas*) during ontogeny". In: *Zoology* 115.6, pp. 354–364.

Hall, M. D. et al. (2010). "Interactions among performance capacities predict male combat outcomes in the field cricket". In: *Functional Ecology* 24.1, pp. 159–164.

Hancock, R. G. et al. (2022). "Mosquitoes Eating Mosquitoes: How *Toxorhynchites amboinensis*, *Psorophora ciliata*, and *Sabethes cyaneus* (Diptera: Culicidae) Capture Prey". In: *Annals of the Entomological Society of America* 115.6, pp. 461–471.

Hao, W. et al. (2018). "Kinematics and Mechanics analysis of trap-jaw ant *Odontomachus monticola*". In: *Journal of Physics: Conference Series*. Vol. 986. IOP Publishing, p. 012029.

Hart, A. G., C. Anderson, and F. L. Ratnieks (2002). "Task partitioning in leafcutting ants". In: *Acta Ethologica* 5.1, pp. 1–11.

Hart, A. G. and F. L. Ratnieks (2001). "Task partitioning, division of labour and nest compartmentalisation collectively isolate hazardous waste in the leafcutting ant *Atta cephalotes*". In: *Behavioral Ecology and Sociobiology* 49.5, pp. 387–392.

Haykin, S. (2001). *Communication Systems*. 4th ed. John Wiley & Sons, Inc. ISBN: 0-471-17869-1.

Hayot, C. M. et al. (2012). "Viscoelastic properties of cell walls of single living plant cells determined by dynamic nanoindentation". In: *Journal of Experimental Botany* 63.7, pp. 2525–2540.

Heethoff, M. and R. A. Norton (2009). "A new use for synchrotron X-ray microtomography: three-dimensional biomechanical modeling of chelicerate mouthparts and calculation of theoretical bite forces". In: *Invertebrate Biology* 128.4, pp. 332–339.

Helanterä, H. and F. L. Ratnieks (2008). "Geometry explains the benefits of division of labour in a leafcutter ant". In: *Proceedings of the Royal Society of London Series B* 275, pp. 1225–1260.

Hepburn, H. and I. Joffe (1974). "Locust solid cuticle - a time sequence of mechanical properties". In: *Journal of Insect Physiology* 20.3, pp. 497–506.

Herrel, A., S. Petrochic, and M. Draud (2018). "Sexual dimorphism, bite force and diet in the diamondback terrapin". In: *Journal of Zoology* 304.3, pp. 217–224.

Herrel, A. et al. (2005). "Evolution of bite force in Darwin's finches: a key role for head width". In: *Journal of Evolutionary Biology* 18.3, pp. 669–675.

Herrel, A. and J. C. O'Reilly (2006). "Ontogenetic scaling of bite force in lizards and turtles". In: *Physiological and Biochemical Zoology* 79.1, pp. 31–42.

Herrel, A. et al. (1999). "Sexual dimorphism of head size in Gallotia galloti: testing the niche divergence hypothesis by functional analyses". In: *Functional Ecology* 13.3, pp. 289–297.

Herrel, A. et al. (2001). "The implications of bite performance for diet in two species of lacertid lizards". In: *Canadian Journal of Zoology* 79.4, pp. 662–670.

Herring, S. W. and S. E. Herring (1974). "The superficial masseter and gape in mammals". In: *The American Naturalist* 108.962, pp. 561–576.

Herz, H., W. Beyschlag, and B. Hölldobler (2007). "Herbivory rate of leaf-cutting ants in a tropical moist forest in Panama at the population and ecosystem scales". In: *Biotropica* 39.4, pp. 482–488.

Hill, A. V. (1938). "The heat of shortening and the dynamic constants of muscle". In: *Proceedings of the Royal Society of London. Series B: Biological Sciences* 126.843, pp. 136–195.

Hinze, B. and R. Leuthold (1999). "Age related polyethism and activity rhythms in the nest of the termite *Macrotermes bellicosus* (Isoptera, Termitidae)". In: *Insectes Sociaux* 46.4, pp. 392–397.

Hite, N. J. et al. (2019). "The better to eat you with: bite force in the naked mole-rat (*Heterocephalus glaber*) is stronger than predicted based on body size". In: *Frontiers in Integrative Neuroscience* 13, p. 70.

Hölldobler, B. and E. O. Wilson (1990). *The ants*. Harvard University Press.

– (2010). *The leafcutter ants: civilization by instinct*. W. W. Norton & Company, New York City, NY, USA.

Hopkins, T. L. and K. J. Kramer (1992). "Insect cuticle sclerotization". In: *Annual Review of Entomology* 37.1, pp. 273–302.

Howard, J. J. (1988). "Leafcutting and diet selection: relative influence of leaf chemistry and physical features". In: *Ecology* 69, pp. 250–260.

Howe, G. A. and A. Schaller (2008). "Direct defenses in plants and their induction by wounding and insect herbivores". In: *Induced plant resistance to herbivory*. Ed. by A. Schaller. Springer Science & Business Media, pp. 7–29.

Hu, D. L., B. Chan, and J. W. Bush (2003). "The hydrodynamics of water strider locomotion". In: *Nature* 424.6949, pp. 663–666.

Hua, L. et al. (2020). "Linking vein properties to leaf biomechanics across 58 woody species from a subtropical forest". In: *Plant Biology* 22.2, pp. 212–220.

Huang, M. H. (2012). "Extreme worker polymorphism in the big-headed Pheidole ants". PhD thesis. The University of Arizona.

Huang, Z.-Y. and G. E. Robinson (1996). "Regulation of honey bee division of labor by colony age demography". In: *Behavioral Ecology and Sociobiology* 39.3, pp. 147–158.

Huber, D. R., M. N. Dean, and A. P. Summers (2008). "Hard prey, soft jaws and the ontogeny of feeding mechanics in the spotted ratfish *Hydrolagus colliei*". In: *Journal of the Royal Society Interface* 5.25, pp. 941–953.

Huber, D. R., C. L. Weggelaar, and P. J. Motta (2006). "Scaling of bite force in the blacktip shark *Carcharhinus limbatus*". In: *Zoology* 109.2, pp. 109–119.

Huber, D. R. et al. (2005). "Analysis of the bite force and mechanical design of the feeding mechanism of the durophagous horn shark *Heterodontus francisci*". In: *Journal of Experimental Biology* 208.18, pp. 3553–3571.

Huber, D. R. et al. (2009). "Is extreme bite performance associated with extreme morphologies in sharks?" In: *Physiological and Biochemical Zoology* 82.1, pp. 20–28.

Hughes, S. M. and P. C. Salinas (1999). "Control of muscle fibre and motoneuron diversification". In: *Current Opinion in Neurobiology* 9.1, pp. 54–64.

Hung, K.-L. J. et al. (2018). "The worldwide importance of honey bees as pollinators in natural habitats". In: *Proceedings of the Royal Society B: Biological Sciences* 285.1870, p. 20172140.

Husak, J. F., A. K. Lappin, and R. A. Van Den Bussche (2009). "The fitness advantage of a high-performance weapon". In: *Biological Journal of the Linnean Society* 96.4, pp. 840–845.

Huxley, J. S. (1924). "Constant differential growth-ratios and their significance". In: *Nature* 114.2877, pp. 895–896.

Ingram, K. K. et al. (2016). "Context-dependent expression of the foraging gene in field colonies of ants: the interacting roles of age, environment and task". In: *Proceedings of the Royal Society B: Biological Sciences* 283.1837, p. 20160841.

Jaffe, K. and P. Howse (1979). "The mass recruitment system of the leaf cutting ant, *Atta cephalotes* (L.)" In: *Animal Behaviour* 27, pp. 930–939.

Jeanson, R. (2019). "Within-individual behavioural variability and division of labour in social insects". In: *Journal of Experimental Biology* 222.10, jeb190868.

Jensen, M. and T. Weis-Fogh (1962). "Biology and physics of locust flight. V. Strength and elasticity of locust cuticle". In: *Philosophical Transactions of the Royal Society of London. Series B, Biological Sciences* 245.721, pp. 137–169.

Jones, A. C., G. W. Felton, and J. H. Tumlinson (2022). "The dual function of elicitors and effectors from insects: reviewing the 'arms race'against plant defenses". In: *Plant Molecular Biology* 109, pp. 457–445.

Jones, M. E. and A. K. Lappin (2009). "Bite-force performance of the last rhynchocephalian (Lepidosauria: *Sphenodon*)". In: *Journal of the Royal Society of New Zealand* 39.2-3, pp. 71–83.

Jones, M. E. et al. (2020). "Reproductive phenotype predicts adult bite-force performance in sex-reversed dragons (*Pogona vitticeps*)". In: *Journal of Experimental Zoology Part A: Ecological and Integrative Physiology* 333.4, pp. 252–263.

Josephson, R. K. (1975). "Extensive and intensive factors determining the performance of striated muscle". In: *Journal of Experimental Zoology* 194.1, pp. 135–153.

Josephson, R. K. and D. R. Stokes (1987). "The contractile properties of a crab respiratory muscle". In: *Journal of Experimental Biology* 131.1, pp. 265–287.

Julian, G. E. and J. H. Fewell (2004). "Genetic variation and task specialization in the desert leaf-cutter ant, *Acromyrmex versicolor*". In: *Animal Behaviour* 68.1, pp. 1–8.

Kaczmarek, E. B. and N. J. Gidmark (2020). "The bite force–gape relationship as an avenue of biomechanical adaptation to trophic niche in two salmonid fishes". In: *Journal of Experimental Biology* 223.20, jeb223180.

Kamatham, S. et al. (2021). "Recent advances in engineering crop plants for resistance to insect pests". In: *Egyptian Journal of Biological Pest Control* 31.1, pp. 1–14.

Kamp, T. van de et al. (2022). "Evolution of flexible biting in hyperdiverse parasitoid wasps". In: *Proceedings of the Royal Society B* 289.1967, p. 20212086.

Kamyab, I., S. Chakrabati, and J. G. Williams (1998). "Cutting cheese with wire". In: *Journal of Materials Science* 33, pp. 2763–2770.

Katzke, J. et al. (2022). "A roadmap to reconstructing muscle architecture from CT data". In: *Integrative Organismal Biology* 4.1, obac001.

Khalife, A. et al. (2018). "Skeletomuscular adaptations of head and legs of *Melissotarsus* ants for tunnelling through living wood". In: *Frontiers in Zoology* 15.30. ISSN: 1-11.

Klocke, D. and H. Schmitz (2011). "Water as a major modulator of the mechanical properties of insect cuticle". In: *Acta Biomaterialia* 7.7, pp. 2935–2942.

Klunk, C. L. et al. (2020). "Mandibular morphology, task specialization, and bite mechanics in Pheidole ants (Hymenoptera: Formicidae)". In: *bioRxiv*.

Kluyver, T. et al. (2016). "Jupyter Notebooks-a publishing format for reproducible computational workflows." In: *Positioning and Power in Academic Publishing: Players, Agents and Agendas*. Ed. by F. Loizides and B. Schmid. IOS Press, pp. 87–90.

Kokko, E. G., B. D. Schaber, and T. Entz (1993). "Quantification of mandibular wear of female alfalfa leafcutter bees, *Megachile rotundata* (F.)(Hymenoptera: Megachilidae), by image analysis". In: *The Canadian Entomologist* 125.1, pp. 93–99.

Kountanya, R. K. and W. J. Endres (2004). "Flank wear of edge-radiused cutting tools under ideal straight-edged orthogonal conditions". In: *Journal of Manufacturing Science and Engineering* 126.3, pp. 496–505.

Krenn, H. W. (2019). *Insect mouthparts: form, function, development and performance*. Springer Nature.

Kundanati, L. et al. (2020). "Cutting mechanics of wood by beetle larval mandibles". In: *Journal of the Mechanical Behavior of Biomedical Materials* 112, p. 104027.

Kuřavová, K., L. Hajduková, and P. Kočárek (2014). "Age-related mandible abrasion in the ground-hopper *Tetrix tenuicornis* (Tetrigidae, Orthoptera)". In: *Arthropod Structure & Development* 43.3, pp. 187–192.

Kvedaras, O. L. et al. (2009). "Influence of plant silicon and sugarcane cultivar on mandibular wear in the stalk borer *Eldana saccharina*". In: *Agricultural and Forest Entomology* 11.3, pp. 301–306.

LaBarbera, M. (1989). "Analyzing body size as a factor in ecology and evolution". In: *Annual review of ecology and systematics*, pp. 97–117.

Labonte, D. and W. Federle (2015). "Rate-dependence of 'wet' biological adhesives and the function of the pad secretion in insects". In: *Soft Matter* 11, pp. 8661–8673.

Labonte, D., A.-K. Lenz, and M. L. Oyen (2017). "On the relationship between indentation hardness and modulus, and the damage resistance of biological materials". In: *Acta Biomaterialia* 57, pp. 373–383.

Labonte, D. et al. (2016). "Extreme positive allometry of animal adhesive pads and the size limits of adhesion-based climbing". In: *Proceedings of the National Academy of Sciences* 113.5, pp. 1297–1302.

Lailvaux, S. P., L. T. Reaney, and P. R. Backwell (2009). "Dishonest signalling of fighting ability and multiple performance traits in the fiddler crab *Uca mjoebergi*". In: *Functional Ecology* 23.2, pp. 359–366.

Lake, G. J. and O. H. Yeoh (1978). "Measurement of rubber cutting resistance in the absence of friction". In: *International Journal of Fracture* 14.5, pp. 509–526.

Lappin, A. K. and M. E. Jones (2014). "Reliable quantification of bite-force performance requires use of appropriate biting substrate and standardization of bite out-lever". In: *Journal of Experimental Biology* 217.24, pp. 4303–4312.

Lappin, A. K. et al. (2017). "Bite force in the horned frog (*Ceratophrys cranwelli*) with implications for extinct giant frogs". In: *Scientific Reports* 7.1, pp. 1–10.

Larabee, F. J., A. A. Smith, and A. V. Suarez (2018). "Snap-jaw morphology is specialized for high-speed power amplification in the Dracula ant, *Mystrium camillae*". In: *Royal Society open science* 5.12, p. 181447.

Larabee, F. J. and A. V. Suarez (2015). "Mandible-powered escape jumps in trap-jaw ants increase survival rates during predator-prey encounters". In: *PLoS One* 10.5, e0124871.

Larabee, F. J. et al. (2022). "Muscle fatigue in the latch-mediated spring actuated mandibles of trap-jaw ants". In: *Integrative and Comparative Biology* 62.5, pp. 1217–1226.

Lemke, S. B. and F. Schnorrer (2017). "Mechanical forces during muscle development". In: *Mechanisms of Development* 144, pp. 92–101.

Levinton, J. and M. Judge (1993). "The relationship of closing force to body size for the major claw of *Uca pugnax* (Decapoda: Ocypodidae)". In: *Functional Ecology* 7.3, pp. 339–345.

Lewis, O. T., M. Martin, and T. J. Czaczkes (2008). "Effects of trail gradient on leaf tissue transport and load size selection in leaf-cutter ants". In: *Behavioural Ecology* 19, pp. 805–809.

Li, D. et al. (2011). "3D configuration of mandibles and controlling muscles in rove beetles based on micro-CT technique". In: *Analytical and bioanalytical chemistry* 401.3, pp. 817–825.

Li, H. et al. (2020). "Biomineral armor in leaf-cutter ants". In: *Nature Communications* 11.1, pp. 1–11.

Lillico-Ouachour, A. et al. (2018). "Internal head morphology of minor workers and soldiers in the hyperdiverse ant genus *Pheidole*". In: *Canadian Journal of Zoology* 96.5, pp. 383–392.

Littledyke, M. and J. M. Cherrett (1976). "Direct ingestion of plant sap from cut leaves by the leaf-cutting ants *Atta cephalotes* (L.) and *Acromyrmex octospinosus* (Reich) (Formicidae, Attini)". In: *Bulletin of Entomological Research* 66, pp. 205–217.

Liu, Y., C.-Y. Hui, and W. Hong (2021). "A clean cut". In: *Extreme Mechanics Letters* 46, p. 101343.

Lowie, A. et al. (2022). "The relationship between head shape, head musculature and bite force in caecilians (Amphibia: Gymnophiona)". In: *Journal of Experimental Biology* 225.1, jeb243599.

Lucas, C., B. N. Hughson, and M. B. Sokolowski (2010). "Job switching in ants: role of a kinase". In: *Communicative & Integrative Biology* 3.1, pp. 6–8.

Lucas, J. R. (1982). "The biophysics of pit construction by antlion larvae (*Myrmeleon*, Neuroptera)". In: *Animal Behaviour* 30.3, pp. 651–664.

Lucas, P. W. (2004). *Dental functional morphology: how teeth work*. Cambridge University Press.

Lucas, P. W. et al. (2000). "Mechanical defences to herbivory". In: *Annals of Botany* 86, pp. 913–920.

Luis, N. M. and F. Schnorrer (2021). "Mechanobiology of muscle and myofibril morphogenesis". In: *Cells & Development* 168, p. 203760.

Magalhães, V. B. et al. (2018). "Secondary seed dispersal by ants in Neotropical cerrado savanna: species-specific effects on seeds and seedlings of *Siparuna guianensis* (Siparunaceae)". In: *Ecological Entomology* 43.5, pp. 665–674.

Malavé, B. M., J. M. Styga, and E. D. Clotfelter (2018). "Size, shape, and sex-dependent variation in force production by crayfish chelae". In: *Journal of Morphology* 279.3, pp. 312–318.

Marshall, C. D. et al. (2012). "The ontogenetic scaling of bite force and head size in loggerhead sea turtles (*Caretta caretta*): implications for durophagy in neritic, benthic habitats". In: *Journal of Experimental Biology* 215.23, pp. 4166–4174.

Marshall, C. D. et al. (2014). "Scaling of bite performance with head and carapace morphometrics in green turtles (Chelonia mydas)". In: *Journal of Experimental Marine Biology and Ecology* 451, pp. 91–97.

Martin, M. M., R. M. Carman, and J. G. MacConnell (1969). "Nutrients derived from the fungus cultured by the fungus-growing ant *Atta colombica tonsipes*". In: *Annals of the Entomological Society of America* 62.1, pp. 11–13.

Martin, M. M. and N. A. Weber (1969). "The cellulose-utilizing capability of the fungus cultured by the attine ant *Atta colombica tonsipes*". In: *Annals of the Entomological Society of America* 62.6, pp. 1386–1387.

McCarthy, C. T., A. N. Annaidh, and M. D. Gilchrist (2010). "On the sharpness of straight edge blades in cutting soft solids: Part II–Analysis of blade geometry". In: *Engineering Fracture Mechanics* 77.3, pp. 437–451.

McCarthy, C. T., M. Hussey, and M. D. Gilchrist (2007). "On the sharpness of straight edge blades in cutting soft solids: Part I - indentation experiments". In: *Engineering Fracture Mechanics* 74.14, pp. 2205–2224.

McLain, D. K. et al. (2015). "Claw-pinching force of sand fiddler crabs in relation to activity and the lunar cycle". In: *Journal of Experimental Marine Biology and Ecology* 471, pp. 190–197.

Meij, M. van der and R. Bout (2004). "Scaling of jaw muscle size and maximal bite force in finches". In: *Journal of Experimental Biology* 207.16, pp. 2745–2753.

Meijden, A. van der, A. Herrel, and A. Summers (2010). "Comparison of chela size and pincer force in scorpions; getting a first grip". In: *Journal of Zoology* 280.4, pp. 319–325.

Meijden, A. van der et al. (2012). "Functional morphology and bite performance of raptorial chelicerae of camel spiders (Solifugae)". In: *Journal of Experimental Biology* 215.19, pp. 3411–3418.

Meijering, E. H., W. J. Niessen, and M. A. Viergever (2001). "Quantitative evaluation of convolution-based methods for medical image interpolation". In: *Medical Image Analysis* 5.2, pp. 111–126.

Metscher, B. D. (2009). "MicroCT for comparative morphology: simple staining methods allow high-contrast 3D imaging of diverse non-mineralized animal tissues". In: *BMC Physiology* 9.1, pp. 1–14.

Meyers, J. J., A. Herrel, and J. Birch (2002). "Scaling of morphology, bite force and feeding kinematics in an iguanian and a scleroglossan lizard". In: *Topics in Functional and Ecological Vertebrate Morphology*, pp. 47–62.

Moll, K., F. Roces, and W. Federle (2010). "Foraging grass-cutting ants (*Atta vollenweideri*) maintain stability by balancing their loads with controlled head movements". In: *Journal of Comparative Physiology A* 196, pp. 471–480.

– (2013). "How load-carrying ants avoid falling over: mechanical stability during foraging in *Atta vollenweideri* grass-cutting ants". In: *Public Library of Science One* 8.1, e52816.

Montoya-Lerma, J. et al. (2012). "Leaf-cutting ants revisited: towards rational management and control". In: *International Journal of Pest Management* 58.3, pp. 225–247.

Moore, B. P. and B. E. Wallbank (1968). "Chemical composition of the defensive secretion in carabid beetles and its importance as a taxonomic character". In: *Proceedings of the Royal Entomological Society of London. Series B: Taxonomy*. Vol. 37. Wiley Online Library, pp. 62–72.

Mueller, U. G. et al. (2001). "The origin of the Attine ant-fungus mutualism". In: *The Quarterly Review of Biology* 76.2, pp. 169–197.

Muscedere, M. L. and J. F. Traniello (2012). "Division of labor in the hyperdiverse ant genus *Pheidole* is associated with distinct subcaste-and age-related patterns of worker brain organization". In: *PLoS One* 7.2, e31618.

Muscedere, M. L., J. F. Traniello, and W. Gronenberg (2011). "Coming of age in an ant colony: cephalic muscle maturation accompanies behavioral development in *Pheidole dentata*". In: *Naturwissenschaften* 98.9, p. 783.

Muscedere, M. L., T. A. Willey, and J. F. Traniello (2009). "Age and task efficiency in the ant *Pheidole dentata*: young minor workers are not specialist nurses". In: *Animal Behaviour* 77.4, pp. 911–918.

Neville, A. (1963). "Daily growth layers for determining the age of grasshopper populations". In: *Oikos*, pp. 1–8.

Nichols-Orians, C. M. and J. C. Schultz (1990). "Interactions among leaf toughness, chemistry, and harvesting by attine ants". In: *Ecological Entomology* 15.3, pp. 311–320.

Nichols-Orians, C. M. and J. C. Schultz (1989). "Leaf Toughness Affects Leaf Harvesting by the Leaf Cutter Ant, *Atta cephalotes* (L.) (Hymenoptera: Formicidae)". In: *Biotropica* 21.1, pp. 80–83.

Nowlan, N. C., P. Murphy, and P. J. Prendergast (2008). "A dynamic pattern of mechanical stimulation promotes ossification in avian embryonic long bones". In: *Journal of Biomechanics* 41.2, pp. 249–258.

Nowlan, N. C. et al. (2012). "Biophysical stimuli induced by passive movements compensate for lack of skeletal muscle during embryonic skeletogenesis". In: *Biomechanics and Modeling in Mechanobiology* 11.1, pp. 207–219.

O'Donnell, S. and R. L. Jeanne (1993). "Methoprene accelerates age polyethism in workers of a social wasp (*Polybia occidentalis*)". In: *Physiological Entomology* 18.2, pp. 189–194.

Oerke, E.-C. (2006). "Crop losses to pests". In: *Journal of Agricultural Science* 144, pp. 31–43.

Oettler, J. and R. A. Johnson (2009). "The old ladies of the seed harvester ant *Pogonomyrmex rugosus*: foraging performed by two groups of workers". In: *Journal of Insect Behavior* 22.3, pp. 217–226.

Oka, S.-i., T. Tomita, and K. Miyamoto (2016). "A mighty claw: pinching force of the coconut crab, the largest terrestrial crustacean". In: *Public Library of Science One* 11.11, e0166108.

Oliveira, C. M. et al. (2014). "Crop losses and the economic impact of insect pests on Brazilian agriculture". In: *Crop Protection* 56, pp. 50–54.

Oliver, W. C. and G. M. Pharr (1992). "An improved technique for determining hardness and elastic modulus using load and displacement sensing indentation experiments". In: *Journal of materials research* 7.6, pp. 1564–1583.

Olsen, K. M. and J. F. Wendel (2013). "A bountiful harvest: genomic insights into crop domestication phenotypes". In: *Annual Review of Plant Biology* 64, pp. 47–70.

Onoda, Y. et al. (2011). "Global patterns of leaf mechanical properties". In: *Ecology Letters* 14, pp. 301–312.

Oster, G. F. and E. O. Wilson (1978). *Caste and ecology in the social insects*. Princeton University Press.

Otten, E. (1987a). "A myocybernetic model of the jaw system of the rat". In: *Journal of Neuroscience Methods* 21.2-4, pp. 287–302.

– (1987b). "Optimal design of vertebrate and insect sarcomeres". In: *Journal of Morphology* 191.1, pp. 49–62.

Paganin, D. et al. (2002). "Simultaneous phase and amplitude extraction from a single defocused image of a homogeneous object". In: *Journal of Microscopy* 206.1, pp. 33–40.

Palchesko, R. N. et al. (2012). "Development of polydimethylsiloxane substrates with tunable elastic modulus to study cell mechanobiology in muscle and nerve". In: *PLoS One* 7.12, e51499.

Palmer, A. R., G. M. Taylor, and A. Barton (1999). "Cuticle strength and the size-dependence of safety factors in *Cancer* crab claws". In: *The Biological Bulletin* 196.3, pp. 281–294.

Parker, A. R. and C. R. Lawrence (2001). "Water capture by a desert beetle". In: *Nature* 414.6859, pp. 33–34.

Parle, E., J.-H. Dirks, and D. Taylor (2017). "Damage, repair and regeneration in insect cuticle: The story so far, and possibilities for the future". In: *Arthropod Structure & Development* 46.1, pp. 49–55.

Parle, E. and D. Taylor (2017). "The effect of aging on the mechanical behaviour of cuticle in the locust *Schistocerca gregaria*". In: *Journal of the Mechanical Behavior of Biomedical Materials* 68, pp. 247–251.

Patek, S. et al. (2006). "Multifunctionality and mechanical origins: ballistic jaw propulsion in trap-jaw ants". In: *Proceedings of the National Academy of Sciences* 103.34, pp. 12787–12792.

Paul, J. (2001). "Review: Mandible movements in ants". In: *Comparative Biochemistry and Physiology Part A* 131, pp. 7–20.

Paul, J. and W. Gronenberg (1999). "Optimizing Force and Velocity: Mandible Muscle Fibre Attachments in Ants". In: *The Journal of Experimental Biology* 202, pp. 797–808.

– (2002). "Motor control of the mandible closer muscle in ants". In: *Journal of Insect Physiology* 48, pp. 255–267.

Paul, J. and F. Roces (2019). "Comparative functional morphology of ant mouthparts and significance for liquid food intake". In: *Insect Mouthparts*. Springer, pp. 335–359.

Peattie, A. and R. Full (2007). "Phylogenetic analysis of the scaling of wet and dry biological fibrillar adhesives". In: *Proceedings of the National Academy of Sciences* 104.47, pp. 18595–18600.

Peeters, C. et al. (2017). "Evolution of cheaper workers in ants: a comparative study of exoskeleton thickness". In: *Biological Journal of the Linnean Society* 121.3, pp. 556–563.

Peeters, P. J., G. Sanson, and J. Read (2007). "Leaf biomechanical properties and the densities of herbivorous insect guilds". In: *Functional Ecology*, pp. 246–255.

Pélabon, C. et al. (2013). "On the relationship between ontogenetic and static allometry". In: *The American Naturalist* 181.2, pp. 195–212.

Pélabon, C. et al. (2014). "Evolution of morphological allometry". In: *Annals of the New York Academy of Sciences* 1320.1, pp. 58–75.

Peña, E. A. and E. H. Slate (2006). "Global validation of linear model assumptions". In: *Journal of the American Statistical Association* 101.473, pp. 341–354.

Penning, D. A. (2017). "The scaling of bite force and constriction pressure in kingsnakes (*Lampropeltis getula*): proximate determinants and correlated performance". In: *Integrative Zoology* 12.2, pp. 121–131.

Pfaller, J. et al. (2010). "Ontogenetic scaling of cranial morphology and bite-force generation in the loggerhead musk turtle". In: *Journal of Zoology* 280.3, pp. 280–289.

Pfuhl, W. (1937). "Die gefiederten Muskeln, ihre Form und ihre Wirkungsweise". In: *Zeitschrift für Anatomie und Entwicklungsgeschichte* 106.6, pp. 749–769.

Pielström, S. and F. Roces (2013). "Sequential soil transport and its influence on the spatial organisation of collective digging in leaf-cutting ants". In: *Public Library of Science One* 8, e57040.

– (2014). "Soil moisture and exvacation behaviour in the Chaco leaf-cutting ant (*Atta vollenweideri*): digging performance and prevention of water inflow into the nest". In: *Public Library of Science One* 9, e95658.

Plum, F. and D. Labonte (2021). "scAnt—an open-source platform for the creation of 3D models of arthropods (and other small objects)". In: *PeerJ* 9, e11155.

Politi, Y., B. Bar-On, and H.-O. Fabritius (2019). "Mechanics of arthropod cuticle-versatility by structural and compositional variation". In: *Architectured Materials in Nature and Engineering*. Springer, pp. 287–327.

Pruim, G., H. De Jongh, and J. Ten Bosch (1980). "Forces acting on the mandible during bilateral static bite at different bite force levels". In: *Journal of Biomechanics* 13.9, pp. 755–763.

Püffel, F., R. Johnston, and D. Labonte (2023a). "A biomechanical model for the relation between bite force and mandibular opening angle in arthropods". In: *Royal Society Open Science* 10.2, p. 221066.

Püffel, F., F. Roces, and D. Labonte (2022). "Strong positive allometry of bite force in leaf-cutter ants increases the range of cuttable plant tissues". In: *bioRxiv*.

Püffel, F. et al. (2021). "Morphological determinants of bite force capacity in insects: a biomechanical analysis of polymorphic leaf-cutter ants". In: *Journal of the Royal Society Interface* 18.182, p. 20210424.

Püffel, F. et al. (2023b). "Developmental biomechanics and age polyethism in leaf-cutter ants". In: *bioRxiv*.

Quinlan, R. and J. Cherrett (1979). "The role of fungus in the diet of the leaf-cutting ant *Atta cephalotes* (L.)" In: *Ecological Entomology* 4.2, pp. 151–160.

R Core Team (2020). *R: A Language and Environment for Statistical Computing*. R Foundation for Statistical Computing. Vienna, Austria. URL: `https://www.R-project.org/`.

– (2021). *R: A Language and Environment for Statistical Computing*. R Foundation for Statistical Computing. Vienna, Austria. URL: `https://www.R-project.org/`.

– (2022). *R: A Language and Environment for Statistical Computing*. R Foundation for Statistical Computing. Vienna, Austria. URL: `https://www.R-project.org/`.

Raupp, M. J. (1985). "Effects of leaf toughness on mandibular wear of the leaf beetle, *Plagiodera versicolora*". In: *Ecological Entomology* 10, pp. 73–79.

Read, J. and A. Stokes (2006). "Plant biomehanics in an ecological context". In: *American Journal of Botany* 93.10, pp. 1546–1565.

Reilly, G. A., B. A. McCormack, and D. Taylor (2004). "Cutting sharpness measurement: a critical review". In: *Journal of Materials Processing Technology* 153-154, pp. 261–267.

Reynolds, O. L., M. G. Keeping, and J. H. Meyer (2009). "Silicon-augmented resistance of plants to herbivorous insects: a review". In: *Annals of Applied Biology* 155, pp. 171–186.

Reyssat, E. et al. (2012). "Slicing softly with shear". In: *Physical Review Letters* 109.24, p. 244301.

Richter, A. et al. (2019). "The cephalic anatomy of workers of the ant species *Wasmannia affinis* (Formicidae, Hymenoptera, Insecta) and its evolutionary implications". In: *Arthropod Structure & Development* 49, pp. 26–49.

Richter, A. et al. (2020). "Comparative analysis of worker head anatomy of *Formica* and *Brachyponera* (Hymenoptera: Formicidae)". In: *Arthropod Systematics & Phylogeny* 78.1, pp. 133–170.

Richter, A. et al. (2021). "The head anatomy of *Protanilla lini* (Hymenoptera: Formicidae: Leptanillinae), with a hypothesis of their mandibular movement". In: *Myrmecological News* 31, pp. 85–114.

Richter, S., G. D. Edgecombe, and G. D. Wilson (2002). "The *lacinia mobilis* and similar structures–a valuable character in arthropod phylogenetics?" In: *Zoologischer Anzeiger-A Journal of Comparative Zoology* 241.4, pp. 339–361.

Roberts, S. P. and M. M. Elekonich (2005). "Muscle biochemistry and the ontogeny of flight capacity during behavioral development in the honey bee, *Apis mellifera*". In: *Journal of Experimental Biology* 208.22, pp. 4193–4198.

Robinson, G. E. (1998). "From society to genes with the honey bee: A combination of environmental, genetic, hormonal and neurobiological factors determine a bee's progression through a series of life stages". In: *American Scientist* 86.5, pp. 456–462.

Robinson, G. E., R. E. Page Jr, and Z. Huang (1994). "Temporal polyethism in social insects is a developmental process". In: *Animal Behaviour* 48.2, pp. 467–469.

Robinson, G. E. et al. (1989). "Hormonal and genetic control of behavioral integration in honey bee colonies". In: *Science* 246.4926, pp. 109–112.

Roces, F. and B. Hölldobler (1994). "Leaf density and a trade-off between load-size selection and recruitment behaviour in the ant *Atta cephalotes*". In: *Oecologia* 97, pp. 1–8.

Roces, F. and J. R. Lighton (1995). "Larger bites of leaf-cutting ants". In: *Nature* 373, p. 392.

Roces, F. (1990). "Leaf-cutting ants cut fragment sizes in relation to the distance from the nest". In: *Animal Behaviour* 40.6, pp. 1181–1183.

– (2002). "Individual complexity and self-organization in foraging by leaf-cutting ants". In: *The Biological Bulletin* 202, pp. 306–312.

– (2022). "Vibrational Communication Outside and Inside the Nest in Leaf-Cutting Ants". In: *Biotremology: Physiology, Ecology, and Evolution*. Springer, pp. 411–435.

Roces, F. and B. Hölldobler (1996). "Use of stridulation in foraging leaf-cutting ants: mechanical support during cutting or short-range recruitment signal?" In: *Behavioral Ecology and Sociobiology*.

Roces, F. and J. A. Núñez (1993). "Information about food quality influences load-size selection in recruited leaf-cutting ants". In: *Animal Behaviour* 45.1, pp. 135–143.

Rockenfeller, R., M. Günther, and S. L. Hooper (2022). "Muscle active force-length curve explained by an electrophysical model of interfilament spacing". In: *Biophysical Journal* 121.10, pp. 1823–1855.

Rockwood, L. L. (1976). "Plant Selection and Foraging Patterns in Two Species of Leaf-Cutting Ants (*Atta*)". In: *Ecology* 57.1, pp. 48–61.

Rodrigues, A. et al. (2008). "Leaf-cutting ant faecal fluid and mandibular gland secretion: effects on microfungi spore germination". In: *Brazilian Journal of Microbiology* 39, pp. 64–67.

Rodríguez-Planes, L. I. and A. G. Farji-Brener (2019). "Extended phenotypes and foraging restrictions: ant nest entrances and resource ingress in leaf-cutting ants". In: *Biotropica* 51.2, pp. 178–185.

Roitberg, B. D. et al. (2005). "The cost of being an omnivore: mandible wear from plant feeding in a true bug". In: *Naturwissenschaften* 92, pp. 431–434.

Röschard, J. and F. Roces (2002). "The effect of load length, width and mass on transport rate in the grass-cutting ant *Atta vollenweideri*". In: *Oecologia* 131, pp. 319–324.

– (2003a). "Cutters, carriers and transport chains: Distance-dependent foraging strategies in the grass-cutting ant *Atta vollenweideri*". In: *Insectes Sociaux* 50, pp. 237–244.

– (2003b). "Fragment-size determination and size-matching in the grass-cutting ant *Atta vollenweideri* depend on the distance from the nest". In: *Journal of Tropical Ecology* 19, pp. 647–653.

– (2011). "Sequential load transport in grass-cutting ants (*Atta vollenweideri*): maximization of plant delivery rate or improved information transfer?" In: *Psyche* 2011, p. ID 643127.

Rose, U., M. Ferber, and R. Hustert (2001). "Maturation of muscle properties and its hormonal control in an adult insect". In: *Journal of Experimental Biology* 204.20, pp. 3531–3545.

Rosenzweig, C. et al. (2014). "Assessing agricultural risks of climate change in the 21st century in a global gridded crop model intercomparison". In: *Proceedings of the National Academy of Sciences of the U.S.A* 111.9, pp. 3268–3273.

Rudolph, S. G. and C. Loudon (1986). "Load size selection by foraging leaf-cutter ants (*Atta cephalotes*)". In: *Ecological Entomology* 11, pp. 401–410.

Rühr, P. T. and A. Blanke (2022). "forceX and forceR: a mobile setup and R package to measure and analyse a wide range of animal closing forces". In: *Methods in Ecology and Evolution*, pp. 1–11.

Rühr, P. T. et al. (2022). "A bite force database of 654 insect species". In: *bioRxiv*.

Sakamoto, M., M. Ruta, and C. Venditti (2019). "Extreme and rapid bursts of functional adaptations shape bite force in amniotes". In: *Proceedings of the Royal Society B* 286.1894, p. 20181932.

Sandhu, S. and M. S. Kang (2017). "Advances in breeding for resistance to insects". In: *Breeding insect resistant crops for sustainable agriculture*. Springer, pp. 67–99.

Sanson, G. et al. (2001). "Measurement of leaf biomechanical properties in studies of herbivory: Opportunities, problems and procedures". In: *Austral Ecology* 26, pp. 535–546.

Sanson, G. (2006). "The biomechanics of browsing and grazing". In: *American Journal of Botany* 93.10, pp. 1531–1545.

Santana, S. E. (2016). "Quantifying the effect of gape and morphology on bite force: biomechanical modelling and *in vivo* measurements in bats". In: *Functional Ecology* 30.4, pp. 557–565.

Santana, S. E., E. R. Dumont, and J. L. Davis (2010). "Mechanics of bite force production and its relationship to diet in bats". In: *Functional Ecology* 24.4, pp. 776–784.

Sartori, J. and H. Stark (2021). "Tracking tendon fibers to their insertion–a 3D analysis of the Achilles tendon enthesis in mice". In: *Acta Biomaterialia* 120, pp. 146–155.

Schindelin, J. et al. (2012). "Fiji: An open-source platform for biological-image analysis". In: *Nature methods* 9.7, pp. 676–682.

Schippers, M.-P., R. Dukas, and G. B. McClelland (2010). "Lifetime-and caste-specific changes in flight metabolic rate and muscle biochemistry of honeybees, *Apis mellifera*". In: *Journal of Comparative Physiology B* 180.1, pp. 45–55.

Schmid-Hempel, P. (1992). "Worker castes and adaptive demography". In: *Journal of Evolutionary Biology* 5.1, pp. 1–12.

Schmidt-Nielsen, K. and S.-N. Knut (1984). *Scaling: why is animal size so important?* Cambridge university press.

Schmitt, C., A. Rack, and O. Betz (2014). "Analyses of the mouthpart kinematics in *Periplaneta americana* (Blattodea, Blattidae) using synchrotron-based X-ray cineradiography". In: *Journal of Experimental Biology* 217.17, pp. 3095–3107.

Schofield, R. M., M. H. Nesson, and K. A. Richardson (2002). "Tooth hardness increases with zinc-content in mandibles of young adult leaf-cutter ants". In: *Naturwissenschaften* 89, pp. 579–583.

Schofield, R. M. et al. (2003). "Zinc is incorporated into cuticular "tools" after ecdysis: The time course of the zinc distribution in "tools" and whole bodies of an ant and a scorpion". In: *Journal of Insect Physiology* 49, pp. 31–44.

Schofield, R. M. et al. (2011). "Leaf-cutter ants with worn mandibles cut half as fast, spend twice the energy, and tend to carry instead of cut". In: *Behavioral Ecology and Sociobiology* 65, pp. 969–982.

Schofield, R. M. et al. (2016). "Is fracture a bigger problem for smaller animals? Force and fracture scaling for a simple model of cutting, puncture and crushing". In: *Interface Focus* 6.

Schofield, R. et al. (2021). "The homogenous alternative to biomineralization: Zn-and Mn-rich materials enable sharp organismal "tools" that reduce force requirements". In: *Scientific Reports* 11.1, pp. 1–23.

Scholz, I. et al. (2010). "Slippery surfaces of pitcher plants: *Nepenthes* wax crystals minimize insect attachment via microscopic surface roughness". In: *The Journal of Experimental Biology* 213, pp. 1115–1125.

Schuldt, S. et al. (2016). "Analysis of the sharpness of blades for food cutting". In: *Journal of Food Engineering* 188, pp. 13–20.

Schuldt, S. et al. (2013). "Defined abrasion procedures for cutting blades and comparative mechanical and geometrical wear characterization". In: *Wear* 300, pp. 38–43.

Seeley, T. D. (1982). "Adaptive significance of the age polyethism schedule in honeybee colonies". In: *Behavioral Ecology and Sociobiology* 11.4, pp. 287–293.

Seghir, R. and S. Arscott (2015). "Extended PDMS stiffness range for flexible systems". In: *Sensors and Actuators A: Physical* 230, pp. 33–39.

Seid, M. A., A. Castillo, and W. T. Wcislo (2011). "The allometry of brain miniaturization in ants". In: *Brain, Behavior and Evolution* 77.1, pp. 5–13.

Seid, M. A. and J. F. Traniello (2006). "Age-related repertoire expansion and division of labor in *Pheidole dentata* (Hymenoptera: Formicidae): a new perspective on temporal polyethism and behavioral plasticity in ants". In: *Behavioral Ecology and Sociobiology* 60.5, pp. 631–644.

Senawi, J. et al. (2015). "Beyond size - morphological predictors of bite force in a diverse insectivorous bat assemblage from Malaysia". In: *Functional Ecology* 29.11, pp. 1411–1420.

Sharma, S., R. Kooner, and R. Arora (2017). "Insect pests and crop losses". In: *Breeding insect resistant crops for sustainable agriculture*. Springer, pp. 45–66.

Sheets, K. G. et al. (2011). "Topical neuroprotectin D1 attenuates experimental CNV and induces activated microglia redistribution". In: *Investigative Ophthalmology & Visual Science* 52.14, pp. 5470–5470.

Shepherd, J. D. (1985). "Adjusting foraging effort to resources in adjacent colonies of the leaf-cutter ant, *Atta colombica*". In: *Biotropica* 17.3, pp. 245–252.

Shimomura, T. et al. (2016). "A beetle flight muscle displays leg muscle microstructure". In: *Biophysical Journal* 111.6, pp. 1295–1303.

Shorter, J. R. and E. A. Tibbetts (2009). "The effect of juvenile hormone on temporal polyethism in the paper wasp *Polistes dominulus*". In: *Insectes Sociaux* 56.1, pp. 7–13.

Shutler, D. and A. Mullie (1991). "Size-related foraging behaviour of the leaf-cutting ant *Atta colombica*". In: *Canadian Journal of Zoology* 69, pp. 1530–1533.

Siebert, T. et al. (2010). "*Cupiennius salei*: biomechanical properties of the tibia–metatarsus joint and its flexing muscles". In: *Journal of Comparative Physiology B* 180.2, pp. 199–209.

Silva, L. C. et al. (2016). "Mandibles of leaf-cutting ants: morphology related to food preference". In: *Sociobiology* 63.3, pp. 881–888.

Silva, T. S. and R. M. Feitosa (2019). "Using controlled vocabularies in anatomical terminology: A case study with *Strumigenys* (Hymenoptera: Formicidae)". In: *Arthropod Structure & Development* 52, p. 100877.

Simon, J.-C. et al. (2015). "Genomics of adaptation to host-plants in herbivorous insects". In: *Briefings in Functional Genomics* 14.6, pp. 413–423.

Singh, I. K. and A. Singh (2021). *Plant-Pest Interactions: From Molecular Mechanisms to: Chemical Ecology*. Springer.

Skandalis, D. A., C. Roy, and C.-A. Darveau (2011). "Behavioural, morphological, and metabolic maturation of newly emerged adult workers of the bumblebee, *Bombus impatiens*". In: *Journal of Insect Physiology* 57.6, pp. 704–711.

Smith, L. D. and A. R. Palmer (1994). "Effects of manipulated diet on size and performance of brachyuran crab claws". In: *Science* 264.5159, pp. 710–712.

Smith, M., O. Kvedaras, and M. Keeping (2007). "A novel method to determine larval mandibular wear of the African stalk borer, Eldana saccharina Walker (Lepidoptera: Pyralidae)". In: *African Entomology* 15.1, pp. 204–208.

Smith, R. J. (2009). "Use and Misuse of the Reduced Major Axis for Line-Fitting". In: *American Journal of Physical Anthropology* 140, pp. 476–486.

Smith, R. J. (1984). "Allometric scaling in comparative biology: problems of concept and method". In: *American Journal of Physiology-Regulatory, Integrative and Comparative Physiology* 246.2, pp. 152–160.

South, J. et al. (2020). "In a pinch: mechanisms behind potential biotic resistance toward two invasive crayfish by native African freshwater crabs". In: *Frontiers in Ecology and Evolution* 8, p. 72.

Souza, A., J. K. Udupa, and P. K. Saha (2005). "Volume rendering in the presence of partial volume effects". In: *IEEE Transactions on Medical Imaging* 24.2, pp. 223–235.

Spagna, J. C. et al. (2008). "Phylogeny, scaling, and the generation of extreme forces in trap-jaw ants". In: *Journal of Experimental Biology* 211.14, pp. 2358–2368.

Sparks, T. C. (2013). "Insecticide discovery: an evaluation and analysis". In: *Pesticide Biochemistry and Physiology* 107.1, pp. 8–17.

Spatz, H., L. Kohler, and K. Niklas (1999). "Mechanical behaviour of plant tissues: composite materials or structures?" In: *Journal of Experimental Biology* 202.23, pp. 3269–3272.

Staniczek, A. H. (2001). "Der Larvenkopf von *Oniscigaster wakefieldi* McLachlan, 1873 (Insecta: Ephemeroptera: Onscigastridae)". PhD thesis. Universität Tübingen.

Stradling, D. J. (1978). "The influence of size on foraging in the ant, *Atta cephalotes*, and the effect of some plant defence mechanisms". In: *The Journal of Animal Ecology*, pp. 173–188.

Stride, G. O. (1953). "The respiratory bubble of the aquatic beetle, *Potamodytes tuberosus*, Hinton". In: *Nature* 171.4359, pp. 885–886.

Sullivan, S. et al. (2019). "3D muscle architecture of the pectoral muscles of European Starling (*Sturnus vulgaris*)". In: *Integrative Organismal Biology* 1.1, pp. 1–18.

Sun, J.-Y. et al. (2012). "Highly stretchable and tough hydrogels". In: *Nature* 489.7414, pp. 133–136.

Sustaita, D. and F. Hertel (2010). "*In vivo* bite and grip forces, morphology and prey-killing behavior of North American accipiters (Accipitridae) and falcons (Falconidae)". In: *Journal of Experimental Biology* 213.15, pp. 2617–2628.

Sutton, G. and M. Burrows (2018). "Insect jumping springs". In: *Current Biology* 28.4, R142–R143.

Sutton, G. P. and M. Burrows (2011). "Biomechanics of jumping in the flea". In: *Journal of Experimental Biology* 214.5, pp. 836–847.

Tautz, J., F. Roces, and B. Hölldobler (1995). "Use of a Sound-Based Vibratome by Leaf-Cutting Ants". In: *Science* 267, p. 84.

Taylor, G. M. (2000). "Maximum force production: why are crabs so strong?" In: *Proceedings of the Royal Society of London. Series B: Biological Sciences* 267.1451, pp. 1475–1480.

Thomas, M. L. and M. A. Elgar (2003). "Colony size affects division of labour in the ponerine ant *Rhytidoponera metallica*". In: *Naturwissenschaften* 90.2, pp. 88–92.

Tilmen, D. et al. (2011). "Global food demand and the sustainable intensification of agriculture". In: *Proceedings of the National Academy of Sciences of the U.S.A* 105.50, pp. 20260–20264.

Tofilski, A. (2002). "Influence of age polyethism on longevity of workers in social insects". In: *Behavioral Ecology and Sociobiology* 51.3, pp. 234–237.

Tofts, C. (1993). "Algorithms for task allocation in ants. (A study of temporal polyethism: theory)". In: *Bulletin of Mathematical Biology* 55.5, pp. 891–918.

Tu, M. S. and T. L. Daniel (2004). "Submaximal power output from the dorsolongitudinal flight muscles of the hawkmoth *Manduca sexta*". In: *Journal of Experimental Biology* 207.26, pp. 4651–4662.

Van Daele, P., A. Herrel, and D. Adriaens (2009). "Biting performance in teeth-digging African mole-rats (*Fukomys*, Bathyergidae, Rodentia)". In: *Physiological and Biochemical Zoology* 82.1, pp. 40–50.

Van Rossum, G. and F. L. Drake (2009). *Python 3 Reference Manual*. Scotts Valley, CA: CreateSpace. ISBN: 1441412697.

Vassallo, A. I. et al. (2016). "Ontogenetic integration between force production and force reception: a case study in Ctenomys (Rodentia: Caviomorpha)". In: *Acta Zoologica* 97.2, pp. 232–240.

Verwaijen, D., R. Van Damme, and A. Herrel (2002). "Relationships between head size, bite force, prey handling efficiency and diet in two sympatric lacertid lizards". In: *Functional Ecology* 16.6, pp. 842–850.

Vieira, S. A., W. D. Fernandes, and W. F. Antonialli-Junior (2010). "Temporal polyethism, life expectancy, and entropy of workers of the ant *Ectatomma vizottoi* Almeida, 1987 (Formicidae: Ectatomminae)". In: *Acta Ethologica* 13.1, pp. 23–31.

Vincent, J. F. (1990). "Fracture properties of plants". In: *Advances in Botanical Research*. Vol. 17. Elsevier, pp. 235–287.

Vincent, J. F. and U. G. Wegst (2004). "Design and mechanical properties of insect cuticle". In: *Arthropod Structure & Development* 33.3, pp. 187–199.

Virtanen, P. et al. (2020). "SciPy 1.0: Fundamental Algorithms for Scientific Computing in Python". In: *Nature Methods* 17, pp. 261–272. DOI: 10.1038/s41592-019-0686-2.

Vogelgesang, M. et al. (2012). "UFO: A scalable GPU-based image processing framework for online monitoring". In: *2012 IEEE 14th International Conference on High Performance Computing and Communication & 2012 IEEE 9th International Conference on Embedded Software and Systems*. IEEE, pp. 824–829.

Vogelgesang, M. et al. (2016). "Real-time image-content-based beamline control for smart 4D X-ray imaging". In: *Journal of Synchrotron Radiation* 23.5, pp. 1254–1263.

Voje, K. L. and T. F. Hansen (2013). "Evolution of static allometries: adaptive change in allometric slopes of eye span in stalk-eyed flies". In: *Evolution: International Journal of Organic Evolution* 67.2, pp. 453–467.

Voje, K. L. et al. (2014). "Allometric constraints and the evolution of allometry". In: *Evolution* 68.3, pp. 866–885.

Wakeling, J. M. et al. (2021). "Modeling muscle function using experimentally determined subject-specific muscle properties". In: *Journal of Biomechanics* 117, p. 110242.

Waller, D. (1982). "Leaf-cutting ants and live oak: the role of leaf toughness in seasonal and intraspecific host choice". In: *Entomologia Experimentalis et Applicata* 32.2, pp. 146–150.

– (1989). "Size-Related Foraging in the Leaf-Cutting Ant *Atta texana* (Buckley) (Formicidae: Attini)". In: *Functional Ecology* 3.4, pp. 461–468.

Walter, E. V., L. Seaton, and A. A. Mathewson (1938). *The Texas leaf-cutting ant and its control*. 494. US Department of Agriculture.

Wang, C. H. (1996). *Introduction to fracture mechanics*. Tech. rep. DSTO Aeronautical and Maritime Research Laboratory.

Wappner, P. and L. A. Quesada-Allué (1996). "Water loss during cuticle sclerotization in the medfly *Ceratitis capitata* is independent of catecholamines". In: *Journal of Insect Physiology* 42.7, pp. 705–709.

War, A. R. et al. (2012). "Mechanisms of plant defense against insect herbivores". In: *Plant Signaling & Behavior* 7.10, pp. 1306–1320.

Warton, D. I. et al. (2006). "Bivariate line-fitting methods for allometry". In: *Biological reviews* 81.2, pp. 259–291.

Warton, D. I. et al. (2012). "smatr 3 - an R package for estimation and inference about allometric lines". In: *Methods in Ecology and Evolution* 3, pp. 257–259.

Weber, N. A. (1972). "The fungus-culturing behaviour of ants". In: *American Zoologist* 12, pp. 577–587.

Weihmann, T. et al. (2015a). "Fast and Powerful: Biomechanics and Bite Forces of the Mandibles in the American Cockroach *Periplaneta americana*". In: *Public Library of Science One* 10, e0141226.

Weihmann, T. et al. (2015b). "Functional morphology of the mandibular apparatus in the cockroach *Periplaneta americana* (Blattodea: Blattidae) – a model species for omnivore insects". In: *Arthropod Systematics & Phylogeny* 73.3, pp. 477–488.

Weisser, W. and E. Siemann (2004). "The various effects of insects on ecosystem functioning". In: *Insects and ecosystem function*. Springer, pp. 3–24.

Wetterer, J. K. (1991a). "Allometry and geometry of leaf-cutting in *Atta cephalotes*". In: *Behavioral Ecology and Sociobiology* 29, pp. 347–351.

– (1991b). "Source distance has no effect on load size in the leaf-cutting ant, *Atta cephalotes*". In: *Psyche* 98, pp. 355–359.

– (1994a). "Forager polymorphism, size-matching, and load delivery in the leaf-cutting ant, *Atta cephalotes*". In: *Ecological Entomology* 19, pp. 57–64.

– (1994b). "Ontogenetic changes in forager polymorphism and foraging ecology in the leaf-cutting ant *Atta cephalotes*". In: *Oecologia* 98, pp. 235–238.

– (1995a). "Forager polymorphism and foraging ecology in the leaf-cutting ant, *Atta colombica*". In: *Psyche* 102, pp. 131–145.

– (1995b). "Forager size and ecology of *Acromyrmex coronatus* and other leaf-cutting ants in Costa Rica". In: *Oecologia* 104, pp. 409–415.

Wetterer, J. K. (1990). "Load-size determination in the leaf-cutter ant, *Atta cephalotes*". In: *Behavioural Ecology* 1.2, pp. 95–101.

– (1999). "The ecology and evolution of worker size-distribution in leaf-cutting ants (Hymenoptera: Formicidae)". In: *Sociobiology* 34.1, pp. 119–144.

Wheater, C. and M. Evans (1989). "The mandibular forces ad pressures of some predacious Coleoptera". In: *Journal of Insect Physiology* 35, pp. 815–820.

Wheeler, D. E. (1991). "The developmental basis of worker caste polymorphism in ants". In: *The American Naturalist* 138.5, pp. 1218–1238.

Wheeler, W. M. (1907). "The Fungus-Growing Ants of North America". In: *Bulletin American Museum of Natural History* 23, pp. 669–807.

Wiens, J. J., R. T. Lapoint, and N. K. Whiteman (2015). "Herbivory increases diversification across insect clades". In: *Nature Communications* 6.1, pp. 1–7.

Williams, C. D. et al. (2013). "The length–tension curve in muscle depends on lattice spacing". In: *Proceedings of the Royal Society B: Biological Sciences* 280.1766, p. 20130697.

Williams, J. G. (2015a). "Stress at a distance fracture criteria and crack self-blunting in rubber". In: *International Journal of Non-Linear Mechanics* 68, pp. 33–36.

– (2015b). "The Griffith Medal Lecture: The fracture mechanics of soft solids". In: *Engineering Fracture Mechanics* 149, pp. 192–198.

Williams, J. G. and Y. Patel (2016). "Fundamentals of cutting". In: *Interface Focus* 6, p. 20150108.

Williams, S. H., E. Peiffer, and S. Ford (2009). "Gape and bite force in the rodents *Onychomys leucogaster* and *Peromyscus maniculatus*: Does jaw-muscle anatomy predict performance?" In: *Journal of Morphology* 270.11, pp. 1338–1347.

Wills, B. D. et al. (2018). "Correlates and consequences of worker polymorphism in ants". In: *Annual Review of Entomology* 63, pp. 575–598.

Wilson, E. O. (1953). "The Origin and Evolution of Polymorphism in Ants". In: *The Quartely Review of Biology* 28.2, pp. 136–156.

– (1980a). "Caste and Division of Labor in Leaf-Cutter ants (Hymenoptera: Formicidae: *Atta*): I. The Overall Pattern in *A. Sextens*". In: *Behavioral Ecology and Sociobiology* 7, pp. 143–156.

– (1980b). "Caste and Division of Labor in Leaf-Cutter ants (Hymenoptera: Formicidae: *Atta*): II. The Ergonomic Optimization of Leaf Cutting". In: *Behavioral Ecology and Sociobiology* 7, pp. 157–165.

– (1983a). "Caste and Division of Labor in Leaf-Cutter ants (Hymenoptera: Formicidae: *Atta*): III. Ergonomic resiliency in foraging by *A. cephalotes*". In: *Behavioral Ecology and Sociobiology* 14.1, pp. 47–54.

– (1983b). "Caste and Division of Labor in Leaf-Cutter ants (Hymenoptera: Formicidae: *Atta*): IV. Colony Ontogeny of *A. cephalotes*". In: *Behavioral Ecology and Sociobiology* 14.1, pp. 55–60.

Wilson, E. O. (1976). "Behavioral discretization and the number of castes in an ant species". In: *Behavioral Ecology and Sociobiology* 1.2, pp. 141–154.

Wilson, R. S. et al. (2007). "Dishonest signals of strength in male slender crayfish (*Cherax dispar*) during agonistic encounters". In: *The American Naturalist* 170.2, pp. 284–291.

Wipfler, B. et al. (2016). "The cephalic morphology of the American cockroach *Periplaneta americana* (Blattodea)". In: *Arthropod Systematics & Phylogeny* 74, pp. 267–297.

Wirth, R. et al. (2003). *Herbivory of Leaf-Cutting Ants: A Case Study on* Atta colombica *in the Tropical Rainforest of Panama*. Berlin, Heidelberg, New York: Springer Science & Business Media.

Withers, P. J. et al. (2021). "X-ray computed tomography". In: *Nature Reviews Methods Primers* 1.1, pp. 1–21.

Wright, W. and J. F. Vincent (1996). "Herbivory and the mechanics of fracture in plants". In: *Biological Reviews* 71.3, pp. 401–413.

Yamada, S. B. and E. G. Boulding (1998). "Claw morphology, prey size selection and foraging efficiency in generalist and specialist shell-breaking crabs". In: *Journal of Experimental Marine Biology and Ecology* 220.2, pp. 191–211.

Yanagihara, S. et al. (2018). "Age-based soldier polyethism: old termite soldiers take more risks than young soldiers". In: *Biology Letters* 14.3, p. 20180025.

Yang, L. H. and C. Gratton (2014). "Insects as drivers of ecosystem processes". In: *Current Opinion in Insect Science* 2, pp. 26–32.

Yap, N. W., Y. Lin, and P. A. Todd (2013). "Chelae force generation at variable gape sizes in the mud crab, *Scylla olivacea* (Brachyura: Portunidae)". In: *Nature in Singapore* 6, pp. 179–185.

Young, W. C. and R. G. Budynas (2002). *Roark's formulas for stress and strain*. 7th ed. McGraw-Hill.

Yushkevich, P. A. et al. (2006). "User-guided 3D active contour segmentation of anatomical structures: significantly improved efficiency and reliability". In: *NeuroImage* 31.3, pp. 1116–1128.

Zachar, J. and D. Zacharová (1966). "The length-tension diagram of single muscle fibres of the crayfish". In: *Experientia* 22.7, pp. 451–452.

Zhang, B. and P. S. Anderson (2022). "Modelling biological puncture: a mathematical framework for determining the energetics and scaling". In: *Journal of the Royal Society Interface* 19.195, p. 20220559.

Zhang, B. and S. B. Hutchens (2021). "On the relationship between cutting and tearing in soft elastic solids". In: *Soft Matter* 17.28, pp. 6728–6741.

Zhang, B. et al. (2019). "Y-shaped cutting for the systematic characterization of cutting and tearing". In: *Experimental Mechanics* 59.4, pp. 517–529.

Zhang, W. et al. (2020a). "A Mathematical Modeling Method Elucidating the Integrated Gripping Performance of Ant Mandibles and Bio-inspired Grippers". In: *Journal of Bionic Engineering* 17.4, pp. 732–746.

Zhang, W. et al. (2020b). "Multifunctional mandibles of ants: Variation in gripping behavior facilitated by specific microstructures and kinematics". In: *Journal of Insect Physiology* 120, p. 103993.

Zhang, Z.-Q. (2013a). "Animal biodiversity: an update of classification and diversity in 2013". In: *Zootaxa* 3703.1, pp. 5–11.

– (2013b). "Phylum Arthropoda". In: *Zootaxa* 3703.1, pp. 17–26.